

Phase Behaviours of Polymeric Blends Containing
Block Copolymers

PHASE BEHAVIOURS OF POLYMERIC BLENDS CONTAINING
BLOCK COPOLYMERS

BY

JIAYU XIE, B.SC.

A THESIS

SUBMITTED TO THE SCHOOL OF GRADUATE STUDIES

IN PARTIAL FULFILLMENT OF THE REQUIREMENTS

FOR THE DEGREE OF

DOCTOR OF PHILOSOPHY

McMaster University

© Copyright by Jiayu Xie December 2023

Doctor of Philosophy (2023)

(Physics & Astronomy)

McMaster University

Hamilton, Ontario

TITLE: Phase Behaviours of Polymeric Blends Containing Block Copolymers

AUTHOR: Jiayu Xie (McMaster University)

SUPERVISOR: Dr. An-Chang Shi

NUMBER OF PAGES: xii, 199

Abstract

Blending different polymers together provides a simple yet effective method for producing unconventional structured materials. However, understanding the interplay between macro- and microphase separations poses a challenge when studying the phase behaviours of polymeric blends containing block copolymers. In this thesis, we advance our knowledge of polymeric blend self-assembly by investigating several informative blending systems using self-consistent field theory (SCFT).

We begin with straightforward blending formulations, such as binary A_1B_1/A_2 and A_1B_1/A_2B_2 blends, to conduct systematic investigations into their phase behaviours. Our focus is on the formation and stability of recently discovered Frank-Kasper (FK) phases. The unveiled correlation between the various system parameters, the behaviours of various polymeric components, and the stability of the FK phases deepens our understanding of the emergence of these unconventional spherical phases in polymeric mixtures composed of simple components.

Expanding our study, we investigate more general AB/C binary blends and AB/C/D ternary blends, resembling surfactant/water and surfactant/water/oil systems. In agreement with recent experiments, we find that the addition of corona-selective C homopolymers into diblock copolymers reduces the critical conformational asymmetry of the diblocks required to stabilize the FK σ phase. Furthermore, the simultaneous presence of core- and corona-selective components greatly enhances the stability of the FK phases,

particularly the Laves phases. Our results provide insights into the formation of FK phases in a broader range of soft matter systems containing amphiphilic molecules and selective additives.

Next, in seeking alternatives to architecturally complex block copolymers for fabricating binary crystalline phases, we turn our attention to AB/CD binary blends. With designed secondary interactions, we demonstrate that this system can stabilize various binary crystals with varying stoichiometries. Our analysis of chain packing within various phases sheds light on the mechanisms governing the selection of the equilibrium crystal in this system.

Lastly, we explore the topological effects of copolymers in their blends with homopolymers. Although the topological nonequivalency between ABA and BAB linear triblock copolymers results in only slight differences in their equilibrium phase behaviours, these differences are dramatically magnified when blended with A homopolymers. Compared to ABA/A blends, BAB/A blends exhibit much poorer miscibility, and the Lifshitz points of these two polymeric blends are qualitatively different.

The results presented in this thesis enhance our understanding of the equilibrium phase behaviours of polymeric blends containing block copolymers, including blend miscibility and structural formation, thus laying a solid foundation for future research into more complex blending systems.

Acknowledgements

I would like to seize this opportunity to express my heartfelt gratitude to those who have been with me, inspiring and supporting me throughout the invaluable and pivotal five and a half years of my graduate studies.

Above all, I am profoundly grateful to have Dr. An-Chang Shi as my supervisor and mentor. Dr. Shi has provided tremendous assistance and support, not only in research but also in life. As the individual with whom I interact and engage with on a daily basis, Dr. Shi has significantly influenced the way I approach research challenges. Thank you for your patience and unwavering commitment to the success and well-being of your students. I am also very appreciative of Dr. Kari Dalnoki-Veress and Dr. Paul Higgs, who have served as members of my Ph.D. committee throughout my academic journey. Your constant support and encouragement have motivated me to strive harder. Kari, I want to express my gratitude for the exceptional polymer course you taught and for your guidance during the challenging moments when I was unsure about my path.

My sincere gratitude extends to all my colleagues who engaged in our daily discussions, with special recognition for Tom Lai, Sarah Dawson, Yang Yang, Yu Li, Cameron Burns and Desiree Rehel. Tom, in particular, holds a special place in my appreciation, not only for his irreplaceable help but also for being my first friend in Canada. The days we spent together discussing research late into the night and our joyous game days stand out as some of the most cherished memories of my Ph.D. journey. My sincere appreciation also

extends to the department secretaries, with a specific mention of Rosemary McNeice, whose invaluable assistance has significantly enhanced my experience at Mac.

Furthermore, I wish to convey my heartfelt acknowledgment to my housemates and friends when I first arrived in Canada – Neo Wang, Tony Qian, and Elvin Drent – and later, Jack Yuan and Hugo Huang, who joined and became integral members of the 137-Broadway-Ave family. I am deeply grateful for the conversations, companionship, and laughter that defined our time together. I can't thank you guys enough for being there, especially during the tough times following the onset of COVID-19.

Throughout my time at Mac, I've had the privilege of making numerous friends. While it is impossible to mention everyone by name, I want to express my deep appreciation to each of you for being a part of my life.

A special thanks goes to the people I met in the ESL class, especially Nelson Buffett, John Ferns, Gillian Ferns, and Margaret Bottley. Nelson, thank you for organizing this wonderful class, which has greatly assisted numerous international students. I'm also grateful for the memorable fishing and hunting trips we all enjoyed up in Northern Ontario. Nelson, John, and Gillian, you are truly some of the most open-minded and kind individuals I've ever had the pleasure of meeting.

An important year in my life was 2022, during which I met my girlfriend, Baoqin Deng. She has been by my side, offering steadfast support in pursuing my goals ever since. Thank you for being such an amazing partner.

Last but certainly not least, I want to express my gratitude to my family for their unconditional love and unwavering support, especially my parents: Qian Li and Quansheng Xie. Without them, I would never have had the opportunity to reach the point where I am today.

I love you all!

Table of contents

Abstract	iii
Acknowledgements	v
List of figures	x
List of tables	xii
1 Introduction	1
1.1 Phase Behaviours of Single-Component Block Copolymer Systems	2
1.1.1 AB Diblock Copolymer	2
1.1.2 More Complex Block Copolymers	10
1.2 Phase Behaviours of Polymeric Blends Containing Block Copolymers . . .	12
1.3 Objective and Outline	17
2 Theoretical Framework	22
2.1 Self-Consistent Field Theory	22
2.1.1 SCFT Applied on Gaussian Chain Model for Diblock Copolymer Melts	23

2.1.2	SCFT Applied on freely jointed Chain Model for Diblock Copolymer Melts	33
2.1.3	SCFT for Polymeric Blends: Binary AB/C Blends	41
2.2	Random-Phase Approximation	45
2.2.1	The \tilde{S}^{-1} Matrix	46
2.2.2	The Form Factors	49
3	Phase Behaviours of Binary Blends of Diblock Copolymers: A Review	51
4	Formation of Complex Spherical Packing Phases in Diblock Copolymer/Homopolymer Blends	72
5	Formation of Complex Spherical Packing Phases in Binary Blends of Diblock Copolymers	86
6	Theory of Complex Spherical Packing Phases in Diblock Copolymer/Homopolymer Blends	102
7	Stabilizing Binary Crystalline Phases in AB/CD Binary Diblock Copolymer Blends via Secondary Interactions	122
8	Phase Behaviour of Triblock Copolymer and Homopolymer Blends: Effect of Copolymer Topology	142
9	Concluding Remarks and Future Outlook	173
	Appendix A Numerical Methods to Solve Modified Diffusion Equations	179
	Appendix B Initial Ansatz for SCFT Calculation	182

List of figures

1.1	Examples of homopolymers and block copolymers. (a) and (b): homopolymers, (c)-(1): block copolymers. Blocks composed of chemically distinct monomers are in different colours.	3
1.2	The (a) homogenous/disordered state and (b) macroscopic-phase-separated state of binary homopolymer mixtures, and (c) the mesoscopic-phase-separated state of diblock copolymers.	4
1.3	Top left and top right depict diblock copolymers with symmetric and asymmetric blocks forming flat and curved domain interface, respectively. Schematics of lamellar, cylindrical and spherical morphologies are listed from left to right at the bottom.	5
1.4	Theoretical phase diagram of AB-diblock copolymer melts with symmetric Kuhn lengths ($\epsilon = 1$) constructed by using SCFT.	6
1.5	The ordered phases that appear in the phase diagram in Fig. 1.4. The surfaces in the plots are isosurfaces defined by the condition that A and B monomers have equal densities.	6

1.6	Schematics to demonstrate different packings of self-assembled domains: (a) perfect circular domains that have optimal chain stretching and interfacial energy but cannot fill the space, (b) space-filling domains with chains stretched as evenly as possible, (c) space-filling domains with a minimal interfacial area and (d) space-filling domains with a balanced chain stretching entropy and interfacial energy.	7
1.7	Theoretical phase diagram of AB-diblock copolymer melts with asymmetric Kuhn lengths ($\epsilon = 3$) constructed by using SCFT.	8
1.8	The Frank-Kasper (a) σ , (b) A15, (c) C14 and (d) C15 phases. The latter two phases also belong to the category of Laves phases, which is a subset of the Frank-Kasper phases. Nonequivalent domains are depicted by distinct colours.	9
1.9	Schematic showcasing the formation of various binary crystalline spherical phases from ABC triblock, AB_2CB_3 tetrablock and $B_1AB_2CB_3$ pentablock terpolymers. Reproduced from [46] with permission.	11
1.10	Schematics of the wet- and dry-brush regimes for the binary blends of AB copolymers and A homopolymers.	14
1.11	The bicontinuous (a) double diamond and (b) plumber's nightmare phases.	15

List of tables

- B.1 Initial density profiles of the core-forming monomers, and, when applicable, the reduced domain-center coordinates, for some typical ordered phases. . 183

Chapter 1

Introduction

As a spontaneous process, self-assembly serves as a fundamental route for materials to organize into a multitude of ordered structures across a wide range of length scales [1]. These self-assembled structures not only contribute to microscopic order but also define the macroscopic properties of materials [2]. Block copolymers, in particular, exemplify materials that display a diverse range of self-assembling behaviours, resulting in valuable properties and a wide array of applications including lithography [3–5], photonics [6–10], drug delivery [11, 12], porous materials [13, 14] and quantum materials [15, 16]. As a concrete example, compared to traditional nanolithography methods, block copolymer self-assembly may offer advantages in achieving high-resolution patterns with feature sizes in the nanometer range, holding promise for integration into semiconductor fabrication processes [17]. Therefore, gaining insights into block copolymer self-assembly and mastering the principles of designing and fabricating polymeric materials with tailored functions is of great importance. Moreover, despite their practical applications, block copolymers also provide an ideal platform to study the spontaneous formation of order in nature, a phenomenon that itself attracts significant research interest.

1.1 Phase Behaviours of Single-Component Block Copolymer Systems

1.1.1 AB Diblock Copolymer

The number of possible block copolymers is infinite. The simplest block copolymer, the AB diblock copolymer, forms by connecting two chemically distinct homopolymers, A and B, at their ends. As the number and types of blocks increase, the complexity of the copolymer chain grows. Fig. 1.1 illustrates some examples of homopolymers and block copolymers with varying degrees of complexity.

To begin understanding the phase behaviour of block copolymers, we can start by considering simple binary blends of chemically incompatible A and B homopolymers. The spatial distribution of the homopolymer chains is determined by a competition between entropy and interfacial energy. On one hand, a uniform distribution of all homopolymers, where A and B homopolymers are homogeneously mixed (Fig. 1.2(a)), maximizes the entropy of the system but results in high interaction energy. On the other hand, macroscopic phase separation into A-rich and B-rich domains (Fig. 1.2(b)) minimizes the interaction energy but leads to suboptimal entropy. According to the theory of binary mixtures for polymers [18, 19], the balance between these opposing tendencies is controlled by several parameters, including the concentrations and molecular weights of the two homopolymers, the interaction between A and B monomers, and temperature. For a given set of homopolymer samples characterized by specific concentrations and length ratios, a critical temperature exists below which the dominance of interaction

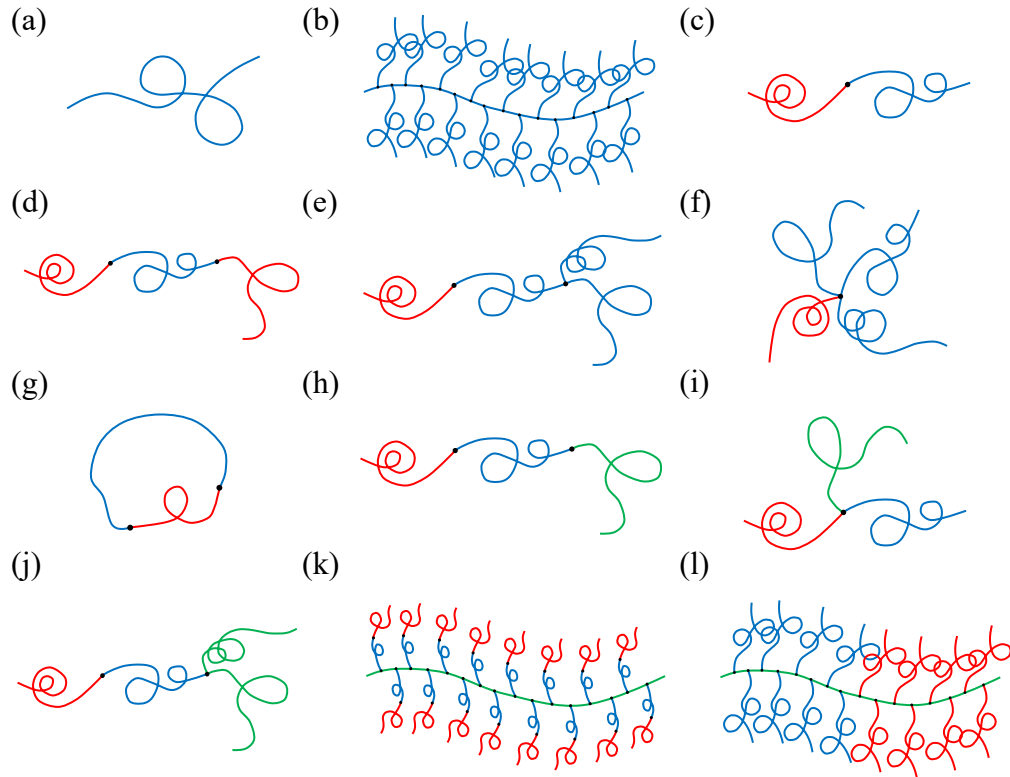


Fig. 1.1 Examples of homopolymers and block copolymers. (a) and (b): homopolymers, (c)-(l): block copolymers. Blocks composed of chemically distinct monomers are in different colours.

energy over translational entropy drives the system towards macroscopic phase separation.

For a system of AB diblock copolymers comprising immiscible A and B blocks, the presence of covalent bonds connecting these blocks precludes macroscopic phase separation. Instead, mesoscopic phase separation occurs below a critical temperature, leading to the formation of A-rich and B-rich domains with a length scale typically ranging from 10 to 100 nanometers (as depicted in Fig. 1.2(c)). The morphology of these mesoscopic domains depends on the volume fractions of the immiscible blocks. As the

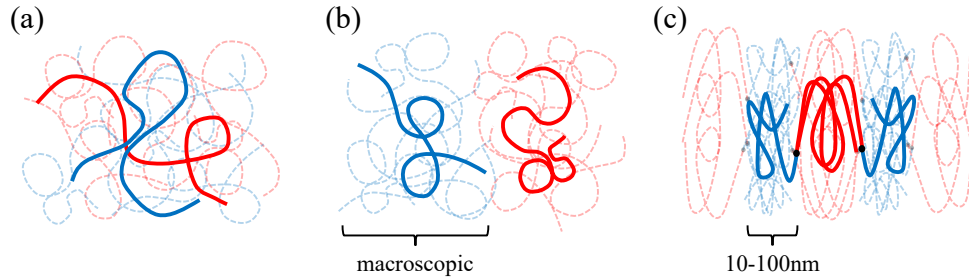


Fig. 1.2 The (a) homogenous/disordered state and (b) macroscopic-phase-separated state of binary homopolymer mixtures, and (c) the mesoscopic-phase-separated state of diblock copolymers.

volume fraction becomes increasingly asymmetric, a progression in domain morphology is commonly observed, transitioning from lamellar to cylindrical, and ultimately to spherical structures, as illustrated in Fig. 1.3. This progression is driven by the necessity to generate a curvature at the AB interface, a critical factor in optimizing chain conformational entropy. Specifically, maximization of conformational entropy leads a polymer chain to form a coil with a certain dimension, which tends to be greater for longer chains. When the distinct blocks of diblock copolymers are symmetrical, the A and B polymer coils have comparable dimensions, favouring a lamellar morphology with flat interfaces, as illustrated by the top-left schematic in Fig. 1.3. In the case of diblock copolymers with asymmetric A and B blocks, the majority blocks prefer to form larger coils than the minority ones, resulting in interfaces that curve towards the minority blocks, as depicted by the top-right schematic in Fig. 1.3. This induced curvature of the interfaces, stemming from the asymmetry between A and B blocks, is commonly referred to as spontaneous curvature [20].

The organization of self-assembled domains can lead to the formation of structures exhibiting long-range order. In the case of the simplest example, AB diblock copoly-

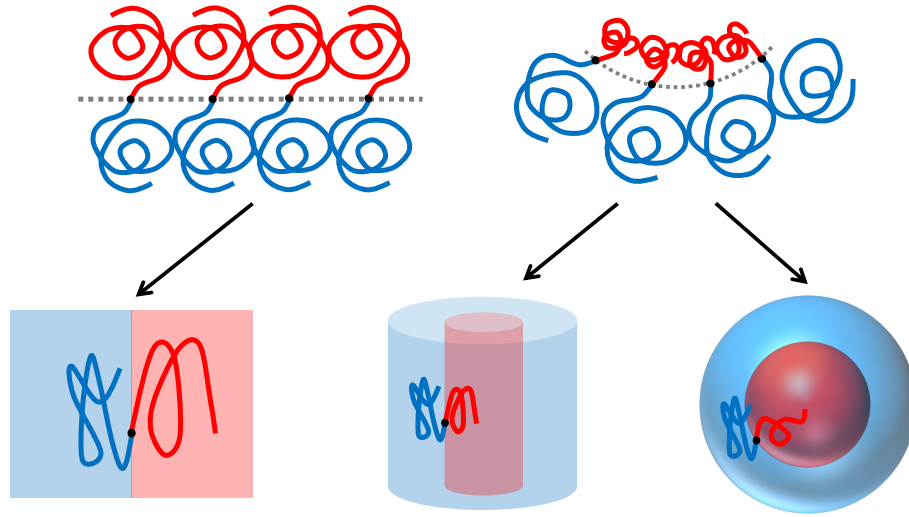


Fig. 1.3 Top left and top right depict diblock copolymers with symmetric and asymmetric blocks forming flat and curved domain interface, respectively. Schematics of lamellar, cylindrical and spherical morphologies are listed from left to right at the bottom.

mer melts, both theoretical studies [21] and experimental investigations [22, 23] have demonstrated that the equilibrium phase behaviour is governed by three key parameters: (1) the volume fractions of A (or B) block, denoted as $f_A = f$ (or $f_B = 1 - f$), (2) the product of the Flory-Huggins interaction parameter and the degree of polymerization, denoted as χN , and (3) the conformational asymmetry determined by the ratio between the Kuhn lengths of the A and B monomers, $\epsilon = b_A/b_B$. The theoretical phase diagram of conformationally symmetric ($\epsilon = 1$) AB diblock copolymer melts, constructed using self-consistent field theory (SCFT), is depicted in Fig. 1.4. This phase diagram exhibits reflection symmetry around $f = 0.5$, where the same phases appear symmetrically on both sides, with the minority and majority blocks swapped. As the parameter f varies from 0.5 to either 0 or 1, a morphological progression is observed, transitioning from lamellae (L) to a $Fddd$ network (O^{70}), then to double Gyroid networks (DG), hexagonally close-packed cylinders (HEX), body-centered cubic spheres (BCC), hexagonally close-packed spheres (HCP), and finally to a disordered (Dis) phase. The DG and O^{70} phases, situated between

HEX and L, are networked phases resembling distorted and interconnected cylinders. Schematic representations of all the ordered phases illustrated in Fig. 1.4 are given in Fig. 1.5.

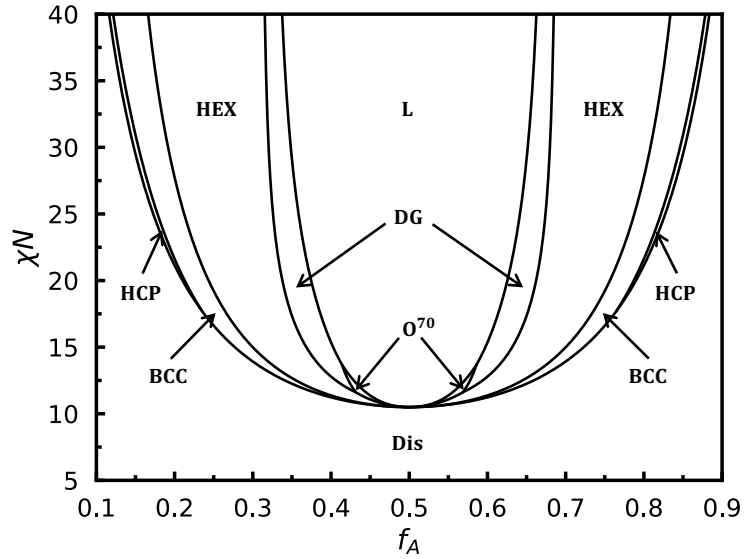


Fig. 1.4 Theoretical phase diagram of AB-diblock copolymer melts with symmetric Kuhn lengths ($\epsilon = 1$) constructed by using SCFT.

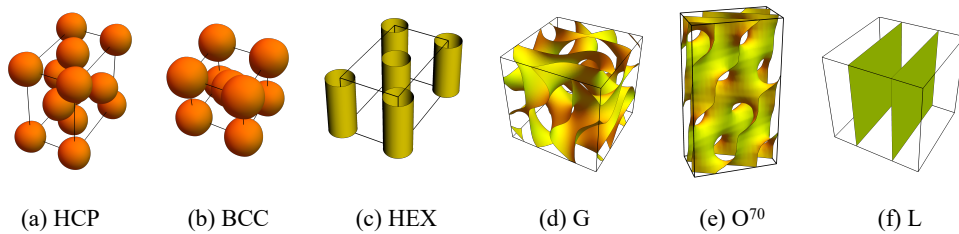


Fig. 1.5 The ordered phases that appear in the phase diagram in Fig. 1.4. The surfaces in the plots are isosurfaces defined by the condition that A and B monomers have equal densities.

The morphological progression of diblock copolymers, transitioning from lamellae to networks, cylinders, and spheres induced by the change in f , can be comprehended through the concept of spontaneous curvature. However, the selection of a specific crystalline structure arises from a complex interplay among conflicting factors within the system. Let us take cylinder-forming diblock copolymers as an illustrative example. The configurational entropy of the copolymer favours uniform chain stretching, resulting in domains with perfectly circular cores and coronas. However, this chain configuration inevitably results in voids in the space (see Fig. 1.6(a)) and is impermissible because polymer melts must occupy the space uniformly. To occupy the space without creating voids, the polymeric domains must conform to the hexagonal shape of their enclosing Wigner-Seitz cells (WSCs). This entails compromising the chain configurational entropy by stretching some chains more than others to reach the regions near the vertices of the hexagons.

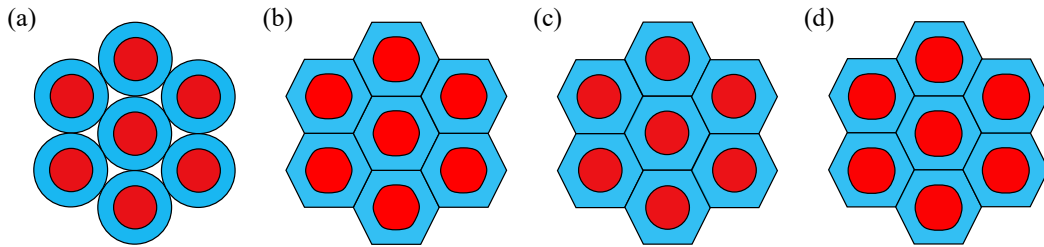


Fig. 1.6 Schematics to demonstrate different packings of self-assembled domains: (a) perfect circular domains that have optimal chain stretching and interfacial energy but cannot fill the space, (b) space-filling domains with chains stretched as evenly as possible, (c) space-filling domains with a minimal interfacial area and (d) space-filling domains with a balanced chain stretching entropy and interfacial energy.

Subject to this space-filling constraint, two other factors come into play. On one hand, the maximization of entropy prefers the copolymer chains to stretch as evenly as possible (Fig. 1.6(b)), while, on the other hand, the minimization of interfacial energy favours a

perfect spherical AB interface (Fig. 1.6(c)). Consequently, the resulting interface assumes an intermediate shape (Fig. 1.6(d)). The inability of block copolymers to simultaneously optimize these competing factors is referred to as “packing frustration” [20, 24]. Such frustration is present in all ordered phases except lamellae self-assembled from symmetric diblock chains, which naturally fill the space with uniformly stretched chains. In the case of conformationally symmetric diblock copolymers, the equilibrium phases illustrated in Fig. 1.5 outperform all other candidate structures known to exist in minimizing packing frustration, thereby establishing themselves as stable morphologies within the phase diagram depicted in Fig. 1.4.

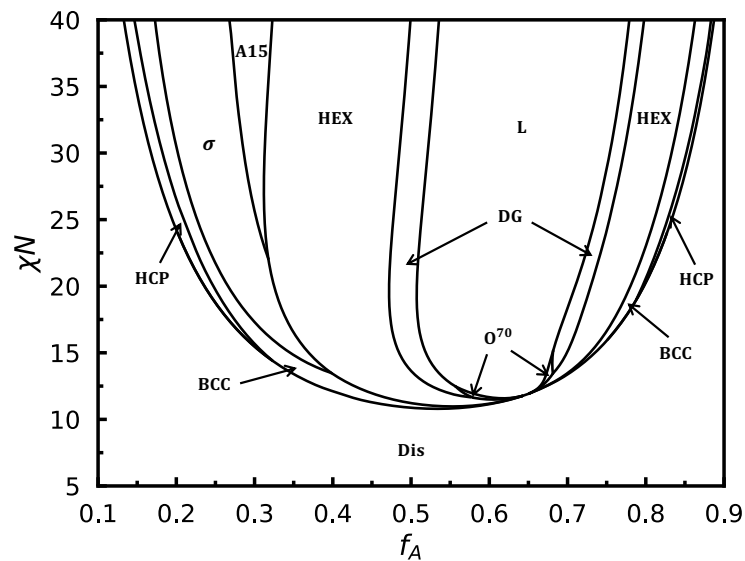


Fig. 1.7 Theoretical phase diagram of AB-diblock copolymer melts with asymmetric Kuhn lengths ($\epsilon = 3$) constructed by using SCFT.

The introduction of conformational asymmetry ($\epsilon > 1$) into the diblock copolymers shifts the phase boundaries in Fig. 1.4 to the right, breaking the reflection symmetry about

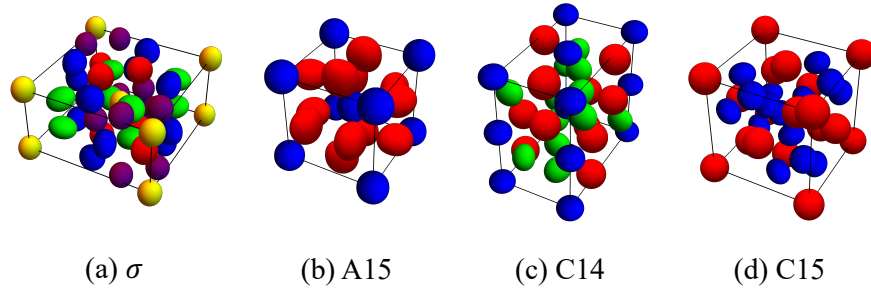


Fig. 1.8 The Frank-Kasper (a) σ , (b) A15, (c) C14 and (d) C15 phases. The latter two phases also belong to the category of Laves phases, which is a subset of the Frank-Kasper phases. Nonequivalent domains are depicted by distinct colours.

$f = 0.5$ and resulting in an asymmetric phase diagram. An example of a SCFT phase diagram for conformationally asymmetric diblock copolymers with $\epsilon = 3$ is presented in Fig. 1.7. It can be observed that, along with the rightward shift of all phase boundaries, the regions occupied by phases on the left expand significantly at the expense of those on the right. Even more intriguingly, two novel equilibrium morphologies, namely the Frank-Kasper (FK) σ and A15 phases, emerge between the HEX and BCC phases on the left-hand side of the phase diagram. In contrast to the “classical” BCC and HCP phases, the FK σ and A15 phases have a more complex unit cell, composed of more than one type of nonequivalent discrete domains [25, 26]. Schematics of the FK σ and A15 phases with nonequivalent domains depicted by distinct colours are provided in Fig. 1.8(a) and (b), respectively.

Since the initial experimental discovery of the FK σ phase in diblock copolymers in 2010 [27], researchers have dedicated extensive efforts to unravel the mechanisms of the emergence of such complex structures in this seemingly simple system [28–34]. Thanks to a decade-long collaborative effort between theorists and experimenters, we have gained a deep understanding of the mechanisms governing the formation of these complex spherical packing phases in single-component diblock copolymer melts. In particular, the

key factor contributing to the stability of these novel phases is their generally rounder Wigner-Seitz cells (WSCs) compared to the traditional BCC and HCP phases. This higher WSC sphericity results in a reduced penalty in interfacial energy when the AB interface undergoes significant deformation towards the WSC. One effective way to induce a more pronounced interface distortion is by increasing the conformational asymmetry of the diblock copolymers. As a result, the FK σ and A15 phases are absent when $\epsilon = 1$ but emerge when ϵ exceeds a critical value. SCFT has determined this critical threshold to be approximately $\epsilon = 1.5$ [28], marking the onset of a stability window for the σ phase on the phase diagram. Intriguingly, experimental observations have revealed the presence of the σ phase in diblock samples with ϵ values much smaller than 1.5 [29, 31, 32].

1.1.2 More Complex Block Copolymers

Restricted by its architectural and chemical simplicity, the number of equilibrium morphologies offered by AB diblock copolymers is limited. One approach to expanding the accessible morphologies involves introducing more complex chain topologies and/or new chemistry. For instance, when a C block is attached to the free end of the B block in an AB diblock copolymer, it produces an ABC linear triblock copolymer. The addition of this extra C block significantly enriches the phase behaviour of the system, opening the door to a multitude of new stable morphologies [35–39]. Another example is an ABC star copolymer, where the C block links to the AB diblock chain at the AB junction. Due to its distinct topology, or architecture, compared to the ABC linear triblock copolymer, the ABC star copolymer can stabilize a number of different phases, including Archimedean tiling patterns [40–45].

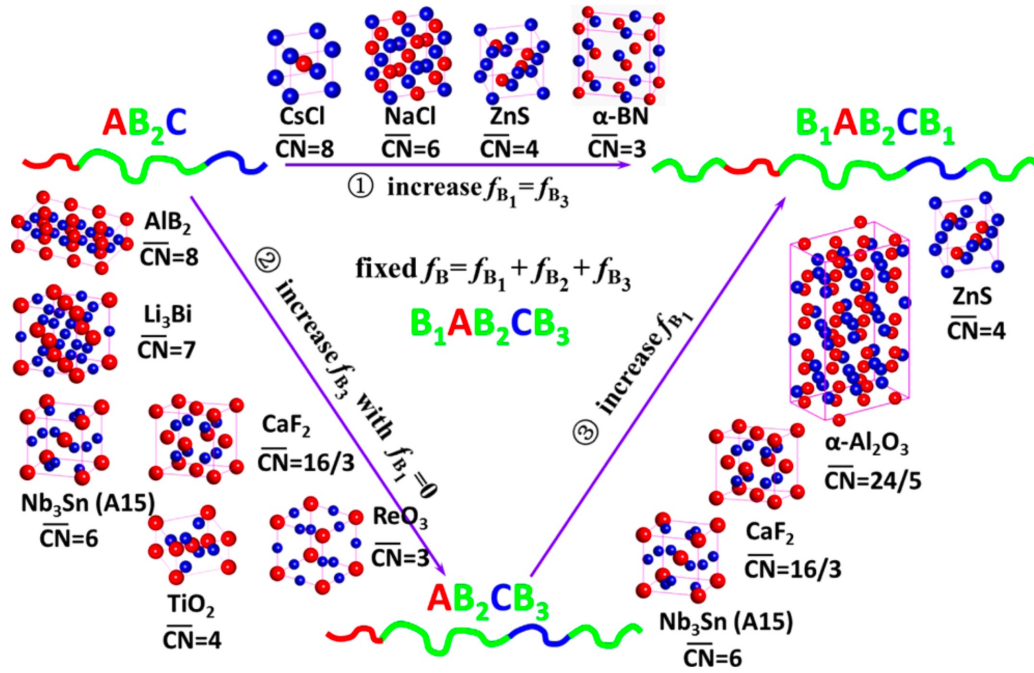


Fig. 1.9 Schematic showcasing the formation of various binary crystalline spherical phases from ABC triblock, AB_2CB_3 tetrablock and $B_1AB_2CB_3$ pentablock terpolymers. Reproduced from [46] with permission.

Beyond triblock architectures, pentablock terpolymers [46], dendritic copolymers [47, 48], and copolymers with more exotic architectures [49–52] offer opportunities for richer phase behaviours and novel morphologies. Fig. 1.9 showcases the formation of various binary crystalline spherical phases from several multiblock copolymers predicted by SCFT. Understanding the phase behaviour of copolymers with complex architectures and designing such architectures to fabricate desired morphologies has been a focal point of research in the field of block polymers over the past decade. Given the enormously large phase space of block copolymer chains, rational and judicious design is crucially important [53].

Despite the fact that block copolymers with complex architectures offer unlimited opportunities to fabricate desired self-assembled nanostructures, their precise synthesis

can be challenging and costly, which hinders their practical application. Therefore, it would be useful to seek a cost-effective alternative to access these structures.

1.2 Phase Behaviours of Polymeric Blends Containing Block Copolymers

One cost-effective alternative to complex block copolymers for producing target morphologies is the use of polymeric blends. Both theoretical and experimental studies have demonstrated that polymeric blends containing block copolymers offer an effective avenue for stabilizing phases that are not available with each of the parent components alone [54–79]. Therefore, it is anticipated that many of the novel morphologies self-assembled from block copolymers with complex architectures could also be achieved by blending simple ingredients together.

One intrinsic characteristic of polymeric blends is their tendency to macroscopically phase separate, which presents a limitation when using blending systems to stabilize single ordered phases [80–84]. In polymeric blends containing block copolymers, the phase behaviours are further complicated by the interplay between microphase and macrophase separations, making the study of their phase behaviours challenging. Notably, two coexisting macroscopically separated phases can occur, and each of these phases may exhibit either disorder or microphase separation. As a result, establishing a good understanding of the mechanisms governing the self-assembling behaviours of different polymeric blends containing block copolymers is extremely important and desirable. Such understanding could enable a more precise morphological control over the self-assembly of these systems.

The simplest polymeric blends containing block copolymers consist of diblock copolymers and homopolymers. Over the past three decades, researchers have made significant efforts to determine the dependency of the phase behaviour on various parameters characterizing this system. One factor found to strongly influence the behaviour of homopolymers when blended with diblock copolymers is the molecular weight of the homopolymers [85–89]. The role played by the homopolymer molecular weight in this blending system can be well understood as the competition between interaction energy and entropy. To elaborate, let us consider binary blends of AB copolymers and A homopolymers. Due to favorable interaction energies, A homopolymers tend to aggregate within or near the microdomains formed by the A blocks of the AB copolymers. When the A homopolymers have significantly lower molecular weights than the A blocks, they tend to penetrate deep into the A-rich microdomains (wet-brush behaviour), driven by a substantial entropy gain that outweighs the increase in their interfacial energy with the B blocks. In contrast, longer homopolymers experience less entropy gain from interpenetration with the A blocks, especially when the homopolymer molecular weight is comparable to or larger than that of the A block. Consequently, longer homopolymers tend to isolate from the A-rich microdomains to minimize interfacial energy (dry-brush behaviour), resulting in a lower overall free energy of the system. Fig. 1.10 shows schematics of the wet- and dry-brush regimes.

The distinct behaviours of the homopolymers, dependent on their molecular weight relative to that of the affinity blocks of the copolymers, significantly influence the miscibility of the blends. In the wet-brush regime, microdomains self-assembled by the diblock copolymers can generally accommodate a larger quantity of homopolymers. In comparison, in the dry-brush regime, microdomains can solubilize fewer homopolymers,

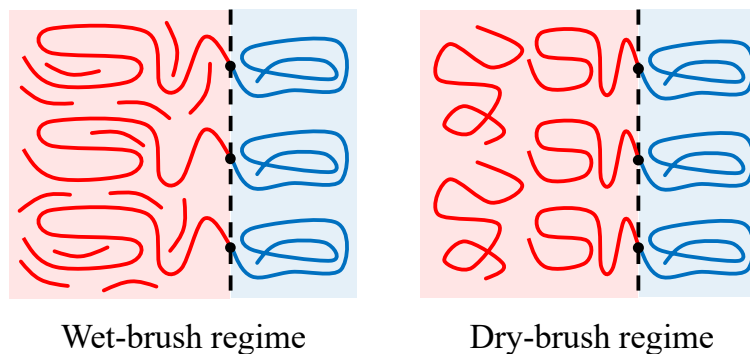


Fig. 1.10 Schematics of the wet- and dry-brush regimes for the binary blends of AB copolymers and A homopolymers.

making the blends more prone to macroscopic phase separation. In other words, diblock copolymers exhibit poorer miscibility with long homopolymers compared to short ones.

The addition of homopolymers into diblock copolymers can induce order-order phase transitions by acting as space fillers. Depending on the selectivity of the homopolymers to the different blocks of the copolymers, their presence can swell the microdomains formed by either blocks, consequently driving the formation of morphologies with either lower or higher interfacial curvature. Specifically, the transition induced by doping core-selective homopolymers generally leads to a phase with flatter interface, while the opposite is true when doping corona-selective homopolymers. Homopolymers also play a significant role in alleviating packing frustration within various ordered structures. They achieve this by localizing in regions that would otherwise be occupied by over-stretching the diblock copolymers. The release of packing frustration significantly enhances the stability of structures with a larger degree of packing frustration, such as the HCP phase.

More interestingly, the incorporation of homopolymers into diblock copolymers leads to the stabilization of entirely new equilibrium morphologies that are absent in neat diblock copolymer melts. A number of theoretical and experimental studies discovered the emergence of novel bicontinuous phases, including the double diamond (DD) and

plumber’s nightmare (P) phases, in binary A_1B_1/A_2 blends [56, 57, 63, 62, 72]. In particular, these structures consist of two disconnected A networks intertwined within a continuous B matrix. Schematics of the DD and P phases are displayed in Fig. 1.11. It was revealed that the localization of homopolymers within the nodes of the DD and P networks effectively release the packing frustration, thus leading to the stabilization of these phases.

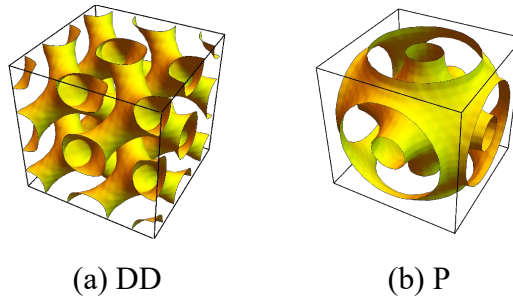


Fig. 1.11 The bicontinuous (a) double diamond and (b) plumber’s nightmare phases.

In a more recent experimental study on binary AB diblock copolymer/A homopolymer mixtures [70], several complex spherical packing phases were observed, including the FK σ and Laves C14 and C15 phases (see Fig. 1.8). In addition, a sensitive dependence of the stability of these phases on the molecular weight of the homopolymer was also discovered. A timely SCFT investigation [90] following the experimental discovery provided evidence of the partitioning, or localization of the homopolymers within the particle cores, which provides a mechanism for this system to accommodate the added homopolymers. As proposed by the authors, the higher asymmetry in particle volumes of the FK phases enables them to accommodate more homopolymers compared to the BCC phase. This delays the onset of macrophase separation and explains the phase transition sequence from phases with lower volume asymmetry to those with higher volume asymmetry, i.e.

from BCC to σ , then to C14, and finally to C15. Moreover, their SCFT results also suggest that the formation of these FK phases does not require conformational asymmetry of the diblock chains in the A_1B_1/A_2 system.

Another polymeric blending system that has been extensively studied is binary blends of diblock copolymers [54, 55, 58, 60, 91, 64, 65, 92, 66, 69, 93–95, 71, 73, 76, 78, 79]. The simplest blending formulation in this category involves combining a parent diblock copolymer (A_1B_1) with an additive diblock copolymer (A_2B_2) that has different degrees of polymerization and/or block compositions. In addition to acting like space fillers, the added diblock copolymers also function as cosurfactants regulating the interfacial properties of the microdomains formed by the parent copolymers [96–102]. It was shown that phases accessed by A_1B_1/A_2 blends, including the novel bicontinuous network and the FK phases, can also be stabilized by blending A_1B_1 and A_2B_2 diblock copolymers with appropriately designed molecular weight ratio and block compositions [66, 69, 71, 73]. Thanks to the cosurfactant effect, binary A_1B_1/A_2B_2 blends typically exhibit better miscibility than A_1B_1/A_2 blends, making them advantageous for fabricating novel structures. Indeed, the stability windows of all the single ordered phases generally span a wider composition range in the A_1B_1/A_2B_2 blends.

Beyond the simple A_1B_1/A_2B_2 formulation, the AB/CB' [92, 76, 78, 79] and AB/CD [91, 68, 93–95, 103] blends can produce more complex phase behaviours. For instance, recent SCFT calculations have revealed that AB/CB' blends with a strong repulsive interaction between the A and C blocks exhibit eutectic phase behaviour akin to that seen in binary alloys. Moreover, a stable binary crystalline phase resembling $MgZn_2$, with an underlying Laves C14 lattice, emerges within a narrow blend composition window. This result stems from the careful selection of molecular parameters for the AB and CB' copolymers, enabling the formation of particles commensurate with the Laves WSCs.

These theoretical findings suggest that AB/CB' blends may have the potential to stabilize other binary crystals previously observed in multiblock terpolymers (see Fig. 1.9), given appropriately designed molecular parameters. However, it is important to note that this system has a pronounced tendency toward macroscopic phase separation.

Due to its simple formulation, the binary blending system composed of two types of diblock copolymers not only serves as a versatile platform for fabricating novel nanostructures but also provides an ideal model system for investigating the formation mechanisms of various ordered phases. Instead of delving into the details of the phase behaviours of binary blends of diblock copolymers here, we will defer this discussion to Chapter 3, where we will explore the historical development, recent advancements, and future opportunities in this field in depth.

The ways in which polymeric blends can be formulated are virtually limitless. More intricate blending schemes, such as binary blends of diblock copolymers and triblock copolymers [61, 104, 105], hold great promise to stabilize a broader spectrum of morphologies. Despite the unlimited opportunities offered by polymeric blends, it is of critical importance to gain a comprehensive understanding of their phase behaviours and the underlying mechanisms governing the stability of different phases. Analogous to the study of block copolymers with complex architectures, such understanding can furnish us with the design principles necessary for inverse molecular engineering, enabling the fabrication of desired structures.

1.3 Objective and Outline

The objective of this thesis is to provide theoretical investigations of the phase behaviours of various polymeric blends composed of architecturally simple ingredients by employing

the self-consistent field theory. Starting from relatively simple polymeric blends that have been previously studied experimentally and theoretically, we provide a more thorough and systematic exploration of their phase space, aiming for reaching a deeper understanding of the formation of the complex spherical phases that have been recently discovered. Subsequently, we shift our focus to polymeric blends of increasing complexity, attempting to acquire new knowledge in the phase behaviours of more complex polymeric blends and establish design principles of polymeric blends to stabilize specific target phases. Our findings provide a solid foundation for future research in even more intricate polymeric blending systems.

This thesis is organized as follows. In Chapter 2, we introduce the main theoretical frameworks used in our study, namely the random-phase approximation (RPA) and self-consistent field theory (SCFT), along with the numerical methods to solve the SCFT equations. Before delving into our examination of polymeric blends containing block copolymers, we begin in Chapter 3 with a comprehensive review of the progress made in the study of phase behaviours of binary blends of diblock copolymers. This review summarizes relevant theoretical and experimental developments spanning over the past three decades on the miscibility and equilibrium morphologies of this blending system.

In Chapter 4, we investigate the formation of complex FK phases in binary blends of A_1B_1 copolymers and A_2 homopolymers. Different from a previous theoretical study by using SCFT based on the Gaussian chain (GC) model of polymers, we opt for the freely-jointed chain (FJC) model. Our choice of the FJC chain model is for two reasons: (1) to assess the sensitivity of theoretical results to the choice of polymer chain model and (2) to better describe low-molecular-weight or short polymers, facilitating direct comparisons with experimental results across a broader spectrum of polymer samples. By constructing a set of phase diagrams with various parameters, we offer a more complete

picture of the phase behaviour of the A_1B_1/A_2 blends. Furthermore, our detailed analysis uncovers the formation mechanisms behind the complex spherical phases in this system.

In Chapter 5, we examine the phase behaviour of binary blends of A_1B_1 and A_2B_2 diblock copolymers, focusing on the stability of the FK phases. Our systematic study extends the previous theoretical findings by constructing a series of phase diagrams on the $\phi_2 - \chi N$ plane, where ϕ_2 is the concentration of the second diblock chains. Our phase diagrams encompass a much wider range of the phase space of the system and can be used to make direct comparison to available experimental data. Additionally, through a detailed analysis of the distributions of the copolymer chains and the properties of self-assembled spherical domains, we uncover the relationship between various system parameters and the two mechanisms responsible for stabilizing the FK phases, namely, intra- and inter-domain segregation, in binary A_1B_1/A_2B_2 diblock copolymer blends.

Chapter 6 is motivated by recent discoveries of FK phases in a broader range of soft matter systems, which involve the blending of amphiphilic molecules with one or more selective additives. Specifically, recent experimental results have shown that the FK σ phase can be stabilized by adding matrix-selective homopolymers to AB diblock copolymers [106, 107]. The stability of the σ phase was found to be highly dependent on the molecular weight of the homopolymer. Another experimental study reported the formation of the C15 phase in salt-doped A/B/AB ternary blends. Furthermore, these various Frank-Kasper packings have also been widely observed in aqueous lyotropic self-assemblies in surfactant/water and surfactant/water/oil systems [108–111]. These experimental observations suggest that the stabilization of these complex spherical packing phases may share common mechanisms across different soft matter systems containing amphiphilic molecules mixed with either matrix-selective or both matrix- and core-

selective components. By applying SCFT to FJCs, we explore these mechanisms by studying two model systems: binary AB/C blends and ternary AB/C/D blends.

In Chapter 7, we explore the possibility of stabilizing the binary spherical crystalline phases in the binary blends of AB/CD diblock copolymers with designed secondary interactions. Previous studies showcased the utilization of AB/CB' blends to stabilize the MgZn₂ crystal through careful molecular engineering. However, the MgZn₂ phase features an extremely narrow stability window in the blend composition due to the pronounced tendency of AB and CB' copolymers to macrophase separate. It is well-established that the introduction of secondary interactions, such as hydrogen bonding, can enhance the miscibility of two otherwise immiscible polymeric components [112, 113]. Therefore, the incorporation of hydrogen bonding into the AB and CB' blends is anticipated to mitigate the macrophase separation and extend the stability range of the binary crystalline phases. We explore this idea by considering the binary AB/CD blends, where A and C blocks are highly repulsive to promote the formation of binary crystals composed of A and C particles, while B and D blocks are mutually attractive to improve the overall miscibility of the mixtures. Through the construction of phase diagrams, we demonstrate that a diverse array of binary crystals can be achieved within the AB/CD blends, and their stability is intricately controlled by various system parameters. Furthermore, we conduct a comprehensive analysis of the chain packing within these binary crystalline phases, shedding light on the selection mechanisms governing the formation of distinct crystal structures.

In Chapter 8, we delve into the topological effects of block copolymers on the phase behaviour of their blends with homopolymers. We choose linear symmetric triblock copolymers as an ideal architecture for this purpose, as they represent the simplest architecture with topologically distinct isomers. Our initial focus centres on lamella-

forming triblock copolymers, where we examine the differences in miscibility among three homologous blending systems: AB/A, ABA/A, and BAB/A blends, using both RPA and SCFT. Our findings reveal a significant disparity in miscibility, with the BAB/A blends displaying notably poorer miscibility compared to the compositionally identical but topologically distinct ABA/A and AB/A blends. We also unravel the distinct natures of the Lifshitz points of these three systems: while the homogeneous phase of the AB/A and ABA/A blends undergoes the transition from microphase to macrophase instability in a manner resembling a “second-order phase transition” at the Lifshitz point, the homogeneous phase of the BAB/A blends undergoes this transition in a manner akin to a “first-order phase transition”. Shifting our focus to sphere-forming triblocks, we further illustrate how the intriguing differences arising from copolymer topologies among these homologous systems lead to significantly varied capabilities in stabilizing the FK phases.

Finally, in the concluding chapter, we summarize the main findings of this thesis and give an outlook to future research.

Chapter 2

Theoretical Framework

2.1 Self-Consistent Field Theory

For the study of the equilibrium phase behaviour of a polymeric system, self-consistent field theory (SCFT) has become one of the most accurate and efficient theoretical tool owing to the development over the past several decades [114–116]. Therefore, we employ SCFT as our theoretical framework. In this chapter, we develop self-consistent field theory for various polymeric systems and introduce the numerical algorithms used to minimize the thermodynamic potential function. Specifically, we start with AB diblock copolymer melts to derive the free energy per chain based on Gaussian chain (GC) and freely jointed chain (FJC) models, respectively. We then extend this theory to polymeric blends, using AB diblock polymer/C homopolymer blends as our example.

2.1.1 SCFT Applied on Gaussian Chain Model for Diblock Copolymer Melts

Free Energy per Chain and SCFT Equations

Let us consider a diblock copolymer melt with n AB diblock copolymers, each of which has degree of polymerization N . The volume fraction of A-block is $f = f_A$ and thus the volume fraction of B-block is $f_B = 1 - f_A$. We assume a uniform segment density ρ_0 so that the total volume of the melt is $V = nN/\rho_0$.

The thermodynamics of the system is fully described by the partition function. In the canonical ensemble, the partition function of the system is written as:

$$\mathcal{Z} = \frac{(V z_0)^n}{n!} \prod_{\alpha=1}^n \int \mathcal{D}\mathbf{r}_i(s) \exp \{-\beta \mathcal{H}\}, \quad (2.1)$$

where $\beta = 1/k_B T$, z_0 represents the momentum integral $(2\pi m/h^2 \beta)^{3/2}$ of each chain, V represents the translational degree of freedom of each chain and \mathcal{H} is the Hamiltonian of the system.

The Hamiltonian contains terms accounting for different energies in the system. In general, regardless of the specific polymer chain model used, it can be written as the summation of the bonded energy and nonbonded energy,

$$\mathcal{H} = \mathcal{H}_{\text{bond}} + \mathcal{H}_{\text{nonbond}}. \quad (2.2)$$

For the GC model, the bonded energy of a linear chain composed of α -monomers with polymerization N has the form [20, 115]:

$$\mathcal{H}_{\text{bond}} = \frac{3k_B T}{2b_\alpha^2} \int_0^N ds \left| \frac{d\mathbf{r}(s)}{ds} \right|^2, \quad (2.3)$$

where b_α is the Kuhn length of α monomers. Since the GC model is a highly coarse-grained model of polymer chains, at the length scale that it describes, the nonbonded energy between segments is normally assumed based on a form of contact interaction:

$$\mathcal{H}_{\text{nonbond}} = k_B T \chi \rho_0 \int d\mathbf{r} \hat{\phi}_A(\mathbf{r}) \hat{\phi}_B(\mathbf{r}), \quad (2.4)$$

where χ is the Flory-Huggins interaction parameter, and $\hat{\phi}_A(\mathbf{r})$ and $\hat{\phi}_B(\mathbf{r})$ are monomer density operators defined as:

$$\hat{\phi}_A(\mathbf{r}) = \frac{1}{\rho_0} \sum_{i=1}^n \int_0^{fN} ds \delta(\mathbf{r} - \mathbf{r}_i(s)), \quad (2.5)$$

$$\hat{\phi}_B(\mathbf{r}) = \frac{1}{\rho_0} \sum_{i=1}^n \int_{fN}^N ds \delta(\mathbf{r} - \mathbf{r}_i(s)). \quad (2.6)$$

Substitute Eq. 2.3 and 2.4 into Eq. 2.2, we have:

$$\mathcal{H} = \frac{3k_B T}{2b_A^2} \sum_{i=1}^n \int_0^{fN} ds \left[\frac{d\mathbf{r}_i(s)}{ds} \right]^2 + \frac{3k_B T}{2b_B^2} \sum_{i=1}^n \int_{fN}^N ds \left[\frac{d\mathbf{r}_i(s)}{ds} \right]^2 + k_B T \chi \rho_0 \int d\mathbf{r} \hat{\phi}_A(\mathbf{r}) \hat{\phi}_B(\mathbf{r}), \quad (2.7)$$

and, by plugging Eq. 2.7 into Eq. 2.1, we get the partition function of the system in the canonical ensemble:

$$\mathcal{Z} = \frac{(Vz_0)^n}{n!} \prod_{\alpha=1}^n \int \mathcal{D}\mathbf{r}_i(s) \exp \left\{ -\frac{3}{2b_A^2} \sum_{i=1}^n \int_0^{fN} ds \left[\frac{d\mathbf{r}_i(s)}{ds} \right]^2 - \frac{3}{2b_B^2} \sum_{i=1}^n \int_{fN}^N ds \left[\frac{d\mathbf{r}_i(s)}{ds} \right]^2 - \chi\rho_0 \int d\mathbf{r} \hat{\phi}_A(\mathbf{r}) \hat{\phi}_B(\mathbf{r}) \right\}. \quad (2.8)$$

Notice that the partition function \mathcal{Z} in Eq. 2.8 depends on the monomer density operators $\hat{\phi}_A(\mathbf{r})$ and $\hat{\phi}_B(\mathbf{r})$ and in turn depends on the coordinates of all the monomers of all chains. In other words, Eq. 2.8 essentially gives us a particle-based theory. In order to transfer to a field-based theory, one mathematical trick is inserting the following identities:

$$\int \mathcal{D}\phi_A(\mathbf{r}) \delta [\phi_A(\mathbf{r}) - \hat{\phi}_A(\mathbf{r})] = 1, \quad (2.9)$$

$$\int \mathcal{D}\phi_B(\mathbf{r}) \delta [\phi_B(\mathbf{r}) - \hat{\phi}_B(\mathbf{r})] = 1, \quad (2.10)$$

into Eq. 2.8, and applying the Fourier transformation of delta functional:

$$\delta [\phi_A(\mathbf{r}) - \hat{\phi}_A(\mathbf{r})] = \int D\omega_A(\mathbf{r}) \exp \left\{ i\rho_0 \int d\mathbf{r} \omega_A(\mathbf{r}) [\phi_A(\mathbf{r}) - \hat{\phi}_A(\mathbf{r})] \right\}, \quad (2.11)$$

$$\delta [\phi_B(\mathbf{r}) - \hat{\phi}_B(\mathbf{r})] = \int D\omega_B(\mathbf{r}) \exp \left\{ i\rho_0 \int d\mathbf{r} \omega_B(\mathbf{r}) [\phi_B(\mathbf{r}) - \hat{\phi}_B(\mathbf{r})] \right\}, \quad (2.12)$$

which leads to the following expression for \mathcal{Z} :

$$\begin{aligned}
 \mathcal{Z} &= \frac{(Vz_0)^n}{n!} \prod_{\alpha=1}^n \int \mathcal{D}\mathbf{r}_i(s) \int \mathcal{D}\phi_A(\mathbf{r}) \int \mathcal{D}\phi_B(\mathbf{r}) \int \mathcal{D}\omega_A(\mathbf{r}) \int \mathcal{D}\omega_B(\mathbf{r}) \\
 &\quad \exp \left\{ i\rho_0 \int d\mathbf{r} \omega_A(\mathbf{r}) [\phi_A(\mathbf{r}) - \hat{\phi}_A(\mathbf{r})] \right\} \exp \left\{ i\rho_0 \int d\mathbf{r} \omega_B(\mathbf{r}) [\phi_B(\mathbf{r}) - \hat{\phi}_B(\mathbf{r})] \right\} \\
 &\quad \exp \left\{ -\frac{3}{2b_A^2} \sum_{i=1}^n \int_0^{fN} ds \left[\frac{d\mathbf{r}_i(s)}{ds} \right]^2 - \frac{3}{2b_B^2} \sum_{i=1}^n \int_{fN}^N ds \left[\frac{d\mathbf{r}_i(s)}{ds} \right]^2 - \chi\rho_0 \int d\mathbf{r} \phi_A(\mathbf{r}) \phi_B(\mathbf{r}) \right\}.
 \end{aligned} \tag{2.13}$$

Note that two real scalar conjugate fields $\omega_A(\mathbf{r})$ and $\omega_B(\mathbf{r})$ have been introduced up to this point. By combining Eq. 2.5, (2.6) and (2.13) and further rearranging, we can arrive at a simplified expression for \mathcal{Z} :

$$\begin{aligned}
 \mathcal{Z} &= \frac{(Vz_0)^n}{n!} \int \mathcal{D}\phi_A(\mathbf{r}) \int \mathcal{D}\phi_B(\mathbf{r}) \int \mathcal{D}\omega_A(\mathbf{r}) \int \mathcal{D}\omega_B(\mathbf{r}) \\
 &\quad Z^n \exp \left\{ \int d\mathbf{r} [\rho_0 i \omega_A(\mathbf{r}) \phi_A(\mathbf{r}) + \rho_0 i \omega_B(\mathbf{r}) \phi_B(\mathbf{r}) - \chi\rho_0 \phi_A(\mathbf{r}) \phi_B(\mathbf{r})] \right\},
 \end{aligned} \tag{2.14}$$

with Z being the single-chain partition function subjected to external fields ω_A and ω_B :

$$\begin{aligned}
 Z &= \int \mathcal{D}\mathbf{r}_i(s) \exp \left\{ - \left[\int_0^{fN} ds i \omega_A(\mathbf{r}_i(s)) + \int_{fN}^N ds i \omega_B(\mathbf{r}_i(s)) \right] \right. \\
 &\quad \left. - \frac{3}{2b_A^2} \int_0^{fN} ds \left[\frac{d\mathbf{r}_i(s)}{ds} \right]^2 - \frac{3}{2b_B^2} \int_{fN}^N ds \left[\frac{d\mathbf{r}_i(s)}{ds} \right]^2 \right\}.
 \end{aligned} \tag{2.15}$$

For computational convenience, the normalized single-chain partition function Q is introduced, which is defined as the ratio between Z and the zero-field single-chain partition function Z_0 , i.e., $Q = Z/Z_0$. Substituting $Z = Q \times Z_0$ into Eq. 2.14 and applying Stirling's approximation,

$$n! \approx \left(\frac{n}{e} \right)^n, \tag{2.16}$$

we obtain:

$$\begin{aligned}
 \mathcal{Z} = & \int \mathcal{D}\phi_A(\mathbf{r}) \int \mathcal{D}\phi_B(\mathbf{r}) \int \mathcal{D}\omega_A(\mathbf{r}) \int \mathcal{D}\omega_B(\mathbf{r}) \\
 & \exp \left\{ \ln \left[\left(\frac{V z_0 e}{n} \right)^n \right] + \ln Q^n + \ln Z_0^n \right. \\
 & \left. + \int d\mathbf{r} [\rho_0 i \omega_A(\mathbf{r}) \phi_A(\mathbf{r}) + \rho_0 i \omega_B(\mathbf{r}) \phi_B(\mathbf{r}) - \chi \rho_0 \phi_A(\mathbf{r}) \phi_B(\mathbf{r})] \right\}.
 \end{aligned} \tag{2.17}$$

Our goal is to obtain a free energy, which can be minimized to get solutions corresponding to various equilibrium structures. However, Eq. 2.17 involves several functional integrals, which are hard to evaluate. To further simplify the theory, we proceed by applying the saddle-point approximation, which is also referred to as the mean-field approximation in the polymer physics literature [115]. For functional integrals like Eq. 2.17, saddle-point approximation amounts to using a single, dominant, stationary-state configuration of the fields to approximate the result. Under this approximation, we have:

$$\begin{aligned}
 \mathcal{Z} \approx & \exp \left\{ \ln \left[\left(\frac{V z_0 e}{n} \right)^n \right] + \ln Q^n \right. \\
 & \left. + \int d\mathbf{r} [\rho_0 \omega_A(\mathbf{r}) \phi_A(\mathbf{r}) + \rho_0 \omega_B(\mathbf{r}) \phi_B(\mathbf{r}) - \chi \rho_0 \phi_A(\mathbf{r}) \phi_B(\mathbf{r})] \right\}.
 \end{aligned} \tag{2.18}$$

It should be noted that due to the analytical structure of the current field theory, the originally introduced real scalar fields, $\omega_\alpha(\mathbf{r})$'s, become purely imaginary after the mean-field approximation [115], and the imaginary unit i has been absorbed into $\omega_\alpha(\mathbf{r})$ in Eq. 2.18, making $\omega_A(\mathbf{r})$ and $\omega_B(\mathbf{r})$ purely real. Using the relation between the partition function and the Helmholtz free energy,

$$\mathcal{Z} = \exp \left(-\frac{F}{k_B T} \right), \tag{2.19}$$

we arrive at an expression of the free energy per chain of the system in the unit of $k_B T$:

$$\begin{aligned} \frac{F}{nk_B T} &= \ln \left(\frac{n}{V z_0 e} \right) - \ln Q - \ln Z_0 \\ &\quad - \frac{1}{V} \int d\mathbf{r} [N\omega_A(\mathbf{r})\phi_A(\mathbf{r}) + N\omega_B(\mathbf{r})\phi_B(\mathbf{r}) - \chi N\phi_A(\mathbf{r})\phi_B(\mathbf{r})]. \end{aligned} \quad (2.20)$$

Because the first and third terms in the above expression are constants that do not affect the differences between the free energies of different local minima, they can be dropped for simplicity. After doing so, a simple form of the free energy of the system reads:

$$\frac{F}{nk_B T} = -\ln Q - \frac{1}{V} \int d\mathbf{r} [N\omega_A(\mathbf{r})\phi_A(\mathbf{r}) + N\omega_B(\mathbf{r})\phi_B(\mathbf{r}) - \chi N\phi_A(\mathbf{r})\phi_B(\mathbf{r})]. \quad (2.21)$$

For the systems that we are interested in, i.e., polymeric melts and blends, the incompressibility condition is assumed, namely,

$$\phi_A(\mathbf{r}) + \phi_B(\mathbf{r}) = 1. \quad (2.22)$$

In minimizing the free energy, Eq. 2.22 can be enforced by introducing a Lagrange multiplier $\eta(\mathbf{r})$, which acts as a pressure field that ensures the incompressibility of the system. The Lagrangian function reads:

$$\begin{aligned} \mathcal{F} &= -\ln Q - \frac{1}{V} \int d\mathbf{r} [N\omega_A(\mathbf{r})\phi_A(\mathbf{r}) + N\omega_B(\mathbf{r})\phi_B(\mathbf{r}) - \chi N\phi_A(\mathbf{r})\phi_B(\mathbf{r}) \\ &\quad + \eta(\mathbf{r}) (1 - \phi_A(\mathbf{r}) - \phi_B(\mathbf{r}))]. \end{aligned} \quad (2.23)$$

Minimizing the above Lagrangian function with respect to $\phi_A(\mathbf{r})$, $\phi_B(\mathbf{r})$, $\omega_A(\mathbf{r})$, $\omega_B(\mathbf{r})$, $\eta(\mathbf{r})$ leads to a set of equations that can be solved self-consistently,

$$\begin{cases} N\omega_A(\mathbf{r}) = \chi N\phi_B(\mathbf{r}) + \eta(\mathbf{r}), \\ N\omega_B(\mathbf{r}) = \chi N\phi_A(\mathbf{r}) + \eta(\mathbf{r}), \\ \phi_A(\mathbf{r}) = \frac{1}{Q} \int_0^f q(s, \mathbf{r}) q^\dagger(s, \mathbf{r}) ds, \\ \phi_B(\mathbf{r}) = \frac{1}{Q} \int_f^1 q(s, \mathbf{r}) q^\dagger(s, \mathbf{r}) ds, \\ \phi_A(\mathbf{r}) + \phi_B(\mathbf{r}) = 1, \end{cases} \quad (2.24)$$

which is referred to as the SCFT equations.

In Eqs. 2.24, the forward propagator $q(s, \mathbf{r})$ and backward propagator $q^\dagger(s, \mathbf{r})$ are calculated by solving the following modified diffusion equations (MDEs):

$$\begin{aligned} \frac{\partial}{\partial s} q(s, \mathbf{r}) &= \nabla^2 q(s, \mathbf{r}) - N\omega_\alpha(\mathbf{r}) q(s, \mathbf{r}), \\ -\frac{\partial}{\partial s} q^\dagger(s, \mathbf{r}) &= \nabla^2 q^\dagger(s, \mathbf{r}) - N\omega_\alpha(\mathbf{r}) q^\dagger(s, \mathbf{r}), \end{aligned} \quad (2.25)$$

with $\alpha = A$ when $s \in [0, f]$ and B when $s \in (f, 1]$. Note that Eq. 2.25 is rescaled such that the unit of length scale is the radius of gyration of the chain, R_g , and the unit of the contour variable s is N . In other words, the N is chosen as the reference degree of polymerization and the contour variable s now represents a fraction of N . This also indicates that the equations should be integrated between 0 and 1, which is consistent with the integration range of the 3rd and 4th equations in Eqs. 2.24. Eqs. 2.25 could be solved efficiently and accurately by using the operator-splitting method and pseudo-spectral scheme [117, 118] with periodic boundary condition and initial conditions, $q(0, \mathbf{r}) = 1$ and $q^\dagger(1, \mathbf{r}) = 1$. A detailed discussion on the pseudo-spectral method used to solve Eqs.

2.25 is provided in Appendix A. With the solved propagators, the single chain partition function can be obtained via:

$$Q = \frac{1}{V} \int d\mathbf{r} q(1, \mathbf{r}). \quad (2.26)$$

Since the free energy of a periodic structure is also a function of the periods, or the lattice parameters θ_l ($l=x, y$ or z in the case of a cuboid unit cell), we also need to minimize the free energy with respect to θ_l . For the GC model, the derivative of the free energy with respect to θ_l , also referred to as stress [119], has the form:

$$d\left(\frac{F}{nk_B T}\right) / d\theta_l = \frac{1}{Q} \sum_{\mathbf{k}} \frac{b^2 dk^2}{6} \frac{dk^2}{d\theta_l} \int_{f_i}^{f_f} ds q(s, \mathbf{k}) q^\dagger(s, -\mathbf{k}). \quad (2.27)$$

The condition for an optimized set of lattice parameters is thus given by:

$$d\left(\frac{F}{nk_B T}\right) / d\theta_l = 0. \quad (2.28)$$

Eqs. 2.24 and Eq. 2.28 are solved for obtaining the minimized free energy of each candidate phase. By comparing the free energies between different phases, we can produce phase diagrams of the system, which, combined with detailed analyses, helps us understand the equilibrium phase behaviour of the system.

Iteration Procedure to Solve SCFT Equations

Because of the non-linearity of Eqs. 2.24 and Eq. 2.25, analytical solution hardly exists. As a result, they need to be solved numerically. Specifically, for each candidate phase, a computational box is set up and discretized into grid points, which contains one unit cell of the target periodic structure during the calculation. Next, we initialize the density fields

$\phi_A(\mathbf{r})$ and $\phi_B(\mathbf{r})$ with an initial guess that attempts to approximate the real field solutions of the target phase. Given the initial density fields, an efficient iterative algorithm to solve Eqs. 2.24 and Eq. 2.28 simultaneously is the variable-cell Anderson mixing [120, 121]. Practically, we firstly use simple mixing to iterate Eqs. 2.24 and gradient descent to iterate Eq. 2.28 for 100-200 steps before switching to variable-cell Anderson mixing to increase the stability of the algorithm. The specific procedure is as follows:

1. Initialize the ϕ fields with initial guesses, and compute the ω fields using the first two equations in Eqs. 2.24 by setting $\eta(\mathbf{r}) = 0$. The procedure to generate the initial guesses for the ϕ fields of the classical morphologies in AB diblock copolymers and several Frank-Kasper phases is discussed in Appendix B.
2. Calculate the forward and backward propagators $q(s, \mathbf{r})$ and $q^\dagger(s, \mathbf{r})$ by solving Eqs. 2.25 and then compute Q via Eq. 2.26. $q(s, \mathbf{k})$ and $q^\dagger(s, \mathbf{k})$ also need to be stored in memory, which will be used to compute the stress later.
3. Calculate $\phi_A(\mathbf{r})$ and $\phi_B(\mathbf{r})$ via the 3rd and 4th equations in Eqs. 2.24 and the stress via Eq. 2.27.
4. Update the pressure field, $\eta(\mathbf{r})$, via:

$$\eta(\mathbf{r}) = \frac{\omega_A(\mathbf{r}) + \omega_B(\mathbf{r}) - \chi N}{2} - \lambda [1 - \phi_A(\mathbf{r}) - \phi_B(\mathbf{r})], \quad (2.29)$$

which is by combining the 1st, 2nd and last equations in Eqs. 2.24. The last term is an additional term added to achieve a faster convergence and λ is an empirical parameter typically chosen within the range of 1 to 20.

5. Obtain the output conjugate fields by 1st and 2nd equations in Eqs. 2.24,

$$\begin{aligned}\omega_{\text{A}}^{\text{out}}(\mathbf{r}) &= \chi N \phi_{\text{B}}(\mathbf{r}) + \eta(\mathbf{r}), \\ \omega_{\text{B}}^{\text{out}}(\mathbf{r}) &= \chi N \phi_{\text{A}}(\mathbf{r}) + \eta(\mathbf{r}).\end{aligned}\tag{2.30}$$

6. Compute the deviations, or called residuals, for the conjugate fields,

$$\begin{aligned}d(\mathbf{r}; \omega_{\text{A}}) &= \omega_{\text{A}}^{\text{out}}(\mathbf{r}) - \omega_{\text{A}}(\mathbf{r}), \\ d(\mathbf{r}; \omega_{\text{B}}) &= \omega_{\text{B}}^{\text{out}}(\mathbf{r}) - \omega_{\text{B}}(\mathbf{r}),\end{aligned}\tag{2.31}$$

and for the lattice parameters,

$$d(\theta_l) = -\frac{d\left(\frac{F}{nk_{\text{B}}T}\right)}{d\theta_l} \Delta\theta_l,\tag{2.32}$$

where $\Delta\theta_l$ is chosen empirically, on the order of magnitude of 10-100.

7. Determine the new conjugate fields for the next iteration. If it is before m^{th} iteration, apply simple mixing,

$$\begin{aligned}\omega_{\text{A}}^{\text{new}}(\mathbf{r}) &= \omega_{\text{A}}(\mathbf{r}) + \lambda_S d(\mathbf{r}; \omega_{\text{A}}), \\ \omega_{\text{B}}^{\text{new}}(\mathbf{r}) &= \omega_{\text{B}}(\mathbf{r}) + \lambda_S d(\mathbf{r}; \omega_{\text{B}}),\end{aligned}\tag{2.33}$$

and gradient descent,

$$\theta_l^{\text{new}} = \theta_l + \lambda_S d(\theta_l),\tag{2.34}$$

with the parameter λ_S typically chosen to be 0.05 or 0.1; otherwise, apply Anderson mixing. The number of the iteration step, m , at which the updating method is switched to Anderson mixing is chosen empirically, and is typically set to 150 in our calculations.

8. Calculate the free energy,

$$\frac{F}{nk_B T} = -\ln Q - \frac{1}{V} \int d\mathbf{r} [N\omega_A(\mathbf{r})\phi_A(\mathbf{r}) + N\omega_B(\mathbf{r})\phi_B(\mathbf{r}) - \chi N\phi_A(\mathbf{r})\phi_B(\mathbf{r})], \quad (2.35)$$

and the error,

$$\text{error} = \left\{ \frac{\sum_{\mathbf{r}} [d^2(\mathbf{r}; \omega_A) + d^2(\mathbf{r}; \omega_B)]}{\sum_{\mathbf{r}} [\omega_A^2(\mathbf{r}) + \omega_B^2(\mathbf{r})]} \right\}^{\frac{1}{2}}. \quad (2.36)$$

9. If all convergence criteria are satisfied, exit; otherwise, go to step 2.

In our calculation, four convergence criteria are inspected at the end of each iteration: (1) $\left| \frac{F^{i+1}}{nk_B T} - \frac{F^i}{nk_B T} \right| < c_1$, (2) $\text{error} < c_2$ (3) $\max(|1 - \phi_A(\mathbf{r}) - \phi_B(\mathbf{r})|) < c_3$ and (4) $\max(|d(\theta_i)|) < c_4$. In the majority of cases, we set $c_1 = 10^{-8}$, $c_2 = 10^{-5}$, $c_3 = 10^{-7}$, and $c_4 = 10^{-5}$. In rare cases where convergence becomes challenging, we use slightly less strict criteria.

2.1.2 SCFT Applied on freely jointed Chain Model for Diblock Copolymer Melts

Free Energy per Chain and SCFT Equations

We consider a AB diblock copolymer melt containing n AB diblock copolymers, each of which is composed of N_A A-segments and N_B B-segments giving a total number of

$N = N_A + N_B$ segments and $N - 1$ bonds per chain. The segments are indexed by integers from 1 to N and the bonds are indexed from 1 to $N - 1$, where bond s connecting segments s and $s + 1$. We note that the contour variable s , which takes continuous values for the GC model, assumes only integer values from 1 to N in the discrete chain models, labelling the discrete segments. We assume a uniform segment density ρ_0 so that the total volume of the melt is $V = nN/\rho_0$.

For the FJC model, the bonded energy of a linear chain containing N α -segments is

$$\mathcal{H}_{\text{bond}} = \sum_{s=1}^{N-1} H_0(\mathbf{R}_s), \quad (2.37)$$

where $\mathbf{R}_s = \mathbf{r}_{s+1} - \mathbf{r}_s$. The bond interaction potential energy H_0 can take different forms

$$H_0(\mathbf{R}_s) = H_0(R_s) = \begin{cases} -k_B T \ln \delta(R_s - b), & \text{for freely jointed chain,} \\ \frac{3k_B T}{2b^2} R_s^2, & \text{for discrete Gaussian chain,} \end{cases} \quad (2.38)$$

where $R_s = |\mathbf{R}_s| = |\mathbf{r}_{s+1} - \mathbf{r}_s|$ and the Kuhn length

$$b = \begin{cases} b_A, & s \leq N_A - 1, \\ b_{AB}, & s = N_A, \\ b_B, & s \geq N_A + 1, \end{cases} \quad (2.39)$$

for the AB diblock copolymer considered.

Given the form of the bond potential energy, the bond transition probability is

$$\begin{aligned}
 g(\mathbf{R}) = g(R) &= \frac{e^{-\frac{H_0(R)}{k_B T}}}{\int e^{-\frac{H_0(\mathbf{R})}{k_B T}} d\mathbf{R}} \\
 &= \begin{cases} \frac{\delta(R-b)}{4\pi b^2}, & \text{for freely jointed chain,} \\ \left(\frac{3}{2\pi b^2}\right)^{\frac{3}{2}} e^{-\frac{3R^2}{2b^2}}, & \text{for discrete Gaussian chain,} \end{cases} \quad (2.40)
 \end{aligned}$$

which also hints that b is the fixed bond length for a freely jointed chain and the root-mean-square bond length for a discrete Gaussian chain.

The Fourier transform of $g(R)$ is:

$$g(k) = \begin{cases} \frac{\sin(kb)}{kb}, & \text{for freely jointed chain,} \\ e^{-\frac{k^2 b^2}{6}}, & \text{for discrete Gaussian chain,} \end{cases} \quad (2.41)$$

which will be used to compute the propagators in solving the SCFT equations later.

The nonbonded interaction energy is introduced with a finite interaction range r_0 :

$$\mathcal{H}_{\text{nonbond}} = k_B T \chi \rho_0 \int u(|\mathbf{r} - \mathbf{r}'|) \hat{\phi}_A(\mathbf{r}) \hat{\phi}_B(\mathbf{r}') d\mathbf{r} d\mathbf{r}', \quad (2.42)$$

where the density operators are defined analogous to those defined for the GC model previously,

$$\hat{\phi}_A(\mathbf{r}) = \frac{1}{\rho_0} \sum_{i=1}^n \sum_{s=1}^{N_A} \delta(\mathbf{r} - \mathbf{r}_{i,s}), \quad (2.43)$$

$$\hat{\phi}_B(\mathbf{r}) = \frac{1}{\rho_0} \sum_{i=1}^n \sum_{s=N_A+1}^{N_B} \delta(\mathbf{r} - \mathbf{r}_{i,s}). \quad (2.44)$$

A Gaussian form is taken for the function $u(|\mathbf{r} - \mathbf{r}'|) = u(R)$ describing the finite range,

$$u(R) = \left(\frac{3}{2\pi r_0^2} \right)^{\frac{3}{2}} e^{-\frac{3R^2}{2r_0^2}}, \quad (2.45)$$

which satisfies the conditions:

$$\int u(R) d\mathbf{R} = 1, \quad (2.46)$$

$$\int R^2 u(R) d\mathbf{R} = r_0^2. \quad (2.47)$$

The Fourier transform of $u(R)$ reads:

$$u(k) = e^{-\frac{k^2 r_0^2}{6}}, \quad (2.48)$$

whose form is also Gaussian. We note that, for the FJC model, a finite inter-segment interaction range is necessary to produce proper scaling behaviour of the domain spacing and interfacial width as the interface becomes narrow in the relatively strong segregation regime [122].

The Hamiltonian of the system is written as:

$$\mathcal{H} = \sum_{i=1}^n \sum_{s=1}^{N-1} H_0(\mathbf{r}_{i,s+1} - \mathbf{r}_{i,s}) + k_B T \chi \rho_0 \int u(|\mathbf{r} - \mathbf{r}'|) \hat{\phi}_A(\mathbf{r}) \hat{\phi}_B(\mathbf{r}') d\mathbf{r} d\mathbf{r}'. \quad (2.49)$$

Performing the same mathematical treatment as that done for the GC model, we can arrive at an expression of the dimensionless free energy per chain within the mean-field

approximation,

$$\frac{F}{nk_B T} = -\ln Q - \frac{1}{V} \int d\mathbf{r} \left[N\omega_A(\mathbf{r})\phi_A(\mathbf{r}) + N\omega_B(\mathbf{r})\phi_B(\mathbf{r}) - \chi N \int u(|\mathbf{r} - \mathbf{r}'|)\phi_A(\mathbf{r})\phi_B(\mathbf{r}')d\mathbf{r}' \right]. \quad (2.50)$$

The conditional minimization of Eq. 2.50 under the incompressibility condition, Eq. 2.22, leads to the SCFT equations:

$$\left\{ \begin{array}{l} N\omega_A(\mathbf{r}) = \chi N \int u(R)\phi_B(\mathbf{r} - \mathbf{R})d\mathbf{R} + \eta(\mathbf{r}), \\ N\omega_B(\mathbf{r}) = \chi N \int u(R)\phi_A(\mathbf{r} - \mathbf{R})d\mathbf{R} + \eta(\mathbf{r}), \\ \phi_A(\mathbf{r}) = \frac{e^{\omega_A(\mathbf{r})}}{QN} \sum_{s=1}^{N_A} q(s, \mathbf{r})q^\dagger(s, \mathbf{r}), \\ \phi_B(\mathbf{r}) = \frac{e^{\omega_B(\mathbf{r})}}{QN} \sum_{s=N_A+1}^{N_B} q(s, \mathbf{r})q^\dagger(s, \mathbf{r}), \\ \phi_A(\mathbf{r}) + \phi_B(\mathbf{r}) = 1. \end{array} \right. \quad (2.51)$$

The forward and backward propagators are computed by iterating the integral equations,

$$\begin{aligned} q(s+1, \mathbf{r}) &= e^{-\omega_\alpha(\mathbf{r})} \int d\mathbf{r}' g_\alpha(\mathbf{r} - \mathbf{r}') q(s, \mathbf{r}'), \\ q^\dagger(s-1, \mathbf{r}) &= e^{-\omega_\alpha(\mathbf{r})} \int d\mathbf{r}' g_\alpha(\mathbf{r} - \mathbf{r}') q^\dagger(s, \mathbf{r}'), \end{aligned} \quad (2.52)$$

with $\alpha = A$ when $1 \leq s \leq N_A$ and B when $N_A + 1 \leq s \leq N$. The initial conditions are $q(1, \mathbf{r}) = e^{-\omega_A(\mathbf{r})}$ and $q^\dagger(N, \mathbf{r}) = e^{-\omega_B(\mathbf{r})}$. Eqs. 2.52 could be computed pseudo-spectrally:

$$\begin{aligned} q(s+1, \mathbf{r}) &= e^{-\omega_\alpha(\mathbf{r})} \mathcal{F}^{-1} \{ g_\alpha(\mathbf{k}) \mathcal{F} \{ q(s, \mathbf{r}') \} \} \\ &= e^{-\omega_\alpha(\mathbf{r})} \mathcal{F}^{-1} \{ g_\alpha(\mathbf{k}) q(s, \mathbf{k}) \}, \\ q^\dagger(s-1, \mathbf{r}) &= e^{-\omega_\alpha(\mathbf{r})} \mathcal{F}^{-1} \{ g_\alpha(\mathbf{k}) q^\dagger(s, \mathbf{k}) \}, \end{aligned} \quad (2.53)$$

which reduces the complexity of computational time by avoiding the convolution via fast Fourier transform. The single chain partition function is computed by:

$$Q = \frac{1}{V} \int d\mathbf{r} q(N, \mathbf{r}). \quad (2.54)$$

The stress for the FJC model has two parts. One is from the bond transition probability,

$$d\left(\frac{F}{nk_B T}\right) / d\theta_l \Big|_{\text{bond}} = -\frac{1}{Q} \sum_{\mathbf{k}} \frac{dg(k)}{dk^2} \frac{dk^2}{d\theta_l} \sum_{s=1}^{N-1} q(s, \mathbf{k}) q^\dagger(s+1, -\mathbf{k}), \quad (2.55)$$

and the other is from the nonbonded interaction,

$$d\left(\frac{F}{nk_B T}\right) / d\theta_l \Big|_{\text{nonbond}} = \chi N \sum_{\mathbf{k}} \frac{du(k)}{dk^2} \frac{dk^2}{d\theta_l} \phi_A(\mathbf{k}) \phi_B(-\mathbf{k}). \quad (2.56)$$

Therefore, the total stress is:

$$\frac{d\left(\frac{F}{nk_B T}\right)}{d\theta_l} = \frac{d\left(\frac{F}{nk_B T}\right)}{d\theta_l} \Big|_{\text{bond}} + \frac{d\left(\frac{F}{nk_B T}\right)}{d\theta_l} \Big|_{\text{nonbond}}, \quad (2.57)$$

which satisfies Eq. 2.28 for an optimized set of lattice parameters.

Iteration Procedure to Solve SCFT Equations

The iteration procedure to solve Eqs. 2.51 and Eq. 2.28 given the initial density fields is as follows:

1. Initialize the ϕ fields with initial guesses, and compute the ω fields using the first two equations in Eqs. 2.51 by setting $\eta(\mathbf{r}) = 0$.

2. Calculate the forward and backward propagators $q(s, \mathbf{r})$ and $q^\dagger(s, \mathbf{r})$ by solving Eqs. 2.53 and Q by Eq. 2.54. $q(s, \mathbf{k})$ and $q^\dagger(s, \mathbf{k})$ also need to be stored in memory, which will be used to compute the stress later.
3. Calculate $\phi_A(\mathbf{r})$ and $\phi_B(\mathbf{r})$ via the 3rd and 4th equations in Eqs. 2.51 and stress from the bond transition probability via Eq. 2.55.
4. Update $\eta(\mathbf{r})$ in real space via:

$$\eta(\mathbf{r}) = \frac{\omega_A(\mathbf{r}) + \omega_B(\mathbf{r}) - \chi N}{2} - \lambda [1 - \phi_A(\mathbf{r}) - \phi_B(\mathbf{r})], \quad (2.58)$$

which is by combining the 1st, 2nd and last equations in Eqs. 2.51. The last term is an additional term added to achieve a faster convergence and λ is an empirical parameter typically chosen within the range of 1 to 20.

5. Forward Fourier transform $\phi_A(\mathbf{r})$, $\phi_B(\mathbf{r})$ and $\eta(\mathbf{r})$ to get $\phi_A(\mathbf{k})$, $\phi_B(\mathbf{k})$ and $\eta(\mathbf{k})$.
6. Compute the stress from the nonbonded interaction via Eq. 2.56 and the total stress via Eq. 2.57.
7. Obtain the output conjugate fields in k space,

$$\begin{aligned} \omega_A^{out}(\mathbf{k}) &= \chi N \phi_B(\mathbf{k}) u(k) + \eta(\mathbf{k}), \\ \omega_B^{out}(\mathbf{k}) &= \chi N \phi_A(\mathbf{k}) u(k) + \eta(\mathbf{k}). \end{aligned} \quad (2.59)$$

8. Backward Fourier transform to obtain the output conjugate fields in real space, $\omega_A^{out}(\mathbf{r})$ and $\omega_B^{out}(\mathbf{r})$.

9. Compute the deviations, or called residuals, for the conjugate fields,

$$\begin{aligned} d(\mathbf{r}; \omega_A) &= \omega_A^{out}(\mathbf{r}) - \omega_A(\mathbf{r}), \\ d(\mathbf{r}; \omega_B) &= \omega_B^{out}(\mathbf{r}) - \omega_B(\mathbf{r}), \end{aligned} \tag{2.60}$$

and for the lattice parameters,

$$d(\theta_l) = -\frac{d\left(\frac{F}{nk_B T}\right)}{d\theta_l} \Delta\theta_l, \tag{2.61}$$

where $\Delta\theta_l$ is chosen empirically, on the order of magnitude of 10-100.

10. Determine the new conjugate fields for the next iteration. If it is before m^{th} iteration, apply simple mixing,

$$\begin{aligned} \omega_A^{new}(\mathbf{r}) &= \omega_A(\mathbf{r}) + \lambda_S d(\mathbf{r}; \omega_A), \\ \omega_B^{new}(\mathbf{r}) &= \omega_B(\mathbf{r}) + \lambda_S d(\mathbf{r}; \omega_B), \end{aligned} \tag{2.62}$$

and gradient descent,

$$\theta_l^{new} = \theta_l + \lambda_S d(\theta_l), \tag{2.63}$$

with the parameter λ_S typically chosen to be 0.05 or 0.1; otherwise, apply Anderson mixing. The number of the iteration step, m , at which the updating method is switched to Anderson mixing is chosen empirically, and is typically set to 150 in our calculations.

11. Calculate the free energy,

$$\frac{F}{nk_B T} = -\ln Q - \sum_{\mathbf{k}} [\omega_A(\mathbf{k})\phi_A(-\mathbf{k}) + \omega_B(\mathbf{k})\phi_B(-\mathbf{k}) - \chi N u(k)\phi_A(\mathbf{k})\phi_B(-\mathbf{k})], \quad (2.64)$$

and error,

$$\text{error} = \left\{ \frac{\sum_{\mathbf{r}} [d^2(\mathbf{r}; \omega_A) + d^2(\mathbf{r}; \omega_B)]}{\sum_{\mathbf{r}} [\omega_A^2(\mathbf{r}) + \omega_B^2(\mathbf{r})]} \right\}^{\frac{1}{2}}. \quad (2.65)$$

12. If all convergence criteria are satisfied, exit; otherwise, go to step 2.

2.1.3 SCFT for Polymeric Blends: Binary AB/C Blends

The mean-field theory derived based on both chain models for diblock copolymer melts can be readily extended to the study of polymeric blends. To demonstrate the application of SCFT in polymeric blends, we will elaborate on the theory applied to binary blends of AB diblock copolymers and C homopolymers, modelled as FJCs. In blending systems, we will use the subscript κ to label quantities, indicating the species they are associated with when necessary. For the current AB/C binary blends, we will use $\kappa=1$ for AB diblock copolymers and $\kappa=0$ for C homopolymers.

The AB/C binary blends considered here consist of n_1 chains of linear AB-type diblock copolymers and n_2 chains of C homopolymers in a volume V . The parameterization of the AB diblock copolymer is the same as the one in Section 2.1.2. For C homopolymer, each chain is composed of N_C C-segments. We define γ_κ as the ratio between the number of segments of a κ -chain and that of a diblock copolymer chain, i.e. $\gamma_\kappa = N_\kappa/N_1 = N_\kappa/N$. With the assumption of a uniform segment density ρ_0 , we have $\rho_0 V = n_1 N + n_2 \gamma_C N$. In

multi-component mixtures, the content of each species in the system could be described by its concentration. More specifically, for AB/C incompressible binary blends, the average concentrations of AB diblock copolymers and C homopolymers are:

$$\phi_1 = \frac{n_1 N}{\rho_0 V} \quad \text{and} \quad \phi_2 = 1 - \phi_1 = \frac{n_2 \gamma_C N}{\rho_0 V},$$

respectively. The bonded and nonbonded interaction potentials take the same form as in Section 2.1.2. A Flory-Huggins interaction parameter $\chi_{\alpha\beta}$ is introduced between each pair of distinct types of segments, i.e. $\alpha, \beta (\neq \alpha) = \text{A, B or C}$, to describe their nonbonded interaction. With the formulation of mean-field theory in the canonical ensemble, we can derive a Helmholtz free energy density:

$$\begin{aligned} \frac{NF}{\rho_0 V k_B T} = & - \sum_{\kappa} \frac{\phi_{\kappa}}{\gamma_{\kappa}} \ln \frac{Q_{\kappa}}{\phi_{\kappa}} - \frac{1}{V} \int d\mathbf{r} \left[\sum_{\alpha} N \omega_{\alpha}(\mathbf{r}) \phi_{\alpha}(\mathbf{r}) \right. \\ & \left. - \sum_{\alpha, \beta (\neq \alpha)} \chi_{\alpha\beta} N \phi_{\alpha}(\mathbf{r}) \phi_{\beta}(\mathbf{r}) + \eta(\mathbf{r}) \left(1 - \sum_{\alpha} \phi_{\alpha}(\mathbf{r}) \right) \right], \end{aligned} \quad (2.66)$$

which fully describes the thermodynamics of the system. The thermodynamic control parameters are the average concentrations, ϕ_1 and ϕ_2 , which are correlated with each other via $\phi_1 = 1 - \phi_2$ due to the incompressibility condition.

Minimization of the free energy density yields a set of SCFT equations:

$$\left\{ \begin{array}{l} \omega_\alpha(\mathbf{r}) = \sum_{\beta(\neq\alpha)} \chi_{\alpha\beta} N \int u(R) \phi_\beta(\mathbf{r} - \mathbf{R}) d\mathbf{R} + \eta(\mathbf{r}), \\ \phi_A(\mathbf{r}) = \frac{1 - \phi}{\gamma_1} \frac{e^{\omega_A(\mathbf{r})}}{Q_1 N} \sum_{s=1}^{N_A} q_1(s, \mathbf{r}) q_1^\dagger(s, \mathbf{r}), \\ \phi_B(\mathbf{r}) = \frac{1 - \phi}{\gamma_1} \frac{e^{\omega_B(\mathbf{r})}}{Q_1 N} \sum_{s=N_A+1}^{N_B} q_1(s, \mathbf{r}) q_1^\dagger(s, \mathbf{r}), \\ \phi_C(\mathbf{r}) = \frac{\phi}{\gamma_2} \frac{e^{\omega_C(\mathbf{r})}}{Q_2 N} \sum_{s=1}^{N_C} q_2(s, \mathbf{r}) q_2(N_C - s + 1, \mathbf{r}), \\ \sum_\alpha \phi_\alpha(\mathbf{r}) = 1, \end{array} \right. \quad (2.67)$$

where $\mathbf{R} = \mathbf{r} - \mathbf{r}'$ and $R = |\mathbf{R}|$. In Eqs. 2.67 ϕ_1 has been replaced by $1 - \phi_2$ and the subscript of ϕ_2 has been dropped for conciseness. The relative stability between different equilibrated phases with a specific concentration of each species could be determined by comparing the minimized free energy density of these phases with a pre-specified ϕ .

The forward and backward propagators and single chain partition function for the diblock copolymers are computed in the same way as in Section 2.1.2. For the homopolymers where each chain is symmetric, only one propagator $q_2(s, \mathbf{r})$ needs to be computed by iterating the first equation in Eqs. 2.53 from $s=1$ to N_C with $\omega_\alpha(\mathbf{r}) = \omega_C(\mathbf{r})$ and initial condition $q_2(1, \mathbf{r}) = e^{-\omega_C(\mathbf{r})}$. The single chain partition function Q_2 is then obtained by:

$$Q_2 = \frac{1}{V} \int d\mathbf{r} q_2(N_C, \mathbf{r}). \quad (2.68)$$

For blending systems, multi-phase coexistence may take place. Specifically, for incompressible binary mixtures, two-phase coexistence region is expected to exist on the phase diagram spanned by ϕ_2 (or ϕ_1) and another arbitrary system parameter besides concentration. Although the two-phase coexistence region can be determined by applying

the double tangent construction to the Helmholtz free energies of the adjacent phases in the canonical ensemble, it is more computationally convenient to locate it by identifying the intersection between the grand potentials of two adjacent phases in the grand canonical ensemble. The mean-field theory formulated in the grand canonical ensemble for the AB/C binary blends leads to a grand potential density,

$$\begin{aligned} \frac{N\Phi}{\rho_0 V k_B T} = & - \sum_{\kappa} e^{\mu_{\kappa}/k_B T} Q_{\kappa} - \frac{1}{V} \int d\mathbf{r} \left[\sum_{\alpha} N \omega_{\alpha}(\mathbf{r}) \phi_{\alpha}(\mathbf{r}) \right. \\ & \left. - \sum_{\alpha, \beta (\neq \alpha)} \chi_{\alpha\beta} N \int u(|\mathbf{r} - \mathbf{r}'|) \phi_{\alpha}(\mathbf{r}) \phi_{\beta}(\mathbf{r}') d\mathbf{r}' + \eta(\mathbf{r}) \left(1 - \sum_{\alpha} \phi_{\alpha}(\mathbf{r}) \right) \right], \end{aligned} \quad (2.69)$$

where the thermodynamic control parameters are the chemical potentials of AB-copolymers, μ_1 , and C homopolymers, μ_2 . Similar to ϕ_1 and ϕ_2 in the canonical ensemble, the two chemical potentials are also correlated because of the incompressibility condition imposed on the system.

By minimizing the grand potential density, we arrive at a set of self-consistent field equations similar to Eqs. 2.67 with slightly modified equations to compute the densities:

$$\begin{aligned} \phi_A(\mathbf{r}) &= \frac{e^{\omega_A(\mathbf{r})}}{N} \sum_{s=1}^{N_A} q_1(s, \mathbf{r}) q_1^{\dagger}(s, \mathbf{r}), \\ \phi_B(\mathbf{r}) &= \frac{e^{\omega_B(\mathbf{r})}}{N} \sum_{s=N_A+1}^{N_B} q_1(s, \mathbf{r}) q_1^{\dagger}(s, \mathbf{r}), \\ \phi_C(\mathbf{r}) &= e^{\mu/k_B T} \frac{e^{\omega_C(\mathbf{r})}}{N} \sum_{s=1}^{N_C} q_2(s, \mathbf{r}) q_2(N_C - s + 1, \mathbf{r}). \end{aligned}$$

Due to the incompressibility condition, only one of two chemical potentials is independent, and therefore we have set the chemical potential μ_1 in the above equations to 0 and dropped the subscript of μ_2 for simplicity. Once the SCFT equations are solved, the

average concentrations for both components can be simply calculated through:

$$\phi_1 = Q_1, \tag{2.70}$$

$$\phi_2 = 1 - \phi_1. \tag{2.71}$$

The SCFT equations for both canonical and grand canonical ensemble could be solved numerically by a similar pseudo-spectral scheme to that introduced in section 2.1.2 with some modifications due to the difference in the detailed form of equations.

2.2 Random-Phase Approximation

Random phase approximation (RPA) is a technique originally invented to study quantum systems. This method was initially introduced to polymer physics by De Gennes [123] and later applied by Leibler to study AB diblock copolymers [124]. Since then, it has found applications in studying the order-disorder transition (ODT) in various polymeric systems [125–128]. We apply RPA to determine the stability limit of the homogeneous phase, known as the spinodal, of a polymeric system.

In the weak segregation limit, the free energy of the homogeneous state of a polymeric system can be written as an expansion,

$$\frac{F}{nk_B T} = f = f^{(0)} + f^{(1)} + f^{(2)} + \dots, \tag{2.72}$$

in terms of the density fluctuations, $\delta\phi_\alpha$. Of particular interest is the second-order term:

$$\begin{aligned}
 f^{(2)} &= \sum_{\alpha,\beta} \int \frac{d\mathbf{k}}{(2\pi)^3} \Gamma_{\alpha\beta}(\mathbf{k}) \delta\phi_\alpha(\mathbf{k}) \delta\phi_\beta(-\mathbf{k}) \\
 &= \sum_{\alpha,\beta} \int \frac{d\mathbf{k}}{(2\pi)^3} S_{\alpha\beta}^{-1}(\mathbf{k}) \delta\phi_\alpha(\mathbf{k}) \delta\phi_\beta(-\mathbf{k}),
 \end{aligned} \tag{2.73}$$

where $\Gamma_{\alpha\beta}(\mathbf{k})(= \tilde{S}_{\alpha\beta}^{-1}(\mathbf{k}))$'s are the entries of the second order coefficient matrix, or the inverse collective structure factor matrix, \tilde{S}^{-1} . $\tilde{S}_{\alpha\beta}(\mathbf{k})$'s are the Fourier-transformed density-density correlation functions. The stability limit of the homogeneous phase, or the spinodal, is identified at point where the smallest eigenvalue of the matrix \tilde{S}^{-1} equals zero for a specific wavevector magnitude, denoted as k^* . Using RPA, one can evaluate \tilde{S}^{-1} .

2.2.1 The \tilde{S}^{-1} Matrix

AB Diblock Copolymer melts

Following the formulation of RPA by Leibler [124], our derivation starts with the second order term of the free energy expansion with respect to small density and conjugate field fluctuations in k space. For AB diblock copolymer melts, using the shorthand notations $\delta\phi_\alpha = \psi_\alpha$ and $\delta\omega_\alpha = w_\alpha$, that is:

$$f^{(2)} = \int \frac{d\mathbf{k}}{(2\pi)^3} \left[-\frac{1}{2} w_A S_{AA} w_A - \frac{1}{2} w_B S_{BB} w_B - w_A S_{AB} w_B - w_A \psi_A - w_B \psi_B + \chi w \psi_A \psi_B \right], \tag{2.74}$$

where the $S_{\alpha\beta}$'s are the correlation functions for an ideal noninteracting single chain, and thus are also termed as the form factors. Because we are interested in the homogenous

phase, the quantities that are a function of \mathbf{k} only depend on the magnitude of \mathbf{k} , i.e. k . In deriving Eq. 2.74, this k dependence has been made implicit for brevity.

Next, we seek the form of $f^{(2)}$ only as a functional of ψ 's. This is done by minimizing Eq. 2.74 with respect to the w_α 's and insert the results back to Eq. 2.74 to eliminate the w_α dependence. After further utilizing the incompressibility condition $\psi_A + \psi_B = 0$, the resulting $f^{(2)}$ is:

$$f^{(2)} = \int \frac{d\mathbf{k}}{(2\pi)^3} \left[\frac{S_{AA} + 2S_{AB} + S_{BB}}{2(S_{AA}S_{BB} - S_{AB}^2)} - \chi u \right] \psi_A^2. \quad (2.75)$$

In this case, the \tilde{S}^{-1} is a scalar:

$$\tilde{S}^{-1} = \frac{S_{AA} + 2S_{AB} + S_{BB}}{2(S_{AA}S_{BB} - S_{AB}^2)} - \chi u. \quad (2.76)$$

Binary AB/C blends

A similar procedure can be carried out for multicomponent systems. We take binary AB/C blends as an example. Following the formulation by Noolandi and coworkers [125, 126], the second order term of the free energy reads:

$$f^{(2)} = \int \frac{d\mathbf{k}}{(2\pi)^3} \left[-\frac{1}{2}\phi_1 N_{AB} w_A g_{AA} w_A - \frac{1}{2}\phi_1 N_{AB} w_B g_{BB} w_B - \phi_1 N_{AB} w_A g_{AB} w_B \right. \\ \left. - \frac{1}{2}\phi_2 N_C w_C g_{CC} w_C - w_A \psi_A - w_B \psi_B - w_C \psi_C \right. \\ \left. + \sum_{\alpha, \beta (\neq \alpha) \in A, B, C} \chi_{\alpha\beta} w \psi_\alpha \psi_\beta \right], \quad (2.77)$$

where $g_{\alpha\beta}$ is related to $S_{\alpha\beta}$ via $S_{\alpha\beta} = Ng_{\alpha\beta}$ with N being the degree of polymerization of the chain composed of the α and β blocks.

After eliminating the w dependence and applying the incompressibility condition, we get:

$$f^{(2)} = \int \frac{d\mathbf{k}}{(2\pi)^3} \left\{ \frac{g_{BB}\psi_A^2 - 2g_{AB}\psi_A\psi_B + g_{AA}\psi_B^2}{2N_{AB}\phi_1(g_{AA}g_{BB} - g_{AB}^2)} + \frac{(\psi_A + \psi_B)^2}{2N_C\phi_2g_{CC}} - u \left[\psi_A^2\chi_{AC} + \psi_B^2\chi_{BC} + \psi_A\psi_B(-\chi_{AB} + \chi_{AC} + \chi_{BC}) \right] \right\}. \quad (2.78)$$

Therefore, the entries, a_{ij} , of the \tilde{S}^{-1} matrix are:

$$a_{11} = -\frac{g_{BB}}{2N(g_{AB}^2 - g_{AA}g_{BB})\phi_1} + \frac{1}{2Ng_{CC}\phi_2} - u\chi_{AC}, \quad (2.79)$$

$$a_{12} = a_{21} = -\frac{g_{AB}}{2N(g_{AB}^2 - g_{AA}g_{BB})\phi_1} + \frac{1}{2Ng_{CC}\phi_2} - \frac{1}{2}u(-\chi_{AB} + \chi_{AC} + \chi_{BC}), \quad (2.80)$$

$$a_{22} = -\frac{g_{AA}}{2N(g_{AB}^2 - g_{AA}g_{BB})\phi_1} + \frac{1}{2Ng_{CC}\phi_2} - u\chi_{BC}. \quad (2.81)$$

For this 2×2 matrix, the smaller eigenvalue is:

$$\lambda_- = \frac{1}{2}(a_{11} + a_{22} - \Delta), \quad (2.82)$$

where,

$$\Delta = \sqrt{(a_{22} - a_{11})^2 + 4a_{12}^2}. \quad (2.83)$$

2.2.2 The Form Factors

The correlation functions, or the form factors, for an ideal noninteracting single chain, are calculated via,

$$S_{\alpha\beta}(\mathbf{k}) = Ng_{\alpha\beta}^{GC}(\mathbf{k}) = \frac{1}{N} \int_0^N ds_i \int_0^N ds_j \Theta_{s_i}^\alpha \Theta_{s_j}^\beta P_{ij}, \quad (2.84)$$

for a continuous GC, and,

$$S_{\alpha\beta}(\mathbf{k}) = Ng_{\alpha\beta}^{DC}(\mathbf{k}) = \frac{1}{N} \sum_{i=1}^N \sum_{j=1}^N \Theta_i^\alpha \Theta_j^\beta P_{ij}, \quad (2.85)$$

for a discrete chain, where,

$$\Theta_i^\alpha = \begin{cases} 1, & \text{if } i\text{th segment is of type } \alpha, \\ 0, & \text{otherwise.} \end{cases} \quad (2.86)$$

In Eqs. 2.84 and 2.84, P_{ij} is the product of the Fourier-transformed bond transition probabilities of all the segments that form the linear sub-chain bridging segments i and j . For the case where all segments have identical Kuhn lengths (so that the bond transition probability $g(k)$ is the same across the whole chain), we simply have $P_{ij} = [g(k)]^{|i-j|}$. As an example, for a continuous Gaussian diblock copolymer chain, the resulting $S_{\alpha\beta}(\mathbf{k})$'s by using Eq. 2.84 are:

$$S_{AA} = \frac{N_A^2}{N} g(x_A), \quad (2.87)$$

$$S_{BB} = \frac{N_B^2}{N} g(x_B), \quad (2.88)$$

$$S_{AB} = \frac{N_A N_B}{N} h(x_A) h(x_B). \quad (2.89)$$

In the above expressions, $x_\alpha = k^2 \frac{b_\alpha^2}{6} N_\alpha$ ($\alpha=A$ or B), $g(x) = 2(e^{-x} + x - 1)/x^2$, which is the Debye function, and $h(x) = (1 - e^{-x})/x$.

Once the form factors are evaluated, they can be substituted into the \tilde{S}^{-1} , from which the spinodal can be further determined.

Chapter 3

Phase Behaviours of Binary Blends of Diblock Copolymers: A Review

Publication: Xie, Jiayu, and An-Chang Shi. "Phase Behavior of Binary Blends of Diblock Copolymers: Progress and Opportunities." *Langmuir* 39.33 (2023): 11491-11509.

Authors: **Jiayu Xie**, An-Chang Shi

Contribution: This is a review article on the study of the phase behaviours of binary blends of diblock copolymers. As the first author, I did the literature review and wrote the first draft. Dr. An-Chang Shi and I revised the manuscript together.

Preface

Over the past three decades, significant research attention has been devoted to studying the equilibrium phase behaviours of binary blends of diblock copolymers, including the miscibility of these blends and the stability of various self-assembled structures. While the most general binary blends of diblock copolymers involve two chemically distinct diblocks, AB and CD, the majority of studies have focused on simpler blends, such as AB/A'B' or AB/A'C mixtures.

In this chapter, we provide a comprehensive review of the phase behaviours of diblock copolymers, with a emphasis on binary mixtures involving two AB diblock copolymers, A_1B_1 and A_2B_2 , which differ only in terms of molecular weights and block compositions. For AB diblock copolymers, homopolymer additives selective to either the A or B blocks serve as space fillers and swell the corresponding microdomains. In contrast, AB-copolymer additives act as both space fillers and cosurfactants, influencing not only the volume of the microdomains but also the properties of the AB interface. Consequently, compared to binary blends comprising diblock copolymers and homopolymers, binary blends of two distinct diblock copolymers exhibit more complex phase behaviours. Our objective is to uncover the self-assembly principles derived from this model system. We believe that these principles will offer valuable insights into the phase behaviors of binary and even more complex blends containing arbitrary block copolymers.

Phase Behavior of Binary Blends of Diblock Copolymers: Progress and Opportunities

Jiayu Xie and An-Chang Shi*



Cite This: *Langmuir* 2023, 39, 11491–11509



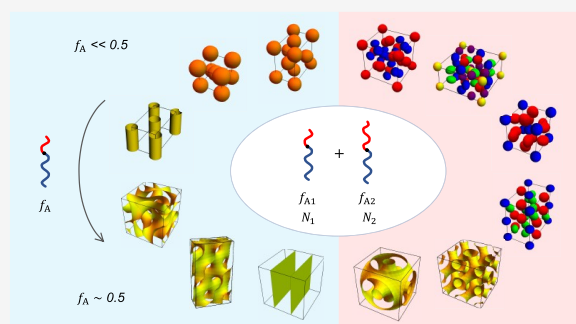
Read Online

ACCESS |

Metrics & More

Article Recommendations

ABSTRACT: The phase behavior of binary blends of diblock copolymers has been examined extensively in the past decades. Experimental and theoretical studies have demonstrated that mixing two different block copolymers provides an efficient and versatile route to regulate their self-assembled morphologies. A good understanding of the principles governing the self-assembly of block copolymer blends has been obtained from the study of A_1B_1/A_2B_2 diblock copolymer blends. The second (A_2B_2) diblocks could act synergistically as fillers and cosurfactants to regulate the domain size and interfacial properties, resulting in the formation of ordered phases not found in the parent (A_1B_1 or A_2B_2) diblock copolymer melts. The study of A_1B_1/A_2B_2 block copolymer blends further provides a solid foundation for future research on more complex block copolymer blends.



INTRODUCTION

Block copolymers are long chain-like macromolecules composed of two or more chemically distinct blocks connected together by covalent bonds.¹ Due to the incompatibility between the block–block repulsion and chain connectivity, block copolymers are intrinsically frustrated.² The repulsion between the chemically distinct blocks drives them to phase separate, whereas chain connectivity prevents macroscopic phase separation. The competition of these two opposing trends provides a mechanism to spontaneously select a finite length scale, resulting in the formation of polymeric domains containing the chemically different blocks. This process is commonly referred to as microphase separation. Generically, the self-assembled polymeric domains assume the shape of spheres, cylinders, and lamellae. For block copolymers in dilute solutions, these polymeric domains and their variations are commonly referred to as micelles of different shapes, such as spherical and wormlike micelles.³ For block copolymer melts, blends, and dense solutions, these polymeric domains pack to fill the space, forming a rich array of self-assembled mesoscopically ordered phases.⁴ The morphology and length scale of the equilibrium ordered phases could be engineered by designing and synthesizing block copolymers with various architectures. Understanding the principles governing the formation of different ordered phases from polymeric systems containing block copolymers has been an active research topic in polymer science for the past several decades.¹ Besides providing a platform for studying fundamental principles of self-assembly, block copolymers have found applications in a

wide range of technologies such as lithography,^{5–8} photonics,^{9–13} and soft-matter enabled quantum materials.¹⁴

An extensively studied system of block copolymers is monodisperse AB diblock copolymers composed of the simplest block copolymer obtained by covalently linking two homopolymers, A and B, through their ends. Due to the tremendous efforts by experimenters and theorists over the past several decades, the phase behavior of AB diblock copolymers is well understood. The self-assembly of monodisperse diblock copolymer melts is mainly determined by three parameters: the composition of the copolymers characterized by the A block volume fraction f_A (and thus f_B since $f_B = 1 - f_A$), the interaction strength between the A and B blocks characterized by the product χN where χ is the Flory–Huggins interaction parameter and N is the copolymer degree of polymerization, and the conformational asymmetry between the A and B blocks quantified by the ratio of their Kuhn lengths $\epsilon = b_A/b_B$.^{1,4,15,16} Phase diagrams of AB diblock copolymers are commonly presented in the $f_A - \chi N$ plane, although it has been revealed recently that the conformational asymmetry parameter (ϵ) should be taken as the third

Received: May 3, 2023

Revised: July 20, 2023

Published: August 3, 2023



coordinate to give a more complete description of the phase behavior.¹⁵ Despite their simplicity, AB diblock copolymers exhibit a surprisingly rich phase behavior containing many ordered phases. As an example of the complexity of block copolymer phase behavior, a theoretical phase diagram for AB diblock copolymers with $\epsilon = b_A/b_B = 3$ produced by the polymeric self-consistent field theory (SCFT) based on the standard Gaussian chain model, along with schematics of the ordered morphologies, is shown in Figure 1. Specifically, the

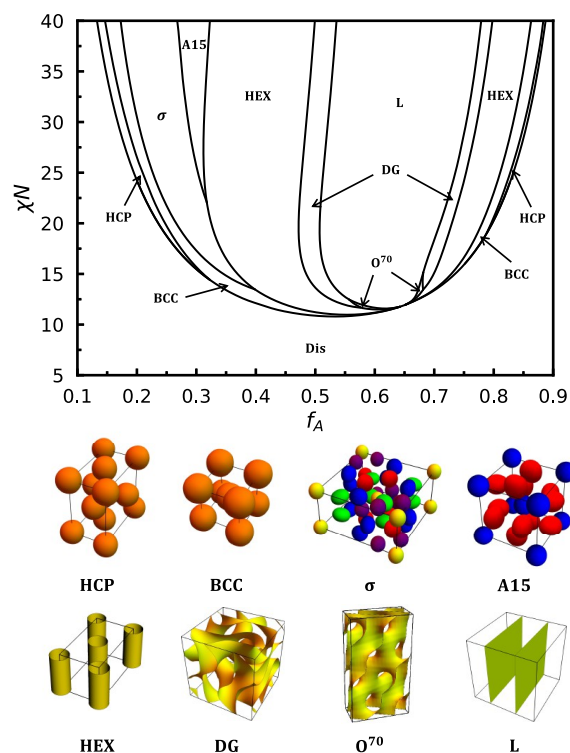


Figure 1. Theoretical phase diagram of AB diblock copolymer melts with $\epsilon = 3$ and schematics of the ordered phases. The spherical domains with different colors for the Frank–Kasper σ and A15 phases highlight the fact that those domains are at nonequivalent positions.

packing of the lamellae, cylinders, and spheres self-assembled from AB diblock copolymers leads to a rich array of equilibrium phases with long-range crystalline order, including simple lamellae (L), hexagonally close packed cylinders (HEX), body-centered cubic spheres (BCC), and hexagonally close packed spheres (HCP), as well as the complex networked morphologies such as the double gyroid network (DG) and $Fddd$ network (O^{70}).⁴ Furthermore, two complex spherical packing phases, namely, the Frank–Kasper σ and A15 phases, have been discovered recently in AB diblock copolymers with large conformational asymmetry.^{15–17}

Although AB diblock copolymers exhibit a very rich phase behavior containing an amazing array of ordered phases (Figure 1), there is a desire to search for block copolymer systems that could form more types of ordered phases, such as the double diamond networked phase and the Laves phases, that are not equilibrium phases of neat diblock copolymer melts. One obvious approach is to extend the block copolymer type and architecture from simple AB diblock copolymer to complex multiblock copolymers containing more types of

blocks and with more complex topology.¹⁸ Examples are ABC linear triblock and star triblock copolymers that exhibit much richer phase behaviors. The number of accessible equilibrium morphologies self-assembled from block copolymers is drastically increased when multiblock copolymers are used. Due to the different choices of the blocks and architecture, there is no limit on the types of block polymers one could design. Therefore, judicious choice of multiblock designs is crucially important.¹⁸ Numerous studies have been carried out to investigate the phase behaviors of multiblock copolymers. It has been demonstrated that the formation of numerous novel structures could be achieved by using tailored multiblock architectures to release the packing frustration.^{19–23}

An alternative approach to regulate the self-assembled morphologies of block copolymers is to add another polymeric species, such as block copolymers or homopolymers, to the system. These added polymeric species are not covalently bonded to the original block copolymers; nevertheless, they can blend into the system and act as fillers and cosurfactants to regulate the volume fraction and interfacial properties of the system. This blending strategy provides an efficient route to obtain desired ordered phases. Numerous experimental and theoretical studies have demonstrated that new equilibrium morphologies could be coassembled from polymeric blends containing block copolymers.^{24–32} More interestingly, block copolymer blends can access ordered phases that are not equilibrium phases of the individual components. Another advantage of block copolymer blends is that the architecture of each polymeric species could remain simple and readily available.^{33–35} Due to the choices of different species, there are unlimited ways to design different formulations of block copolymer blends. Among the vast number of possible polymeric blends, binary mixtures of diblock copolymers are of particular interest and have attracted much attention. In particular, binary blends of diblock copolymers not only provide a simple route to obtain novel structures but also serve as an ideal model system to understand the mechanisms governing the self-assembly of multicomponent macromolecular systems.

Over the past three decades, tremendous progress has been made on the study of binary blends of diblock copolymers, including their phase behaviors in bulk, under confinement, and in solutions. In this feature article, we shall focus on the study of the phase behavior of binary blends of diblock copolymers by providing a review on the past progress and offering our perspective on future opportunities. In general, binary blends of diblock copolymers are composed of two different diblocks, AB and CD, where all four blocks could be chemically different. A comprehensive understanding of this complex blending system is, however, still not complete. Instead, most of the existing studies are on simpler blends such as AB/A'B' or AB/A'C mixtures. We will mainly focus on the phase behavior of binary mixtures composed of one AB diblock copolymer (A_1B_1) and another AB diblock copolymer (A_2B_2) with different molecular weights and compositions, aiming to reveal the self-assembly principles obtained from this simple model system. We believe these principles will be helpful for the study of the phase behaviors of binary and even ternary blends composed of arbitrary block copolymers. Furthermore, we do not discuss block copolymer blends under confinement or in solutions. Instead, we would like to mention some references on the phase behaviors of block copolymer blends under confinement^{36–44} and in solution.^{45–52}

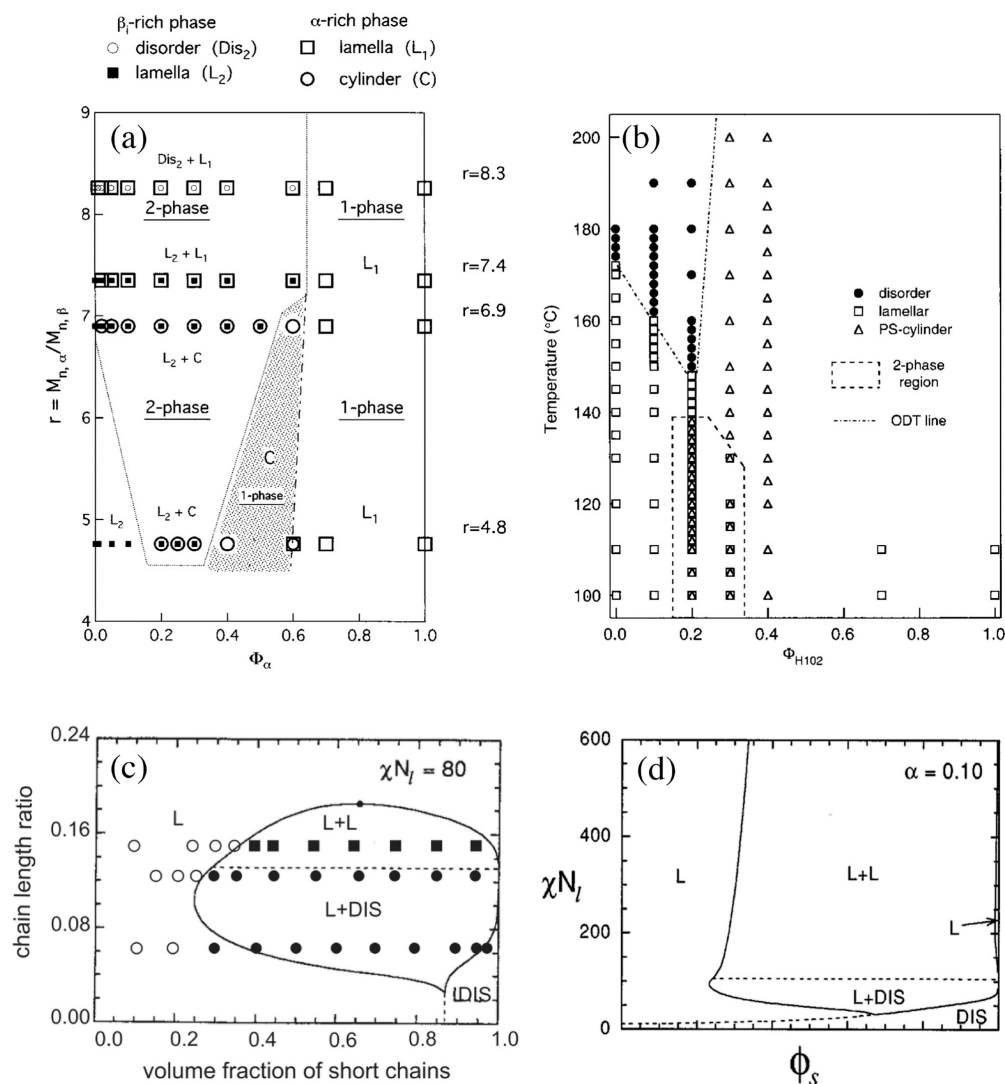


Figure 2. Experimental phase diagrams on the plane spanned by (a) the weight fraction of the longer α copolymers and the molecular weight ratio between the long and short copolymers and (b) the weight fraction of the longer copolymers and temperature, where all the samples are SI diblock copolymers; (c) SCFT phase diagram on the plane spanned by the volume fraction of short chains and chain length ratio, overlaid with experimental data and (d) SCFT phase diagram on the $\phi_s - \chi N_l$ plane with subscripts s and l representing short and long, respectively. Part (a) is reprinted with permission from ref 67, Copyright 2001 American Chemical Society; (b) is reprinted with permission from ref 69, Copyright 2001 American Chemical Society; (c) is reprinted with permission from ref 66, Copyright 1998 Springer Nature; (d) is reprinted with permission from ref 73, Copyright 1995 AIP Publishing.

BLEND MISCIBILITY: MACROPHASE VS MICROPHASE SEPARATION

Miscibility of a multicomponent system refers to the ability of the chemically distinct components to form a homogeneously mixed state, instead of macroscopically separating into two or more coexisting phases. For the simplest binary polymer blend composed of A and B homopolymers, it is either in a homogeneously mixed state or in a biphasic state where A-rich and B-rich phases coexist. The equilibrium phase behavior of this blending system can be well described by the Flory–Huggins theory.^{53,54} For two homopolymers with degrees of polymerization N_A and N_B and Flory–Huggins interaction parameter χ , the system forms a homogeneous phase when χ is

below the critical value $\chi < \chi_c = \frac{1}{2} \left(\frac{1}{\sqrt{N_A}} + \frac{1}{\sqrt{N_B}} \right)^2$ and phase separates into two coexisting phases when χ is above the critical value $\chi > \chi_c$. When the two homopolymers are covalently bonded to form AB diblock copolymers, the driving force of phase separation still exists. However, the bonding of the A and B blocks prevents phase separation at the macroscopic scale and thus the system becomes frustrated.² This frustration leads to local phase separation, or the system undergoes microphase separation, resulting in the formation of inhomogeneous phases composed of periodically or aperiodically arranged A and B domains, or mesoscopically ordered phases.^{2,6}

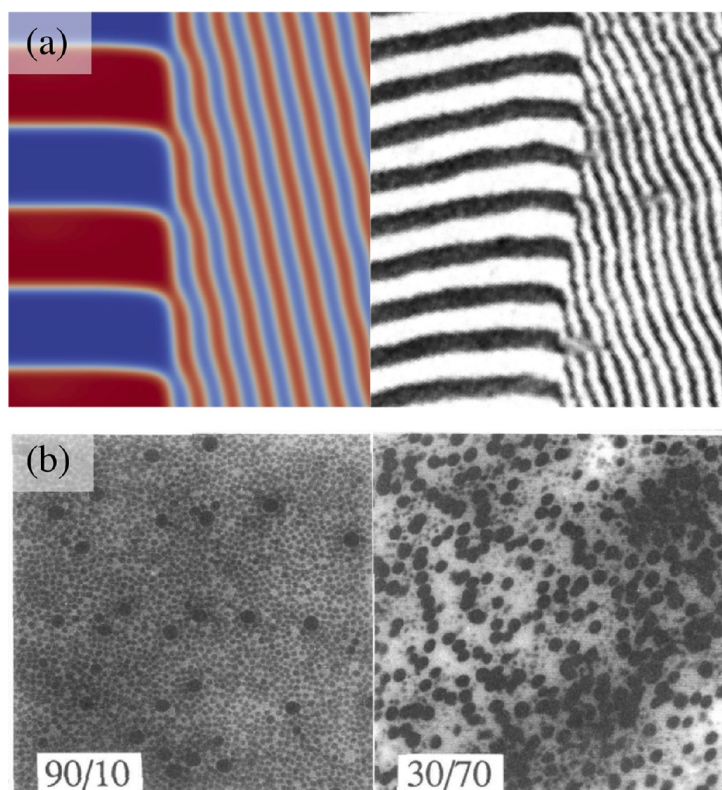


Figure 3. (a) Theoretically predicted (left) and experimentally observed (right) “kink” boundary morphology and (b) TEM images showing randomly mixed big and small spheres in binary mixtures of immiscible sphere-forming SI diblock copolymers. Part (a) is reprinted with permission from ref 81, Copyright 2015 American Chemical Society; (b) is reprinted with permission from ref 59, Copyright 1994 American Chemical Society.

A ubiquitous feature of polymer blends is their tendency to phase separate, forming two or more coexisting phases. When one or more of the components in the blends are block copolymers, the coexisting phases could themselves be inhomogeneous states with microphase-separated domains. Therefore, studying the miscibility of multicomponent blends containing block copolymers is a complicated topic because the mixing/demixing behavior of the blends is entangled with the formation of the mesoscopically ordered structures. Specifically, both microphase separation, where the components are miscible at the molecular scale and form coassembled microdomains, and macrophase separation, where the components are immiscible and phase separate at a macroscopic length scale to form coexisting phases whereas each of them could undergo microphase separation, are possible. Since the 1980s, numerous studies of the phase behaviors of block copolymer blends have been carried out experimentally and theoretically, revealing a sensitive dependence of the equilibrium morphology on the parameters of the system. In this section, we briefly review these early studies on the micro- and macrophase-separated morphologies of binary mixtures of diblock copolymers and summarize their key findings.

The phase behavior of block copolymer blends is controlled by a large number of parameters. Even the relatively simple binary blends composed of A_1B_1 and A_2B_2 diblock copolymers are characterized by seven control parameters, namely, the Flory–Huggins interaction parameter χ , the degrees of polymerization of the two copolymers N_1 and N_2 , the compositions or A block volume fractions of the two

copolymers f_{A1} and f_{A2} , the conformational asymmetry parameter ϵ , and the concentration of the copolymers ϕ_1 or ϕ_2 ($\phi_1 + \phi_2 = 1$ for incompressible systems). As a result of the large number of system parameters, the phase space of block copolymer blends is enormously large. For binary blends of A_1B_1/A_2B_2 diblock copolymers, part of the phase space has been explored by early experimental^{55–70} and theoretical^{24,71–77} studies carried out by several groups.

Experimentally, copolymer samples with desired degrees of polymerization and block compositions can be synthesized by techniques such as living anionic polymerization.⁷⁸ Their self-assembled mesoscopic structures can then be probed by combining different characterization techniques such as small-angle X-ray scattering (SAXS) and transmission electron micrograph (TEM).⁷⁹ For binary mixtures of A_1B_1/A_2B_2 diblock copolymers with comparable block compositions ($f_{A1} \approx f_{A2}$), the dependence of the equilibrium morphology on the chain length ratio $\alpha = N_2/N_1$ and the blend composition ϕ_1 (or $\phi_2 = 1 - \phi_1$) has been investigated experimentally for both lamella-forming and sphere/cylinder-forming diblock copolymer samples.^{56,59,60,66,67,69,70} It is noted that α can be assumed to be larger than 1 since both components of the blends are AB diblock copolymers. It was observed that samples composed of binary mixtures of lamella-forming polystyrene (PS)-*block*-polyisoprene (PI) diblock copolymers were miscible over the entire blend composition range ($0 < \phi_1 < 1$) when α was small, whereas the system was only miscible within the range $\phi_1 < \phi_{1,CS}$ or $\phi_1 > \phi_{1,CL}$ when α was sufficiently large,⁵⁶ where $\phi_{1,CS}$ and $\phi_{1,CL}$ denote the small and large critical concentration

between which macrophase separation takes place. For the case with a large α , transmission electron micrographs revealed that macrodomains consisting of large- and small-period lamellae coexisted within the range $\phi_{1,CS} < \phi_1 < \phi_{1,CL}$. It was also found that $\phi_{1,CS} \ll 1 - \phi_{1,CL}$, indicating that long copolymers could solubilize more short copolymers in their lamellar microdomains, whereas short copolymers could solubilize much fewer long copolymers. In the case of sphere/cylinder-forming copolymers, the blends were shown to exhibit similar behavior but with different values of α , $\phi_{1,CS}$ and $\phi_{1,CL}$ or shifted boundary between microphase and macrophase separation and with the lamellar morphology replaced by spheres or cylinders.⁵⁹ An intriguing behavior that two lamella-forming diblock copolymers coassembled into cylinders was discovered by Yamaguchi et al.,^{26,67,69} which was predicted by strong segregation theory (SST)⁸⁰ and later confirmed by self-consistent field theory (SCFT) calculations.²⁷

Parallel to the experimental work, extensive theoretical studies were also carried out by several researchers to understand and predict the phase behavior of binary mixtures of A_1B_1/A_2B_2 diblock copolymers.^{24,71,73,75} Matsen examined the miscibility of lamella-forming diblock copolymers by SCFT and showed good agreement between theoretical and experimental results.⁷³ For a direct comparison, the experimental phase diagrams from refs 66, 67, and 69 and the theoretical phase diagram from ref 73 are reproduced in Figure 2. In particular, Figure 2c reproduced from ref 66 is a combined figure where the experimental data with binary blends of polystyrene-*b*-polybutadiene diblock copolymers from ref 66 and the SCFT phase diagram from ref 73 are overlaid together, clearly showing excellent agreement between experiment and theory. Qualitative agreement could also be seen by comparing the phase diagrams in Figure 2a and c and the phase diagrams in parts b and d, despite the fact that the parameters might not be the same and that the cylindrical phase was not considered in those early theoretical calculations.

Detailed structures of the boundaries between macrophase-separated domains could be revealed from the experimental studies. One example is that the boundary between the macrodomains formed in binary blends of immiscible diblock copolymers exhibited some characteristic patterns resolved by transmission electron micrographs.^{56,57,59} In the binary blends of immiscible lamella-forming diblock copolymers with a large difference in their molecular weights, nonparallel-oriented lamellar macrodomains with long and short periods were experimentally observed by Hashimoto and co-workers, which were jointed together with a “kink” boundary.⁵⁷ This observation was partially explained by Spencer and Matsen 20 years later using SCFT, showing that the one-sided inclination of the kink boundary has lower boundary tension and thus is more preferred than the parallel boundary.⁸¹ Figure 3a highlights the comparison between the experimentally observed and theoretically predicted boundary morphologies. On the other hand, for binary mixtures of immiscible sphere-forming diblock copolymers, the experimentally observed morphology appeared to be randomly mixed big and small spheres (Figure 3b), rather than macroscopic domains of big/small spheres packed on a crystalline lattice.⁵⁹ This observation implies that microphase separation could enhance the miscibility of the diblock copolymers. However, this effect has not yet been explored theoretically.

Experimental and theoretical studies were also conducted to investigate the phase behavior of binary mixtures of two diblock copolymers with different f_A and comparable degrees of polymerization.^{24,58,62,63,65,68,74,82} These studies mainly focused on the miscibility of the two block copolymers and the ability of the system to form intermediate structures. Yamaguchi et al.⁶⁸ discovered that, for binary blends of PS-*b*-PI diblock copolymers with complementary compositions $f_{A1} \approx 1 - f_{A2} \approx 0.2$ and comparable N , the system formed a single phase with $T \lesssim 130$ °C and a macroscopically separated phase with $T \gtrsim 130$ °C. This finding was qualitatively consistent with the theoretical results by Matsen et al.⁷⁴ Furthermore, theoretical calculations based on SCFT suggested that the phase behavior of binary blends composed of two diblock copolymers with roughly equal N could be well approximated by the phase diagram of neat diblock copolymers with the same overall block composition, provided that neither f_{A1} nor f_{A2} is too close to 0 or 1.^{24,74} This one-component approximation provides a useful and efficient route to access a desired morphology without synthesizing precisely tailored block copolymers.⁸³ Direct experimental confirmation of this one-component approximation was provided by the observation that two-complementary cylinder-forming copolymers self-assembled into the intermediate lamellar phase.^{58,62} However, the formation of a gyroid phase in the blends of two lamella-forming diblocks could not be explained by the one-component approximation.⁶⁵

We have so far focused on the phase behavior of binary mixtures of A_1B_1/A_2B_2 diblock copolymers. The complexity of the binary diblock copolymer blends is greatly increased if chemically distinct blocks are introduced, forming binary AB/B'C or AB/CD blends. For example, in the most general case of AB/CD blends, there are four chemically distinct blocks, each with its own statistical segment lengths, and six interaction parameters, i.e., $\chi_{\alpha\beta}$ where $\alpha, \beta (\neq \alpha) = A, B, C,$ or D , describing the different monomer–monomer interactions. The hugely expanded parameter space for the general binary blends of diblock copolymers makes a thorough investigation of their phase behaviors formidable via either experimental or theoretical approaches. However, several interesting studies of these systems have been carried out, shedding light on the understanding of their phase behaviors.

The phase behavior of binary mixtures of AB/B'C diblock copolymers has been examined by several groups theoretically and experimentally.^{84–88} These case studies on different samples showed evidence of the formation of novel macro- and microphase structures. For instance, in an experimental study of binary blend of polystyrene-*block*-poly(ethylenepropylene) (PS-*b*-PEP) and polystyrene-*block*-(partially hydrogenated polyisoprene) (PS-*b*-HPI) by Kimishima et al., different morphologies were observed with different degrees of segregation power between the PEP and HPI blocks, which was controlled by the degree of hydrogenation reaction.⁸⁶ For a relatively low degree of PEP-HPI segregation power, the observed lamellar morphology contained alternating PS-layers and PEP-HPI-layers in which the PEP and HPI blocks segregated only in the direction perpendicular to the lamellar interface. When the degree of PEP-HPI segregation power was stronger due to the lower degree of hydrogenation reaction, the PEP and HPI blocks segregated in the direction both parallel and perpendicular to the lamellar interface between the PS-layers and PEP-HPI-layers. This observation was attributed to the interplay between phase separation and

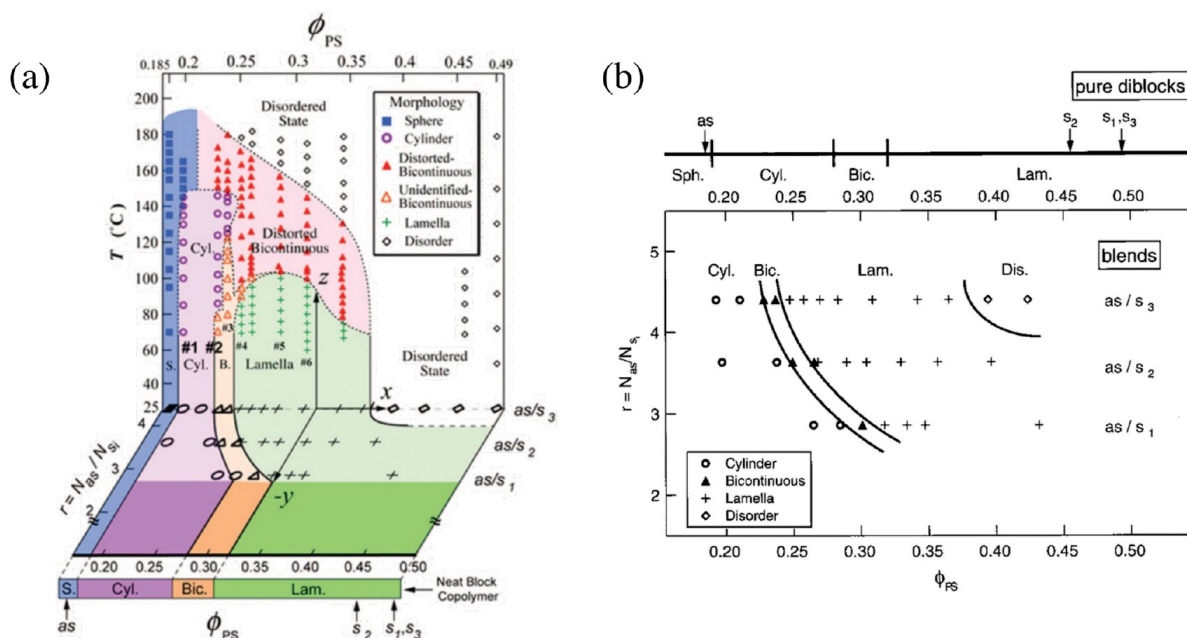


Figure 4. (a) Three-dimensional phase diagram summarizing a series of experimental results from Hashimoto and co-workers in the parameter space of the overall PS block volume fraction ϕ_{PS} , the chain length ratio r between long and short SI copolymers and temperature T and (b) the magnified version of the $\phi_{PS} - r$ plane in (a). The full names of the phases labeled by their abbreviated names in both diagrams are given in the legends. The phase transition boundaries for pure diblock copolymers in terms of the PS block fraction are included in both parts (a) (bottom) and (b) (top). Part (a) is reprinted with permission from ref 92, Copyright 2008 American Chemical Society; (b) is reprinted with permission from ref 93, Copyright 2001 American Chemical Society.

vitrification of the polymer chains. Furthermore, it was observed that the binary blends were dominated by macrophase separation when the repulsive interaction between distinct blocks was strong.^{86–88} The morphologies of AB/B/C or AB/CD blends could be further enriched by introducing other types of secondary interactions, such as hydrogen bonding.

SELF-ASSEMBLY MECHANISMS: SPACE FILLERS VS INTERFACE MODIFIERS

Understanding the mechanisms governing the morphological transformations when two diblock copolymers are mixed is of great importance. For the simple binary blends of A_1B_1/A_2B_2 diblock copolymers, the effects of adding the second diblock copolymers into the microdomains formed by the first diblock copolymers could be classified into two types depending on the spatial distribution of the added diblock. Asymmetric AB diblock copolymers with $f_{A,2}$ close to 0 or 1 would be mainly located in the middle of the B or A domains, whereas symmetric AB diblock copolymers with $f_{A,2} \sim 0.5$ tend to localize at the AB interfaces. When the added diblock copolymers are located in their preferred domains, they act as fillers, regulating the volume of the corresponding domains. This effect could be approximated by an effective volume fraction of the different, A or B, diblocks. When the added diblock copolymers are located at the AB interfaces, they would act as cosurfactants or compatibilizers, decreasing the AB interfacial tension and modifying the interfacial curvature. The phase behavior of the A_1B_1/A_2B_2 diblock copolymer blends is, therefore, strongly influenced by the behavior of the added second diblock copolymers, which in turn depends on the various system parameters.

The different behaviors of short AB diblock copolymers added into microdomains formed by long AB diblock copolymers were first elucidated in theoretical studies by Shi et al. using SST and SCFT.^{89–91} It was demonstrated that, when small amounts ($\phi_s \ll 0.5$) of short diblocks with $f_{A,s}$ are mixed into the ordered microdomains formed from long diblocks with $f_{A,b}$, the spatial distribution of the short chains is regulated by the short block composition $f_{A,s}$. Specifically, short diblock copolymers with $f_{A,s} \approx 0$ or 1 behave as homopolymer fillers localized in the B or A domains, whereas the added diblocks with $f_{A,s} \approx 0.5$ behave more as cosurfactants localized at the AB interfaces. The homopolymer-like short diblocks localized in the A or B domains swell these microdomains, leading to an increased domain spacing and reduced stretching free energy. On the other hand, the surfactant-like short diblocks localize at the AB interfaces, resulting in reduced interfacial tension and a shrunken domain size. In general, these two mechanisms are in effect at the same time, shifting the phase boundary significantly.⁹⁰

Experimentally, the cosurfactant effect of the added diblock copolymers was studied extensively by Hashimoto and co-workers, who also considered cases of relatively large concentrations of short copolymers with different degrees of polymerization.^{70,92–96} Two representative experimental phase diagrams obtained from this series of studies on polystyrene-*b*-polyisoprene (PS-*b*-PI), adopted from refs 92 and 93, are shown in Figure 4a and b. The phase diagram in Figure 4a summarizes the major phase behaviors probed by a series of experiments by Hashimoto and co-workers. The three-dimensional diagram in Figure 4a is in the parameter space of the overall PS block volume fraction ϕ_{PS} , the chain length ratio r between long and short SI copolymers, and temperature

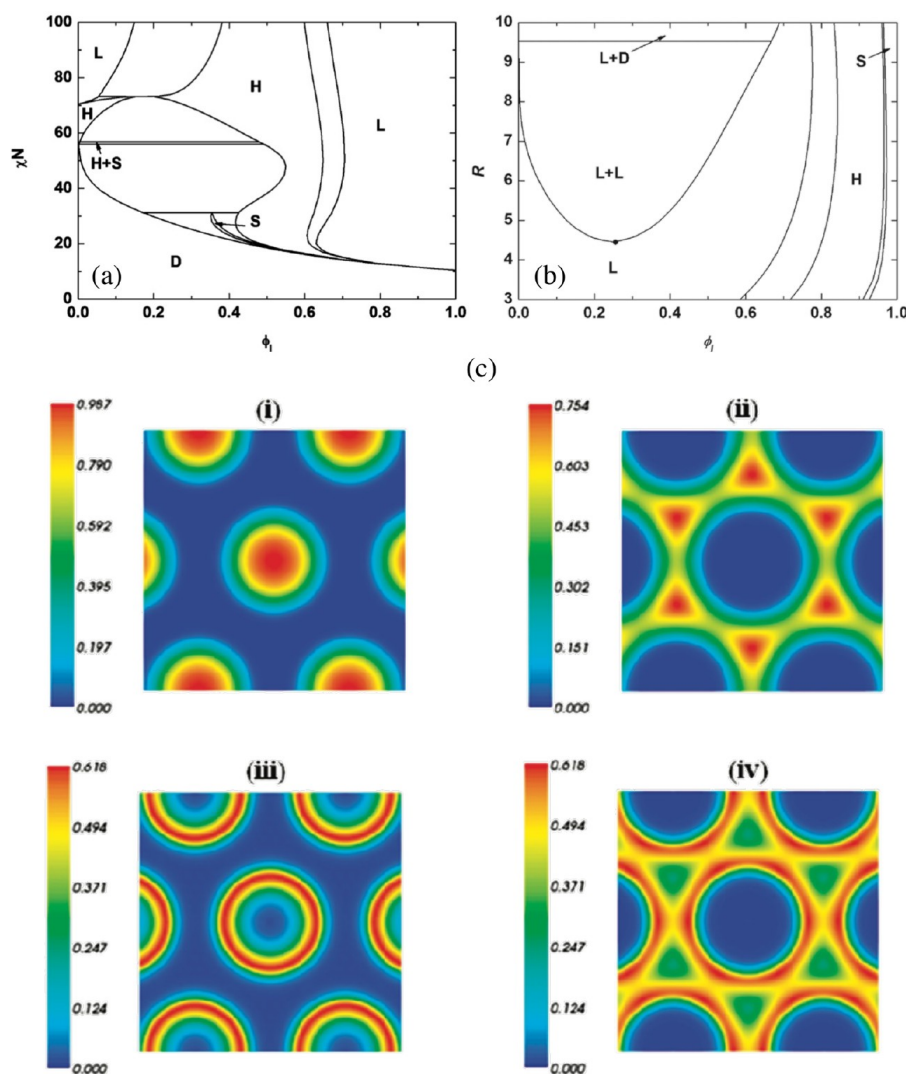


Figure 5. SCFT phase diagrams in the (a) $\phi_1 - \chi N (= \chi N_l)$ plane with fixed $f_{SA} = 0.4$, $f_{LA} = 0.5$, and $R = N_l/N_s = 5$ and (b) $\phi_1 - R$ plane with fixed $f_{SA} = 0.5$, $f_{LA} = 0.1$, and $\chi N_l = 100$, where s and l appearing in all subscripts represent short and long, respectively; (c) density profiles (i) ϕ_{1A} , (ii) ϕ_{1B} , (iii) ϕ_{1SA} , and (iv) ϕ_{1SB} solved by SCFT under $f_{SA} = 0.4$, $f_{LA} = 0.5$, $R = N_l/N_s = 5$, $\chi N_l = 100$, and 1:1 volume fraction between the long and short copolymers. Parts (a) and (c) are reprinted with permission from ref 27, Copyright 2010 American Chemical Society; (b) is reprinted with permission from ref 28, Copyright 2011 American Chemical Society.

T , and the one in Figure 4b is a magnified version of the $\phi_{PS} - r$ plane in Figure 4a. Most of the observed phases are labeled by their abbreviated names in both diagrams in Figure 4 and their full names are given in the legends. For both phase diagrams, the composition f_A of the long copolymers is fixed at 0.185 and the short copolymers are all nearly symmetric so that the left ($\phi_{PS} = 0.185$) and right ($\phi_{PS} \approx 0.5$) edges correspond to neat long and short diblock copolymers, respectively. The phase transition boundaries for pure diblock copolymers in terms of the PS block fraction are included in both figures for comparison. In Figure 4b, the expansion of the lamellar phase toward lower ϕ_{PS} relative to the neat diblocks with increasing r indicates an enhancement of the cosurfactant effect when the difference between the chain length becomes larger. Furthermore, there exists a re-entrant transition Cyl. \rightarrow Bic. \rightarrow Cyl. along the 3D path at $\phi_{PS} \approx 0.24$ in Figure 4a.

Specifically, when T is increased, the transition from Bic. back to Cyl., which is the stable morphology in the neat long diblock copolymers, is due to the weakening of cosurfactant effect caused by delocalizing the junctions of the short copolymers away from the PS–PI interface.⁹²

Built on the earlier success of applying SCFT to study binary mixtures of A_1B_1/A_2B_2 diblock copolymers,^{24,74,90} extensive SCFT calculations were carried out to construct complete phase diagrams of the system. In particular, Wu et al. systematically explored a large area of the phase space of binary blends of A_1B_1/A_2B_2 diblock copolymers, resulting in a relatively complete picture of the phase behavior of the system.^{27,28} Two typical phase diagrams selected from refs 27, 28 are reproduced in Figure 5a and b, respectively, where ϕ_1 refers to the concentration of the long diblock chains and $R = N_{\text{long}}/N_{\text{short}}$. The SCFT calculations predicted that the mixing

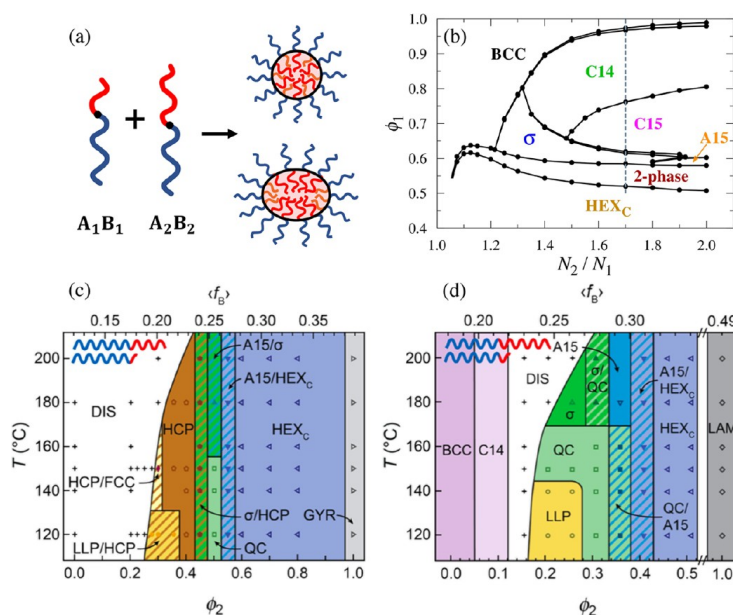


Figure 6. (a) Schematics of the discrete domains with distinct volumes and shapes formed in A₁B₁/A₂B₂ binary mixtures, (b) SCFT phase diagram in the $N_2/N_1 - \phi_1$ plane, (c) experimental phase diagram of SB binary blends on the $\phi_2 - T$ plane with $f_{B1} = 0.12$, $f_{B2} = 0.39$, and $N_2/N_1 = 1.4$, and (d) experimental phase diagram in the same parameter space as that in (c) but with $f_{B1} = 0.18$, $f_{B2} = 0.53$, and $N_2/N_1 = 1.6$. Note that in the diagrams in (c) and (d) B instead of A denotes the minority core blocks. Part (b) is reprinted with permission from ref 97, Copyright 2018 National Academy of Sciences; (c) and (d) are reprinted with permission from ref 98, Copyright 2021 American Chemical Society.

of two lamella-forming diblock copolymers can indeed stabilize the HEX phase as seen from the top of Figure 5a, which is consistent with the experimental observation by Yamaguchi et al.^{26,67,69} Another qualitative agreement between theory and experiment can be found by comparing Figure 5b to the horizontal plane in Figure 4a. In both phase diagrams the transitions as increasing the concentration of the short copolymers (or decreasing that of the long ones) are from S → H → L. It is noted that the bicontinuous phase was not included in these SCFT calculations. One discrepancy between theory and experiment is that macrophase separation is predicted by SCFT, but it is absent in Figure 4a. This could be attributed to the relatively low degree of segregation accessed in the experiments. As a result, macrophase separation may not have taken place or may have occurred within a narrow window and was not detected. The density profiles of the A and B blocks of the long chains, i.e., $\phi_{IA}(\mathbf{r})$ and $\phi_{IB}(\mathbf{r})$, and those of the short chains, i.e., $\phi_{sA}(\mathbf{r})$ and $\phi_{sB}(\mathbf{r})$, are also depicted in Figure 5c(i)–(iv). It is obvious that the short AB diblocks primarily localize near the interface, demonstrating clearly the cosurfactant behavior.

■ STRUCTURAL ENGINEERING: COMPLEX MORPHOLOGIES

Based on the results presented above, it is clear that block copolymer blends have a rich phase behavior and provide an efficient and cost-effective platform to obtain desired ordered polymeric phases. The principles governing the formation of different ordered phases are the spatial distribution of the added species, which could act as fillers and cosurfactants to regulate the equilibrium morphology. On the other hand, prior to 2010 most of the ordered phases observed in experiments and/or predicted by theory are the “classical” ones. It is therefore desirable to investigate the possibility of using block

copolymer blends to obtain new morphologies that are not the equilibrium phases of each of their parent block copolymers.

One interesting example of obtaining new morphologies is the recent theoretical prediction and experimental observation of the complex spherical packing phases such as the Frank–Kasper phases and the Laves phases.¹⁶ Exciting progress has been made in the study of the formation of these novel phases in binary blends of diblock copolymers, including the discovery of new morphologies, the understanding of their formation mechanisms, and the accessing of desired morphologies through rational molecular design. In this section, we review these recent developments in the self-assembly of binary blends of diblock copolymers.

One very exciting progress on the possibility of using blends to obtain new morphologies is the discovery of Frank–Kasper (FK) phases in binary blends composed of A₁B₁/A₂B₂ diblock copolymers.^{29,31,97–99} The FK phases are a family of complex spherical packing phases composed of more than one nonequivalent Wigner-Seitz cells (WSCs), with distinct shapes and sizes, partitioning the three-dimensional space.^{100,101} In contrast, the so-called “classical” spherical packing phases such as the body-centered cubic (BCC), face-centered cubic (FCC), and hexagonal close-packed (HCP) phases all have only one type of WSC. Prior to 2010, it was believed that neat diblock copolymers could only form the BCC, FCC, and HCP phases. This assumption was broken in 2010 when Lee et al. reported the discovery of a Frank–Kasper σ phase from diblock copolymers.¹⁷ Later SCFT calculations by Xie et al.¹⁵ showed that the mechanism for the formation of complex spherical packing phases in neat diblock copolymers could be attributed to the conformational asymmetry of the different blocks, which could be manipulated by using blocks with very different Kuhn lengths or by changing the copolymer architecture from linear AB to miktoarm AB_n. This theoretical

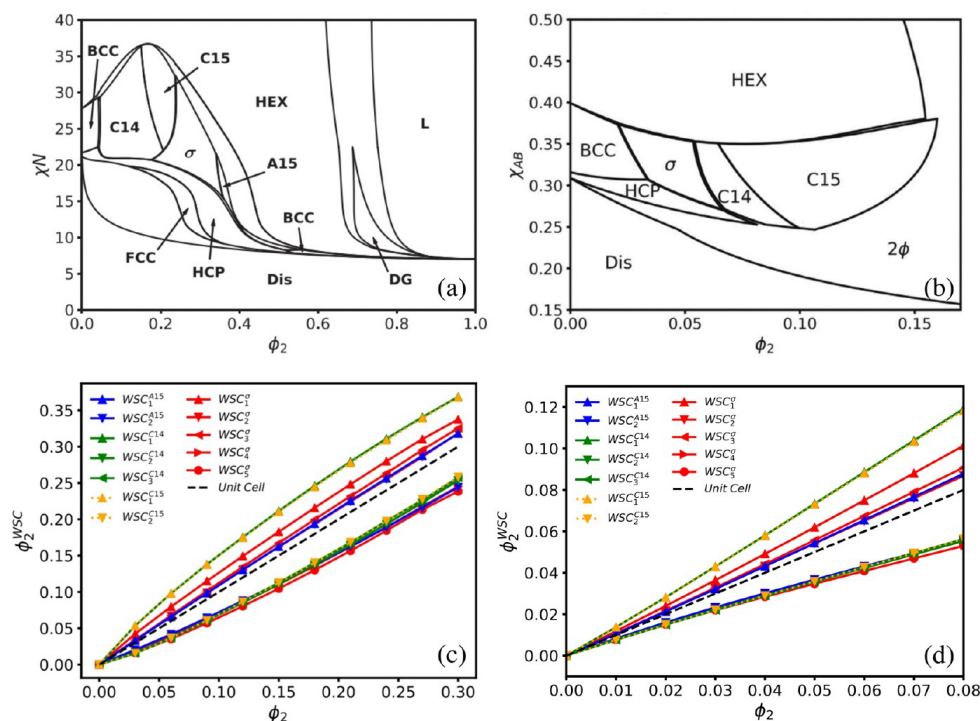


Figure 7. (a) SCFT phase diagram of conformationally symmetric A_1B_1/A_2B_2 binary blends modeled as Gaussian chains on the $\phi_2 - \chi N (= \chi N_1)$ plane with $f_{A1} = 0.2$, $f_{A2} = 0.5$, and $\gamma = N_2/N_1 = 1.5$; (b) SCFT phase diagram of A_1B_1/A_2 binary blends modeled as freely jointed chains on the $\phi_2 - \chi_{AB}$ plane with $N_1 = 80$, $f_{A1} = 0.2$, and $\alpha = N_{A2}/N_{A1} = 1.0$; (c) average concentrations of the second components in the A_1B_1/A_2B_2 blend within distinct WSCs for different complex phases as a function of ϕ_2 (average concentrations of the second components in the entire unit cell) with fixed $f_1 = 0.2$, $f_2 = 0.7$, $\gamma = 1.5$, and $\chi N = 30$; and (d) similar to (c) but for the A_1B_1/A_2 blend with fixed $N_1 = 80$, $\epsilon = 1.25$, $f_{A1} = 0.2$, $\alpha = 1.0$, $\chi_{AB} = 0.45$. The dashed lines in (c,d) are ϕ_2 over the entire unit cell. Parts (a) and (c) are reprinted with permission from ref 99, Copyright 2021 John Wiley and Sons; (b) and (d) are reprinted with permission from ref 32, Copyright 2021 Elsevier.

prediction was confirmed in subsequent experiments.^{33,102–104} Based on the idea that differential distribution of diblock copolymers could promote the formation of polymeric domains with different shapes and volumes, as schematically depicted in Figure 6a, Liu et al.²⁹ predicted theoretically that there is a very large stable window of the Frank–Kasper σ and A15 phases in the phase diagram of binary blends of A_1B_1/A_2B_2 diblock copolymers. Furthermore, their results are insensitive to the conformational asymmetry of the blocks. Moreover, refined SCFT calculations predicted that the Laves C14 and C15 phases, which are members of the FK family but with much larger WSC volume dispersity compared with the A15 and σ phases, can become equilibrium phases in the same binary blending system as can be seen in the phase diagram in Figure 6b.⁹⁷ The theoretical prediction that complex spherical packing phases could be stabilized by blending two different AB diblock copolymers was confirmed by Lindsay et al.^{31,98} in their careful experiments on binary mixtures of polystyrene-*block*-1,4-polybutadiene (PS-*b*-PB) diblock copolymers. In their experimental design, all the diblock copolymer chains had the same lengths of the corona blocks and various lengths of the core blocks. The resultant blends were obtained by mixing the disorder-forming diblock sample with other samples having different core block lengths. Besides the classical phases, the FK σ , A15, and C14 phases, and a dodecahedral quasicrystal (QC) phase were observed, demonstrating the effectiveness of the blending strategy in stabilizing these novel structures. Two of their experimental phase portraits are shown in Figure 6c

and d. It is interesting to note that the experimental phase behaviors of the binary diblock copolymer blends observed by Lindsay et al.^{31,98} are qualitatively in agreement with the theoretical predictions.^{29,97,99}

Mechanisms stabilizing the Frank–Kasper and Laves phases in binary blends of A_1B_1/A_2B_2 diblock copolymers have been elucidated from detailed SCFT calculations. Based on the theoretical results, it was argued that the synergy of the inter- and intradomain segregation of the two diblock copolymers plays a crucial role in alleviating the packing frustration of the polymeric domains, thus stabilizing the complex spherical phases.²⁹ A good understanding of the effects of copolymer segregation on the promotion of complex spherical packing is provided by Xie et al.,⁹⁹ who performed a detailed study using SCFT on BCC-forming diblock copolymers ($f_{A1} = 0.2$) mixed with other diblock chains with different f_{A2} and $\alpha = N_2/N_1$. A typical phase diagram with $f_{A2} = 0.5$ and $\alpha = 1.5$ favoring the formation of FK phases is given in Figure 7a, which contains stable regions for an amazing array of FK phases, including the σ , A15, C14, and C15 phases, spanning a large range over $\chi N (= \chi N_1)$ and ϕ_2 . The partition of the longer copolymers ($f_{A2} = 0.5$) into the different WSCs quantified by its average concentration in these cells ϕ_2^{WSC} are shown in Figure 7c, where the scattering of ϕ_2^{WSC} around the average ϕ_2 over the entire unit cell is obvious, indicating a differential interdomain segregation of the copolymers. The unequal partition of the longer diblock chains, i.e., more longer copolymers are found in larger domains, fulfills the need to form domains with

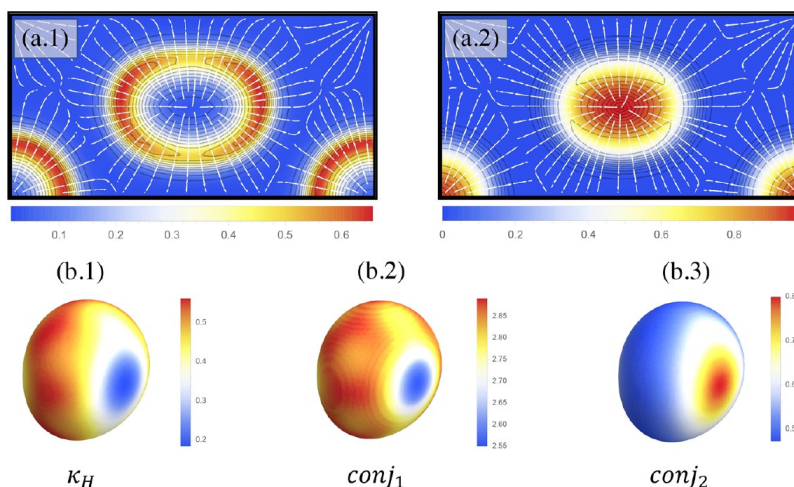


Figure 8. (a) Segment density and bond orientation distributions of (a.1) A_1B_1 and (a.2) A_2B_2 copolymers and (b) interfacial mean curvature (κ_H) and A,B junction distributions ($conj_i$, $i = 1, 2$) projected on the interface in the A_1B_1/A_2B_2 binary mixtures. Both (a) and (b) are obtained by SCFT and for the $CN = 14$ domain of an equilibrated A15 structure with $f_1 = 0.2$, $f_2 = 0.75$, and $\gamma = 1.5$, $\phi_2 = 0.15$, and $\chi N = 30$. Reprinted with permission from ref 99, Copyright 2021 John Wiley and Sons.

different sizes required by the FK phases. It is interesting to compare the distribution of the longer copolymers in the A_1B_1/A_2B_2 blends and that of the homopolymers in the binary diblock copolymer/homopolymer (A_1B_1/A_2) blends.³² A typical phase diagram and homopolymer distribution (ϕ_2^{WSC}) plot for the A_1B_1/A_2 blends are shown in Figure 7b and d, respectively. Figure 7b shows the formation of the FK phases in the A_1B_1/A_2 system, which results from the nonuniformly distributed homopolymers (Figure 7d). The similarity between Figure 7c and d indicates the homopolymer-like behavior of the longer diblock copolymers, i.e., acting as space fillers and swelling distinct domains by different degrees in the A_1B_1/A_2B_2 blends, which in turn drives the formation of large and small spheres.

Unlike homopolymers that could only act as fillers, the added diblock copolymers could act as fillers and cosurfactants simultaneously, depending on whether they are located in the middle of the domains or at the AB-interfacial regions. The effects of this dual function of the added diblock copolymers are threefold: 1. Compared with binary A_1B_1/A_2 blends, the miscibility of the two AB diblock copolymers is increased so that the stable region of spherical morphologies could be extended to a relatively high ϕ_2 . 2. A core-shell structure is formed in the spherical domains such that the longer A blocks extend to the core regions of the domains, which, coupled with interdomain segregation, results in swollen domains with different sizes. 3. The lateral distribution of the AB junctions on the interface provides a mechanism to regulate the interfacial curvature favoring the formation of domains with different shapes.⁹⁹ The second and third effects are illustrated by Figure 8a and b, respectively.³² As shown in Figure 8a, the A blocks of the shorter diblock copolymers form a shell (Figure 8a.1), whereas those of the longer copolymers form the core (Figure 8a.2) of the A-rich domain. Figure 8b displays the mean curvature of the interface (Figure 8b.1) along with the distribution of the AB junctions of the diblocks with $f_{A1} = 0.2$ (Figure 8b.2) and those of the diblocks with $f_{A2} = 0.5$ (Figure 8b.3). It is clearly seen that the segregation of the AB junctions of the A_1B_1 and A_2B_2 copolymers coincides with the interfacial

areas with high and low mean curvatures, respectively. The interplay between the inter- and intradomain segregations should be responsible for the larger region of the FK phases and the stabilization of the A15 phase in Figure 7a compared to Figure 7b.

Following the previous study by Liu et al. on the A_1B_1/A_2B_2 mixtures,^{29,97} Zhao et al.¹⁰⁵ extended the SCFT calculations to investigate the phase behavior when the two diblock copolymers have a much larger difference in their lengths, i.e., $\gamma = N_2/N_1 > 2$. It is very interesting that their theoretical study predicted that a novel “binary” HCP (HCP^b) phase, composed of larger and smaller spheres with vastly different volumes, becomes stable when $\gamma \gtrsim 2.6$. Figure 9 shows their phase diagram covering a large region of $0.5 \lesssim \phi_1 \lesssim 1$ and $1.6 \lesssim \gamma \lesssim 4.1$, in which a stability window for the HCP^b phase

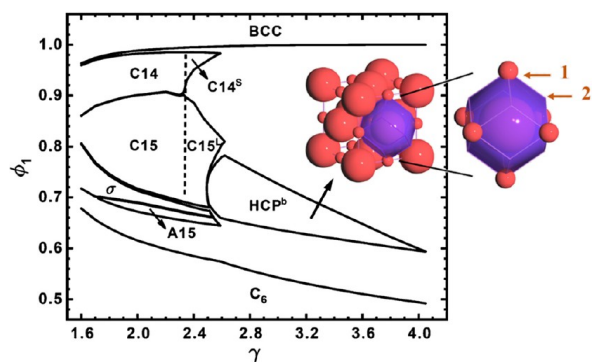


Figure 9. SCFT phase diagram of the conformationally symmetric A_1B_1/A_2B_2 binary blend in the $\gamma - \phi_1$ plane where $\gamma = N_2/N_1$. The phase diagram was constructed under fixed $f_1 = 0.23$, $\chi N_1 = 20$, and 1:1 corona block length ratio featuring the formation of the HCP^b phase composed of large spheres packing on a HCP lattice and small spheres located at those vertices of the HCP WSCs with larger interstitial voids. A schematic of the novel HCP^b phase is also included, along with the phase diagram. Reprinted with permission from ref 105, Copyright 2022 American Chemical Society.

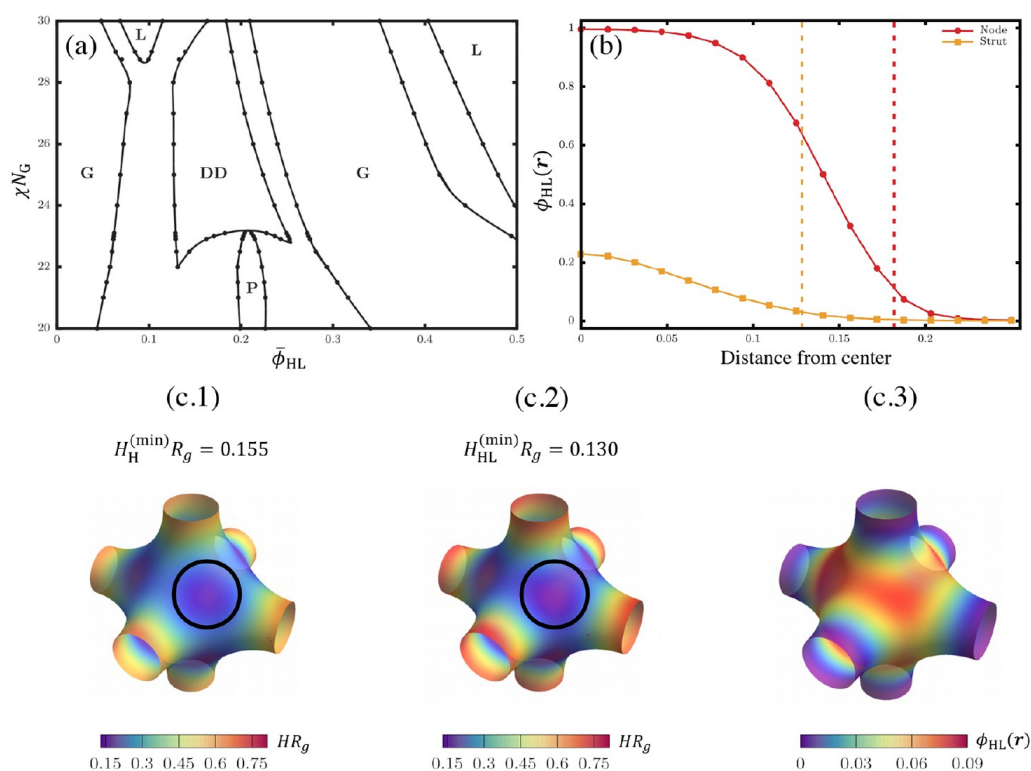


Figure 10. (a) SCFT phase diagram of conformationally symmetric A_1B_1/A_2B_2 binary blend in the $\bar{\phi}_{HL}(= \phi_2) - \chi N_G(= \chi N_1)$ plane with fixed $f_{A1} = 0.34$, $f_{A1} = 0.95$ and $\alpha = N_2/N_1 = 2.32$ featuring the formation of DD and P phases with sizable stability windows, (b) the variation of the volume fraction $\phi_{HL}(r)$ of the A_2B_2 copolymers as going away from the center of a node/strut along the $[111]/[100]$ direction for the P phase and (c) the AB-interfacial mean curvature for (c.1) A_1B_1/A_2B_2 and (c.2) A_1B_1/A_2 blends as well as (c.3) the A_2B_2 copolymer density projected on one representative node of the P phase with $\phi_2 = 0.16$, $f_1 = 0.34$, $f_{A2} = 0.95$ (for the A_2B_2 copolymers), $\chi N_1 = 25$, and $\alpha = 2.32$. Reprinted with permission from ref 107, Copyright 2021 John Wiley and Sons.

opens up at $\gamma \approx 2.5$, gradually tapers off after reaching the maximum width ($\Delta\phi_1 \sim 0.12$) at $\gamma \approx 2.62$, and eventually disappears at $\gamma \approx 4.05$. In the HCP^b phase, the larger spheres pack on a HCP lattice, while the smaller spheres are located at the vertices of the HCP WSCs with larger interstitial voids (Figure 9). Similar “binary” phases where the larger spheres sit on FCC, BCC, C14, and C15 lattices interspersed by smaller spheres locating at the interstitial positions were also found as metastable phases. The HCP^b phase is stable when the reduced chain stretching free energy of the longer copolymers outweighs the extra interfacial free energy induced by forming small spheres to fill the interstitial voids. The discovery of the HCP^b phase unveiled another type of chain arrangement in binary A_1B_1/A_2B_2 blends, consisting of copolymers with a great difference in degrees of polymerization, i.e., forming larger and smaller spheres and packing in a way that conforms to Horsfield close packing model.^{105,106} It would be interesting to confirm the formation of this novel HCP^b phase in experiments.

Besides stabilizing complex spherical packing phases, it has been predicted that binary mixtures of A_1B_1/A_2B_2 diblock copolymers also offer opportunities to stabilize novel bicontinuous phases.¹⁰⁷ The bicontinuous phases self-assembled by AB-type copolymers are characterized by two intertwining networks composed of the minority A or B blocks immersed in the majority B- or A-rich matrix. There exist several bicontinuous morphologies such as the double gyroid

(DG), double diamond (DD), and plumber’s nightmare (P) phases, categorized by the number of struts jointed at each node, p . Among all the candidate morphologies, the DG phase with $p = 3$ is the only equilibrium bicontinuous morphology for neat AB diblock copolymer melts.^{108,109} The stabilization of DG ($p = 3$) over DD ($p = 4$) and P ($p = 6$) is attributed to the higher excessive chain stretching at the nodes in structures with larger p , which, regarded as a form of packing frustration, is induced by the competition between the preference of having uniform interfacial curvature and the need to maintain a constant monomer density.¹¹⁰ One way to alleviate such packing frustration is by introducing homopolymers as space fillers, which could give rise to the stabilization of bicontinuous structures with higher p .^{25,111–114} However, this blending scheme is limited by the small amount of homopolymers that could solubilize into the polymeric domains, thus making the blends prone to macrophase separation between the ordered phases and the homopolymer-rich disordered phase and prohibiting the formation of the desired phases in a large range in the phase space.

In comparison to homopolymer additives, appropriate block copolymer additives may be capable of accessing the bicontinuous morphologies with high p over a larger blend composition range because of their dual role as homopolymer-like fillers and cosurfactants. Based on this idea, Lai and Shi¹⁰⁷ examined the phase behavior of binary mixtures of A_1B_1/A_2B_2 diblock copolymer blends in selected regions in the phase

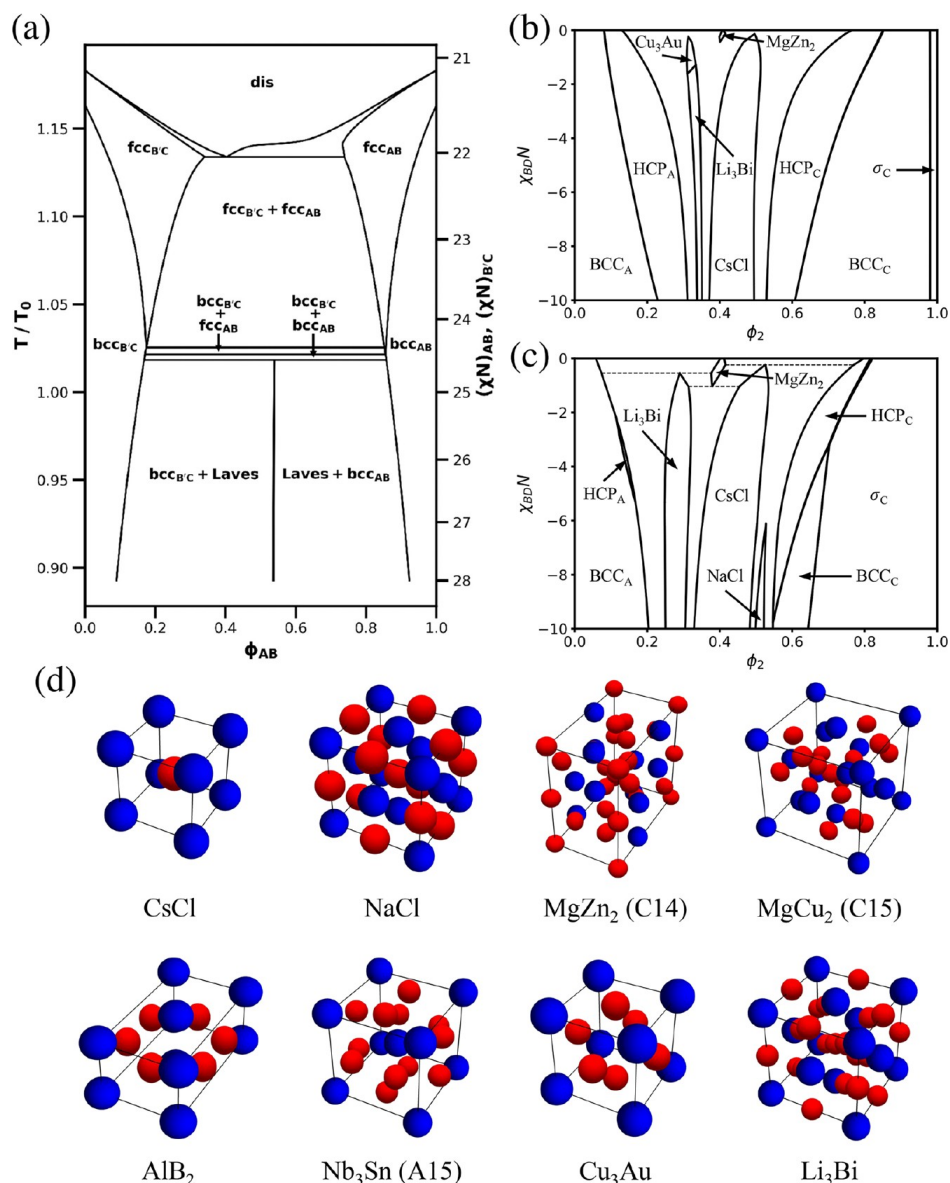


Figure 11. (a) SCFT phase diagram of the AB/B'C blend mimicking the eutectic phase diagram of a binary metallic alloy, (b) SCFT phase diagram of the AB/CD (the AB and CD chains are labeled by 1 and 2, respectively) binary mixture in the $\phi_2 - \chi_{BD}N$ plane with $\epsilon_1 = \epsilon_2 = 1.0$, $f_1 = 0.18$, $f_2 = 0.21$, $\gamma = N_2/N_1 = 1.0$, and all other positive χN fixed at 30, (c) SCFT phase diagram similar to that in (b) but with $\epsilon_1 = 1$, $\epsilon_2 = 2.0$, and $f_1 = f_2 = 0.19$, and (d) schematic plots of all the stable binary alloy phases that have so far been discovered in the AB/CD blends (except C15, who has only been metastable in the phase space explored). Note that in (b) and (c), subscripts A and C indicate that these phases contain core-shell-structured AC-mixed domains with a higher A and C content, respectively. Part (a) is reprinted with permission from ref 115, Copyright 2022 American Chemical Society; (b), (c), and (d) are adapted with permission from ref 117.

space and showed that both the DD and P phases could be stabilized with sizable stability windows. The binary A_1B_1/A_2B_2 phase diagram constructed by Lai and Shi featuring the emergence of the DD and P phases is shown in Figure 10a, which is on the $\phi_{HL} (= \phi_2) - \chi N_G (= \chi N_1)$ plane with fixed $f_{A1} = 0.34$, $f_{A2} = 0.95$, and $\alpha = N_2/N_1 = 2.32$. The key observation from their study is that the added homopolymer-like AB diblock copolymers with $f_{A2} = 0.95$ can act as fillers and cosurfactants at the same time. When the homopolymer-like diblock copolymers ($f_{A2} = 0.95$) are added into the DG-forming copolymers, order-order phase transition sequences

of $DG \rightarrow DD$ and $DG \rightarrow P$ are induced in the ranges of higher and lower χN_G , respectively. Compared to the A_1B_1/A_2B_2 blends,^{25,111–113} the blend composition range over which the DD and P phases are stable in the A_1B_1/A_2B_2 blends is generally larger, which is advantageous as a platform to obtain these phases in experiments. Another feature revealed by Figure 10a is the re-entrant transition to the DG phase upon further increasing ϕ_{HL} , which replaces the transition to the dominant order-disorder coexistence region and finally to the homopolymer-rich disordered phase generally occurring in the A_1B_1/A_2B_2 blends. The behavior of the copolymer additives in

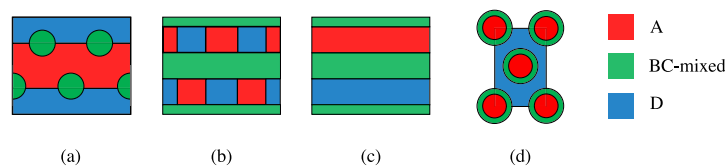


Figure 12. Schematics of (a) BC cylinders in A/D lamellae, (b) lamellae composed of BC-mixed layers and B/D-separated layers, (c) three-layer lamellae, and (d) core-shell cylinders formed in supramolecular AC/CD binary blends.

the binary blends was examined by detailed analyses of their spatial distribution.¹⁰⁷ The homopolymer-like behavior could be recognized in Figure 10b, which shows the variation of the volume fraction $\phi_{HL}(\mathbf{r})$ of the A_2B_2 copolymers as going from the center of a node/strut along the [111]/[100] direction for the P phase. Both curves peak at zero, suggesting the segregation of the A_2B_2 copolymers inside the A-rich networks especially at the nodes. This helps to reduce the excessive stretching of the host copolymers. Furthermore, the authors also showed that, in comparison to homopolymer additives, the copolymer additives accumulate in the regions on the AB interface with reversed curvature (curving toward the majority blocks). This region is disfavored by the DG-forming diblocks, and the segregated A_2B_2 copolymers help to alleviate this frustration due to the much longer A blocks. This modification of the interfacial curvature further benefits the conformational entropy for the high- p bicontinuous phases and, thus, enhances their stability. This cosurfactant behavior is demonstrated in Figure 10c, where the minimum curvature is much lower in the A_1B_1/A_2B_2 blends (Figure 10c.1) than that in the A_1B_1/A_2 blends (Figure 10c.2) with A_2 homopolymer having the same N as the A_2B_2 copolymer, and the segregation of the copolymer additives (Figure 10c.3) coincides with the regions with the lowered curvature. The cooperation between the homopolymer-like filler and cosurfactant effects explains the superiority of the A_1B_1/A_2B_2 over A_1B_1/A_2 binary mixtures in stabilizing the novel bicontinuous phases.

■ BEYOND BINARY A_1B_1/A_2B_2 BLENDS: MESOATOMIC ALLOYS

The recent progress reviewed above has focused on binary blends composed of A_1B_1 and A_2B_2 diblock copolymers. Despite their simplicity, this system exemplifies the possibility to obtain desired ordered phases via rational molecular engineering based on design principles elucidated from the extensive experimental and theoretical investigations. One obvious extension of this research topic is the study of binary blends composed of block copolymers with more than two types of chemically distinct blocks, as well as going beyond the simple diblock copolymer architecture. There is an infinite number of possibilities in formulating such block copolymer blends with great opportunities to access desired morphologies. Efforts have been made to investigate the phase behaviors of more complicated binary diblock copolymer blends, which will be of our focus in this section.

Although the stability of Laves phases in the A_1B_1/A_2B_2 diblock copolymer blends is anticipated according to SCFT calculations, their formation in many of the theoretically predicted regions has not been successfully confirmed in experiments.⁹⁸ In search of a more robust approach to stabilize the Laves phases, Magruder et al. proposed to go beyond the A_1B_1/A_2B_2 formulation and use binary blends composed of AB/B'C diblock copolymers, where the interaction parameters

and block compositions were judiciously adjusted to favor the formation of binary Laves phases composed of A and C spheres mimicking crystals from metallic alloys.¹¹⁵ The phase diagrams obtained by SCFT calculations highly resemble the eutectic phase diagrams of binary alloys, where a narrow composition window for the C14 phase is present (Figure 11). The stability of the C14 phase results from the ratio between the degrees of polymerization of the BCC-forming AB and B'C copolymers ($N_{B'C}/N_{AB} = 1.3$, and $f_A = f_C = 0.2$), which were purposely designed to match the volume asymmetry of the Laves phases. Soon after, Case et al. demonstrated that this blending system enables a decoupled control over the polyhedral imprinting of the inequivalent particles via conformational asymmetry.¹¹⁶ Particularly, enhancing the polyhedral imprinting by increasing the conformational asymmetry for the larger or smaller spherical particles in Laves phases proved to be beneficial or detrimental to their stability, respectively.

As pointed out by Case et al.,¹¹⁶ one feature hindering practical applications of the AB/B'C blends in producing the Laves phases is the strong tendency for the system to macrophase separate. This tendency could be suppressed by introducing some associations between the corona blocks such as hydrogen bonding. In a recent SCFT study, Xie et al.¹¹⁷ considered a more complicated binary blending system composed of AB and CD diblock copolymers. Their system is similar to the AB/B'C system studied by Magruder et al. and Case et al. but with adjustable compatibility between the corona blocks, i.e., the B and D blocks. In their calculations, the enhanced miscibility between the B and D blocks was modeled by using a negative χ_{BD} . Two phase diagrams in the $\phi_2 - \chi_{BD}N$ plane, where ϕ_2 is the concentration of the CD copolymers and $\chi_{BD}N$ quantifies the favorable association between the corona blocks, are shown in Figure 11b and c. A list of binary alloy phases is also included in Figure 11d. In the phase space explored by Xie et al.,¹¹⁷ stability windows for all of the binary crystals in Figure 11d have been discovered in the AB/CD blends via SCFT, except the MgCu₂ (C15) phase which has only been metastable. Interestingly, a weak corona block association slightly enlarges the C14 window, while a stronger association stabilizes other mesoatomic alloy phases in place of the C14 phase, as could be seen in both Figure 11b and c. These results are still preliminary, and systematic studies covering more regions in the phase space of the binary blends composed of AB and CD diblock copolymers are required in order to understand the rich phase behavior of this system.

It is worth mentioning that although the negative χ approach is commonly used, the hydrogen bonding effect should be modeled as reversible intermolecular complexations.¹¹⁸ By using the AB/C binary blends with hydrogen-bonded A and C blocks as a model system, Dehghan and Shi showed that both approaches produced qualitatively correct phase behavior in comparison to experiments, but only the complexation model predicted the correct lamellar spacing in the strong hydrogen

bonding regime.¹¹⁹ Compared to the more complicated intermolecular complexation model, the simplicity of the negative χ model makes it the preferred approach to obtain a qualitative understanding of the phase behavior in many cases.

Experimentally, the role played by hydrogen bonding in the phase behaviors of block copolymer blends has been studied in a series of publications by Kuo and co-workers,^{50,120–124} as well as by other research groups.^{125,126} Some peculiar self-assembled structures have been reported by these authors for supramolecular binary diblock copolymer blends involving hydrogen bonding. For instance, highly asymmetric lamellar phase having thin and thick layers¹²⁶ could be formed in an AB/A'C blend where B and C are compatibilized by hydrogen bonding. Another example is an AB/CD blend with B and C associated via hydrogen bonding, which is capable of forming hierarchical structures including BC cylinders in A/D lamellae and lamellae composed of BC-mixed layers and B/D-separated layers, as illustrated schematically in Figure 12a and b, respectively.¹²⁵ Moreover, when hydrogen bonding exists between more than one pairs of blocks but with different strengths, the competing interactions could also drive the system to form novel phases such as three-layer lamellae and core-shell cylinders, as illustrated schematically in Figure 12c and d, respectively.^{120–122,124} Many of these structures also exist in self-assembled linear triblock copolymers;^{127,128} thus, the supramolecular blending strategy provides a simple route to access phases whose formation would otherwise require more complicated chain architectures. Theoretical studies of these systems by various methods were also conducted,^{129–131} and part of the experimental observed phases have been predicted.¹³⁰ However, a direct and systematic comparison between theory and experiments is still lacking. Exploring the phase behaviors of polymeric blends containing supramolecular block copolymers is an interesting topic with great opportunities to explore the formation of more exotic morphologies.

CONCLUSIONS

Due to the presence of block copolymers, polymeric blends containing block copolymers possess the ability to self-assemble into various ordered phases. Compared with multiblock copolymers that would require sophisticated synthetic techniques, block copolymer blends provide a flexible and cost-effective route to obtain polymeric systems containing many chemically distinct components, which, in turn, could be used as a platform to fabricate structured materials with desired morphologies. On the other hand, mixing different polymeric components together introduces many new ingredients into the system, resulting in an enormously enlarged phase space. In particular, the macrophase separation of the different components is an eminent feature of polymer blends. Together with the additional system parameters, the phase behaviors of polymeric blends containing block copolymers become extremely complex. Comprehensive studies of the phase behaviors of block copolymer blends using a combination of experimental and theoretical approaches are required to gain a good understanding of the phase behaviors of these systems.

A polymer blend can contain any number and type of components, resulting in unlimited formations. The simplest block copolymer blends are binary blends obtained by mixing two different, AB and CD, diblock copolymers. Most of the work reviewed in this article is further restricted to the case of binary mixtures of A_1B_1 and A_2B_2 diblock copolymers. It is

important to regulate the miscibility of the two diblock copolymers such that macroscopic phase separation of the system is suppressed, which could be achieved by judiciously selecting the system parameters, such as the relative molecular weights and the block compositions. The phase behavior of this seemingly simple system is surprising complex. Besides self-assembling into the stable phases of AB diblock copolymer melts, the A_1B_1/A_2B_2 binary blends can form ordered phases that are not equilibrium ones for the parent diblock copolymer melts.

Extensive experimental and theoretical studies have revealed that the function of the added A_2B_2 diblock copolymers can be classified as fillers and cosurfactants, depending on their spatial distribution in the polymeric domains formed by the A_1B_1 diblock copolymers. The spatial distribution of the A_2B_2 diblocks depends on the A block composition or volume fraction f_{A_2} . The asymmetric homopolymer-like added diblocks with $f_{A_2} \sim 0$ or 1 would predominantly distribute in the central regions of the B or A domains, acting as fillers to regulate the volume of the corresponding domains. On the other hand, the symmetric added diblocks with $f_{A_2} \sim 0.5$ are most likely to localize at the AB interfaces acting as cosurfactants to regulate interfacial properties. These behaviors will be further modified by the molecular weights of the two diblock copolymers. Taken together, the added diblock copolymers act synergistically to alleviate the packing frustration of the polymeric domains and therefore stabilize structures with very different domain volumes such as the Laves C14 and C15 phases or structures with very different interfacial curvatures such as the double diamond and plumber's nightmare networked structures. The principles governing the self-assembly of A_1B_1/A_2B_2 diblock copolymer blends could be extended to other blending systems such as mixtures of AB and CD diblock copolymers, thus providing a solid foundation for further investigation of the more complex polymeric blends containing block copolymers.

Compared with the simple case of A_1B_1/A_2B_2 diblock copolymer blends, binary mixtures of AB/CD diblock copolymers, or more complex variations such as mixtures of diblock and triblock copolymers,^{132,133} could provide more opportunities to fabricate novel nanoscopic structures via self-assembly. One example is the formation of superlattices composed of A and C spherical domains. While it is possible to form such superlattices by using BABCB pentablock copolymers,¹⁹ it would be more efficient and cost-effective by using block copolymer blends.^{115–117} On the other hand, different block copolymers, such as AB and CD diblock copolymers, tend to macrophase separate due to the chemical differences between the AB and CD blocks. One possible solution to this problem is to introduce attractive interactions between the different types of block copolymers. For example, introducing hydrogen bonding between monomers B and D could increase the miscibility of AB and CD diblock copolymers, thus, encouraging the formation of mixed phases and providing opportunities to form novel morphologies.

There are some major challenges for the theoretical and experimental study of the equilibrium phase behaviors of binary blends of diblock copolymers. Due to the great complexity of the binary blends of diblock copolymers, particularly the AB/CD blends, a systematic experimental exploration of their phase space is a daunting task. On the other hand, obtaining informative guidance on the phase behaviors of such systems by using theoretical frameworks

such as SCFT relies on the choice of candidate phases, which is a well-known difficult task in the design of complex multiblock copolymers.¹³⁴ The interplay between microphase and macrophase separations makes the design of multicomponent block copolymer systems even more challenging. To overcome these obstacles, it is important to obtain insights and establish an understanding of the self-assembling mechanisms by a concerted collaboration of theorists and experimenters. Such an effort could achieve more precise morphological control over AB/CD or even more complicated polymeric blends.

In this feature article, we have given a brief account on the progress made in the past decades in the study of the phase behaviors of binary blends of diblock copolymers. We have mainly focused on the simple system composed of two, A_1B_1/A_2B_2 , diblock copolymers that differ only by their molecular weights and block compositions. The studies of this system have led to a good understanding of the principles governing the self-assembly of polymeric blends and design rules to alleviate frustrations in the self-assembled structures. We hope this review will stimulate further studies of the phase behaviors of polymeric blends containing block copolymers.

■ AUTHOR INFORMATION

Corresponding Author

An-Chang Shi – Department of Physics & Astronomy,
McMaster University, Hamilton, Ontario L8S 4M1,
Canada;  orcid.org/0000-0003-1379-7162; Email: shi@mcmaster.ca

Author

Jiayu Xie – Department of Physics & Astronomy, McMaster
University, Hamilton, Ontario L8S 4M1, Canada

Complete contact information is available at:

<https://pubs.acs.org/10.1021/acs.langmuir.3c01175>

Notes

The authors declare no competing financial interest.

Biographies



Jiayu Xie received his B.Sc. in Applied Physics from Beijing Jiaotong University in 2018, after which he joined the research group of Dr. An-Chang Shi in the Department of Physics & Astronomy at McMaster University to pursue his Ph.D. in theoretical and computational soft matter physics. During his Ph.D., he has worked on different research topics on the formation of self-assembled ordered structures. His current research focuses on investigating the equilibrium phase behaviors of polymeric blends and interacting hard spheres by means of statistical field theory.



Dr. An-Chang Shi is a professor of physics at McMaster University. He earned B.Sc. in physics from Fudan University in 1982 and Ph.D. in physics from University of Illinois at Urbana–Champaign in 1988. From 1988 to 1992 he was a Post-Doctoral Fellow and Research Associate at McMaster University. He joined Xerox Research Centre of Canada as a Member of Research Staff in 1992 and moved to McMaster University as an Associate Professor in 1999. Dr. Shi received a Premier's Research Excellent Award in 2000 and was elected to Fellow of American Physical Society in 2010. He has worked on a wide range of topics in condensed matter physics, including crystal shapes, superconductivity, and polymer physics. His current research activities center on the development of theoretic models and methods for soft matter, the investigation of phase behavior of self-assembling macromolecules such as block copolymers, and the study of kinetic pathways connecting stable and metastable states.

■ ACKNOWLEDGMENTS

We thank Frank S. Bates, Kevin D. Dorfman, Chi To (Tom) Lai, Wehua Li, Yu Li, Meijiao Liu, Mark W. Matsen, and Marcus Müller for stimulating discussions and fruitful collaborations. This manuscript is completed while ACS is visiting the Kavli Institute for Theoretical Physics at UC Santa Barbara. This research is supported by the Natural Sciences and Engineering Research Council (NSERC) of Canada and in part by the National Science Foundation under Grant No. PHY-1748958.

■ REFERENCES

- (1) Bates, C. M.; Bates, F. S. 50th Anniversary Perspective: Block Polymers—Pure Potential. *Macromolecules* **2017**, *50*, 3–22.
- (2) Shi, A.-C. Frustration in block copolymer assemblies. *J. Phys.: Condens. Matter* **2021**, *33*, 253001.
- (3) Mai, Y.; Eisenberg, A. Self-assembly of block copolymers. *Chem. Soc. Rev.* **2012**, *41*, 5969–5985.
- (4) Bates, F. S.; Fredrickson, G. H. Block copolymers—designer soft materials. *Phys. Today* **1999**, *52*, 32–38.
- (5) Cushen, J. D.; Otsuka, I.; Bates, C. M.; Halila, S.; Fort, S.; Rochas, C.; Easley, J. A.; Rausch, E. L.; Thio, A.; Borsali, R.; Willson, C. G.; Ellison, C. J. Oligosaccharide/silicon-containing block copolymers with 5 nm features for lithographic applications. *ACS Nano* **2012**, *6*, 3424–3433.
- (6) Bates, C. M.; Maher, M. J.; Janes, D. W.; Ellison, C. J.; Willson, C. G. Block copolymer lithography. *Macromolecules* **2014**, *47*, 2–12.
- (7) Durand, W. J.; Blachut, G.; Maher, M. J.; Sirard, S.; Tein, S.; Carlson, M. C.; Asano, Y.; Zhou, S. X.; Lane, A. P.; Bates, C. M.; Ellison, C. J.; Willson, C. G. Design of high- χ block copolymers for lithography. *J. Polym. Sci., Part A: Polym. Chem.* **2015**, *53*, 344–352.
- (8) Huang, C.; Zhu, Y.; Man, X. Block copolymer thin films. *Phys. Rep.* **2021**, *932*, 1–36.
- (9) Fink, Y.; Urbas, A. M.; Bawendi, M. G.; Joannopoulos, J. D.; Thomas, E. L. Block copolymers as photonic bandgap materials. *Journal of Lightwave Technology* **1999**, *17*, 1963–1969.

- (10) Urbas, A.; Sharp, R.; Fink, Y.; Thomas, E. L.; Xenidou, M.; Fetters, L. J. Tunable block copolymer/homopolymer photonic crystals. *Adv. Mater.* **2000**, *12*, 812–814.
- (11) Parnell, A. J.; Pryke, A.; Mykhaylyk, O. O.; Howse, J. R.; Adawi, A. M.; Terrill, N. J.; Fairclough, J. P. A. Continuously tuneable optical filters from self-assembled block copolymer blends. *Soft Matter* **2011**, *7*, 3721–3725.
- (12) Liu, S.; Yang, Y.; Zhang, L.; Xu, J.; Zhu, J. Recent progress in responsive photonic crystals of block copolymers. *Journal of Materials Chemistry C* **2020**, *8*, 16633–16647.
- (13) Wang, Z.; Chan, C. L. C.; Zhao, T. H.; Parker, R. M.; Vignolini, S. Recent advances in block copolymer self-assembly for the fabrication of photonic films and pigments. *Advanced Optical Materials* **2021**, *9*, 2100519.
- (14) Thedford, R. P.; Yu, F.; Tait, W. R.; Shastri, K.; Monticone, F.; Wiesner, U. The Promise of Soft-Matter-Enabled Quantum Materials. *Adv. Mater.* **2023**, *35*, 2203908.
- (15) Xie, N.; Li, W.; Qiu, F.; Shi, A.-C. σ phase formed in conformationally asymmetric AB-type block copolymers. *ACS Macro Lett.* **2014**, *3*, 906–910.
- (16) Dorfman, K. D. Frank-Kasper Phases in Block Polymers. *Macromolecules* **2021**, *54*, 10251–10270.
- (17) Lee, S.; Bluemle, M. J.; Bates, F. S. Discovery of a Frank-Kasper σ phase in sphere-forming block copolymer melts. *Science* **2010**, *330*, 349–353.
- (18) Bates, F. S.; Hillmyer, M. A.; Lodge, T. P.; Bates, C. M.; Delaney, K. T.; Fredrickson, G. H. Multiblock Polymers: Panacea or Pandora's Box? *Science* **2012**, *336*, 434.
- (19) Xie, N.; Liu, M.; Deng, H.; Li, W.; Qiu, F.; Shi, A.-C. Macromolecular metallurgy of binary mesocrystals via designed multiblock terpolymers. *J. Am. Chem. Soc.* **2014**, *136*, 2974–2977.
- (20) Gao, Y.; Deng, H.; Li, W.; Qiu, F.; Shi, A.-C. Formation of Nonclassical Ordered Phases of A B-Type Multiarm Block Copolymers. *Phys. Rev. Lett.* **2016**, *116*, 068304.
- (21) Xie, Q.; Qiang, Y.; Chen, L.; Xia, Y.; Li, W. Synergistic effect of stretched bridging block and released packing frustration leads to exotic nanostructures. *ACS Macro Lett.* **2020**, *9*, 980–984.
- (22) Xie, Q.; Qiang, Y.; Li, W. Regulate the stability of gyroids of ABC-type multiblock copolymers by controlling the packing frustration. *ACS Macro Lett.* **2020**, *9*, 278–283.
- (23) Xu, Z.; Li, W. Control the Self-assembly of Block Copolymers by Tailoring the Packing Frustration. *Chin. J. Chem.* **2022**, *40*, 1083–1090.
- (24) Shi, A.-C.; Noolandi, J. Binary Mixtures of Diblock Copolymers. Phase Diagrams with a New Twist. *Macromolecules* **1995**, *28*, 3103–3109.
- (25) Matsen, M. W. Stabilizing new morphologies by blending homopolymer with block copolymer. *Phys. Rev. Lett.* **1995**, *74*, 4225.
- (26) Yamaguchi, D.; Shiratake, S.; Hashimoto, T. Ordered structure in blends of block copolymers. 5. Blends of lamella-forming block copolymers showing both microphase separation involving unique morphological transitions and macrophase separation. *Macromolecules* **2000**, *33*, 8258–8268.
- (27) Wu, Z.; Li, B.; Jin, Q.; Ding, D.; Shi, A.-C. Phase behavior of binary blends of diblock copolymers. *J. Phys. Chem. B* **2010**, *114*, 15789–15798.
- (28) Wu, Z.; Li, B.; Jin, Q.; Ding, D.; Shi, A.-C. Microphase and macrophase separations in binary blends of diblock copolymers. *Macromolecules* **2011**, *44*, 1680–1694.
- (29) Liu, M.; Qiang, Y.; Li, W.; Qiu, F.; Shi, A.-C. Stabilizing the Frank-Kasper phases via binary blends of AB diblock copolymers. *ACS Macro Lett.* **2016**, *5*, 1167–1171.
- (30) Mueller, A. J.; Lindsay, A. P.; Jayaraman, A.; Lodge, T. P.; Mahanthappa, M. K.; Bates, F. S. Emergence of a C15 Laves phase in diblock polymer/homopolymer blends. *ACS Macro Lett.* **2020**, *9*, 576–582.
- (31) Lindsay, A. P.; Lewis, R. M., III; Lee, B.; Peterson, A. J.; Lodge, T. P.; Bates, F. S. A15, σ , and a quasicrystal: Access to complex particle packings via bidisperse diblock copolymer blends. *ACS Macro Lett.* **2020**, *9*, 197–203.
- (32) Xie, J.; Shi, A.-C. Formation of complex spherical packing phases in diblock copolymer/homopolymer blends. *Giant* **2021**, *5*, 100043.
- (33) Sun, Y.; Tan, R.; Ma, Z.; Gan, Z.; Li, G.; Zhou, D.; Shao, Y.; Zhang, W.-B.; Zhang, R.; Dong, X.-H. Discrete block copolymers with diverse architectures: resolving complex spherical phases with one monomer resolution. *ACS Central Science* **2020**, *6*, 1386–1393.
- (34) Duan, S.; Yang, X.; Yang, Z.; Liu, Y.; Shi, Q.; Yang, Z.; Wu, H.; Han, Y.; Wang, Y.; Shen, H.; Huang, Z.; Dong, X.-H.; Zhang, Z. A Versatile Synthetic Platform for Discrete Oligo- and Polyesters Based on Optimized Protective Groups Via Iterative Exponential Growth. *Macromolecules* **2021**, *54*, 10830–10837.
- (35) Zhou, D.; Xu, M.; Ma, Z.; Gan, Z.; Zheng, J.; Tan, R.; Dong, X.-H. Discrete Diblock Copolymers with Tailored Conformational Asymmetry: A Precise Model Platform to Explore Complex Spherical Phases. *Macromolecules* **2022**, *55*, 7013–7022.
- (36) Edwards, E. W.; Stoykovich, M. P.; Nealey, P. F.; Solak, H. H. Binary blends of diblock copolymers as an effective route to multiple length scales in perfect directed self-assembly of diblock copolymer thin films. *Journal of Vacuum Science & Technology B: Microelectronics and Nanometer Structures Processing, Measurement, and Phenomena* **2006**, *24*, 340–344.
- (37) Zhu, Y.; Jiang, W. Self-assembly of diblock copolymer mixtures in confined states: a Monte Carlo study. *Macromolecules* **2007**, *40*, 2872–2881.
- (38) Guo, R.; Huang, H.; Chen, Y.; Gong, Y.; Du, B.; He, T. Effect of the nature of annealing solvent on the morphology of diblock copolymer blend thin films. *Macromolecules* **2008**, *41*, 890–900.
- (39) Tang, C.; Hur, S.-m.; Stahl, B. C.; Sivanandan, K.; Dimitriou, M.; Pressly, E.; Fredrickson, G. H.; Kramer, E. J.; Hawker, C. J. Thin film morphology of block copolymer blends with tunable supramolecular interactions for lithographic applications. *Macromolecules* **2010**, *43*, 2880–2889.
- (40) Shi, L.-Y.; Zhou, Y.; Shen, Z.; Fan, X.-H. Hierarchical structures in thin films of macrophase- and microphase-separated AB/AC diblock copolymer blends. *Macromolecules* **2012**, *45*, 5530–5537.
- (41) Pan, J.-X.; Zhang, J.-J.; Wang, B.-F.; Wu, H.-S.; Sun, M.-N. Phase behaviors in a binary mixture of diblock copolymers confined between two parallel walls. *Chinese Physics B* **2013**, *22*, 026401.
- (42) Rao, J.; Ma, H.; Baettig, J.; Woo, S.; Stuparu, M. C.; Bang, J.; Khan, A. Self-assembly of an interacting binary blend of diblock copolymers in thin films: a potential route to porous materials with reactive nanochannel chemistry. *Soft Matter* **2014**, *10*, 5755–5762.
- (43) Williamson, L. D.; Nealey, P. F. Macrophase separation of blends of diblock copolymers in thin films. *Macromolecules* **2015**, *48*, 3997–4003.
- (44) Yan, N.; Liu, X.; Zhang, Y.; Sun, N.; Jiang, W.; Zhu, Y. Confined co-assembly of AB/BC diblock copolymer blends under 3D soft confinement. *Soft Matter* **2018**, *14*, 4679–4686.
- (45) Sens, P.; Marques, C.; Joanny, J.-F. Mixed micelles in a bidisperse solution of diblock copolymers. *Macromolecules* **1996**, *29*, 4880–4890.
- (46) Li, X.; Tang, P.; Qiu, F.; Zhang, H.; Yang, Y. Aggregates in solution of binary mixtures of amphiphilic diblock copolymers with different chain length. *J. Phys. Chem. B* **2006**, *110*, 2024–2030.
- (47) Palyulin, V. V.; Potemkin, I. I. Mixed versus ordinary micelles in the dilute solution of AB and BC diblock copolymers. *Macromolecules* **2008**, *41*, 4459–4463.
- (48) Kuo, S.-W.; Tung, P.-H.; Lai, C.-L.; Jeong, K.-U.; Chang, F.-C. Supramolecular micellization of diblock copolymer mixtures mediated by hydrogen bonding for the observation of separated coil and chain aggregation in common solvents. *Macromol. Rapid Commun.* **2008**, *29*, 229–233.
- (49) Zhuang, Y.; Lin, J.; Wang, L.; Zhang, L. Self-assembly behavior of AB/AC diblock copolymer mixtures in dilute solution. *J. Phys. Chem. B* **2009**, *113*, 1906–1913.

- (50) Kuo, S.-W. Hydrogen bond-mediated self-assembly and supramolecular structures of diblock copolymer mixtures. *Polymer international* **2009**, *58*, 455–464.
- (51) Yabu, H.; Motoyoshi, K.; Higuchi, T.; Shimomura, M. Hierarchical structures in AB/AC type diblock-copolymer blend particles. *Phys. Chem. Chem. Phys.* **2010**, *12*, 11944–11947.
- (52) Cui, J.; Han, Y.; Jiang, W. Asymmetric vesicle constructed by AB/CB diblock copolymer mixture and its behavior: A Monte Carlo study. *Langmuir* **2014**, *30*, 9219–9227.
- (53) Jones, R. A. *Soft condensed matter*; Oxford University Press, 2002; Vol. 6; pp 26–31.
- (54) Rubinstein, M.; Colby, R. H. *Polymer physics*; Oxford University Press: New York, 2003; Vol. 23; pp 137–154.
- (55) Almdal, K.; Rosedale, J. H.; Bates, F. S. The order-disorder transition in binary mixtures of nearly symmetric diblock copolymers. *Macromolecules* **1990**, *23*, 4336–4338.
- (56) Hashimoto, T.; Yamasaki, K.; Koizumi, S.; Hasegawa, H. Ordered structure in blends of block copolymers. 1. Miscibility criterion for lamellar block copolymers. *Macromolecules* **1993**, *26*, 2895–2904.
- (57) Hashimoto, T.; Koizumi, S.; Hasegawa, H. Ordered structure in blends of block copolymers. 2. Self-assembly for immiscible lamella-forming copolymers. *Macromolecules* **1994**, *27*, 1562–1570.
- (58) Vilesov, A. D.; Floudas, G.; Pakula, T.; Melenevskaya, E. Y.; Birshtein, T. M.; Lyatskaya, Y. V. Lamellar structure formation in the mixture of two cylinder-forming block copolymers. *Macromol. Chem. Phys.* **1994**, *195*, 2317–2326.
- (59) Koizumi, S.; Hasegawa, H.; Hashimoto, T. Ordered structure in blends of block copolymers. 3. Self-assembly in blends of sphere-or cylinder-forming copolymers. *Macromolecules* **1994**, *27*, 4371–4381.
- (60) Kane, L.; Satkowski, M. M.; Smith, S. D.; Spontak, R. J. Phase behavior and morphological characteristics of compositionally symmetric diblock copolymer blends. *Macromolecules* **1996**, *29*, 8862–8870.
- (61) Floudas, G.; Vlassopoulos, D.; Pitsikalis, M.; Hadjichristidis, N.; Stamm, M. Order-disorder transition and ordering kinetics in binary diblock copolymer mixtures of styrene and isoprene. *J. Chem. Phys.* **1996**, *104*, 2083–2088.
- (62) Spontak, R. J.; Fung, J. C.; Braunfeld, M. B.; Sedat, J. W.; Agard, D. A.; Kane, L.; Smith, S. D.; Satkowski, M. M.; Ashraf, A.; Hajduk, D. A.; Gruner, S. M. Phase behavior of ordered diblock copolymer blends: effect of compositional heterogeneity. *Macromolecules* **1996**, *29*, 4494–4507.
- (63) Yamaguchi, D.; Hashimoto, T.; Han, C. D.; Baek, D. M.; Kim, J. K.; Shi, A.-C. Order-Disorder Transition, Microdomain Structure, and Phase Behavior in Binary Mixtures of Low Molecular Weight Polystyrene-block-polyisoprene Copolymers. *Macromolecules* **1997**, *30*, 5832–5842.
- (64) Sakurai, S.; Umeda, H.; Yoshida, A.; Nomura, S. Anomalous temperature behavior of lamellar microdomain structures in binary blends of polystyrene-block-polyisoprene diblock copolymers. *Macromolecules* **1997**, *30*, 7614–7617.
- (65) Sakurai, S.; Irie, H.; Umeda, H.; Nomura, S.; Lee, H. H.; Kim, J. K. Gyroid structures and morphological control in binary blends of polystyrene-block-polyisoprene diblock copolymers. *Macromolecules* **1998**, *31*, 336–343.
- (66) Papadakis, C.; Mortensen, K.; Posselt, D. Phase behavior of binary blends of symmetric polystyrene-polybutadiene diblock copolymers studied using SANS. *European Physical Journal B-Condensed Matter and Complex Systems* **1998**, *4*, 325–332.
- (67) Yamaguchi, D.; Hashimoto, T. A phase diagram for the binary blends of nearly symmetric diblock copolymers. 1. Parameter space of molecular weight ratio and blend composition. *Macromolecules* **2001**, *34*, 6495–6505.
- (68) Yamaguchi, D.; Takenaka, M.; Hasegawa, H.; Hashimoto, T. Macro- and microphase transitions in binary blends of block copolymers with complementarily asymmetric compositions. *Macromolecules* **2001**, *34*, 1707–1719.
- (69) Yamaguchi, D.; Hasegawa, H.; Hashimoto, T. A phase diagram for the binary blends of nearly symmetric diblock copolymers. 2. Parameter space of temperature and blend composition. *Macromolecules* **2001**, *34*, 6506–6518.
- (70) Hashimoto, T.; Yamaguchi, D.; Court, F. Self-assembly in mixtures of block copolymers: “co-surfactant effects” on morphology control. *Macromol. Symp.* **2003**, *195*, 191–200.
- (71) Spontak, R. J. Self-Consistent Field Theory of Ordered Block Copolymer Blends. 1.(AB). α ./.(AB). β . Blends. *Macromolecules* **1994**, *27*, 6363–6370.
- (72) Dan, N.; Safran, S. Self-assembly in mixtures of diblock copolymers. *Macromolecules* **1994**, *27*, 5766–5772.
- (73) Matsen, M. Immiscibility of large and small symmetric diblock copolymers. *J. Chem. Phys.* **1995**, *103*, 3268–3271.
- (74) Matsen, M. W.; Bates, F. S. One-component approximation for binary diblock copolymer blends. *Macromolecules* **1995**, *28*, 7298–7300.
- (75) Morita, H.; Kawakatsu, T.; Doi, M.; Yamaguchi, D.; Takenaka, M.; Hashimoto, T. Competition between micro- and macrophase separations in a binary mixture of block copolymers. A dynamic density functional study. *Macromolecules* **2002**, *35*, 7473–7480.
- (76) Wang, Y.; Li, X.; Tang, P.; Yang, Y. Dynamics and order-disorder transitions in bidisperse diblock copolymer blends. *Physica B: Condensed Matter* **2011**, *406*, 1132–1138.
- (77) Padmanabhan, P.; Martinez-Veracoechea, F. J.; Araque, J. C.; Escobedo, F. A. A theoretical and simulation study of the self-assembly of a binary blend of diblock copolymers. *J. Chem. Phys.* **2012**, *136*, 234905.
- (78) Ndoni, S.; Papadakis, C. M.; Bates, F. S.; Almdal, K. Laboratory-scale setup for anionic polymerization under inert atmosphere. *Review of scientific instruments* **1995**, *66*, 1090–1095.
- (79) Bates, F. S.; Fredrickson, G. H. Block copolymer thermodynamics: theory and experiment. *Annu. Rev. Phys. Chem.* **1990**, *41*, 525–557.
- (80) Lyatskaya, J. V.; Zhulina, E.; Birshtein, T. Theory of supermolecular structures in polydisperse block copolymers: 4. Cylindrical domains in binary mixtures of diblock copolymers and cylinder-lamellae transition. *Polymer* **1992**, *33*, 343–351.
- (81) Spencer, R. K.; Matsen, M. W. Boundary Tension Between Coexisting Phases of a Block Copolymer Blend. *Macromolecules* **2015**, *48*, 2840–2848.
- (82) Sakurai, S.; Umeda, H.; Furukawa, C.; Irie, H.; Nomura, S.; Hyun Lee, H.; Kon Kim, J. Thermally induced morphological transition from lamella to gyroid in a binary blend of diblock copolymers. *J. Chem. Phys.* **1998**, *108*, 4333–4339.
- (83) Zhao, J.; Majumdar, B.; Schulz, M. F.; Bates, F. S.; Almdal, K.; Mortensen, K.; Hajduk, D. A.; Gruner, S. M. Phase behavior of pure diblocks and binary diblock blends of poly(ethylene)-poly(ethylene). *Macromolecules* **1996**, *29*, 1204–1215.
- (84) Olmsted, P. D.; Hamley, I. W. Lifshitz points in blends of AB and BC diblock copolymers. *EPL (Europhysics Letters)* **1999**, *45*, 83.
- (85) Jeon, H. G.; Hudson, S. D.; Ishida, H.; Smith, S. D. Microphase and macrophase transitions in binary blends of diblock copolymers. *Macromolecules* **1999**, *32*, 1803–1808.
- (86) Kimishima, K.; Jinnai, H.; Hashimoto, T. Control of self-assembled structures in binary mixtures of A-B diblock copolymer and A-C diblock copolymer by changing the interaction between B and C block chains. *Macromolecules* **1999**, *32*, 2585–2596.
- (87) Frielinghaus, H.; Hermsdorf, N.; Almdal, K.; Mortensen, K.; Messé, L.; Corvazier, L.; Fairclough, J.; Ryan, A.; Olmsted, P.; Hamley, I. Micro- vs. macro-phase separation in binary blends of poly(styrene)-poly(isoprene) and poly(isoprene)-poly(ethylene oxide) diblock copolymers. *EPL (Europhysics Letters)* **2001**, *53*, 680.
- (88) Frielinghaus, H.; Hermsdorf, N.; Sigel, R.; Almdal, K.; Mortensen, K.; Hamley, I.; Messé, L.; Corvazier, L.; Ryan, A.; Van Dusschoten, D.; Wilhelm, M.; Floudas, G.; Fytas, G. Blends of AB/BC diblock copolymers with a large interaction parameter χ . *Macromolecules* **2001**, *34*, 4907–4916.

- (89) Shi, A.-C.; Noolandi, J.; Hoffmann, H. Diblock copolymer blends as mixtures of surfactants and cosurfactants. *Macromolecules* **1994**, *27*, 6661–6664.
- (90) Shi, A.-C.; Noolandi, J. Effects of short diblocks at interfaces of strongly segregated long diblocks. *Macromolecules* **1994**, *27*, 2936–2944.
- (91) Lin, E. K.; Gast, A. P.; Shi, A.-C.; Noolandi, J.; Smith, S. D. Effect of short diblock copolymers at internal interfaces of large diblock copolymer mesophases. *Macromolecules* **1996**, *29*, 5920–5925.
- (92) Court, F.; Yamaguchi, D.; Hashimoto, T. Morphological and scattering studies of binary mixtures of block copolymers: Cosurfactant effects observed in the parameter space of temperature, blend composition, and molecular weight ratio. *Macromolecules* **2008**, *41*, 4828–4837.
- (93) Court, F.; Hashimoto, T. Morphological studies of binary mixtures of block copolymers. 1. Cosurfactant effects and composition dependence of morphology. *Macromolecules* **2001**, *34*, 2536–2545.
- (94) Court, F.; Hashimoto, T. Morphological studies of binary mixtures of block copolymers. 2. Chain organization of long and short blocks in lamellar microdomains and its effect on domain size and stability. *Macromolecules* **2002**, *35*, 2566–2575.
- (95) Court, F.; Yamaguchi, D.; Hashimoto, T. Morphological studies of binary mixtures of block copolymers: Temperature dependence of cosurfactant effects. *Macromolecules* **2006**, *39*, 2596–2605.
- (96) Chen, F.; Kondo, Y.; Hashimoto, T. Control of nanostructure in mixtures of block copolymers: Curvature control via cosurfactant effects. *Macromolecules* **2007**, *40*, 3714–3723.
- (97) Kim, K.; Arora, A.; Lewis III, R. M.; Liu, M.; Li, W.; Shi, A.-C.; Dorfman, K. D.; Bates, F. S. Origins of low-symmetry phases in asymmetric diblock copolymer melts. *Proc. Natl. Acad. Sci. U. S. A.* **2018**, *115*, 847–854.
- (98) Lindsay, A. P.; Cheong, G. K.; Peterson, A. J.; Weigand, S.; Dorfman, K. D.; Lodge, T. P.; Bates, F. S. Complex Phase Behavior in Particle-Forming AB/AB' Diblock Copolymer Blends with Variable Core Block Lengths. *Macromolecules* **2021**, *54*, 7088–7101.
- (99) Xie, J.; Li, Y.; Shi, A.-C. Binary Blends of Diblock Copolymers: An Efficient Route to Complex Spherical Packing Phases. *Macromol. Theory Simul.* **2021**, *30*, 2100053.
- (100) Frank, F. C.; Kasper, J. S. Complex alloy structures regarded as sphere packings. I. Definitions and basic principles. *Acta Crystallogr.* **1958**, *11*, 184–190.
- (101) Frank, F. C.; Kasper, J. S. Complex alloy structures regarded as sphere packings. II. Analysis and classification of representative structures. *Acta Crystallogr.* **1959**, *12*, 483–499.
- (102) Schulze, M. W.; Lewis III, R. M.; Lettow, J. H.; Hickey, R. J.; Gillard, T. M.; Hillmyer, M. A.; Bates, F. S. Conformational asymmetry and quasicrystal approximants in linear diblock copolymers. *Physical review letters* **2017**, *118*, 207801.
- (103) Bates, M. W.; Lequeieu, J.; Barbon, S. M.; Lewis III, R. M.; Delaney, K. T.; Anastasaki, A.; Hawker, C. J.; Fredrickson, G. H.; Bates, C. M. Stability of the A15 phase in diblock copolymer melts. *Proc. Natl. Acad. Sci. U. S. A.* **2019**, *116*, 13194–13199.
- (104) Bates, M. W.; Barbon, S. M.; Levi, A. E.; Lewis III, R. M.; Beech, H. K.; Vonk, K. M.; Zhang, C.; Fredrickson, G. H.; Hawker, C. J.; Bates, C. M. Synthesis and self-assembly of AB n miktoarm star polymers. *ACS Macro Lett.* **2020**, *9*, 396–403.
- (105) Zhao, F.; Dong, Q.; Li, Q.; Liu, M.; Li, W. Emergence and Stability of Exotic “Binary” HCP-Type Spherical Phase in Binary AB/AB Blends. *Macromolecules* **2022**, *55*, 10005–10013.
- (106) Hudson, D. R. Density and packing in an aggregate of mixed spheres. *J. Appl. Phys.* **1949**, *20*, 154–162.
- (107) Lai, C. T.; Shi, A.-C. Binary blends of diblock copolymers: An effective route to novel bicontinuous phases. *Macromol. Theory Simul.* **2021**, *30*, 2100019.
- (108) Matsen, M. W.; Schick, M. Stable and unstable phases of a diblock copolymer melt. *Phys. Rev. Lett.* **1994**, *72*, 2660.
- (109) Meuler, A. J.; Hillmyer, M. A.; Bates, F. S. Ordered network mesostructures in block polymer materials. *Macromolecules* **2009**, *42*, 7221–7250.
- (110) Matsen, M. W. The standard Gaussian model for block copolymer melts. *J. Phys.: Condens. Matter* **2002**, *14*, R21.
- (111) Matsen, M. W. Phase behavior of block copolymer/homopolymer blends. *Macromolecules* **1995**, *28*, 5765–5773.
- (112) Martinez-Veracoechea, F. J.; Escobedo, F. A. Bicontinuous phases in diblock copolymer/homopolymer blends: Simulation and self-consistent field theory. *Macromolecules* **2009**, *42*, 1775–1784.
- (113) Martinez-Veracoechea, F. J.; Escobedo, F. A. The Plumber's Nightmare Phase in Diblock Copolymer/Homopolymer Blends. A Self-Consistent Field Theory Study. *Macromolecules* **2009**, *42*, 9058–9062.
- (114) Takagi, H.; Yamamoto, K. Effect of Block Copolymer Composition and Homopolymer Molecular Weight on Ordered Bicontinuous Double-Diamond Structures in Binary Blends of Polystyrene-Polyisoprene Block Copolymer and Polyisoprene Homopolymer. *Macromolecules* **2021**, *54*, 5136–5143.
- (115) Magruder, B. R.; Park, S. J.; Collanton, R. P.; Bates, F. S.; Dorfman, K. D. Laves Phase Field in a Diblock Copolymer Alloy. *Macromolecules* **2022**, *55*, 2991–2998.
- (116) Case, L. J.; Bates, F. S.; Dorfman, K. D. Tuning conformational asymmetry in particle-forming diblock copolymer alloys. *Soft Matter* **2022**, *19*, 90–97.
- (117) Xie, J.; Lai, C. T.; Shi, A.-C. Regulating the Self-Assembly of AB/CD Diblock Copolymer Blends via Secondary Interactions. *J. Polym. Sci.* **2023**, *1* DOI: 10.1002/pol.20230306.
- (118) Feng, E. H.; Lee, W. B.; Fredrickson, G. H. Supramolecular diblock copolymers: A field-theoretic model and mean-field solution. *Macromolecules* **2007**, *40*, 693–702.
- (119) Dehghan, A.; Shi, A.-C. Modeling hydrogen bonding in diblock copolymer/homopolymer blends. *Macromolecules* **2013**, *46*, 5796–5805.
- (120) Chen, W.-C.; Kuo, S.-W.; Chang, F.-C. Self-assembly of an A-B diblock copolymer blended with a C homopolymer and a C-D diblock copolymer through hydrogen bonding interaction. *Polymer* **2010**, *51*, 4176–4184.
- (121) Tseng, T.-C.; Kuo, S.-W. Hydrogen-bonding strength influences hierarchical self-assembled structures in unusual miscible/immiscible Diblock copolymer blends. *Macromolecules* **2018**, *51*, 6451–6459.
- (122) Tseng, T.-C.; Kuo, S.-W. Hierarchical self-assembled structures from Diblock copolymer mixtures by competitive hydrogen bonding strength. *Molecules* **2018**, *23*, 2242.
- (123) Tseng, T.-C.; Kuo, S.-W. Hydrogen bonding induces unusual self-assembled structures from mixtures of two miscible disordered diblock copolymers. *Eur. Polym. J.* **2019**, *116*, 361–369.
- (124) Tsou, C.-T.; Kuo, S.-W. Competing hydrogen bonding interaction creates hierarchically ordered self-assembled structures of PMMA-b-P4VP/PVPh-b-PS mixtures. *Macromolecules* **2019**, *52*, 8374–8383.
- (125) Asari, T.; Matsuo, S.; Takano, A.; Matsushita, Y. Three-phase hierarchical structures from AB/CD diblock copolymer blends with complementary hydrogen bonding interaction. *Macromolecules* **2005**, *38*, 8811–8815.
- (126) Han, S. H.; Pryamitsyn, V.; Bae, D.; Kwak, J.; Ganesan, V.; Kim, J. K. Highly asymmetric lamellar nanopatterns via block copolymer blends capable of hydrogen bonding. *ACS Nano* **2012**, *6*, 7966–7972.
- (127) Tang, P.; Qiu, F.; Zhang, H.; Yang, Y. Morphology and phase diagram of complex block copolymers: ABC linear triblock copolymers. *Phys. Rev. E* **2004**, *69*, 031803.
- (128) Liu, M.; Li, W.; Qiu, F.; Shi, A.-C. Theoretical study of phase behavior of frustrated ABC linear triblock copolymers. *Macromolecules* **2012**, *45*, 9522–9530.
- (129) Pryamitsyn, V.; Han, S. H.; Kim, J. K.; Ganesan, V. Curvature modification of block copolymer microdomains using blends of block

copolymers with hydrogen bonding interactions. *Macromolecules* **2012**, *45*, 8729–8742.

(130) Zhang, X.; Lin, J.; Wang, L.; Zhang, L.; Lin, J.; Gao, L. Supramolecular assembly of diblock copolymer blends with hydrogen-bonding interactions modeled by Yukawa potentials. *Polymer* **2015**, *78*, 69–80.

(131) Ahmadian, I.; Peters, A. J. Phase behavior of AB/CD diblock copolymer blends via coarse-grained simulation. *Soft Matter* **2020**, *16*, 3069–3081.

(132) Park, S. J.; Bates, F. S.; Dorfman, K. D. Complex Phase Behavior in Binary Blends of AB Diblock Copolymer and ABC Triblock Terpolymer. *Macromolecules* **2023**, *56*, 1278–1288.

(133) He, W.; Wang, F.; Qiang, Y.; Pan, Y.; Li, W.; Liu, M. Asymmetric Binary Spherical Phases Self-Assembled by Mixing AB Diblock/ABC Triblock Copolymers. *Macromolecules* **2023**, *56*, 719.

(134) Bates, F. S.; Hillmyer, M. A.; Lodge, T. P.; Bates, C. M.; Delaney, K. T.; Fredrickson, G. H. Multiblock polymers: Panacea or Pandora's box? *Science* **2012**, *336*, 434–440.

Chapter 4

Formation of Complex Spherical Packing Phases in Diblock Copolymer/Homopolymer Blends

Publication: Xie, Jiayu, and An-Chang Shi. “Formation of complex spherical packing phases in diblock copolymer/homopolymer blends.” *Giant* 5 (2021): 100043.

Authors: **Jiayu Xie**, An-Chang Shi

Contribution: As the first author, my contributions included developing the theoretical model and computational code, data generation and analysis, and drafting the initial manuscript. Dr. An-Chang Shi and I collaborated on manuscript revisions, with guidance from Dr. Shi throughout the research.

Preface

In this chapter, we investigate the formation of complex Frank-Kasper phases in binary blends of A_1B_1 copolymers and A_2 homopolymers. Recent experiments on A_1B_1/A_2 blends revealed a novel morphological progression: $\sigma \rightarrow C14 \rightarrow C15$ phases [70, 77]. SCFT calculations based on the Gaussian chain model confirmed these observations [90]. While previous SCFT studies indicated a positive correlation between particle-size differences in equilibrium morphologies and the capacity to accommodate homopolymers, the formation and transition mechanisms of these structures remain unclear. Additionally, a significant portion of the phase space of this system remains unexplored.

In our study, we address these gaps by systematically exploring the phase behaviour of A_1B_1/A_2 blends. Instead of the standard SCFT based on Gaussian chains, we adopt the freely-jointed chain model. This allows us to assess if the theoretical results are sensitive to the choice of polymer chain model and also provides a better description of low-molecular-weight or short polymers. Through the construction of phase diagrams with various parameters, the dependence of the phase behaviour on the different parameters is uncovered. Moreover, we perform a detailed analysis of the homopolymer distribution and its effects on the domain properties of different phases, which sheds light on the mechanisms behind the formation of complex spherical phases and the novel morphological transitions observed in experiments.



Formation of complex spherical packing phases in diblock copolymer/homopolymer blends

Full-length article

Jiayu Xie, An-Chang Shi*

Department of Physics and Astronomy, McMaster University, 1280 Main Street West, Hamilton, Ontario, Canada L8S 4M1

Keywords: Self-Assembly, Block copolymers, Self-Consistent field theory, Frank-Kasper phases

The formation and relative stability of spherical packing phases in binary blends composed of AB-diblock copolymers and A-homopolymers are systematically studied using the self-consistent field theory applied to the freely-jointed chain model of polymers. Phase diagrams with different model parameters of the blends are constructed, revealing that the emergence of various complex spherical packing phases, including the Frank-Kasper σ phase and the Laves C14 and C15 phases, could be induced by the addition of the homopolymers. For BCC-forming diblock copolymers, a phase transition sequence of BCC \rightarrow σ \rightarrow C14 \rightarrow C15 is predicted when the homopolymer concentration is increased. An analysis of the properties of A-domains reveals that their sizes are regulated by the differential localization of A-homopolymers. The resultant spherical domains of different sizes is a key factor to stabilize complex spherical packing phases, especially the Laves C14 and C15 phases. Furthermore, the phase behaviour is strongly affected by the chain length of the homopolymers. In particular, the addition of short homopolymers results in an expanded region of the cylindrical phase, whereas the addition of long homopolymers stabilizes the complex spherical packing phases. The theoretical results from current study are in good agreement with recent experiments and theory, and shed light to the formation of complex spherical packing phases in other self-assembling soft matter systems.

Introduction

The packing problem is a fascinating topic with a long history that could be traced back to the early 17th century [1]. One example is the Kepler problem concerning the ordered close packing of hard spheres. It is now well-established that, for identical hard spheres in three-dimensional space, the close packing structures are the face-centered cubic (FCC) and hexagonal close packing (HCP) lattices. The packing problem becomes drastically complicated

if the objects being packed are deformable and/or nonuniform, resulting in multiple possible solutions depending on the property of the system [1]. In particular, the Frank-Kasper (FK) phases, composed of at least two distinct types of particles with different coordination numbers, *i.e.* CN=12, 14, 15 or 16, represent a class of possible solutions to the packing problems of nonidentical and/or soft spheres [2,3].

In hard condensed matter, complex spherical packing phases are commonly observed in metallic alloys, in which atoms of different sizes pack into ordered structures [4]. In soft condensed matter, the spherical domains are usually deformable. Therefore, complex spherical packing phases are expected to occur. Indeed,

* Corresponding author.

E-mail addresses: xiej33@mcmaster.ca (J. Xie), shi@mcmaster.ca (A.-C. Shi).

Received 3 November 2020; Received in revised form 18 December 2020; Accepted 20 December 2020

in recent years complex spherical packing phases, *e.g.* the FK A15, σ phases and Laves C14, C15 phases, have been experimentally observed in various soft matter systems including block copolymers (BCPs) [5–17], supramolecular dendrimer systems [18–20], giant surfactants or shape amphiphiles [21–23] and aqueous surfactant solutions [24–27]. Along with the experimental studies on polymeric systems containing block copolymers, a considerable number of theoretical studies have been carried out aiming to reveal the formation mechanisms of these novel and complex spherical packing phases [28–37].

In soft matter systems with long-range order, the “atoms” or particles are usually self-assembled from smaller molecules such as block copolymers or surfactants. In order to form a crystalline structure, the particles need to be deformed from a perfect sphere towards the polyhedral shape resembling the enclosing Wigner-Seitz cell (WSC) in order to fill out the space with a uniform spatial density [38]. The average sphericity can be measured by the average isoperimetric quotient (IQ) of the WSCs. The deformation of the self-assembled particles away from their ideal spherical shape costs a free energy penalty so that structures with rounder WSCs is preferred from this perspective. A generic feature of the complex FK phases is that their Wigner-Seitz cells have higher average sphericity than those of the classical spherical phases such as body-centered cubic (BCC) phase [32,38]. Based on this argument, it has been proposed that one possible mechanism to stabilize FK phases is to enlarge the particles so that larger particle deformations are required to form the ordered packing, whereas at the same time to prevent the system transferring to non-spherical (cylindrical) phases. For example, it has been predicted theoretically [29] and confirmed experimentally [6,7,13] that introducing conformational asymmetry for diblock copolymers is one of such approaches to stabilize the FK A15 and σ phases in AB diblock copolymer melts. At the same time, theoretical results have demonstrated that the Laves C14 and C15 phases are metastable phases of AB diblock copolymer melts [14]. It is important to note that the complex spherical packing phases contain a number of symmetrically inequivalent WSCs with different volumes. The volume difference of the different cells is relatively small for the FK A15 and σ phases but becomes quite large for the Laves C14 and C15 phases. Therefore, the formation of the Laves phases in monodisperse block copolymer melts is not favoured because it requires larger volume exchange among the spherical domains.

An effective route to alleviate the free energy cost of domain-size variation in block copolymers is to blend different polymeric species into the system. For example, it has been shown theoretically [30,39] and experimentally [15] that a large region of complex spherical packing phases including FK A15 and σ and Laves C14 and C15 phases appears in binary AB/AB blends composed of AB diblock copolymers with different molecular weights and compositions. Furthermore, stable Laves C14 and/or C15 phases have been observed in experiments carried out by Baez-Cotto *et al.* [26] on oil-containing aqueous surfactant solutions and by J. Mueller *et al.* [17] on binary blends composed of AB diblock polymers and A-homopolymers. One common feature of these two systems is the existence of a component that is compatible with, and localizes inside, the core of the

spherical domains thus regulating the volume of the particles. Specifically, it has been argued that the uneven distribution of the swelling component (oil or homopolymer) facilitates the formation of domains with sizes commensurate with the structure of the C14 and C15 phases. This qualitative argument could be made concrete by quantitative theoretical studies. Indeed the phase behaviour of binary blends composed of AB-type block copolymers and A-homopolymers has been studied theoretically using the self-consistent field theory (SCFT) applied to Gaussian chain models by Zhao *et al.* for AB₄/A blends [33] and very recently by Cheong *et al.* [34] for AB/A blends. These theoretical studies provide a quantitative confirmation of the mechanism associated with homopolymer localization in different domains. Predictions from these theoretical studies are in good agreement with the experimentally observed phase transition sequences. Furthermore, these studies also considered the role played by the molecular weight of the homopolymer additives on the phase behaviour of the blending system. It has been found that the phase behaviour of the AB/A blends depends on the chain length ratio (α) between the A-homopolymer and the A-block of the copolymer. In agreement with experiments, the theoretical phase diagrams reveal that the FK σ , Laves C14 and C15 phases are stabilized in the phase portrait in the case of $\alpha \geq 1$ but they disappear and replaced by hexagonal close packing cylinders (HEX) in the case of $\alpha < 1$.

The aforementioned recent experimental observations and theoretical calculations have offered a good insight to the formation principles of complex spherical packing phases in various block copolymer blends including binary AB/AB and AB/A blends. For the simplest model system composed of AB-diblock copolymers and A-homopolymers, the recent SCFT study of Cheong *et al.* [34] provided a timely examination on the effect of homopolymer additives to the phase behaviour of the system. However, a systematic theoretical investigation with phase diagrams covering a larger parameter space for polymer blends containing various block copolymers is still lacking. It is therefore desirable to carry out a systematic theoretical study for polymeric blends containing block copolymers that exhibit various complex spherical packing phases. Such a systematic study would provide a comprehensive understanding of the complex spherical packing problem in soft matter systems.

In the current work, we carry out a systematic study of the phase behaviour of binary AB/A blends composed of AB diblock copolymers and A-homopolymers using the self-consistent field theory applied to the freely jointed chain model. Compared with the commonly used Gaussian chain model, the freely-jointed chain (FJC) model has a great computational advantage when proper numerical methods are adopted [40,41]. More importantly, the FJC model provides a more proper description of experimental systems containing low-molecular weight polymers. The FJC model is characterized by a finite segment number N and an interaction potential with a finite interaction range. It approaches the Gaussian chain model at the large- N limit. Therefore, the theoretical results obtained from the FJC model should be consistent with those based on Gaussian chain model. We focus on the effects of the following four parameters on the phase behaviour of the AB/A blends: (1) the conformational asymmetry

ϵ of the diblock copolymers, (2) the average concentration ϕ_2 of the A-homopolymers, (3) the chain length ratio α between that of the A-homopolymer and the A-block of the diblock copolymer, and (4) the volume fraction of A-block f . We will start with the construction of phase diagrams in the $\chi_{AB} - \phi_2$ plane in a large range of χ_{AB} from 0.15 to 0.5 and ϕ_2 from 0 to 0.17 with different values of ϵ , α and f . The phase diagrams will be compared with the experimental phase portraits reported by Mueller et al. [17] and the theoretical phase diagrams of Cheong et al. [34]. Next, we will provide a detailed examination on the partitioning of the A-homopolymers in different WSCs for each phase, and the properties of the enclosing minority domains. A free energy analysis of the different phases is also given, thus shedding light on the mechanisms regulating the phase behaviour of the system.

Theoretical Model and Method

Our theoretical model is a binary blend composed of n_1 linear AB-type diblock copolymers and n_2 A-homopolymers in a volume V . Each AB diblock copolymer is composed of N_A A-segments and N_B B-segments, thus the total number of segments is $N = N_A + N_B$ with $N - 1$ bonds. The volume fractions of the A and B blocks are given by $f_A = f$ and $f_B = 1 - f$, respectively. Each A-homopolymer has N_{Ah} A-segments, the ratio between the length of the homopolymer and A-block of the diblock copolymer is $\alpha = N_{Ah}/N_A = N_{Ah}/fN$. We assume a uniform segment density ρ_0 so that we have $\rho_0 V = n_1 N + n_2 \alpha f N$ according to incompressibility condition. The average concentrations of the AB diblock copolymers and the A-homopolymers are given by,

$$\phi_1 = \frac{n_1 N}{\rho_0 V}, \quad \phi_2 = 1 - \phi_1 = \frac{n_2 \alpha f N}{\rho_0 V}.$$

The interaction potential between the segments can be divided into bonded and non-bonded contributions. The bonded potential $b_\alpha(R_i)$ and non-bonded interaction energy U are chosen to have the form,

$$b_\alpha(R_i) = -k_B T \ln \delta(R_i - b_\alpha),$$

$$U = k_B T \rho_0 \chi_{AB} \int u(|\vec{r} - \vec{r}'|) \hat{\phi}_A(\vec{r}) \hat{\phi}_B(\vec{r}') d\vec{r} d\vec{r}',$$

where χ_{AB} is the Flory-Huggins parameter quantifying the interaction between A and B segments, b_α is the Kuhn length of the α -segment, $\hat{\phi}_\alpha(\vec{r}) = (1/\rho_0) \sum_i \delta(\vec{r} - \vec{r}_{\alpha i})$, is the density (concentration) operator of α -segment with $\alpha=A$ or B and $u(|\vec{r} - \vec{r}'|)$ is the interaction potential function accounting for the finite range interactions.

For polymer blends, it is convenient to formulate the theory in grand canonical ensemble where the thermodynamic control parameters are the chemical potentials of the AB-copolymers, μ_1 , and the A-homopolymers, μ_2 . Within the scope of the self-consistent field theory [42], the grand potential Φ of the system can be expressed as,

$$\frac{N\Phi}{\rho_0 V k_B T} = -e^{\mu_1/k_B T} Q_1 - e^{\mu_2/k_B T} Q_2 - \frac{1}{V} \int d\vec{r} [\omega_A(\vec{r}) \phi_A(\vec{r}) + \omega_B(\vec{r}) \phi_B(\vec{r}) - \chi_{AB} N \int u(|\vec{r} - \vec{r}'|) \phi_A(\vec{r}) \phi_B(\vec{r}') d\vec{r}' + \eta(\vec{r}) (1 - \phi_A(\vec{r}) - \phi_B(\vec{r}))]. \quad (1)$$

where the quantity Q_κ with $\kappa=1$ or 2 denotes the single chain partition function of the AB-copolymer and the A-homopolymer, respectively. $\phi_\alpha(\vec{r})$ is the ensemble average of $\hat{\phi}_\alpha(\vec{r})$, $\omega_\alpha(\vec{r})$ is the conjugate field of the α -segments and $\eta(\vec{r})$ is the Lagrange

multiplier that enforces the incompressibility condition. The total A-concentration is given by,

$$\phi_A(\vec{r}) = \phi_{Ad}(\vec{r}) + \phi_{Ah}(\vec{r}),$$

where $\phi_{Ad}(\vec{r})$ and $\phi_{Ah}(\vec{r})$ are the concentrations of the A-segments from the AB diblock copolymers and the A-homopolymers, respectively. Minimizing the grand potential with respect to the concentrations and conjugate fields leads to the following set of self-consistent equations,

$$\begin{cases} \omega_A(\vec{r}) = \chi_{AB} N \int u(R) \phi_B(\vec{r} - \vec{R}) dR + \eta(\vec{r}), \\ \omega_B(\vec{r}) = \chi_{AB} N \int u(R) \phi_A(\vec{r} - \vec{R}) dR + \eta(\vec{r}), \\ \phi_A(\vec{r}) = \frac{e^{\mu_1(\vec{r})}}{N} \sum_{i=1}^{N_A} q_1(i, \vec{r}) q_1^\dagger(i, \vec{r}), \\ \quad + e^{\mu_1/k_B T} \frac{e^{\mu_2(\vec{r})}}{N} \sum_{i=1}^{N_{Ah}} q_2(i, \vec{r}) q_2^\dagger(i, \vec{r}), \\ \phi_B(\vec{r}) = \frac{e^{\mu_2(\vec{r})}}{N} \sum_{i=N_A+1}^{N_B} q_1(i, \vec{r}) q_1^\dagger(i, \vec{r}), \\ \phi_A(\vec{r}) + \phi_B(\vec{r}) = 1, \end{cases} \quad (2)$$

where $\vec{R} = \vec{r} - \vec{r}'$ and $R = |\vec{R}|$. We have used the incompressibility condition to set the chemical potential μ_1 for the diblock copolymers to 0, so that the subscript of μ_2 has been dropped for simplicity. Once the SCFT equations (Eqs 2) are solved, the average concentrations of the different components can be simply calculated by, $\phi_1 = Q_1$ and $\phi_2 = 1 - \phi_1$. In Eqs 2, the forward propagator $q(i, \vec{r})$ is calculated iteratively by,

$$q_\kappa(\vec{r}_{i+1}, i+1) = e^{-\omega_\alpha(\vec{r}_{i+1})} \int d\vec{r}' g_\alpha(\vec{r}_{i+1} - \vec{r}_i) q_\kappa(\vec{r}_i, i), \quad (3)$$

where $g_\alpha(\vec{r}_{i+1} - \vec{r}_i)$ is the bond transition probability and it has the form,

$$g_\alpha(\vec{R}_i) = \frac{1}{4\pi b_\alpha^2} \delta(|\vec{R}_i| - b_\alpha),$$

where $\vec{R}_i = \vec{r}_{i+1} - \vec{r}_i$. The initial condition of the propagator is $q_\kappa(\vec{r}, 1) = \exp[-\omega_\alpha(\vec{r})]$. The computation of the backward propagator is performed similarly with iterations running in the opposite direction. Finally, the single chain partition function Q_κ is determined by,

$$Q_\kappa = \frac{1}{V} \int d\vec{r} N_\kappa q_\kappa(\vec{r}_{N_\kappa}, N_\kappa). \quad (4)$$

One efficient numerical method to solve the above SCFT equations is the pseudo-spectral method. In the pseudo-spectral scheme, firstly, the iteration equation Eq. 3 is performed in real space and Fourier space alternately by transferring $q(\vec{r}_i, i)$ forth and back between these two spaces,

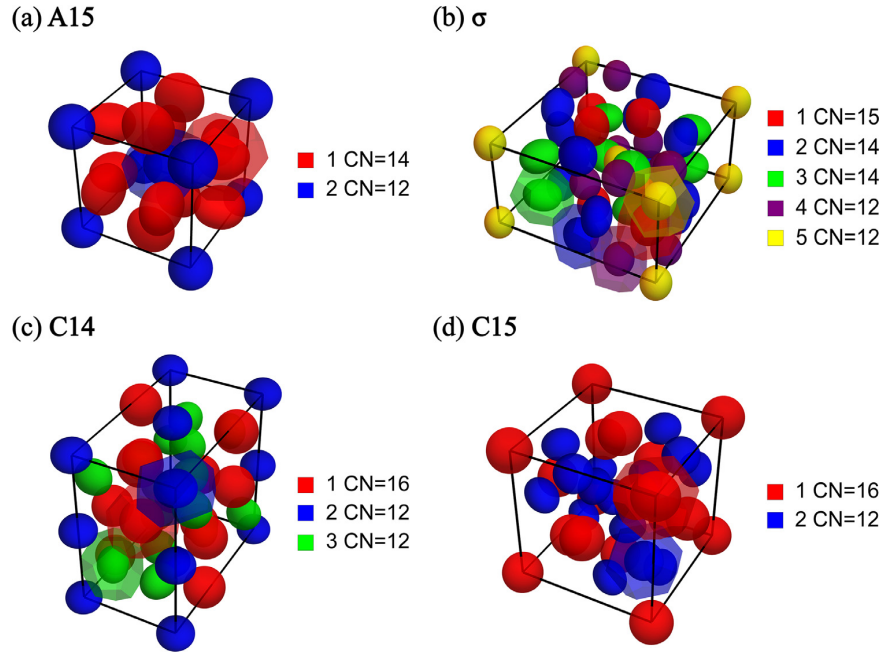
$$\begin{aligned} q_\kappa(\vec{r}_{i+1}, i+1) &= e^{-\omega_\alpha(\vec{r}_{i+1})} \mathcal{F}^{-1} \left\{ g_\alpha(\vec{k}) \mathcal{F} \left\{ q_\kappa(\vec{r}_i, i) \right\} \right\}, \\ &= e^{-\omega_\alpha(\vec{r}_{i+1})} \mathcal{F}^{-1} \left\{ g_\alpha(\vec{k}) q_\kappa(\vec{k}, i) \right\}. \end{aligned} \quad (5)$$

Secondly, the first two equations in Eq. 2 are performed in Fourier space,

$$\begin{aligned} \omega_A^{out}(\vec{k}) &= \chi_{AB} N \phi_B(\vec{k}) u(\vec{k}) + \eta(\vec{k}), \\ \omega_B^{out}(\vec{k}) &= \chi_{AB} N \phi_A(\vec{k}) u(\vec{k}) + \eta(\vec{k}). \end{aligned} \quad (6)$$

Finally, the grand potential density is also calculated in Fourier space by,

$$\frac{N\Phi}{\rho_0 V k_B T} = -e^{\mu_1/k_B T} Q_1 - e^{\mu_2/k_B T} Q_2 - \sum_{\vec{k}} \left[\omega_A(\vec{k}) \cdot \phi_A(\vec{k}) + \omega_B(\vec{k}) \cdot \phi_B(\vec{k}) - \chi_{AB} N u(k) \phi_A(\vec{k}) \cdot \phi_B(\vec{k}) \right].$$


Fig. 1

The $\phi_A(\vec{r}) = \phi_B(\vec{r})$ isosurface plots and representative WSCs for the complex spherical packing phases. (a)A15, (b) σ , (c)C14 and (d)C15. Each WSC is color coded and numbered, along with its coordination number (CN) for each type of particle.

(7)

where the dot product between two functions in k -space is defined by,

$$f(\vec{k}) \cdot g(\vec{k}) = f(\vec{k})g(-\vec{k}).$$

The period of each ordered structure needs to be optimized. This optimization is carried out simultaneously with the other SCFT equations by using the variable-cell Anderson-mixing scheme [43–45] with a modified stress residual due to the different chain model,

$$d\left(\frac{-N\Phi}{\rho_0 V k_B T}\right)/d\theta_l = -\sum_{\kappa=1}^2 e^{\mu_{\kappa}/k_B T} \sum_{\vec{k}} \frac{dg_{\kappa}(k)}{dk^2} \frac{dk^2}{d\theta_l} \sum_{i=1}^{N_{\kappa}-1} q_{\kappa}(\vec{k}, i) \cdot q_{\kappa}^{\dagger}(\vec{k}, i+1) + \chi_{AB} N \sum_{\vec{k}} \frac{du(k)}{dk^2} \frac{dk^2}{d\theta_l} \phi_A(\vec{k}) \cdot \phi_B(\vec{k}). \quad (8)$$

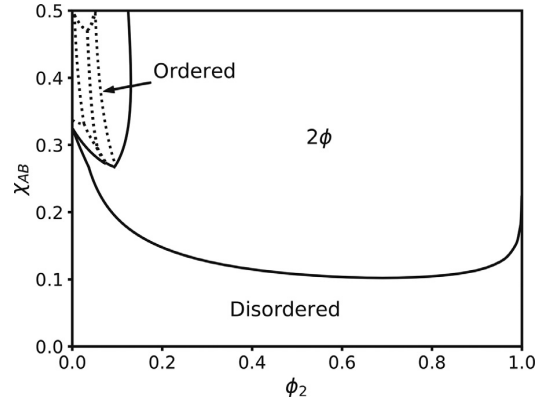
For the freely-jointed chain model, the bond transition probability and its Fourier transform are given by,

$$g(R) = \frac{1}{4\pi b^2} \delta(R-b), \quad g(k) = \frac{\sin(kb)}{kb}.$$

The non-bonded finite range interaction potential is assumed to have the Gaussian form,

$$u(R) = \left(\frac{3}{2\pi r_0^2}\right)^{\frac{3}{2}} e^{-\frac{3R^2}{2r_0^2}}, \quad u(k) = e^{-\frac{k^2 r_0^2}{6}},$$

which is normalized over the whole space, *i.e.* $\int u(R)d\vec{R} = 1$. In the current study we fix the number of segments of each AB-copolymer chain to be $N_{AB} = N=80$ and the interaction range to be $r_0 = \sqrt{3}b_A$, with which the FJC behaves closely as


Fig. 2

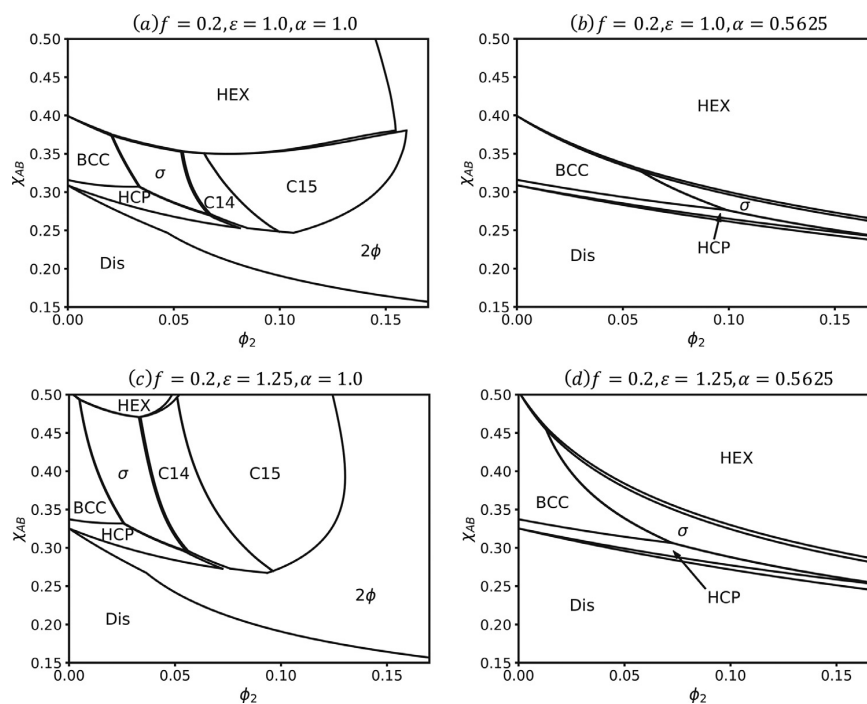
Phase diagram in the $\chi_{AB} - \phi_2$ plane with $f = 0.2$, $\epsilon = 1.25$ and $\alpha = 1.0$. The phase diagram is dominated by a large two-phase region. However, a rich phase behaviour featuring numerous order-order transitions is found in the block copolymer rich region. Detailed phase boundaries between the ordered phases are shown in Fig. 3(c).

Gaussian chain with a slight shifts of the phase boundaries[40]. Furthermore, the conformationally asymmetry of the AB diblock copolymers is characterized by the parameter $\epsilon = b_A/b_B$.

Results and Discussion

Phase behaviour of the AB/A blends

The phase behaviour of the AB/A blends is controlled by a number of parameters. In what follows the theoretical results are

**Fig. 3**

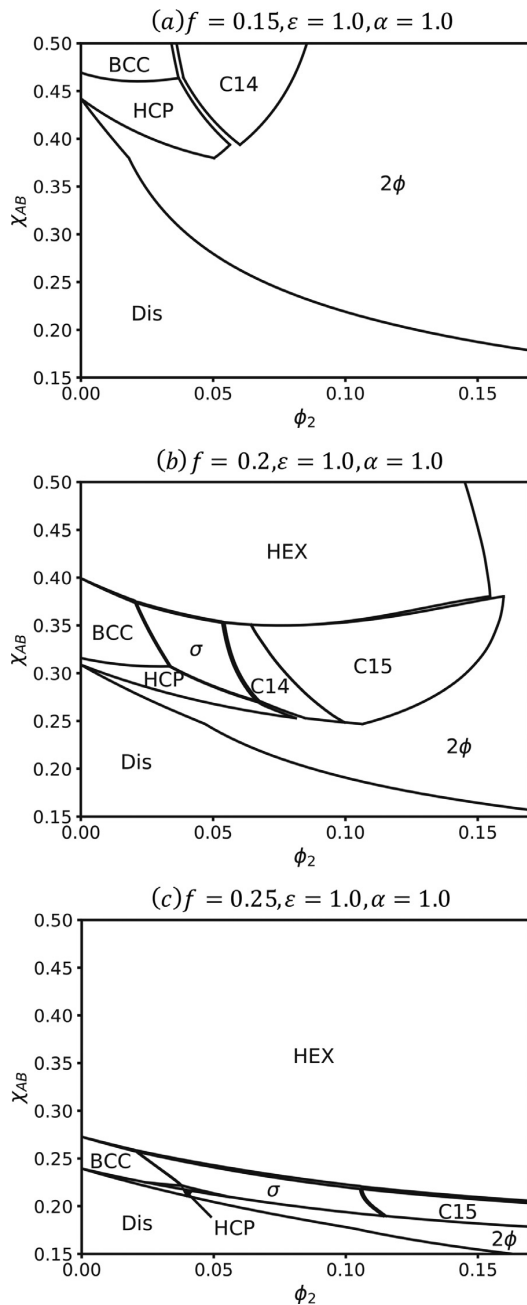
Phase diagrams in the $\chi_{AB} - \phi_2$ plane with (a) $f = 0.2, \epsilon = 1.0, \alpha = 1.0$ (b) $f = 0.2, \epsilon = 1.0, \alpha = 0.5625$ (c) $f = 0.2, \epsilon = 1.25, \alpha = 1.0$, (d) $f = 0.2, \epsilon = 1.25, \alpha = 0.5625$. The unlabeled regions are the two-phase coexistence region between two adjacent single phases. This set of phase diagrams highlights the effects of varying α and ϵ .

summarized in a set of phase diagrams constructed to cover a large region of the parameter space of the system. Specifically, phase diagrams are presented in the $\chi_{AB} - \phi_2$ plane for different values of f , ϵ and α . The phase diagrams are constructed by comparing the grand potential density of different candidate phases. The set of candidate ordered phases used in the current study includes the complex spherical packing phases, *i.e.* A15, σ , C14 and C15 shown schematically in Fig. 1, and the classical ordered phases, *i.e.* lamellae (L), BCC, HCP, HEX and the double gyroid (DG). In order to focus on the spherical packing phases, the A-block volume fraction of the AB diblock copolymers is chosen to be the minority block with $f = 0.15, 0.20$ and 0.25 . At the same time, the effect of the conformational asymmetry of the AB diblock copolymers on the phase behaviour is examined by constructing phase diagrams for $\epsilon = 1.0$ and $\epsilon = 1.25$. For each value of ϵ , two cases with $\alpha = 1.0$ and $\alpha = 0.5625$, representing dry and wet brush regimes of the A-blocks, have been investigated to demonstrate the effect of the homopolymer length. Finally, to study the effect of the volume fraction of A-blocks (f), phase diagrams with $\epsilon = 1.0, \alpha = 1.0$ and different values of f ($=0.15, 0.2, 0.25$) are constructed. This choice of parameters results in a set of phase diagrams in the $\chi_{AB} - \phi_2$ plane covering a rather large region of the parameter space.

One important feature of polymer blends is the existence of two-phase regions due to macroscopic phase separation. The phase diagram of the AB/A blends in the whole range of $0 < \phi_2 < 1$ would naturally contain a large two-phase region due to the macroscopic separation of the homopolymer-rich and block-

copolymer-rich phases. A typical phase diagram containing a large two-phase region is shown in Fig. 2 for the case of $f = 0.2, \epsilon = 1.25$ and $\alpha = 1.0$. It is obvious that the phase diagram in the whole range of $0 < \phi_2 < 1$ is dominated by a very large and featureless two-phase (2ϕ) region, whereas the single-phase region of the ordered phases is located at the small ϕ_2 area where the diblock copolymers are the majority component. Because the current study focuses on the spherical packing phases, in what follows we present a set of phase diagrams, shown in Fig. 3 and 4, in the $\chi_{AB} - \phi_2$ plane with the $0.15 < \chi_{AB} < 0.5$ and $0 < \phi_2 < 0.17$, respectively. This choice of parameters covers the order-to-disorder transitions and, at the same time, highlights the order-to-order transitions of the system.

The representative phase diagrams of binary blends composed of AB diblock copolymers and A-homopolymers shown in Figs. 3 and 4 exhibit a number of interesting features. The vertical axis at $\phi_2 = 0$ on the phase diagrams represents the phase behaviour of neat AB diblock copolymers with a given volume fraction (f) of the A-blocks. When χ_{AB} is increased, the neat AB diblock copolymers ($\phi_2 = 0$) with $f = 0.15, 0.20$ and 0.25 undergoes a disorder to order transition into the spherical packing phases, eventually reaching the hexagonally-packed cylindrical phase (HEX). The spherical packing phases of the neat diblock copolymers are the classical ones (HCP and BCC) because the conformational asymmetry parameter ($\epsilon = 1$ and 1.25) used in the current study is not large enough to stabilize the complex spherical packing phases [29]. The region of $\phi_2 > 0$ on the phase diagrams (Fig. 3 and 4) represents binary blends of AB

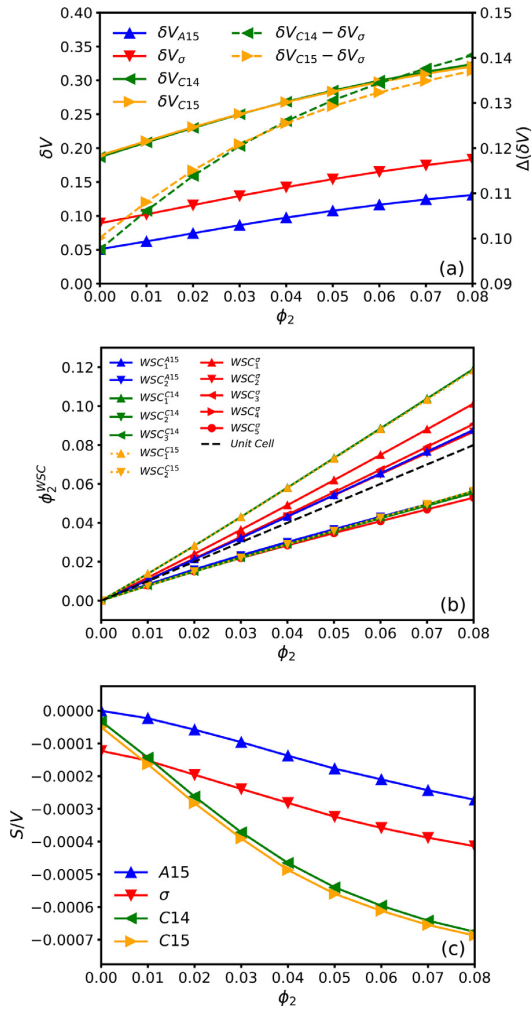
**Fig. 4**

Phase diagrams in the $\chi_{AB} - \phi_2$ plane with (a) $f = 0.15$, $\epsilon = 1.0$, $\alpha = 1.0$ (b) $f = 0.20$, $\epsilon = 1.0$, $\alpha = 1.0$ (c) $f = 0.25$, $\epsilon = 1.0$, $\alpha = 1.0$. The unlabeled regions are the two-phase coexistence region between two adjacent single phases. Fig. 4(b) is the same as Fig. 3(a), which is reproduced here to highlight the effects of varying f .

diblock copolymers and A-homopolymers. An obvious, albeit nontrivial, conclusion from the phase diagrams is that the addition of the A-homopolymers induces more order-to-order phase transitions, particularly transitions from classical spherical phases (BCC or HCP) to the complex spherical packing phases. The two-phase region between the copolymer-rich ordered phases and homopolymer-rich disordered phase is very large as illustrated in Fig. 2. On the other hand, the two-phase regions between the ordered phases are generally very narrow as shown in Figs. 3 and 4. The occurrence of complex spherical packing phases depends sensitively on the chain length ratio α between the homopolymers and the A-blocks. For the case of $\alpha < 1$, the complex spherical packing phases are largely suppressed while the relative stability of the cylindrical phase (HEX) is enhanced. This feature is clearly evidenced by the drastic change of the phase behaviours when α is changed from $\alpha = 1$ (Figs. 3(a) and (c)) to $\alpha = 0.5625$ (Figs. 3(b) and (d)). Another interesting feature is that increasing A-volume fraction f of the block copolymers also leads to an enhanced stability of the cylindrical phase as shown by a comparison of the phase diagrams shown in Figs. 4(a), (b), and (c), corresponding to $f = 0.15$, 0.20 and 0.25. A larger value of f favours the ordering of the blends and the occurrence of the cylindrical phase.

For diblock copolymers with $f = 0.20$, the addition of A-homopolymers, or the increase of ϕ_2 , results in a phase transition sequence from BCC to σ , C14 and C15 in a sizeable window of χ_{AB} (Figs. 3(a) and (c)). It should be noted that conformational asymmetry is not a prerequisite for the emergence of the complex spherical packing phases (σ , C14 and C15), although larger conformational asymmetry does lead to a wider χ_{AB} -window for the complex spherical packing phases (Fig. 3(c) vs. (a)). For example, for the case of $\alpha = 1.0$, increasing ϵ from 1.0 to 1.25 pushes the phase boundary between the spherical phases and HEX phase from $\chi_{AB} \approx 0.36$ to ≈ 0.475 . For neat block copolymer melts, it has been established theoretically [29] and experimentally [6,7,13] that conformational asymmetry of the block copolymers, quantified by the parameter ϵ , is a key factor to stabilize the FK A15 and σ phases. However, the Laves C14 and C15 phases have been shown to be metastable phases of neat diblock copolymers [14]. In agreement with previous experimental [17] and theoretical studies [34], the phase diagrams shown in Fig. 3 predict that the FK σ phase as well as the Laves C14 and C15 phases could become stable phases when A-homopolymers are added to the system. In particular, the predicted phase transition sequence (Fig. 3(a) and (c)) of BCC \rightarrow $\sigma \rightarrow$ C14 \rightarrow C15 when ϕ_2 is increased is in excellent agreement with that observed from the experiments of Mueller et al. [17] and theoretical studies of Cheong et al. [34]. Consistently, the emergence of complex spherical packing phases is also observed to occur in binary mixtures of AB/AB diblock copolymers [15,30,39] or in binary blend of A-homopolymer and AB₄ miktoarm star copolymer [33]. One interesting observation is that the FK A15 phase is missing from the phase diagrams shown in Fig. 3 and 4, implying that a larger conformational asymmetry parameter might be required to stabilize the A15 phase.

The theoretically predicted emergence of complex spherical packing phases in binary blends of diblock copolymers and homopolymers is in good agreement with the recent experimental


Fig. 5

(a) The standard deviation of particle volume δV , (b) the normalized concentration of A-homopolymers in different WSCs and (c) the interfacial area per unit volume of complex phases relative to that of the BCC with $\epsilon = 1.25$, $\alpha = 1.0$ and $\chi_{AB} = 0.45$. In (a), the solid lines follow the y-axis on the left side and the dashed lines follow the y-axis on the right side. The lines for the C15 phase in (b) are plotted in dotted style to distinguish them from those for the C14 phase because they almost overlap.

results of binary blends of poly(styrene-*b*-1,4-butadiene)/(1,4-butadiene) by Mueller et al. [17] and theoretical results of AB/A blends by Cheong et al. [34]. It should be noted that, although the recent SCFT study of Cheong et al. [34] and the current study share the same theoretical framework of the self-consistent field theory, a number of differences exist between these two contributions. First of all, the current study employs the FJC model of polymers, whereas Cheong et al. modelled the polymers as Gaussian chains. Therefore the current model may provide a better description for low molecular weight block copolymers and homopolymers. Secondly, the current study provides a more complete picture of the phase behaviour of the AB/A blends by extending the phase

diagrams in the $\chi_{AB} - \phi_2$ plane for a set of parameters (f , ϵ and α). It should also be emphasized that the agreement between the theoretical results from Gaussian chain model and FJC model is a strong indication of the universality of the predicted phase behaviour for AB/A blends. In particular, it is expected that many of the theoretical predictions would apply to generic amphiphilic molecules mixed with appropriate swelling species [26].

Quantitative analysis of the spherical domains

Information on possible mechanisms stabilizing the complex spherical packing phases could be inferred from a quantitative analysis of the properties of the spherical domains. Several quantities could be extracted from the SCFT solutions of the different ordered phases. The first quantity is the standard deviation δV of domain volumes, which quantifies the volume variation of the minority domains. Specifically, δV is defined by,

$$\delta V = \frac{1}{\bar{v}} \sqrt{\frac{\sum_i (v_i - \bar{v})^2}{N_d}},$$

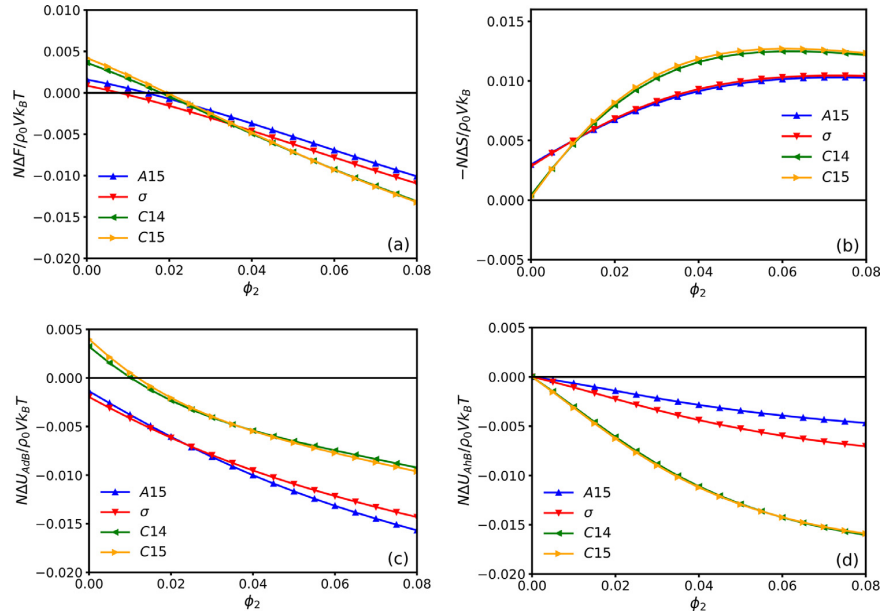
where the summation is over all the domains in a unit cell for a given phase. N_d , v_i and \bar{v} denote the total number of non-equivalent domains in a unit cell, the volume of the i -th domain and the average domain volume. In the unit cell of a phase, a domain is defined as the enclosing space of $\phi_A(\vec{r}) = \phi_B(\vec{r})$ isosurface. The space is partitioned into equivalent close-packed WSCs for the classical spherical phases but multiple inequivalent WSCs for complex spherical phases. The different symmetries of different WSCs naturally result in nonuniform distribution of A-homopolymers among WSCs. This nonuniform homopolymer distribution could be quantified by the normalized concentration of A-homopolymers within the distinct WSCs. Specifically, this normalized concentration is defined by,

$$\phi_2^{WSC} = \frac{1}{V_{WSC}} \int_{WSC} \phi_{A_i}(\vec{r}) d\vec{r}.$$

Due to the favourable interactions, the A-homopolymers are expected to be concentrated at the core-region of the A-domains, thus the total homopolymer concentration in different WSCs could be used to describe the swelling of the spherical particles. The last quantity used in our analysis is the interfacial area per unit volume defined by,

$$S/V = \frac{1}{V} \sum_i S_i,$$

where S_i and V are the surface area of i -th domain and the volume of the unit cell, respectively. The summation is over all the domains in a unit cell. From the solutions of the SCFT equations, these three quantities for different phases have been computed. An example of the results is shown in Fig. 5, where δV , ϕ_2^{WSC} and S/V are plotted as a function of ϕ_2 with fixed $\epsilon = 1.25$, $\alpha = 1.0$ and $\chi_{AB} = 0.45$. Results of the A15 phase is also included in these plots and in our analysis, even though A15 phase is not a stable phase in this region of the phase diagrams. On the other hand, results of δV and ϕ_2^{WSC} for the BCC phase are not shown in these plots because BCC only has one type of WSC, thus $\delta V = 0$ and $\phi_2^{WSC} \approx \phi_2$. In the S/V plot, the BCC phase is chosen as a reference to better display the difference between the different phases.

**Fig. 6**

(a) The total free energy, (b) the entropic contribution (c) the interaction free energy between A- and B-blocks of the copolymers and (d) the interaction free energy between A-homopolymers and B-blocks relative to those of BCC phase as functions of ϕ_2 with $\epsilon = 1.25$, $\alpha = 1.0$ and $\chi_{AB}=0.45$.

The $\phi_A(\vec{r}) = \phi_B(\vec{r})$ isosurface of domains within the unit cell for complex spherical phases are depicted in Fig. 1 for the case of $\epsilon = 1.25$, $\alpha = 1.0$, $\phi_2 = 0.05$ and $\chi_{AB}=0.45$, where inequivalent domains are shown in different colors. We also plot one representative WSC for each type of domains and number them for the following analysis. As shown in Fig. 1, the FK σ phase has five different types of WSCs with CN=12, 14 and 15 whereas the Laves C14 and C15 phases are composed of WSCs with CN=12 and 16. Naturally, the C14 and C15 packing requires particles having larger size difference thus resulting in larger packing frustration, which explains why these phases are not stable in neat AB-diblock copolymer melts. However, in AB/A blends the addition of A-homopolymers provides a mechanism to alleviate frustrations caused by the large size difference via differential segregation in different domains. The nonuniform distribution of A-homopolymers in different domains is well confirmed by the behaviour of δV , ϕ_2^{WSC} and S/V as functions of ϕ_2 shown in Fig. 5.

For neat diblock copolymers, the plot of Fig. 5(a) shows that a significant volume difference ($\delta V \sim 5\%$ for A15 and $\sim 9\%$ for σ) already exists for the FK phases. Noticeably, the Laves C14 and C15 phases exhibit a much larger volume difference of $\delta V \sim 19\%$. With the addition of A-homopolymers or the increase of ϕ_2 , δV for all the complex phases increases but the increase is more rapid for the C14 and C15 phases. This rapid increase of δV is shown more clearly by the monotonically increasing trend of the difference, $\delta V - \delta V_\sigma$, for the two Laves phases. The segregation of the homopolymers among the different spherical domains is shown in Fig. 5(b), where ϕ_2^{WSC} is plotted as a function of ϕ_2 for different WSCs of the spherical phases. Differential segregation of the homopolymers is quantified by the spreading of the ϕ_2^{WSC}

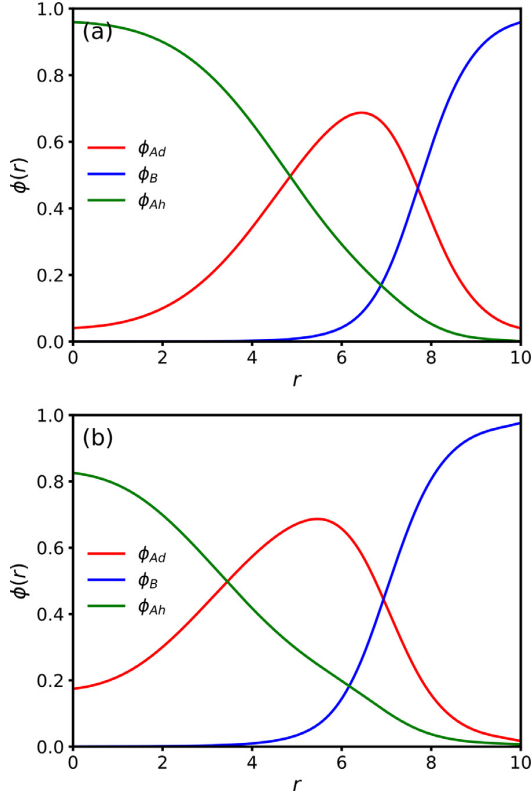
curves for each phase. It is obvious that the spreading of ϕ_2^{WSC} values for C14 and C15 is wider than that of A15 and σ . This observation confirms that enhanced volume deviation around the average value is regulated by the nonuniform distribution of A-homopolymers among distinct WSCs. A direct result of larger particle volume difference is the reduction of the interfacial energy caused by the smaller interfacial area per unit volume shown in Fig. 5(c). It is seen that the S/V for all complex spherical phases decreases relative to BCC phase as increasing ϕ_2 and it decreases more pronouncedly for the C14 and C15 phases than the A15 and σ phases, consistent with the changing tendency predicted from δV , hence well explaining the transition sequence from BCC to σ then to Laves phases. The reason why C15 phase is stable at higher ϕ_2 than C14 phase should be a result of more detailed compromise between the competing interfacial and stretching energies.

Free energy comparison of the different phases

Correlation between the emergence of complex spherical packing phases and the free energy change provides another quantitative insight into the formation mechanisms of these ordered phases. The total Helmholtz free energy density could be separated into enthalpic and entropic contributions. In order to clearly show the free energy difference, the BCC phase is chosen as the reference state. The total free energy density difference between a phase and that of the BCC phase, $N\Delta F/\rho_0 V k_B T$, can be separated into the following three contributions,

$$\frac{N\Delta F}{\rho_0 V k_B T} = \frac{N\Delta U_{AdB}}{\rho_0 V k_B T} + \frac{N\Delta U_{AhB}}{\rho_0 V k_B T} - T \frac{N\Delta S}{\rho_0 V k_B T}.$$

Here ΔU_{AdB} and ΔU_{AhB} are the enthalpic contributions from the A-B interactions between A- and B-blocks and that between

**Fig. 7**

Radial distribution of the segment densities near domain centers for C14 phase with (a) $\alpha = 1.0$ and (b) $\alpha = 0.5625$. The other parameters are: $\epsilon = 1.25$, $\phi_2 = 0.07$ and $\chi_{AB} = 0.45$. The r is in the unit of b_A . There are three types of spherical domains for the C14 phase. The segment distributions are similar for these different domains, thus these distributions are shown only for domain 1 with CN=16 for clarity.

A-homopolymer and B-blocks, respectively, and $-T\Delta S$ is the entropic contribution to the free energy. Within the SCFT, these contributions are given by,

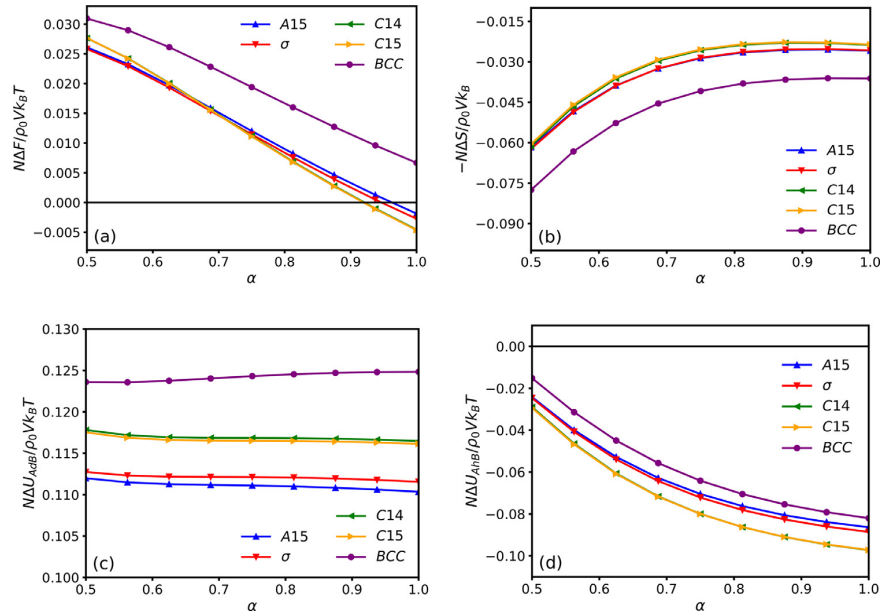
$$\begin{aligned} \frac{N(-TS)}{\rho_0 V k_B T} &= -\phi_1 \ln \frac{Q_1}{\phi_1} - \frac{\phi_2}{\gamma_2} \ln \frac{Q_2}{\phi_2} - \frac{1}{V} \int d\vec{r} [\omega_A(\vec{r}) \phi_A(\vec{r}) + \omega_B(\vec{r}) \phi_B(\vec{r})], \\ \frac{N U_{AB}}{\rho_0 V k_B T} &= \frac{1}{V} \chi_{AB} N \int u(|\vec{r} - \vec{r}'|) \phi_{Ad}(\vec{r}) \phi_B(\vec{r}') d\vec{r}', \\ \frac{N U_{Ah}}{\rho_0 V k_B T} &= \frac{1}{V} \chi_{AB} N \int u(|\vec{r} - \vec{r}'|) \phi_{Ah}(\vec{r}) \phi_B(\vec{r}') d\vec{r}'. \end{aligned} \quad (9)$$

The sum of these three contributions gives the total Helmholtz free energy density. The results of the various contributions to the free energy density are shown in Fig. 6. As we can see from the total free energy density plot (Fig. 6(a)), the complex spherical packing phases become increasingly stable than the BCC phase for larger value of ϕ_2 . From the plots of the different components of the free energy, it is evident that the interaction free energies are the main factors contributing to the decrease of free energy of the complex spherical packing phases relative to the BCC phase, as shown in Figure 6(c) and (d). Furthermore, the free energy density for the Laves C14 and C15 phases are decreasing faster than that of the FK A15 and σ phases. This mainly results from the interaction

free energy between the A-homopolymers and B-blocks as could be seen in Fig. 6(d). This free energy decrease could be attributed to the localization of A-homopolymers in the core of the A-domains, resulting in larger domain size difference thus less A-B interfacial areas. Another interesting observation is that the interaction free energy between A- and B-blocks becomes more favourable for the C15 phase than C14 phase at larger ϕ_2 , which should be the main contribution triggering the C14 \rightarrow C15 transition at high ϕ_2 .

One interesting observation from the phase diagrams shown in Fig. 3 is that the cylindrical HEX phase occupies a much larger region when α changes from 1.0 to 0.5625, which is in good agreement with the experimental observations by Mueller et al. [17] and the SCFT calculations by Cheong et al. [34]. It has been pointed out that this drastic change of phase behaviour is correlated with whether the A-homopolymers penetrate into the A-layers formed by the A-blocks (wet brushes) or not (dry brushes). The penetration of A-homopolymers into the A-blocks is dictated by the homopolymer localization in the A-domains. For A-homopolymers with larger molecular weight than that of the A-blocks, entropic penalty prevents the penetration of homopolymers into the A-blocks, resulting in dry brushes [46–48]. The distributions of A-homopolymers obtained from SCFT calculations could be used to clearly illustrate the occurrence of dry- and wet-brushes in our model system. The distinct density distributions could be clearly seen by using the C14 phase as an example. Specifically, we first define the center of a spherical domain as the position where $\phi_{Ah}(\vec{r})$ reaches a local maximum. Then we divide the space surrounding the center into thin spherical shells and compute the angular average of $\phi(\vec{r})$ within each shell, resulting in the average radial distribution of segments within each domain. The results for the C14 phase with $\epsilon = 1.25$, $\phi_2 = 0.07$, $\chi_{AB} = 0.45$ and two values of $\alpha = 1.0$ and 0.5625 are shown in Fig. 7(a) and (b), respectively. It is noted that the radial segment distributions of the three domains exhibit similar behaviour. Therefore, only the result for domain 1 with CN=16 is presented in Fig. 7 for clarity. The degrees of localization of these two cases can be evaluated by comparing the peak values of $\phi(r)$. For example, the maximum value of $\phi_{Ah}(r)$ at the domain center ($r = 0$) is close to 0.97 when $\alpha = 1.0$ but it is about 0.82 when $\alpha = 0.5625$. In addition, the curve of $\phi_{Ah}(r)$ decreases more rapidly as moving away from the domain center for the case of $\alpha = 1.0$ than that of $\alpha = 0.5625$. These observations provide convincing indication of a stronger localization of A-homopolymers at the center of the domains when $\alpha = 1.0$.

It is known that the cylindrical phase becomes more favoured over the spherical phases when the spontaneous interfacial curvature becomes smaller. In the case of wet brushes, the penetration of A-homopolymers into the A-blocks naturally leads to a smaller interfacial curvature because the effective volume of the A-domains is increased. In the case of dry brushes, there is less penetration of A-homopolymers into the A-blocks. Thus, the property of the A-B interface is less affected and the system would prefer to maintain in spherical phases. This effect could be illustrated by the free energy plot. The different contributions to the free energy density of each phase relative to those of the HEX phase are plotted as functions of α in Fig. 8 with fixed $\epsilon = 1.25$, $\phi_2 = 0.07$ and $\chi_{AB} = 0.45$. It can be seen that the dominant

**Fig. 8**

(a) The total free energy, (b) the entropic contribution (c) the interaction free energy between A- and B-blocks of the copolymers and (d) the interaction free energy between A-homopolymers and B-blocks relative to those of HEX phase as functions of α with $\epsilon = 1.25$, $\phi_2 = 0.07$ and $\chi_{AB} = 0.45$.

contribution that determines the total free energy tendency is the interaction free energy between A-homopolymers and B-blocks, which decreases for all spherical phases relative to HEX phase as α becomes larger. Therefore it is the decreasing of the A-homopolymer and B-block interactions that enlarges the region of the spherical phases.

Conclusion

In summary, we have systematically studied the emergence and relative stability of complex spherical packing phases in binary blends composed of AB diblock copolymers and A-homopolymers by using the self-consistent field theory applied to a freely-jointed chain model of polymers. We focus on the effects of four molecular parameters characterizing the conformational asymmetry ϵ , homopolymer concentration ϕ_2 , homopolymer length α and diblock copolymer composition f . The phase behaviours of the binary AB/A blends are investigated by constructing a set of phase diagrams covering a large parameter space. In agreement with previous theoretical and experimental studies, the theoretical results from the current study confirm the conclusion that conformational asymmetry of the AB-diblock copolymer is not a necessary condition to promote the formation of complex spherical packing phases in polymeric blends containing block copolymers, although a larger value of ϵ could drastically enlarge the spherical phase region on the phase diagram. For a particular set of system parameters, the theory predicts a phase transition sequence, from BCC \rightarrow σ \rightarrow C14 \rightarrow C15, with the addition of A-homopolymers. A detailed quantitative analysis on the properties of spherical domains reveals that the phase transition from BCC to the complex spherical packing phases is

strongly correlated with the nonuniform distribution of the A-homopolymers among the different packing A-domains. The emergence of the complex spherical packing phases is induced by the localization of the A-homopolymers in the core region of the A-domains that provides an effective mechanism to regulate the domain volumes. The rich phase behaviour by simply adding homopolymers to diblock copolymers provides a simple and efficient route to engineer complex spherical packing phases.

Compared with the previous theoretical studies of AB/A blends [34], the current extensive SCFT calculations cover a significantly larger parameter space, thus providing a more complete study of the formation of complex spherical packing phases in polymeric blends containing block copolymers. Furthermore, we have employed a freely-jointed chain model suitable for polymers with low molecular weight, rather than the commonly used Gaussian model that is more suitable for polymers with high molecular weight. Because of the larger parameter space and polymer model, the results obtained in the current study could be used to make direct comparison to experiments. Furthermore, we would like to point out that the agreement between theoretical studies employing different chain models provides a strong indication that the emergence and relative stability of complex spherical packing phases in soft matter systems containing amphiphilic molecules is a generic phenomenon independent of the molecular details of the system. This universality of phase behaviours will shed light to the understanding of the emergence of complex ordered phases in non-polymeric soft matter systems, including surfactant suspensions [24–26], giant surfactants [21–23] and supramolecular assemblies [18–20], to name a few.

Declaration of Competing Interest

The authors declare that they have no known competing financial interests or personal relationships that could have appeared to influence the work reported in this paper.

Acknowledgements

This research was supported by the Natural Science and Engineering Research Council (NSERC) of Canada and was enabled in part by support provided by the facilities of SHARCNET (<https://www.sharcnet.ca>) and Compute Canada (<http://www.computeCanada.ca>).

References

- [1] T. Aste, D. Weaire, *The Pursuit of Perfect Packing*, 2nd, Taylor & Francis, 2008.
- [2] F.C. Frank, J.S. Kasper, Complex alloy structures regarded as sphere packings. I. definitions and basic principles, *Acta Crystallogr* 11 (1958) 184–190, doi:10.1107/s0365110x58000487.
- [3] F.C. Frank, J.S. Kasper, Complex alloy structures regarded as sphere packings. II. analysis and classification of representative structures, *Acta Crystallogr* 12 (1959) 483–499, doi:10.1107/s0365110x59001499.
- [4] M. De Graef, M.E. McHenry, *Structure of materials: An introduction to crystallography, diffraction and symmetry*, 2nd, Cambridge University Press, 2012.
- [5] S. Lee, M.J. Bluemle, F.S. Bates, Discovery of a frank-kasper phase in sphere-forming block copolymer melts, *Science* 330 (2010) 349–353, doi:10.1126/science.1195552.
- [6] M.W. Schulze, R.M. LewisIII, J.H. Lettow, R.J. Hickey, T.M. Gillard, M. Hillmyer, F.S. Bates, Conformational asymmetry and quasicrystal approximants in linear diblock copolymers, *Phys. Rev. Lett.* 118 (2017), doi:10.1103/physrevlett.118.207801.
- [7] M.W. Bates, J. Lequeieu, S.M. Barbon, R.M. LewisIII, K.T. Delaney, A. Anastasaki, C.J. Hawker, G.H. Fredrickson, C.M. Bates, Stability of the A15 phase in diblock copolymer melts, *Proceedings of The National Academy of Sciences* 116 (2019) 13194–13199, doi:10.1073/pnas.1900121116.
- [8] S. Jeon, T. Jun, S. Jo, H. Ahn, S. Lee, B. Lee, D.Y. Ryu, Frank-kasper phases identified in PDMS-b-PTFEA copolymers with high conformational asymmetry, *Macromol. Rapid Commun.* 40 (2019) 1900259, doi:10.1002/marc.201900259.
- [9] K.K. Lachmayr, C.M. Wentz, L.R. Sita, An exceptional stable and scalable sugar-polyolefin frank-kasper a15 phase, *Angew. Chem. Int. Ed* 58 (2019) 1–7, doi:10.1002/anie.201912648.
- [10] A.B. Chang, F.S. Bates, Impact of architectural asymmetry on frank-kasper phase formation in block polymer melts, *ACS Nano* 14 (2020) 11463–11472, doi:10.1021/acsnano.0c03846.
- [11] S.M. Barbon, J. Song, D. Chen, C. Zhang, J. Lequeieu, K.T. Delaney, A. Anastasaki, M. Rolland, G.H. Fredrickson, M.W. Bates, C.J. Hawker, C.M. Bates, Architecture effects in complex spherical assemblies of (AB)_n-type block copolymers, *ACS Macro Letters*. 9 (2020) 1745–1752, doi:10.1021/acsmacrolett.0c00704.
- [12] M.W. Bates, S.M. Barbon, A.E. Levi, R.M. LewisIII, H.K. Beech, K.M. Vonk, C. Zhang, G.H. Fredrickson, C.J. Hawker, C.M. Bates, Synthesis and self-assembly of AB_n miktoarm star polymers, *ACS Macro Lett* 9 (2020) 396–403, doi:10.1021/acsmacrolett.0c00061.
- [13] M. Watanabe, Y. Asai, J. Suzuki, A. Takano, Y. Matsushita, Frank-kasper a15 phase formed in AB_n block-graft copolymers with large number of graft chains, *Macromolecules* 53 (2020) 10217–102244, doi:10.1021/acs.macromol.0c01097.
- [14] K. Kim, M.W. Schulze, A. Arora, R.M. LewisIII, M.A. Hillmyer, K.D. Dorfman, F.S. Bates, Thermal processing of diblock copolymer melts mimics metallurgy, *Science* 356 (2017) 520–523, doi:10.1126/science.aam7212.
- [15] A.P. Lindsay, R.M. LewisIII, B. Lee, A.J. Peterson, T.P. Lodge, F.S. Bates, A15, σ , and a quasicrystal: Access to complex particle packings via bidisperse diblock copolymer blends, *ACS Macro Letters*. 9 (2020) 197–203, doi:10.1021/acsmacrolett.9b01026.
- [16] H. Takagi, K. Yamamoto, Phase boundary of Frank-Kasper σ phase in phase diagrams of binary mixtures of block copolymers and homopolymers, *Macromolecules* 52 (2019) 2007–2014.
- [17] A.J. Mueller, A.P. Lindsay, A. Jayaraman, T.P. Lodge, M.K. Mahanthappa, F.S. Bates, Emergence of a c15 laves phase in diblock polymer/homopolymer blends, *ACS Macro Lett* 9 (2020) 576–582, doi:10.1021/acsmacrolett.0c00124.
- [18] G. Ungar, Y. Liu, X. Zeng, V. Percec, W.D. Cho, Giant supramolecular liquid crystal lattice, *Science* 299 (2003) 1208–1211, doi:10.1126/science.1078849.
- [19] X. Zeng, G. Ungar, Y. Liu, V. Percec, A.E. Dulcey, J.K. Hobbs, Supramolecular dendritic liquid quasicrystals, *Nature* 428 (2004) 157–160, doi:10.1038/nature02368.
- [20] H.J. Sun, S. Zhang, V. Percec, From structure to function via complex supramolecular dendrimer systems, *Chem. Soc. Rev.* 44 (2015) 3900–3923, doi:10.1039/c4cs00249k.
- [21] K. Yue, M. Huang, R.L. Marson, J. He, J. Huang, Z. Zhou, J. Wang, C. Liu, X. Yan, K. Wu, Z. Guo, H. Liu, W. Zhang, P. Ni, C. Wedemiotis, W.B. Zhang, S.C. Glotzer, S.Z.D. Cheng, Geometry induced sequence of nanoscale Frank-Kasper and quasicrystal mesophases in giant surfactants, *Proceedings of The National Academy of Sciences* 113 (2016) 14195–14200, doi:10.1073/pnas.1609422113.
- [22] Z. Su, C. Hsu, Z. Gong, X. Feng, J. Huang, Z. R. Y. Wang, M. Huang, S.Z.D. Cheng, Identification of a Frank-Kasper σ phase from shape amphiphile self-assembly, *Nat Chem* 11 (2019) 899–905, doi:10.1038/s41557-019-0330-x.
- [23] Y. Liu, T. Liu, X. Yan, Q. Guo, J. Wang, R. Zhang, S. Zhang, Z. Su, J. Huang, G. Liu, W. Zhang, Z. W. T. Aida, K. Yue, M. Huang, S.Z.D. Cheng, Mesotom alloys via self-sorting approach of giant molecules blends, *Giant* 4 (2020) 100031, doi:10.1016/j.giant.2020.100031.
- [24] S.A. Kim, K. Jeong, A. Yethiraj, M.K. Mahanthappa, Low-symmetry sphere packings of simple surfactant micelles induced by ionic sphericity, *Proceedings of The National Academy of Sciences* 114 (2017) 4072–4077, doi:10.1073/pnas.1701608114.
- [25] A. Jayaraman, M.K. Mahanthappa, Counterion-dependent access to low-symmetry lyotropic sphere packings of ionic surfactant micelles, *Langmuir*. 34 (2018) 2290–2301, doi:10.1021/acs.langmuir.7b03833.
- [26] C. Baez-Cotto, M.K. Mahanthappa, Micellar mimicry of intermetallic c14 and c15 laves phases by aqueous lyotropic self-assembly, *ACS Nano*. 12 (2018) 3226–3234, doi:10.1021/acsnano.7b07475.
- [27] C. Baez-Cotto, G.L. Jackson, M.K. Mahanthappa, Aqueous lyotropic mesophase behavior of gemini dicarboxylate surfactants swollen with n-decane, *Langmuir* 36 (2019) 2307–2321, doi:10.1021/acs.langmuir.9b03408.
- [28] W. Li, C. Duan, A.C. Shi, Nonclassical spherical packing phases self-assembled from AB-type block copolymers, *ACS Macro Letters*. 6 (2017) 1257–1262, doi:10.1021/acsmacrolett.7b00756.
- [29] N. Xie, W. Li, F. Qiu, A.C. Shi, σ phase formed in conformationally asymmetric AB-type block copolymers, *ACS Macro Letters*. 3 (2014) 906–910, doi:10.1021/mz500445v.
- [30] M. Liu, Y. Qiang, W. Li, F. Qiu, A.C. Shi, Stabilizing the Frank-Kasper phases via binary blends of AB diblock copolymers, *ACS Macro Letters*. 5 (2016) 1167–1171, doi:10.1021/acsmacrolett.6b00685.
- [31] M. Liu, W. Li, F. Qiu, A.C. Shi, Stability of the frank-kasper σ -phase in BABC linear triblock terpolymers, *Soft Matter*. 12 (2016) 6412–6421, doi:10.1039/c6sm00798h.
- [32] A. Reddy, M.B. Buckley, A. Arora, F.S. Bates, K.D. Dorfman, G.M. Grason, Stable Frank-Kasper phases of self-assembled, soft matter spheres, *Proceedings of The National Academy of Sciences*. 115 (2018) 10233–10238, doi:10.1073/pnas.1809655115.
- [33] M. Zhao, W. Li, Laves phases formed in the binary blend of AB₄ miktoarm star copolymer and a-homopolymer, *Macromolecules* 52 (2019) 1832–1842, doi:10.1021/acs.macromol.8b02407.
- [34] G.K. Cheong, F.S. Bates, K.D. Dorfman, Symmetry breaking in particle-forming diblock polymer/homopolymer blends, *Proceedings of The National Academy of Sciences* 117 (2020) 16764–16769, doi:10.1073/pnas.2006079117.
- [35] L. Chen, Y. Qiang, W. Li, Tuning arm architecture leads to unusual phase behaviors in a (BAB)₂ star copolymer melt, *Macromolecules* 51 (2018) 9890–9900, doi:10.1021/acs.macromol.8b01484.
- [36] W. Li, C. Duan, A.C. Shi, Stabilizing phases of block copolymers with gigantic spheres via designed chain architectures, *ACS Macro Letters*. 9 (2020) 668–673, doi:10.1021/acsmacrolett.0c00193.
- [37] Q. Xie, Y. Qiang, L. Chen, Y. Xia, W. Li, Synergistic effect of stretched bridging block and released packing frustration leads to exotic nanostructures, *ACS Macro Letters*. 9 (2020) 980–984, doi:10.1021/acsmacrolett.0c00313.
- [38] S. Lee, C. Leighton, F.S. Bates, Sphericity and symmetry breaking in the formation of Frank-Kasper phases from one component materials, *Proceedings of The National Academy of Sciences* 111 (2014) 17723–17731, doi:10.1073/pnas.1408678111.
- [39] K. Kim, A. Arora, R.M. LewisIII, M. Liu, W. Li, A.-C. Shi, K.D. Dorfman, F.S. Bates, Origins of low-symmetry phases in asymmetric diblock copolymer melts, *Proceedings of The National Academy of Sciences* 115 (2018) 847–854, doi:10.1073/pnas.1717850115.
- [40] M.W. Matsen, Self-consistent field theory for melts of low-molecular-weight diblock copolymer, *Macromolecules* 45 (2012) 8502–8509, doi:10.1021/ma301788q.
- [41] S. Park, D. Yong, Y. Kim, J. Kim, Numerical implementation of pseudo-spectral method in self-consistent mean field theory for discrete polymer chains, *J Chem Phys* 150 (2019) 234901, doi:10.1063/1.5094227.
- [42] A.C. Shi, Self-consistent field theory of inhomogeneous polymeric systems, in: J. Wu (Ed.), *Variation Methods in Molecular Modeling*, Springer, 2017.
- [43] A. Arora, D.C. Morse, F.S. Bates, K.D. Dorfman, Accelerating self-consistent field theory of block polymers in a variable unit cell, *J Chem Phys* 146 (2017) 244902, doi:10.1063/1.4986643.

- [44] R.B. Thompson, K.O. Rasmussen, T. Lookman, Improved convergence in block copolymer self-consistent field theory by anderson mixing, *J Chem Phys* 120 (2004) 31–34, doi:[10.1063/1.1629673](https://doi.org/10.1063/1.1629673).
- [45] C.A. Tyler, D.C. Morse, Stress in self-consistent-field theory, *Macromolecules* 36 (2003) 8184–8188, doi:[10.1021/ma034601x](https://doi.org/10.1021/ma034601x).
- [46] T. Hashimoto, H. Tanaka, H. Hasegawa, Ordered structure in mixtures of a block copolymer and homopolymers, 2. Effects of molecular weights of homopolymers, *Macromolecules* 23 (1990) 4378–4386, doi:[10.1021/ma00222a009](https://doi.org/10.1021/ma00222a009).
- [47] K.I. Winey, E.L. Thomas, L.J. Fetters, Swelling of lamellar diblock copolymer by homopolymer: influences of homopolymer concentration and molecular weight, *Macromolecules* 24 (1991) 6182–6188, doi:[10.1021/ma00023a020](https://doi.org/10.1021/ma00023a020).
- [48] S. Koizumi, H. Hasegawa, T. Hashimoto, Spatial distribution of homopolymers in block copolymer microdomains as observed by a combined SANS and SAXS method, *Macromolecules* 27 (1994) 7893–7906, doi:[10.1021/ma00104a053](https://doi.org/10.1021/ma00104a053).

Chapter 5

Formation of Complex Spherical Packing Phases in Binary Blends of Diblock Copolymers

Publication: Xie, Jiayu, Yu Li, and An-Chang Shi. “Binary blends of diblock copolymers: An efficient route to complex spherical packing phases.” *Macromolecular Theory and Simulations* 30.6 (2021): 2100053.

Authors: **Jiayu Xie**, Yu Li, An-Chang Shi

Contribution: As the first author, I developed the theoretical model and computational code. Yu Li and I collaborated on generating and analyzing the data, as well as drafting the initial manuscript. All authors contributed to manuscript revisions, with guidance from Dr. Shi throughout the research.

Preface

In this chapter, we examine the phase behaviour of binary blends of A_1B_1 and A_2B_2 diblock copolymers, with a focus on the stability of the Frank-Kasper phases. The emergence of the FK phases in A_1B_1/A_2B_2 blends was initially predicted by SCFT [66] and later confirmed by experiments [71, 74]. Previous SCFT calculations demonstrated that the differential distributions of distinct diblock copolymers across different domains (inter-domain segregation) and within the same domain (intra-domain segregation) serve as effective mechanisms to regulate the domain volumes and shapes, respectively, leading to the stabilization of the complex FK phases.

In the current study, we deepen our understanding of the stability of the FK phases in the A_1B_1/A_2B_2 blends by conducting a systematic SCFT study covering an unprecedentedly large phase space. Phase diagrams on the $\phi_2 - \chi N$ plane, where ϕ_2 is the concentration of the second diblock chains, are constructed. These diagrams consider different combinations of block compositions of the two diblock copolymers, f_1 and f_2 , and their length ratio, γ . Additionally, through a detailed analysis of both inter- and intra-domain distributions of the second copolymer chains and the properties of self-assembled spherical domains, we unveil the relationship between various system parameters and the two mechanisms, i.e. intra- and inter-domain segregations, responsible for stabilizing the FK phases in this system.

RESEARCH ARTICLE

Binary Blends of Diblock Copolymers: An Efficient Route to Complex Spherical Packing Phases

Jiayu Xie, Yu Li, and An-Chang Shi*

The phase behavior of binary blends composed of A_1B_1 and A_2B_2 diblock copolymers is systematically studied using the polymeric self-consistent field theory, focusing on the formation and relative stability of various spherical packing phases. The results are summarized in a set of phase diagrams covering a large phase space of the system. Besides the commonly observed body-centered-cubic phase, complex spherical packing phases including the Frank–Kasper A15, σ and the Laves C14, C15 phases could be stabilized by the addition of longer A_2B_2 -copolymers to asymmetric A_1B_1 -copolymers. Stabilizing the complex spherical packing phases requires that the added A_2B_2 -copolymers have a longer A-block and an overall chain length at least comparable to the host copolymer chains. A detailed analysis of the block distributions reveals the existence of inter- and intra-domain segregation of different copolymers, which depends sensitively on the copolymer length ratio and composition. The predicted phase behaviours of the A_1B_1/A_2B_2 diblock copolymer blends are in good agreement with previous experimental and theoretical results. The study demonstrates that binary blends of diblock copolymers provide an efficient route to regulate the emergence and stability of complex spherical packing phases.

The FK phases are a class of complex spherical packing phases initially discovered in metallic alloys. An important feature of the FK phases is the existence of at least two non-equivalent particles or Wigner–Seitz cells (WSCs) in the unit cell of the lattice, which compactly pack together in a complex manner to fill the space.^[13,14] Besides hard condensed matter systems,^[15] the FK phases have been discovered in various soft matter systems, such as block copolymer melts and blends,^[3,6–8] surfactant solutions,^[16–18] and giant molecules.^[19,20] In the case of polymeric systems containing block copolymers, the FK σ phase was first discovered in AB diblock copolymer melts.^[3] Since then a large number of studies have been carried out to understand the emergence of complex spherical packing phases in polymeric systems containing block copolymers both experimentally^[4,6–8,21] and theoretically.^[9–12]

Different from hard condensed matter, in soft matter systems such as block copolymer melts, the particles or the spherical

domains are deformable. Due to the broken spherical symmetry in a crystalline lattice, the packed soft spheres tend to deform toward the polyhedral shape of the WSCs by which they are enclosed in order to maintain a uniform monomer density. Such distortion would inevitably increase the free energy of the polymeric domains, which prefers their native spherical shapes. Thus, phases with higher average sphericity of the WSCs would be preferred when the domain is large enough to induce severe distortion. Based on this argument, the FK phases, whose WSCs have higher average sphericity than that of the classical body-centered cubic (BCC) and close-packed (HCP or FCC) phases, could become stable if the spherical domain can be enlarged and, at the same time, the transition to cylindrical domains could be prevented.^[12,22]

A key feature of the complex spherical packing phases is the formation of large spherical domains. There are a number of routes to regulate the size of the polymeric domains.^[2,11] Introducing conformational or configurational asymmetry into diblock copolymers is an effective approach to enlarge spherical domains. Indeed, a theoretical study based on the polymeric self-consistent field theory (SCFT) showed that the FK A15 and σ phases could be stabilized in conformationally asymmetric linear AB-diblock copolymers and configurationally asymmetric linear AB₄ miktoarm copolymers.^[9] This theoretical prediction has been

1. Introduction

Block copolymers are macromolecules composed of two or more chemically distinct sub-chains or blocks.^[1] Due to the intrinsic frustration originated from a competition between the monomer–monomer interactions and chain connectivity, block copolymers tend to self-assemble into mesoscopic polymeric domains of various shapes, loosely classified as lamellae, cylinders and spheres.^[2] In block copolymer melts or concentrated block copolymer solutions, the packing of these domains leads to the formation of various ordered phases or mesocrystals. The formation and relative stability of these ordered phases have been an actively researched topic attracting sustained attention.^[1] In particular, the emergence of complex spherical packing phases such as the Frank–Kasper (FK) phases has attracted tremendous attention in recent years.^[3–12]

J. Xie, Y. Li, A.-C. Shi
 Department of Physics and Astronomy
 McMaster University
 1280 Main Street West, Hamilton, Ontario L8S 4M1, Canada
 E-mail: shi@mcmaster.ca

 The ORCID identification number(s) for the author(s) of this article can be found under <https://doi.org/10.1002/mats.202100053>

DOI: 10.1002/mats.202100053

confirmed in experiments on conformationally asymmetric diblock copolymers^[4] and on miktoarm AB block copolymers.^[5] Moreover, a recent SCFT study by Qiang et al.^[23] demonstrated that by employing specially designed dendritic AB-type block copolymers, the spherical domains could be maintained up to $f_A \approx 0.7$ resulting in large windows of FK A15 and σ phases in the phase diagram. These studies offer a good understanding of the formation of FK phases in single component systems composed of asymmetric block copolymers.

Another feature of the complex spherical packing phases is that the sizes of the nonequivalent particles or polymeric domains are different. For example, there are two different types of particles in the A15 phase and five different particles in the σ phase. These nonequivalent polymeric domains have different volumes, which is in contrast to the classical BCC, FCC, and HCP phases having only one type of domains. This feature is more pronounced for the Laves C14 and C15 phases, which have spherical domains with much larger volume differences when compared with the A15 and σ phases. The fact that the Laves phases have not been found to be stable in diblock copolymer melts could be attributed to the fact that their formation requires considerable volume exchange among distinct domains, which is not favored in single-component systems. From this perspective, one mechanism to stabilize the complex spherical packing phases is to regulate the sizes of the polymeric domains, which could be effectively accomplished by mixing another species into the system.^[2,11]

Indeed, experimental and theoretical studies have suggested that blending different components together could provide an efficient route to regulate the domain sizes thus stabilizing the complex spherical packing phases. The simplest blending system is obtained by mixing A-homopolymers with sphere-forming AB diblock copolymers. The added A-homopolymers would be localized in the central region, or the core, of the spherical domains resulting in larger spheres. At the same time, differential segregation of the A-homopolymers would lead to the formation of spherical domains with different sizes. The combined effects could stabilize the formation of complex spherical packing phases. This route has been demonstrated experimentally by Mueller et al. showing that the FK σ , Laves C14 and C15 phases could become stable phases in AB/A binary blends in the dry brush regime.^[6] Moreover, the local segregation of the A-homopolymers has been illustrated by SCFT calculations for AB/A^[24,25] and AB₄/A^[26] binary blends. Another blending platform is mixing AB diblock copolymers with different lengths and compositions. The formation of complex spherical packing phases in block copolymer blends has been examined theoretically,^[10,27] predicting that complex spherical packing phases, including the A15, σ , C14 and C15 phases, could be formed by mixing A₁B₁ and A₂B₂ diblock copolymers. In agreement with the theoretical predictions, these complex spherical packing phases have been observed in recent experiments^[7,8] on binary blends of A₁B₁/A₂B₂ diblock copolymers. These previous experimental and theoretical studies have shown that the binary blends composed of A₁B₁/A₂B₂ diblock copolymers provide a flexible platform to stabilize complex spherical packing phases, as well as a useful model system to study the mechanism of the formation of these complex phases. The fundamental difference between the addition of A-homopolymers and AB diblock copolymers to an AB diblock copolymer melt is

that the added AB diblock copolymers could be localized inside one domain or at the AB-interfaces. As such, the added AB diblock copolymers could act as fillers similar to A-homopolymers and as co-surfactants which could modify the property of the AB-interfaces. A synergetic interplay of these two functions could lead to a much enhanced effect on the stabilization of the complex spherical packing phases.

The self-assembly of binary blends of A₁B₁/A₂B₂ diblock copolymers has been investigated experimentally^[7,8,28–33] and theoretically^[10,27,34–39] in the past years. It has been well established that mixing A₁B₁ and A₂B₂ diblock copolymers could lead to a rich phase behavior including macroscopic phase separation and the emergence of new phases. In particular, previous experiments^[7,8] and theory^[10,27] have laid a foundation of the self-assembly of complex spherical packing phases in A₁B₁/A₂B₂ diblock copolymer blends. However, a complete set of phase diagrams covering a large phase space of the system and a detailed investigation of the effect of different molecular parameters are still lacking. Therefore, it is desirable to carry out a systematic study on the binary A₁B₁/A₂B₂ diblock copolymer blends covering a large phase space. In the current work, we fill this gap by carrying out a comprehensive study of A₁B₁/A₂B₂ blends using the polymeric self-consistent field theory. We will mainly focus on the effects of three parameters: 1) the concentration of the A₂B₂-copolymers ϕ_2 ; 2) the composition of the A₂B₂-copolymers f_2 ; and 3) the length ratio between the A₁B₁- and A₂B₂-copolymers γ . A set of phase diagrams in the $\phi_2 - \chi N$ plane with different values of f_2 and γ are constructed and presented. The phase diagrams cover a large range of ϕ_2 from 0 to 1 and χN from 0 to 40. These phase diagrams span a large region of the phase space and give a systematic overview of the phase behavior of the binary blends. The predicted phase transition sequences could be used to make direct comparison with experimental phase diagrams in the concentration versus temperature plane. Furthermore, we perform a detailed analysis of the effects of different molecular parameters on the inter- and intra-domain segregation of the copolymers. Our results provide a comprehensive picture of the phase behavior of binary A₁B₁/A₂B₂ diblock copolymer blends, thus shedding light on the mechanisms of the stabilization of complex spherical packing phases.

2. Theoretical Model

We consider an incompressible binary blend composed of linear A₁B₁ and A₂B₂ diblock copolymers in a volume V . Specifically, the model system contains n_1 A₁B₁ diblock copolymer chains and n_2 A₂B₂-diblock copolymer chains. The degree of polymerization of the A₁B₁- and A₂B₂-copolymers is $N_1 = \gamma_1 N = N$ and $N_2 = \gamma_2 N = \gamma N$ ($\gamma_1 = 1, \gamma_2 = \gamma$), respectively. The volume fraction of the A-blocks for the two copolymers is $f_1 = N_{1A}/N_1$ and $f_2 = N_{2A}/N_2$, respectively. We assume a uniform segment density $\rho_{A,0} = \rho_{B,0} = \rho_0$ such that $\rho_0 V = n_1 N + n_2 \gamma N$ according to the incompressibility condition. The average concentrations of the A₁B₁- and A₂B₂-copolymers are given by, $\phi_1 = \frac{n_1 \gamma_1 N}{\rho_0 V}$ and $\phi_2 = \frac{n_2 \gamma_2 N}{\rho_0 V} = 1 - \phi_1$, respectively. Furthermore, we denote the Kuhn length of the A- and B-segments by b_A and b_B , which can take different values to model chains with different stiffness or conformational asymmetry.

In order to consider two phase coexistence, it is convenient to formulate the theory in the grand canonical ensemble in which the thermodynamic parameters are the chemical potentials of the two copolymers, μ_1 and μ_2 . Because the system is assumed to be incompressible, these two chemical potentials are not independent and can be chosen as $\mu_1 = 0$ and $\mu_2 = \mu$ for convenience. Within the mean-field approximation, the grand potential density of the system can be expressed as^[40,41]

$$\frac{N\bar{\mu}}{\rho_0 V k_B T} = -Q_1 - e^{\frac{\mu}{k_B T}} Q_2 + \frac{1}{V} \int d\vec{r} \left\{ \chi N \phi_A(\vec{r}) \phi_B(\vec{r}) - \omega_A(\vec{r}) \phi_A(\vec{r}) - \omega_B(\vec{r}) \phi_B(\vec{r}) - \eta(\vec{r}) [1 - \phi_A(\vec{r}) - \phi_B(\vec{r})] \right\} \quad (1)$$

By minimizing the grand potential with respect to the densities and fields, we obtain the SCFT equations

$$\begin{cases} \omega_A(\vec{r}) = \chi N \phi_B(\vec{r}) + \eta(\vec{r}) \\ \omega_B(\vec{r}) = \chi N \phi_A(\vec{r}) + \eta(\vec{r}) \\ \phi_A(\vec{r}) = \sum_{i=1}^2 e^{\frac{\mu_i}{k_B T}} \int_0^{\gamma_i f_i} ds q_i(s, \vec{r}) q_i^\dagger(s, \vec{r}) \\ \phi_B(\vec{r}) = \sum_{i=1}^2 e^{\frac{\mu_i}{k_B T}} \int_{\gamma_i f_i}^{\gamma_i} ds q_i(s, \vec{r}) q_i^\dagger(s, \vec{r}) \\ \phi_A(\vec{r}) + \phi_B(\vec{r}) = 1 \end{cases} \quad (2)$$

where we have used N as the scale of the polymer arc-length.

In Equation (2), the forward propagators $q_i(s, \vec{r})$ and backward propagators $q_i^\dagger(s, \vec{r})$ ($i = 1, 2$) are obtained by solving the modified diffusion equations

$$\begin{aligned} \frac{\partial}{\partial s} q_i(s, \vec{r}) &= \epsilon_i^2(s) \nabla^2 q_i(s, \vec{r}) - \omega_i(s, \vec{r}) q_i(s, \vec{r}) \\ -\frac{\partial}{\partial s} q_i^\dagger(s, \vec{r}) &= \epsilon_i^2(s) \nabla^2 q_i^\dagger(s, \vec{r}) - \omega_i(s, \vec{r}) q_i^\dagger(s, \vec{r}) \end{aligned} \quad (3)$$

where $s \in [0, \gamma_i]$ for the $A_i B_i$ -copolymers ($i = 1, 2$). The function $\epsilon_i^2(s)$ represents the conformational asymmetry parameter, which is defined by $\epsilon_i^2(s) = (\rho_{A,0} b_A^2) / (\rho_{B,0} b_B^2) = b_A^2 / b_B^2$ for $s \in [0, \gamma_i f_i]$ and $\epsilon_i^2(s) = 1$ for $s \in [\gamma_i f_i, \gamma_i]$. The self-consistent fields $\omega_i(s, \vec{r})$ for the $A_i B_i$ copolymers are given by, $\omega_i(s, \vec{r}) = \omega_A(\vec{r})$ when $s \in [0, \gamma_i f_i]$ and $\omega_i(s, \vec{r}) = \omega_B(\vec{r})$ when $s \in [\gamma_i f_i, \gamma_i]$. The initial conditions of the propagators are specified by $q_i(0, \vec{r}) = 1$ and $q_i^\dagger(\gamma_i, \vec{r}) = 1$.

The single chain partition functions are obtained from the solutions of the propagators by

$$Q_i = \frac{1}{V} \int d\vec{r} q_i(\gamma_i, \vec{r}) \quad (4)$$

Once the SCFT equations [Equation (2)] are solved, the average concentrations of the two components can be simply calculated by

$$\phi_1 = Q_1, \quad \phi_2 = 1 - \phi_1 \quad (5)$$

In many cases it is advantageous to specify the concentration of each components, or equivalently the numbers of polymer

chains, in the system explicitly. In this case it is convenient to work in the canonical ensemble, where the concentration of the $A_i B_i$ -copolymers (ϕ_i , $i = 1, 2$) are the thermodynamic control parameters. Within the mean-field theory, the Helmholtz free energy density of the system is expressed as^[40,41]

$$\frac{NF}{\rho_0 V k_B T} = -\phi_1 \ln \frac{Q_1}{\phi_1} - \frac{\phi_2}{\gamma} \ln \frac{Q_2}{\phi_2} + \frac{1}{V} \int d\vec{r} \left\{ \chi N \phi_A(\vec{r}) \phi_B(\vec{r}) - \omega_A(\vec{r}) \phi_A(\vec{r}) - \omega_B(\vec{r}) \phi_B(\vec{r}) - \eta(\vec{r}) [1 - \phi_A(\vec{r}) - \phi_B(\vec{r})] \right\} \quad (6)$$

Minimization of this free energy with respect to the densities and fields results in the following SCFT equations

$$\begin{cases} \omega_A(\vec{r}) = \chi N \phi_B(\vec{r}) + \eta(\vec{r}) \\ \omega_B(\vec{r}) = \chi N \phi_A(\vec{r}) + \eta(\vec{r}) \\ \phi_A(\vec{r}) = \sum_{i=1}^2 \frac{\phi_i}{\gamma_i Q_i} \int_0^{\gamma_i f_i} ds q_i(s, \vec{r}) q_i^\dagger(s, \vec{r}) \\ \phi_B(\vec{r}) = \sum_{i=1}^2 \frac{\phi_i}{\gamma_i Q_i} \int_{\gamma_i f_i}^{\gamma_i} ds q_i(s, \vec{r}) q_i^\dagger(s, \vec{r}) \\ \phi_A(\vec{r}) + \phi_B(\vec{r}) = 1 \end{cases} \quad (7)$$

where the propagators are computed by the same modified diffusion equations in Equation (3).

The SCFT equations are a set of coupled nonlinear and non-local equations. For most of the cases, solutions of the SCFT equations should be obtained numerically. We employ the pseudo-spectral method to solve the modified diffusion equations.^[42,43] Moreover, the variable-cell Anderson mixing scheme^[44,45] is used to speed up the self-consistent iteration and minimize the free energy or grand-potential with respect to the unit-cell dimensions simultaneously. Starting from specific initial configurations, a set of solutions corresponding to different ordered phases can be obtained. The relative stability of these different phases is determined by comparing their free energy or grand potential density. The phase boundaries between two phases are found by locating the intersections between their thermodynamic potentials.

3. Results and Discussion

3.1. Phase Behavior

For the model binary $A_1 B_1 / A_2 B_2$ diblock copolymer blends, their phase behavior is controlled by six independent parameters, namely, the A-block volume fractions f_1 and f_2 , molecular weight ratio γ , conformational asymmetry parameter ϵ , copolymer concentration ϕ_2 , and segregation strength χN . In the current study we consider conformationally symmetric diblock copolymers with a fixed $\epsilon = 1$ because we are focusing on the effect of blending rather than conformational asymmetry. It is noted that the effect of conformational asymmetry has been studied extensively for AB-diblock copolymer melts by theory^[9] and experiments.^[4]

In order to obtain a comprehensive overview of the phase behavior of the A_1B_1/A_2B_2 diblock copolymer blends, we will construct two sets of phase diagrams in the ϕ_2 - χN plane, highlighting the effect of f_2 and γ , respectively. There are two main benefits of this construction. First, different from previous works,^[10,27] where the length of either the majority or the minority block of the longer chain are fixed relative to the shorter chain so that f_2 and γ are coupled, we choose to decouple the effects of these two parameters to provide an understanding of the phase behaviors from different perspectives. Specifically, we are able to examine the effects of f_2 and γ separately to reveal the synergetic effects of f_2 and γ on the stabilization of the complex spherical packing phases. Second, we choose to construct the phase diagrams in the ϕ_2 - χN plane so that the results can be compared directly with experimental observations.^[7,8]

Phase diagrams of the blends are constructed by comparing the free energy of various candidate phases including the disordered (Dis), lamellar (L), double gyroid (DG), hexagonally-packed cylinders (HEX), body-centered-cubic (BCC), face-centered-cubic (FCC), hexagonally close-packed spheres (HCP) as well as the FK A15, σ and Laves C14, C15 phases. This choice of candidate phases is motivated by our knowledge of potential equilibrium phases obtained from previous experimental and theoretical studies. We have obtained SCFT solutions of several FK phases, such as the Z and H phases, beyond this list. However, these phases have not found to become stable phase within the parameter space explored in the current study. The phase behaviors of the binary A_1B_1/A_2B_2 diblock copolymers are summarized in two sets of phase diagrams shown in Figures 1 and 2, respectively. The first set of phase diagrams (Figure 1) are for the cases with $f_1 = 0.2$ and $\gamma = 1.5$ and three typical values of $f_2 = 0.3, 0.5$, and 0.7 . This choice of f_2 covers both symmetric case and two oppositely asymmetric cases for the A_2B_2 -copolymers. The second set of phase diagrams (Figure 2) are for the cases with $f_1 = 0.2$ and $f_2 = 0.5$ and three typical values of $\gamma = 0.5, 1.0$ and 1.5 . This choice of γ covers the cases where the overall chain length of the A_2B_2 -copolymers is shorter, equal, and longer than that of the A_1B_1 -copolymers. All phase diagrams are computed in the full range of ϕ_2 from 0 to 1 and a large range of χN from 0 to 40. Taking together, these two sets of phase diagrams represent the phase behavior of the model system in a large region of the phase space.

In the phase diagrams shown in Figures 1 and 2, the vertical lines at $\phi_2=0$ and 1 represent the phase behaviors of the neat A_1B_1 and A_2B_2 diblock copolymers, respectively. Because these two diblock copolymers are conformationally symmetric ($b_A = b_B$), the stable phases of the neat diblock copolymers are the classical phases. For example, the phase transition of the neat diblock copolymers follows the generic sequence of Dis \rightarrow HCP \rightarrow BCC \rightarrow HEX for $f_i = 0.2$ when the segregation strength χN is increased. Upon the blending of the two diblock copolymers, new ordered stable phases including the complex spherical packing phases could emerge as stable phases. As the A_2B_2 -copolymer concentration (ϕ_2) is increased, the system undergoes a series of phase transitions from the neat, f_1 -dependent, A_1B_1 phase to the neat, f_2 -dependent, A_2B_2 phase. The phase transition sequence of the blends as ϕ_2 changes from 0 (neat A_1B_1) to 1 (neat A_2B_2) depends sensitively on the segregation strength χN , the volume fractions of the A-blocks f_i , and the

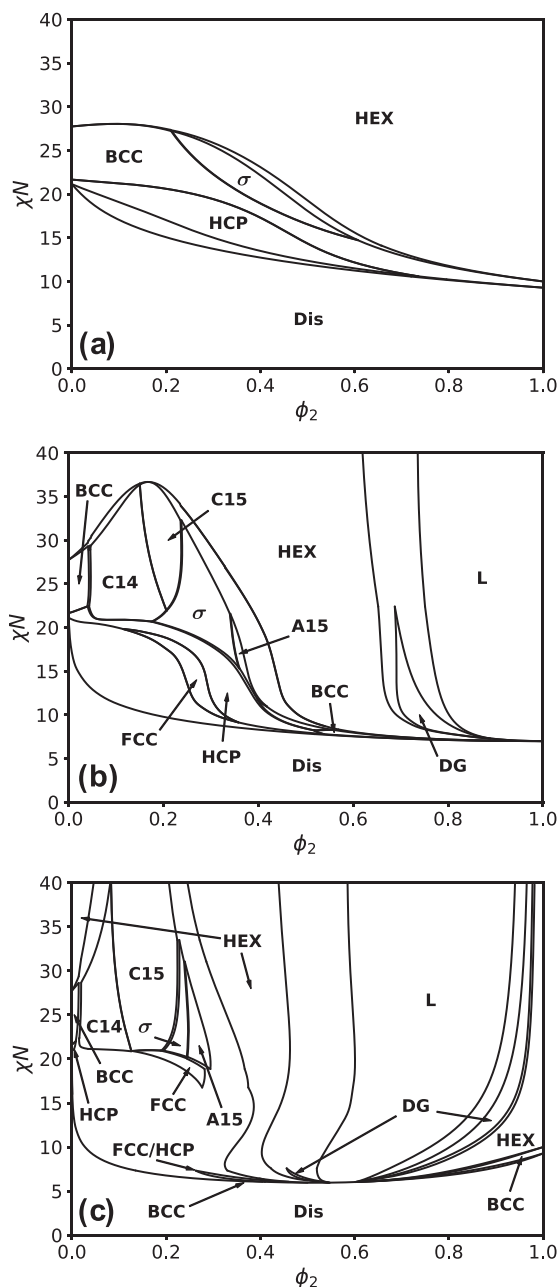


Figure 1. Phase diagram in the ϕ_2 - χN plane for a) $f_2 = 0.3$, b) $f_2 = 0.5$, and c) $f_2 = 0.7$ with fixed $f_1 = 0.2$ and $\gamma = 1.5$. The unlabeled regions are two-phase coexistence regions where two adjacent single phases are connected by a horizontal tie-line. In (c), the FCC/HCP indicates that these two phases are degenerate within the accuracy of the SCFT calculations and the phases on the right hand side of L are the inverse phases.

chain length ratio γ . In particular, the phase transition sequence could vary from no phase transition at all to a complex one involving up to a dozen ordered phases. It is noted that the SCFT calculations are within the framework of mean-field theory and the order-disorder transition boundary is expected to be modified

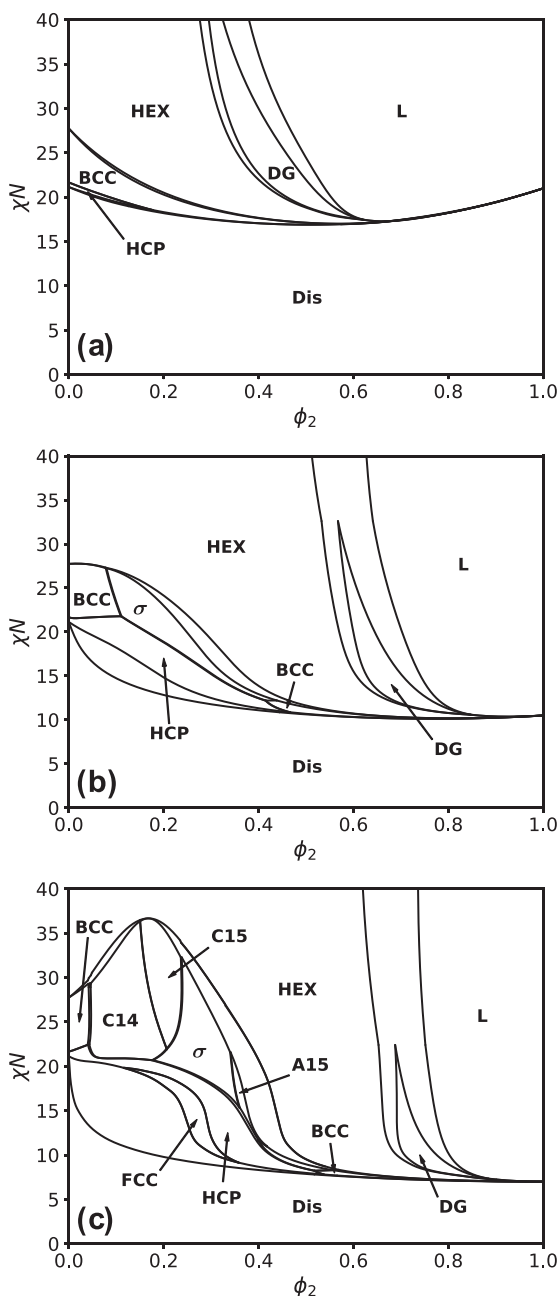


Figure 2. Phase diagrams in the ϕ_2 - χN plane for a) $\gamma = 0.5$, b) $\gamma = 1.0$, and c) $\gamma = 1.5$ with fixed $f_1 = 0.2$ and $f_2 = 0.5$. The unlabeled regions are the two-phase coexistence regions between two adjacent single phases. Note that (c) is identical to Figure 1b, which is reproduced here for easy comparison.

by fluctuation effects. Nevertheless, we expect that the phase transition sequence at larger χN are less affected by fluctuations.

The phase diagrams for $f_1 = 0.2$ and $\gamma = 1.5$ shown in Figure 1 highlight the effects of varying f_2 on the phase behavior of the A_1B_1/A_2B_2 diblock copolymer blends. For $f_1 = 0.2$, the neat A_1B_1 diblock copolymers undergoes phase transitions following

the sequence of Dis \rightarrow HCP \rightarrow BCC \rightarrow HEX as χN is increased from 0 to 40. For $f_2 = 0.3$ that is similar to $f_1 = 0.2$, the neat A_2B_2 diblock copolymers exhibit a phase transition sequence of Dis \rightarrow BCC \rightarrow HEX as χN is increased. In this case the phase behavior of the A_1B_1/A_2B_2 blends (Figure 1a) is relatively simple. At small ($\chi N \leq 10$) and large ($\chi N \geq 27$) values of χN , the addition of the A_2B_2 diblock copolymers does not induce any phase transitions. That is, the binary A_1B_1/A_2B_2 blends would be in the disordered phase at small χN and the hexagonally-packed cylindrical phase at large χN , respectively. In the intermediate region ($10 \leq \chi N \leq 27$), order-to-order phase transitions could be induced with the addition of the A_2B_2 diblock copolymers. In particular, a small window of the FK σ phase appears in the middle ($0.2 \leq \phi_2 \leq 0.6$) of the phase diagrams. The predicted phase transition sequence as a function of ϕ_2 follows the generic sequence of Dis \rightarrow HCP \rightarrow BCC \rightarrow σ \rightarrow HEX in which some of the phases could be missing for a given χN . Notably, although the two diblock copolymers have similar A-block volume fractions and there is no conformational asymmetry, the addition of the A_2B_2 -copolymers could stabilize a complex spherical packing phase, albeit in a small region on the phase diagram, suggesting that even a modest difference in the A-block lengths is sufficient to stabilize the σ phase.

The phase behavior becomes much more richer for the cases of larger f_2 , as shown in the phase diagrams for $f_2 = 0.5$ (Figure 1b) and $f_2 = 0.7$ (Figure 1c). When $f_2 = 0.5$, the neat ($\phi_2 = 1.0$) A_2B_2 diblock copolymers transitions from the disordered (Dis) phase to the lamellar (L) phase at $\chi N_2 = \gamma \chi N = 10.5$. The addition of this symmetric, lamella-forming diblock copolymers to the asymmetric A_1B_1 diblock copolymers results in an extremely rich phase behavior as shown in Figure 1b. Comparing with the phase diagram for $f_2 = 0.3$ (Figure 1a) containing four ordered phases (HCP, BCC, σ , and HEX), 10 ordered phases (HCP, FCC, BCC, C14, C15, σ , A15, HEX, DG, and L) can become equilibrium phases in the phase diagram for $f_2 = 0.5$. It is amazing that a seemingly small change from $f_2 = 0.3$ to $f_2 = 0.5$ leads to such a drastic change of the phase behavior. When f_2 is increased further to $f_2 = 0.7$ (Figure 1c), the neat A_2B_2 -copolymers form inverted BCC and HEX phases since the B-blocks are the domain-forming minority component. The phase diagram for the binary blends of diblock copolymers with $f_1 = 0.2$ and $f_2 = 0.7$ becomes even more complex as shown in Figure 1c. The formation of complex spherical packing phases persists in this case, except that the window of the complex spherical phases is pushed to smaller values of ϕ_2 . Furthermore, the region of the FK phases extends to higher χN and the region of Laves phases grows at the cost of the σ phase. Based on the phase diagrams shown in Figure 1, we can conclude that the addition of the A_2B_2 -copolymers with $f_2 \geq 0.5$ stabilizes the complex spherical packing phases, such that the FK σ and A15 phases and the Laves C14 and C15 phases appear as equilibrium phases in the phase diagrams. This prediction provides an efficient route to obtain these complex spherical packing phases via blending of two diblock copolymers.

Besides the volume fraction of the A-blocks f_2 , the chain length or the degree of polymerization ($N_2 = \gamma N$) of the A_2B_2 diblock copolymers could also have a large effect on the phase behavior of the binary blends. The effect of varying γ on the phase behavior of binary A_1B_1/A_2B_2 diblock copolymer blends is revealed in the phase diagrams shown in Figure 2 for the cases

with $f_1 = 0.2$ and $f_2 = 0.5$. This set of phase diagrams clearly demonstrate the importance of the chain length of the added A_2B_2 -copolymers. When the A_2B_2 -copolymers are shorter than the A_1B_1 -copolymers as exemplified by $\gamma = 0.5$, the phase behavior is relatively simple (Figure 2a). In particular, the addition of short A_2B_2 -copolymers does not stabilize the complex spherical packing phases and the order-to-order phase transition follows the generic sequence of HCP \rightarrow BCC \rightarrow HEX \rightarrow DG \rightarrow L (Figure 2a). When the chain length of the A_2B_2 -copolymers is increased to be the same as that of the A_1B_1 -copolymers ($\gamma = 1.0$), a small window of the FK σ phase appears along the BCC/HEX phase boundary (Figure 2b). Further increasing γ from $\gamma = 1$ to $\gamma = 1.5$ results in the rich phase behavior containing a set of 10 ordered phases including the complex spherical packing phases as shown in Figure 2c that is the same as Figure 1b. An important conclusion from these theoretical results is that, in order to stabilize the complex spherical packing phases in the A_1B_1/A_2B_2 binary blends, sufficiently large values of f_2 and γ are required. As shall be presented in the next section, the reason of this behavior is that the additive A_2B_2 -copolymers with much shorter chain length than the host A_1B_1 -copolymers tend to segregate at the AB-interface, which does not affect the packing of the A-blocks at the center of the domains.

It is interesting to compare the phase behaviors presented in Figures 1 and 2 to previous theoretical and experimental results. A set of theoretical phase diagrams of binary A_1B_1/A_2B_2 diblock copolymer blends have been constructed by Wu et al.^[37,38] Because the complex spherical packing phases were not included in these previous studies, a detailed comparison of the phase boundaries is not straightforward. Nevertheless, the overall phase behavior obtained in these previous studies is consistent with the current results summarized in Figures 1 and 2. In particular, both sets of phase diagrams exhibit the trend of the expansion of the HEX phase and the shrinking of the L phase when γ is increased. In a more recent SCFT study,^[10,27] it was predicted that the FK A15 and σ phases and the Laves C14 and C15 phases could be stabilized in binary A_1B_1/A_2B_2 diblock copolymer blends. Phase diagrams in the $\phi_2 - \gamma$ plane were obtained for a fixed $\chi N = 40$ and two sets of $f_1 = 0.15$ and 0.45 , whereas the value of f_2 varies with γ as $f_2 = 0.85/\gamma$. Although the phase diagrams in the current work are provided in a different phase plane, the phase behaviors obtained from these two studies are completely consistent. It should be emphasized that the phase diagrams shown in Figures 1 and 2 cover an unprecedented large phase space of the system, thus provide more information about the phase behavior of the A_1B_1/A_2B_2 blends.

Experimentally, the formation of complex spherical packing phases in binary A_1B_1/A_2B_2 diblock copolymer blends has been examined by Lindsay et al.^[7,8] These authors observed a number of complex spherical packing phases including A15, σ , C14, C15, and a quasicrystal. The overall observed phase behavior from these experiments is consistent with the theoretical predictions. In particular, the experiments reported by Lindsay et al.^[7] revealed a phase transition sequence from $\sigma \rightarrow$ A15 \rightarrow HEX as ϕ_2 is increased from 0.25 to 0.5. The same phase transition sequence is found in the phase diagram shown in Figure 1b, which has similar molecular parameters as that of the experiments, along the path at $\chi N \approx 20$ with ϕ_2 varies from 0.3 to 0.5. This good agreement between theory and experiment is very encouraging.

3.2. Segregation of Diblock Copolymers

The phase diagrams presented above clearly reveal that the addition of a second A_2B_2 diblock copolymer with a larger A-volume fraction and longer chain length to sphere-forming A_1B_1 diblock copolymers provides an efficient route to stabilize complex spherical packing phases. It is desirable to understand the mechanisms favoring the formation of these complex ordered phases in the blends. The complex spherical packing phases are characterized by polymeric domains with different sizes and shapes. The formation of these complex structures would be favored if the free energy cost of deforming the polymeric domains is reduced. As proposed by Liu et al.,^[10] there are two possible mechanisms stabilizing the complex spherical packing phases in binary A_1B_1/A_2B_2 diblock copolymer blends, involving the segregation of the A_1B_1 - and A_2B_2 -copolymers among different polymeric domains (inter-domain segregation) and within each domain (intra-domain segregation). The inter- and intra-domain segregation of the copolymers provides mechanisms to regulate the size and shape of the polymeric domains or mesoatoms. In this subsection, we provide a detailed analysis of the two mechanisms based on a number of quantities extracted from the SCFT results. Additionally, we will demonstrate how the local copolymer segregation is affected by the molecular parameters, that is, ϕ_2 , f_2 , and γ .

3.2.1. Inter-Domain Segregation

The structure of the spherical phases could be regarded as the close packing of the space by unit cells. One particularly useful method to describe the packing pattern is to partition the space by closely-packed Wigner–Seitz cells (WSCs), such that each WSC encloses one minority A-domain or one “particle.” For the classical spherical packing phases (HCP, FCC, and BCC), all the particles are symmetrically equivalent, so that there is only one type of WSC with the same volume or equivalently the same number of copolymers contained in each WSC. In contrast, the complex spherical packing phases such as the FK and Laves phases have at least two types of non-equivalent WSCs as illustrated in Figure 3.^[15] These non-equivalent WSCs would naturally have different volumes or contain different number of copolymers. Furthermore, the shape of these WSCs is non-spherical in general. The formation of complex spherical packing phases requires the deformation of the polymeric domains from their natural state, that is, a sphere with a given size, into different non-spherical domains with different sizes. Any mechanisms favoring these domain deformations would be advantageous for the formation of the complex spherical packing phases.^[2,11,12]

It has been proposed that the formation of the complex spherical packing phases in binary A_1B_1/A_2B_2 diblock copolymer blends is enhanced by the differential distributions of the two types of copolymers among the different WSCs. In particular, this inter-domain segregation of the different copolymers offers a mechanism to regulate the size of the spherical domains because the two diblock copolymers will occupy different volumes specified by N/ρ_0 and $\gamma N/\rho_0$, respectively. In order to demonstrate the non-uniform distribution, or local segregation, of the copolymers among the different WSCs quantitatively, we compute the concentration of the A_2B_2 -copolymers (ϕ_2^{WSC})

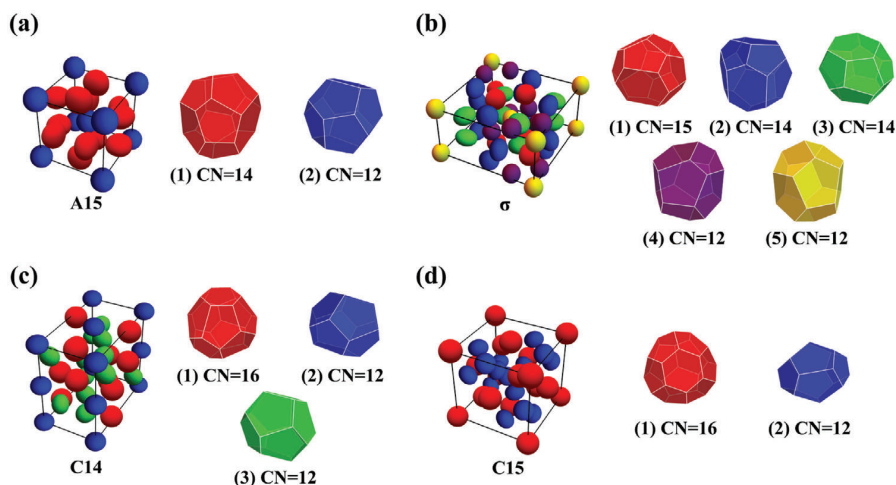


Figure 3. The unit cell of a) A15, b) σ , c) C14, and d) C15 phases. Each type of WSC is plotted along with its coordination number.

within the different WSCs. The calculated ϕ_2^{WSC} is plotted as a function of three molecular parameters, that is, ϕ_2 , f_2 , and γ , along certain phase paths in **Figure 4a–c**.

One interesting and important observation from **Figure 4** is that the A_2B_2 concentrations ϕ_2^{WSC} in different WSCs deviate from the mean value ϕ_2 , for all the complex spherical packing phases. This inter-domain segregation of diblock copolymers is especially apparent in **Figure 4a**, where ϕ_2^{WSC} is plotted as a function of ϕ_2 . If there was no inter-domain segregation, all the curves should follow the straight line $\phi_2^{\text{WSC}} = \phi_2$. The deviations from this straight line indicate that the local concentration of the A_2B_2 -copolymers in different WSCs becomes different from the average concentration. The WSCs could be roughly divided into two populations containing less or more A_2B_2 -copolymers, corresponding to smaller and larger domains for the case with $\gamma = 1.5$ shown in **Figure 4a**. It is interesting to note that the smaller WSCs of the different ordered phases have similar values of ϕ_2^{WSC} , whereas the ϕ_2^{WSC} of the larger WSCs are more scattered. A detailed examination of these curves reveals that the value of ϕ_2^{WSC} is correlated with the coordination number (CN) of the WSCs. Specifically, the smallest values of ϕ_2^{WSC} are found for the WSCs with CN = 12, whereas the largest values of ϕ_2^{WSC} are for the WSCs with CN = 16. It is also interesting to observe that the ϕ_2^{WSC} values are approximately the same for the WSCs with the same CN, regardless of the phases. In particular, all the WSCs with the smallest CN = 12 roughly have the same value of ϕ_2^{WSC} . This grouping of ϕ_2^{WSC} according to the CN is also found when ϕ_2^{WSC} is plotted as a function of f_2 (**Figure 4b**) or γ (**Figure 4c**). For the same ordered phase, the dispersity of the ϕ_2^{WSC} values among the different WSCs becomes larger when the molecular parameters (ϕ_2 , f_2 , or γ) are increased. Namely, for a given value of ϕ_2 a larger value of f_2 or γ would enhance the inter-domain segregation. From these observations, it can be concluded that the formation of WSCs with different CN is correlated with the distribution of the A_2B_2 -copolymers among the different WSCs.

The difference between the maximum and minimum values of ϕ_2^{WSC} , $\epsilon\phi_2^{\text{WSC}}$, follows the order of $\epsilon\phi_{2,A15}^{\text{WSC}} < \epsilon\phi_{2,\sigma}^{\text{WSC}} < \epsilon\phi_{2,C15}^{\text{WSC}} \approx$

$\epsilon\phi_{2,C14}^{\text{WSC}}$. This order of differences in ϕ_2^{WSC} is in agreement with the standard deviation of the WSC volumes of the different phases shown schematically in **Figure 3**, which have the ascending order of BCC/FCC/HCP(0.0) < A15(≈ 0.0135316) < σ (≈ 0.0421305) < C14(≈ 0.0987861) \lesssim C15(≈ 0.100634). It is noted that the volume deviation for the WSCs of the Laves phases is much larger than that of the A15 and σ phases. In order to be quantitative, we have computed the standard deviation of the A-domain volumes (δV) for different phases and plotted the results as a function of ϕ_2 , f_2 and γ in **Figure 5**. It is obvious that $\delta V > 0$ for all the complex spherical phases and the δV for the Laves phases is always the greatest in the whole parameter range shown in **Figure 5**.

One interesting behavior seen in **Figure 5a** is that the δV is not a monotonically increasing function of ϕ_2 . Specifically, when ϕ_2 is beyond certain critical value, δV becomes saturated and then starts to decrease slightly. This suggests that an optimal ratio of the concentrations of longer and shorter chains exists that maximizes the benefit from raising the size difference through inter-domain segregation, exceeding which there is no further benefit upon adding the longer chains. The optimal ratio should be structure-dependent. Phases that have similar property of WSCs, such as C14 and C15 phases, have similar critical $\phi_2 \approx 0.1$ while σ and A15 phases with smaller δV have higher critical ϕ_2 . Another interesting observation is that δV increases as increasing f_2 and γ . The mechanism of this tendency could be elucidated in the discussion of intra-domain segregation presented in the next subsection.

It is worth to mention that the behavior of ϕ_2^{WSC} and δV at low ϕ_2 (**Figures 4** and **5**) is similar to that of the AB/A binary blends where the A-homopolymers act as fillers localized in the central region of the A-domains.^[25] In the case of A_1B_1/A_2B_2 block copolymer blends, the long A_2 -blocks of the A_2B_2 -copolymers play a similar role to occupy the central region of the A-domains. The differential segregation of these additives provides a mechanism to regulate the sizes of the domains, thus stabilizing the complex spherical packing phases, such as the Laves C14 and C15 phases, with large domain size dispersity. However, there

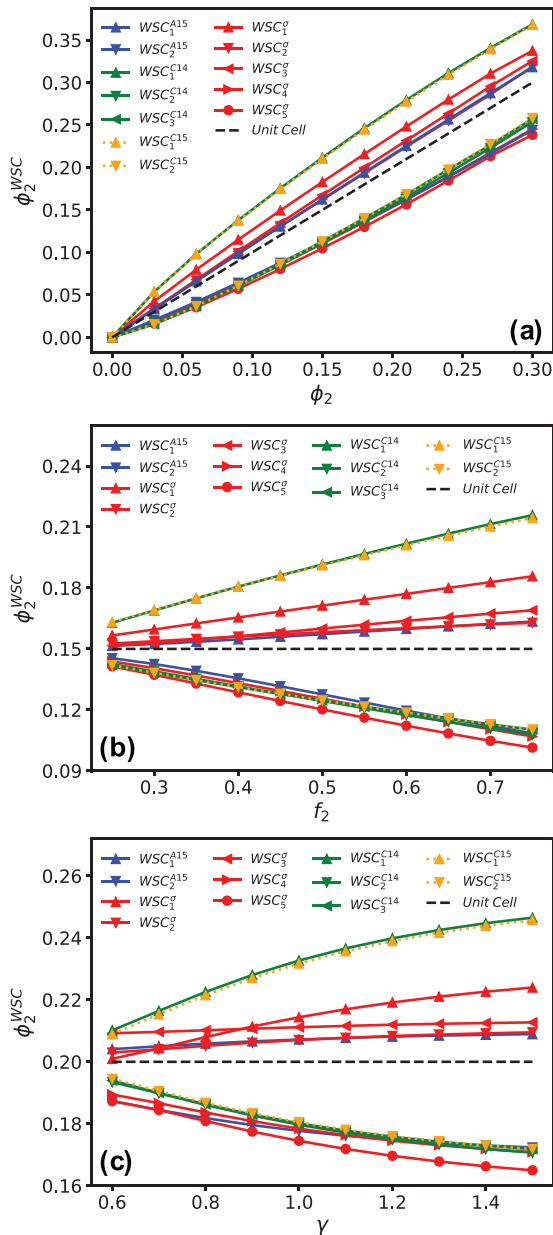


Figure 4. A₂B₂ concentration (ϕ_2^{WSC}), in different WSCs for the A15, C14, C15, and σ phases, as a function of a) ϕ_2 (with fixed $f_1 = 0.2, f_2 = 0.7, \gamma_1 = 1.5$, and $\chi N = 30$), b) f_2 (with fixed $f_1 = 0.2, \gamma_1 = 1.5, \phi_2 = 0.15, \chi N = 30$, and $\chi N = 30$) and c) γ (with fixed $f_1 = 0.2, f_2 = 0.5, \phi_2 = 0.2$, and $\chi N = 30$).

is a noticeable difference between these two types of additives. In the case of AB/A binary blends, the A-homopolymers are localized at the central region of the domains to form a core composed mostly of A-homopolymers. On the other hand, in A₁B₁/A₂B₂ diblock copolymer blends, there is a radial segregation of the long and short A-blocks forming a “core-shell” structure, as will be illustrated in the next section.

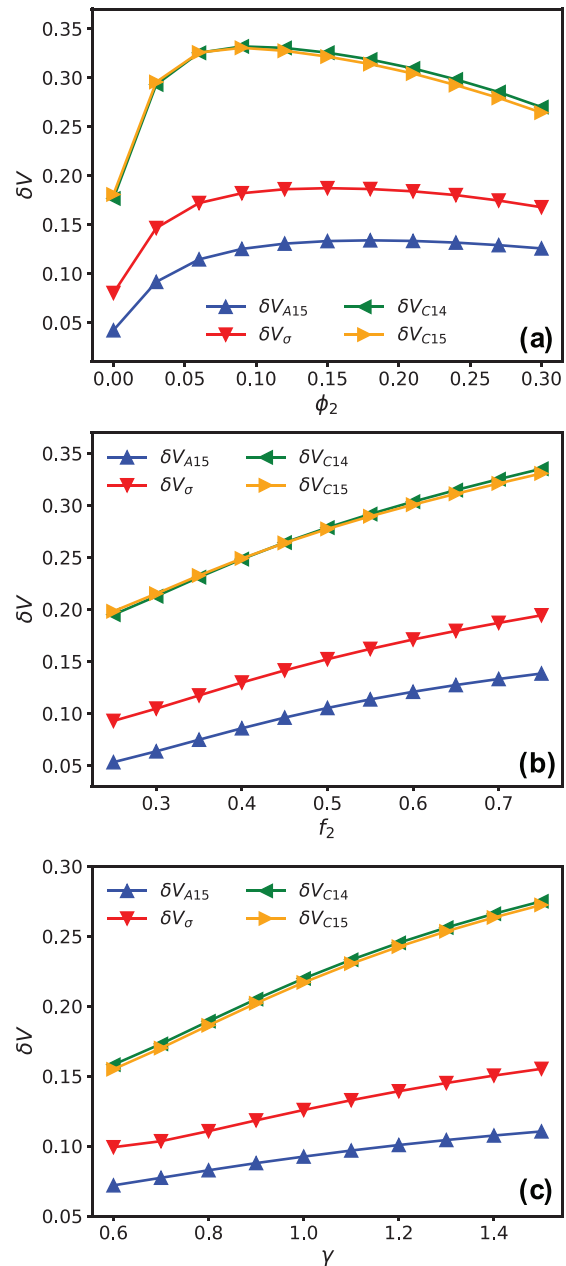


Figure 5. The standard deviation of domain volume, δV , for the FK and Laves phases, as a function of a) ϕ_2 , b) f_2 , and c) γ . The other parameters are chosen as the same as those in Figure 4.

3.2.2. Intra-Domain Segregation

In contrast to the case of binary AB/A diblock copolymer/homopolymer blends, in which the A-homopolymers mainly act as fillers localizing inside the core of each domain, the added A₂B₂ diblock copolymers in the binary A₁B₁/A₂B₂ block copolymer blends will distribute across the A- and B-domains

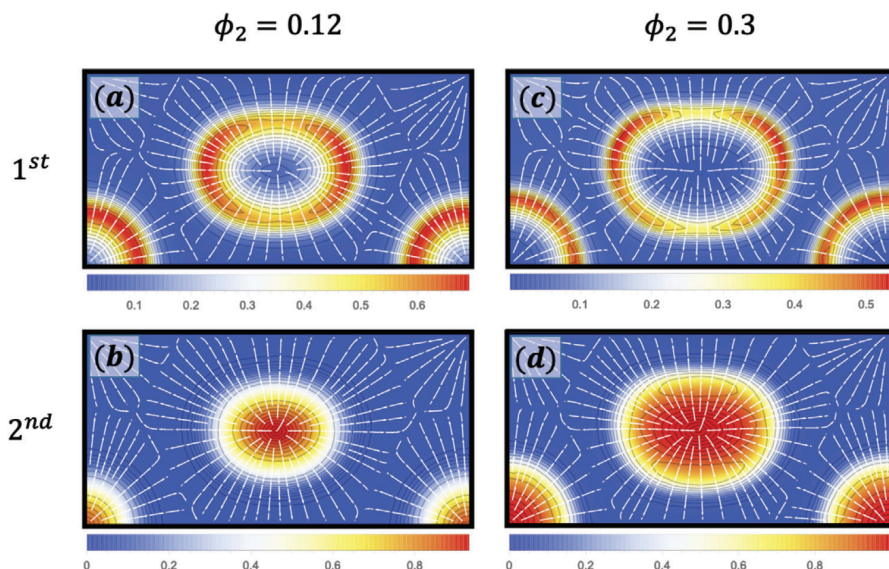


Figure 6. The A-segment density and bond orientation distributions for a,c) A_1B_1 , and b,d) A_2B_2 , with a,b) $\phi_2 = 0.12$ and c,d) $\phi_2 = 0.30$. The other fixed parameters are $f_1 = 0.2$, $f_2 = 0.7$, $\gamma_1 = 1.5$, and $\chi N = 30$. The plot is for the CN = 14 domain of an equilibrated A15 structure.

because of the architecture of the A_2B_2 -copolymers. Specifically, the AB-junctions of the A_2B_2 -copolymers will be localized at the AB-interfaces of the structure. In this case the A_2B_2 -copolymers can act as fillers such that the long A-blocks will be stretched into the center of the A-domain and, at the same time, as co-surfactants due to the localization of the AB-junctions. Therefore, the distribution of the A_2B_2 -copolymers in the system possesses interesting internal patterns, in the form of radial segregation of the A-blocks and lateral segregation of the copolymers on the AB-interfaces, that will play a dual role as fillers to regulate the size of the polymeric domains and as co-surfactants to modify the interfacial properties.^[10] These two effects provide efficient mechanisms to stabilize the complex spherical packing phases. In what follows, we provide a detailed quantitative analysis of the internal structure of domains using the SCFT results and examine the effects of ϕ_2 , f_2 , and γ on the such structures.

Due to the separation of the A- and B-blocks, the A-blocks are stretched from the AB-interface into the A-domains. Because the A_1 - and A_2 -blocks usually have different lengths, their degrees of stretching are different, resulting in a radial segregation of the two different A-blocks to form a “core-shell” structure. The segregation of the A-blocks or the formation of the “core-shell” structure could be revealed by the density distribution of the A-segments of the two copolymers. As an example, we plot the density and average bond orientation distributions of the A-segments for the CN = 14 domain of an equilibrated A15 structure in **Figures 6–8**. The average bond orientation distribution was proposed by Prasad et al. to depict the average extension and orientation of the A-backbones.^[46] The inclusion of this quantity in the figures provides information about the average stretching of the block copolymers. The existence of a radial separation of the A_1 - and A_2 -blocks is clearly visible in the density plots shown in **Figures 6–8**. Specifically, the longer A-blocks are stretched to

reach the center of the domain to form a core, whereas the shorter A-blocks are distributed near the AB-interface to form a shell. It is also interesting to observe that the orientation of the polymeric segments is perpendicular to the interface, especially in the region near the interface.

For the A_iB_i ($i = 1, 2$) diblock copolymers, the length of the A-blocks is specified by $N_{i,A} = f_i\gamma_i N$, thus the length ratio of the two A-blocks is $N_{2,A}/N_{1,A} = \gamma_2 f_2 / \gamma_1 f_1$. For the case shown in **Figure 6**, we have $\gamma = 1.5$, $f_1 = 0.2$ and $f_2 = 0.7$, thus $N_{2,A}/N_{1,A} = 5.25$ so that the A_2 -block is much longer than the A_1 -block. In this case a well-defined core-shell structure is found in **Figure 6**, in which the longer A_2 -blocks form the core of the domain and the shorter A_1 -blocks form a shell enclosing the core. This core-shell structure is found for different values of $\phi_2 = 0.12$ and 0.30 . The size of the domain increases significantly when the concentration of the longer A_2B_2 diblock copolymers is increased from 0.12 to 0.30. At the same time, noticeable deformation of the domain occurs such that the overall domain shape approaches to that of the WSC. For a polymeric domain formed from monodisperse diblock copolymers, enlarging its size would result in extra stretching of the A-blocks. Such unfavorable stretching is avoided in the case of binary A_1B_1/A_2B_2 diblock copolymer blends because the longer A-blocks can be stretched toward the center of the domain so that no excess stretching is required. Furthermore, the concentration of the longer diblock copolymers acts as a control parameter to regulate the domain size as illustrated by **Figure 6**. The inter-domain segregation shown in the **Figure 4** provides a mechanism to form polymeric domains with different sizes, which in turn pack into the complex spherical phases.

The effects of f_2 and γ on the “core-shell” structure are examined in **Figures 7** and **8**, respectively. An obvious observation is that a well-defined “core-shell” structure requires a large value of $N_{2,A}/N_{1,A} = \gamma f_2 / f_1$. In the case shown in **Figure 7** with $\gamma = 1.5$ and $f_1 = 0.2$, we have $N_{2,A}/N_{1,A} = 1.875$ and

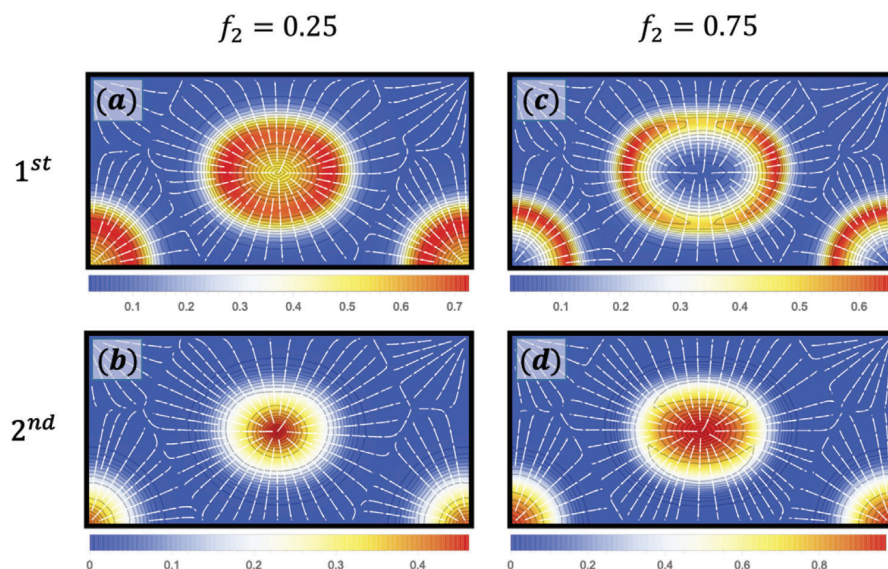


Figure 7. The A-segment density and bond orientation distributions for a,c) A_1B_1 and b,d) A_2B_2 , with a,b) $f_2 = 0.25$ and c,d) $f_2 = 0.75$. The other fixed parameters are $f_1 = 0.2$, $\gamma_1 = 1.5$, $\phi_2 = 0.15$, and $\chi N = 30$. The plot is for the CN = 14 domain of an equilibrated A15 structure.

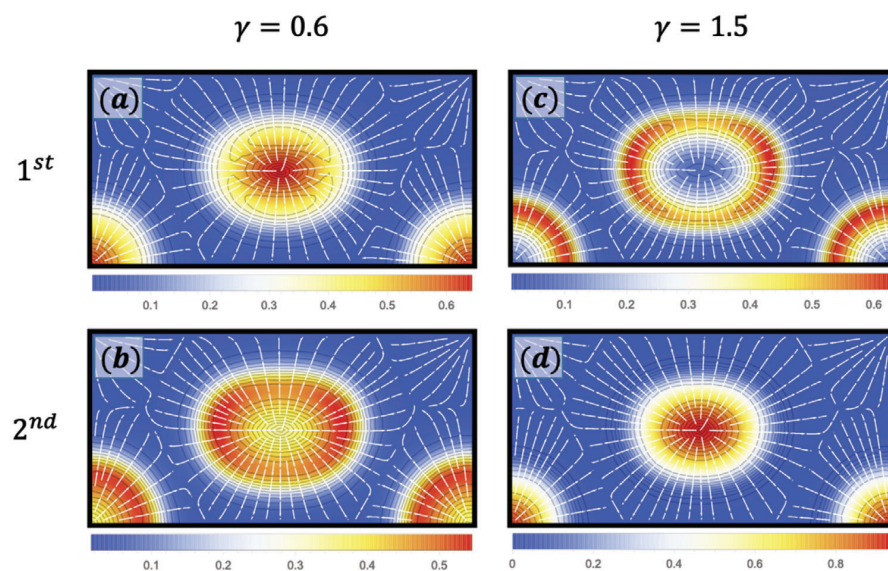


Figure 8. The A-segment density and bond orientation distributions for a,c) A_1B_1 and b,d) A_2B_2 , with a,b) $\gamma = 0.6$ and c,d) $\gamma = 1.5$. The other fixed parameters are $f_1 = 0.2$, $f_2 = 0.5$, $\phi_2 = 0.2$, and $\chi N = 30$. The plot is for the CN = 14 domain of an equilibrated A15 structure.

$N_{2,A}/N_{1,A} = 5.625$ for $f_2 = 0.25$ and 0.75 , respectively. As shown in Figure 7 and in agreement with the expectation from the $N_{2,A}/N_{1,A}$ values, a well-defined core-shell structure is observed for $f_2 = 0.75$ whereas the shell becomes quite thick for $f_2 = 0.25$. Besides the length of the A-blocks, the overall length of the diblock copolymers could have significant effects on the radial segregation of the A-blocks inside a domain. This effect is illustrated by the case shown in Figure 8 with $f_1 = 0.2$ and $f_2 = 0.5$, the ratio of $N_{2,A}/N_{1,A}$ is given by $N_{2,A}/N_{1,A} = 1.5$ and 3.75 for

$\gamma = 0.6$ and 1.5 , respectively. Although the A_2 -block is slightly longer than the A_1 -block for $\gamma = 0.6$, Figure 8a and b reveal that the A_2 -blocks form a rather thick shell whereas the A_1 -blocks mostly localized at the core. This result suggests that in the binary blends of A_1B_1/A_2B_2 diblock copolymers, the copolymers with much shorter overall chain length tend to segregate at the interface even though their A-block is slightly longer. Based on these observations, it can be concluded that the formation of the complex spherical packing phases via the “core-shell” structure

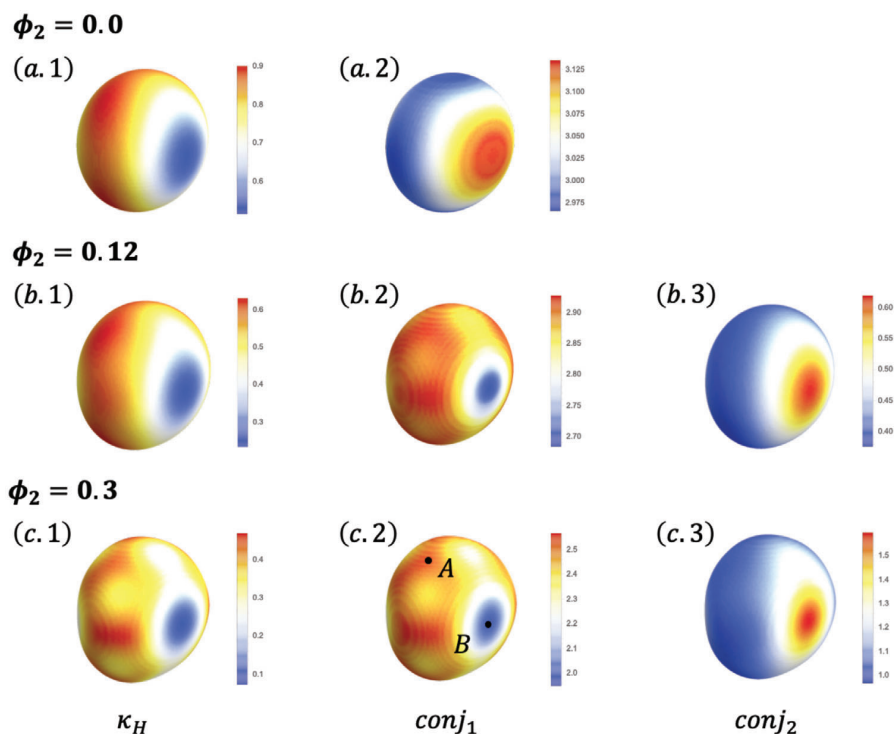


Figure 9. Interfacial mean curvature (κ_H) and A_1B_1 junction distributions ($conj_i$, $i = 1, 2$) projected on the interface for a) $\phi_2 = 0$, b) 0.12, and c) 0.30 and fixed $f_1 = 0.2$, $f_2 = 0.7$, $\gamma_1 = 1.5$, and $\chi N = 30$. The plot is for the CN = 14 domain of an equilibrated A15 structure.

requires that the additive A_2B_2 -copolymers have a large $N_{2,A}/N_{1,A}$ ratio and a chain length longer than, or at least comparable to, that of the A_1B_1 -copolymers. As an example, none of the complex spherical phases are stable in the phase diagrams shown in Figure 2a even though $N_{2,A}/N_{1,A} = \gamma f_2/f_1 = 1.25 > 1$, presumably due to the significantly shorter A_2B_2 -copolymers.

Due to the broken rotational symmetry in a crystalline structure, the WSCs assume the shape of a polyhedron. The AB-interface in the spherical packing phases would assume a non-spherical shape resembling the shape of the WSCs. On the other hand, the native shape of the polymeric domains is spherical with a uniform interfacial curvature. In the case of block copolymer blends, different diblock copolymers would have different preferred interfacial curvatures. It is therefore expected that the diblock copolymers would have an inhomogeneous distribution on the AB-interface and the distribution is coupled with the interfacial curvature. The interfacial distribution of the diblock copolymers could be revealed by the density of the AB-junction points of the two copolymers projected on the interface defined by the $\phi_A(\vec{r}) = \phi_B(\vec{r})$ isosurface. To facilitate the comparison between the distribution of AB-junctions and the interfacial curvature, we also compute the mean curvature of the interface, κ_H , based on level set method.^[47] As an example, the mean-curvature and interfacial AB-junction distributions have been computed for the CN = 14 domain of an equilibrated A15 structure and are shown in **Figures 9–11** for three sets of molecular parameters.

The plots shown in **Figures 9–11** clearly reveal the existence of a curvature driven lateral segregation of the AB-junctions on the

AB-interfaces. It is interesting to observe that a curvature driven lateral segregation of the AB-junctions occurs, albeit with a very small amplitude, even for the neat A_1B_1 -copolymers as shown in Figure 9a where a relatively higher density of AB-junctions is found in the area with a smaller curvature. When the longer and less asymmetric A_2B_2 -copolymers are added to the system, a curvature driven segregation of the A_1B_1 - and A_2B_2 -copolymers on the AB-interface takes place, such that the A_2B_2 -copolymers are localized in the area with low curvature whereas the A_1B_1 -copolymers concentrate in the area with high curvature. Specifically, as shown in Figure 9, the pattern of the mean curvature and junction distributions coincide with the shape of the WSC, especially when ϕ_2 is large. For example, the points A and B in Figure 9(c.2) represent roughly a local maximum and minimum of the A_1B_1 -junction density and they correspond to the vertex and face of the WSC, respectively. Because the vertices and faces of the WSC correspond to high and low interfacial curvature areas, the accumulation and depletion of the A_1B_1 -junctions in these areas are expected.

As shown in Figure 10, the A-volume fraction f_2 of the A_2B_2 -copolymers affects significantly the interfacial segregation of the diblock copolymers. When $f_2 = 0.25$ which is slightly larger than $f_1 = 0.2$, the interfacial segregation behavior is very similar to that for the neat A_1B_1 -copolymers (Figure 9a) such that there is a weak accumulation of the A_1B_1 -junctions at the low curvature area. On the other hand, when f_2 changes to $f_2 = 0.75$, the interfacial segregation pattern is inverted such that the A_1B_1 -junctions are depleted in the low curvature area. Similar to the formation

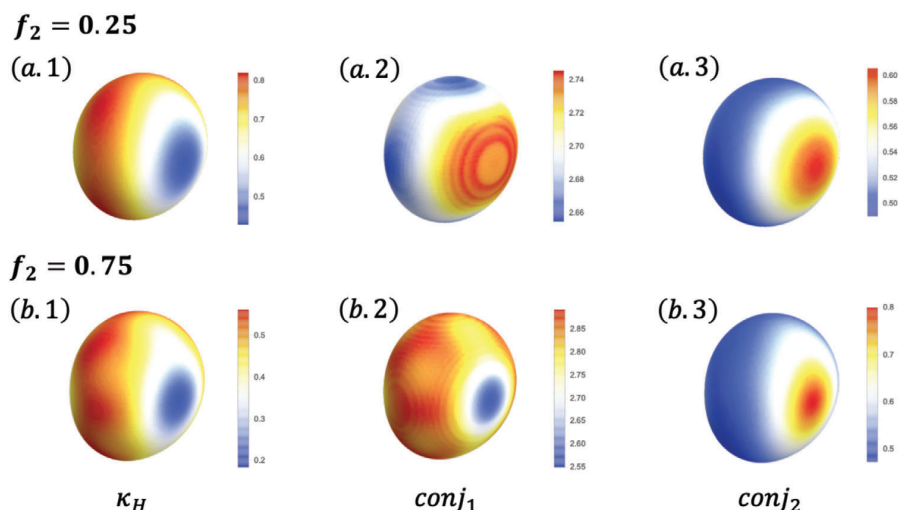


Figure 10. Interfacial mean curvature (κ_H) and A_1B_1 junction distributions ($conj_i$, $i = 1, 2$) projected on the interface for a) $f_2 = 0.25$ and b) 0.75 , with fixed $f_1 = 0.2$, $\gamma_1 = 1.5$, $\phi_2 = 0.15$, and $\chi N = 30$. The plot is for the CN = 14 domain of an equilibrated A15 structure.

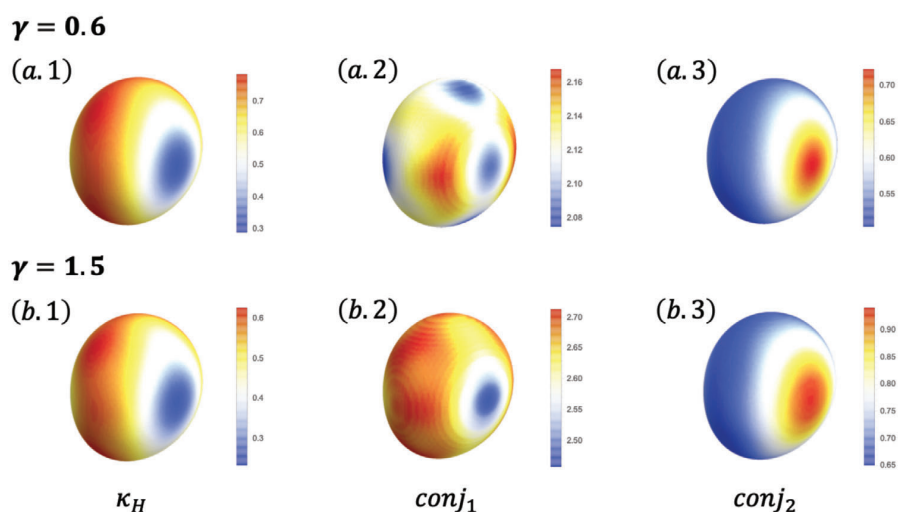


Figure 11. Interfacial mean curvature (κ_H) and A_1B_1 junction distributions ($conj_i$, $i = 1, 2$) projected on the interface for a) $\gamma = 0.6$ and b) 1.5 , with fixed $f_1 = 0.2$, $f_2 = 0.5$, $\phi_2 = 0.2$, and $\chi N = 30$. The plot is for the CN = 14 domain of an equilibrated A15 structure.

of the “core–shell” structure, the interfacial segregation also requires simultaneously large f_2 and γ as revealed by Figures 10 and 11. Particularly, for the chains with a large f_2 but significantly smaller total chain length or smaller γ , the distribution of the A_1B_1 -junctions are nearly constant on the interface as indicated by Figure 11(a.2), where the variation of the junction density is extremely small as depicted on the scale bar.

4. Conclusion

In summary, we have systematically studied the formation and relative stability of complex spherical packing phases in binary blends composed of A_1B_1 and A_2B_2 diblock copolymers with dif-

ferent chain lengths and compositions by using the polymeric self-consistent field theory. A set of phase diagrams of the binary blends have been constructed, representing the phase behavior of the system in a large parameter space. The effects of three molecular parameters, that is, the concentration ϕ_2 , composition f_2 , and relative chain length γ of the A_2B_2 diblock copolymers, have been examined. Our results predict that the complex spherical packing phases, that is, the FK A15, σ and the Laves C14, C15 phases, can become stable equilibrium phases with proper choices of f_2 and γ . In particular, the theoretical results reveal that large values of f_2 and γ are required simultaneously to stabilize the complex spherical packing phases. The phase diagrams could be used to predict the phase transition sequence for a given set of parameters.

For example, for BCC-forming A_1B_1 diblock copolymers with $f_1 = 0.2$, the addition of A_2B_2 , or increasing ϕ_2 from 0 to 1, with $f_2 = 0.7$ and $\gamma = 1.5$ is predicted to induce order-order phase transitions following the sequence of BCC \rightarrow C14 \rightarrow C15 \rightarrow σ \rightarrow A15 \rightarrow HEX \rightarrow L \rightarrow DG \rightarrow HEX. The predicted phase behavior is in agreement with available theoretical studies and experiments. More importantly, the theoretical results predict that the binary A_1B_1/A_2B_2 diblock copolymer blends provide an efficient and versatile platform to obtain complex spherical packing phases.

The mechanisms stabilizing the complex spherical packing phases have been explored by a detailed and quantitative analysis of the SCFT solutions. Specifically, the spatial distributions of the different polymeric species are used to establish correlations between structural formation and polymer segregation. A detailed examination of the A_2B_2 -concentration in different Wigner–Seitz cells reveals that inter-domain segregation of the different diblock copolymers occurs in the blends, resulting in domains of different sizes. At the same time, an examination of the A-segment density and AB-junction distributions demonstrates that two types of intra-domain segregation take place. The radial segregation of the long and short A-blocks inside the A-domains results in a core–shell structure. The simultaneous stretching of the long and short chains enables the formation of large spherical domains. The lateral segregation of the AB diblock copolymers on the AB-interfaces releases the frustration of forming non-spherical cells. These mechanisms operate synergistically resulting in a large stable region for the complex spherical packing phases.

The current study focused on the simplest binary blends of diblock copolymers, that is, blends containing A_1B_1 and A_2B_2 diblock copolymers. It is natural to expect that more complex binary blends composed of AB/CD diblock copolymers will exhibit more complex phase behaviors, thus providing more opportunities to form novel ordered phases, for example, other FK phases and quasicrystals. Extension of the current study to more complex blends containing block copolymers is straightforward, however, care must be taken when one chooses the molecular parameters and possible ordered candidate phases.

The results obtained in the current study provide a useful foundation for further investigation of more complex polymeric blends containing block copolymers. The mechanisms identified in the study will be helpful for the understanding of the formation of complex structures via polymer self-assembly. In particular, the mechanism of local segregation of distinct components in polymer blends provides a simple and effective route to access complex ordered phases, particularly the complex spherical packing phases.

Acknowledgements

The authors acknowledge delightful discussions on the phase behavior of block copolymers with Frank Bates, Kevin Dorfman, Weihua Li, Meijiao Liu, and Rob Wickham. This research was supported by the Natural Sciences and Engineering Research Council (NSERC) of Canada and was enabled in part by support provided by the facilities of SHARCNET (<https://www.sharcnet.ca>) and Compute Canada (<http://www.compute-canada.ca>).

Conflict of Interest

The authors declare no conflict of interest.

Data Availability Statement

The data that support the findings of this study are available from the corresponding author upon reasonable request.

Keywords

block copolymers, Frank–Kasper phases, polymer blends, self-assembly

Received: July 29, 2021

Revised: August 26, 2021

Published online:

- [1] C. M. Bates, F. S. Bates, *Macromolecules* **2017**, *50*, 3.
- [2] A.-C. Shi, *J. Phys.: Condens. Matter* **2021**, *33*, 253001.
- [3] S. Lee, M. J. Bluemle, F. S. Bates, *Science* **2010**, *330*, 349.
- [4] M. W. Schulze, R. M. Lewis III, J. H. Lettow, R. J. Hickey, T. M. Gillard, M. A. Hillmyer, F. S. Bates, *Phys. Rev. Lett.* **2017**, *118*, 207801.
- [5] M. W. Bates, S. M. Barbon, A. E. Levi, R. M. Lewis, H. K. Beech, K. M. Vonk, C. Zhang, G. H. Fredrickson, C. J. Hawker, C. M. Bates, *ACS Macro Lett.* **2020**, *9*, 396.
- [6] A. J. Mueller, A. P. Lindsay, A. Jayaraman, T. P. Lodge, M. K. Mahanthappa, F. S. Bates, *ACS Macro Lett.* **2020**, *9*, 576.
- [7] A. P. Lindsay, R. M. Lewis III, B. Lee, A. J. Peterson, T. P. Lodge, F. S. Bates, *ACS Macro Lett.* **2020**, *9*, 197.
- [8] A. P. Lindsay, G.-K. Cheong, A. J. Peterson, S. n Weigand, K. D. Dorfman, T. P. Lodge, F. S. Bates, *Macromolecules* **2021**, *54*, 7088.
- [9] N. Xie, W. Li, F. Qiu, A.-C. Shi, *ACS Macro Lett.* **2014**, *3*, 906.
- [10] M. Liu, Y. Qiang, W. Li, F. Qiu, A.-C. Shi, *ACS Macro Lett.* **2016**, *5*, 1167.
- [11] W. Li, C. Duan, A.-C. Shi, *ACS Macro Lett.* **2017**, *6*, 1257.
- [12] A. Reddy, M. B. Buckley, A. Arora, F. S. Bates, K. D. Dorfman, G. M. Grason, *Proc. Natl. Acad. Sci. USA* **2018**, *115*, 10233.
- [13] F. C. Frank, J. S. Kasper, *Acta Crystallogr.* **1958**, *11*, 184.
- [14] F. C. Frank, J. S. Kasper, *Acta Crystallogr.* **1959**, *12*, 483.
- [15] M. De Graef, M. E. McHenry, *Structure of Materials: An Introduction to Crystallography, Diffraction and Symmetry*, Cambridge University Press, Cambridge **2012**.
- [16] S. Kim, K.-J. Jeong, A. Yethiraj, M. K. Mahanthappa, *Proc. Natl. Acad. Sci. USA* **2017**, *114*, 4072.
- [17] A. Jayaraman, M. K. Mahanthappa, *Langmuir* **2018**, *34*, 2290.
- [18] C. M. Baez-Cotto, M. K. Mahanthappa, *ACS Nano* **2018**, *12*, 3226.
- [19] K. Yue, M. Huang, R. L. Marson, J. He, J. Huang, Z. Zhou, J. Wang, C. Liu, X. Yan, K. Wu, Z. Guo, H. Liu, W. Zhang, P. Ni, C. Wesdemiotis, W.-B. Zhang, S. C. Glotzer, S. Z. D. Cheng, *Proc. Natl. Acad. Sci. USA* **2016**, *113*, 14195.
- [20] Z. Su, J. Huang, W. Shan, X. Yan, R. Zhang, T. Liu, Y. Liu, Q. Guo, F. Bian, X. Miao, M. Huang, S. Z. D. Cheng, *CCS Chem.* **2020**, *3*, 1434.
- [21] R. M. Lewis III, A. Arora, H. K. Beech, B. Lee, A. P. Lindsay, T. P. Lodge, K. D. Dorfman, F. S. Bates, *Phys. Rev. Lett.* **2018**, *121*, 208002.
- [22] S. Lee, C. Leighton, F. S. Bates, *Proc. Natl. Acad. Sci. USA* **2014**, *111*, 17723.
- [23] Y. Qiang, W. Li, A.-C. Shi, *ACS Macro Lett.* **2020**, *9*, 668.
- [24] G.-K. Cheong, F. S. Bates, K. D. Dorfman, *Proc. Natl. Acad. Sci. USA* **2020**, *117*, 16764.
- [25] J. Xie, A.-C. Shi, *Giant* **2021**, *5*, 100043.
- [26] M. Zhao, W. Li, *Macromolecules* **2019**, *52*, 1832.
- [27] K. Kim, A. Arora, A. M. Lewis, M. Liu, W. Li, A.-C. Shi, K. D. Dorfman, F. S. Bates, *Proc. Natl. Acad. Sci. USA* **2018**, *115*, 847.
- [28] T. Hashimoto, S. Koizumi, H. Hasegawa, *Macromolecules* **1994**, *27*, 1562.

- [29] D. Yamaguchi, T. Hashimoto, C. D. Han, D. M. Baek, J. K. Kim, A.-C. Shi, *Macromolecules* **1997**, *30*, 5832.
- [30] D. Yamaguchi, S. Shiratake, T. Hashimoto, *Macromolecules* **2000**, *33*, 8258.
- [31] D. Yamaguchi, M. Takenaka, H. Hasegawa, T. Hashimoto, *Macromolecules* **2001**, *34*, 1707.
- [32] F. Court, T. Hashimoto, *Macromolecules* **2002**, *35*, 2566.
- [33] F. Chen, Y. Kondo, T. Hashimoto, *Macromolecules* **2007**, *40*, 3714.
- [34] A.-C. Shi, J. Noolandi, *Macromolecules* **1994**, *27*, 2936.
- [35] A.-C. Shi, J. Noolandi, *Macromolecules* **1995**, *28*, 3103.
- [36] M. W. Matsen, F. S. Bates, *Macromolecules* **1995**, *28*, 7298.
- [37] Z. Wu, B. Li, Q. Jin, D. Ding, A.-C. Shi, *J. Phys. Chem. B* **2010**, *114*, 15789.
- [38] Z. Wu, B. Li, Q. Jin, D. Ding, A.-C. Shi, *Macromolecules* **2011**, *44*, 1680.
- [39] C. T. Lai, A.-C. Shi, *Macromol. Theory Simul.* **2021**, *33*, 2100019.
- [40] G. H. Fredrickson, *The Equilibrium Theory of Inhomogeneous Polymers*, volume 134. Oxford University Press, Oxford **2006**.
- [41] A.-C. Shi, in *Self-Consistent Field Theory of Inhomogeneous Polymeric Systems, in Variation Methods in Molecular Modeling* (Ed: J. Wu), Springer, Singapore **2017**, pp. 155–180.
- [42] K. Ø. Rasmussen, G. Kalosakas, *J. Polym. Sci., Part B: Polym. Phys.* **2002**, *40*, 1777.
- [43] G. Tzeremes, K. Ø. Rasmussen, T. Lookman, A. Saxena, *Phys. Rev. E* **2002**, *65*, 041806.
- [44] R. B. Thompson, K. Ø. Rasmussen, T. Lookman, *J. Chem. Phys.* **2004**, *120*, 31.
- [45] A. Arora, D. C. Morse, F. S. Bates, K. D. Dorfman, *J. Chem. Phys.* **2017**, *146*, 244902.
- [46] I. Prasad, Y. Seo, L. M. Hall, G. M. Grason, *Phys. Rev. Lett.* **2017**, *118*, 247801.
- [47] E. Albin, R. Knikker, S. Xin, C.-O. Paschereit, Y. d'Angelo, in *Int. Conf. on Mathematical Methods for Curves and Surfaces*, Springer, Cham **2016**, pp. 1–22.

Chapter 6

Theory of Complex Spherical Packing Phases in Diblock Copolymer/Homopolymer Blends

Publication: Xie, Jiayu, and An-Chang Shi. “Theory of Complex Spherical Packing Phases in Diblock Copolymer/Homopolymer Blends.” *Macromolecules* 56.24 (2023): 10296–10312.

Authors: **Jiayu Xie**, An-Chang Shi

Contribution: As the first author, my contributions included constructing the theoretical model and computational code, generating and analyzing the data, and drafting the initial manuscript. Dr. An-Chang Shi and I collaborated on manuscript revisions, with guidance from Dr. Shi throughout the research.

Preface

In this chapter, we systematically explore the phase behaviours of two illuminating model systems: binary AB/C blends and ternary AB/C/D blends, focusing on the stability of the Frank-Kasper phases. Recent experiments have revealed the formation of FK phases not only in polymeric blends [106, 129, 107] but also in surfactant systems [108–111]. These systems involve the mixing of amphiphilic molecules with a matrix-selective component alone, or both core-selective and matrix-selective components together. Unlike the effect of adding a core-selective component, thoroughly discussed in Chapter 4, the addition of a matrix-selective component swells the matrix. It remains unclear how the stability of the FK phases is impacted with the existence of a matrix-selective component. Motivated by the need to understand the experimentally observed emergence of the FK phases in the broad range of soft matter systems, our study concerns the case where the AB copolymer is A-sphere-forming, and the C and D homopolymers are B- and A-selective, respectively. Free-jointed chain model is used to model all polymer chains, which provides a reasonable description of low-molecular-weight polymers and even small molecules compared to the commonly used continuous Gaussian chain model. Self-consistent field theory is then employed to probe the phase behaviours of the systems.

For binary AB/C blends, phase diagrams are presented in the $\phi_2 - \chi$ plane. In the case of ternary AB/C/D blends, phase diagrams are constructed in both the $\phi_2 - \chi$ plane and the $\phi_1 - \phi_2 - \phi_3$ triangle, utilizing different thermodynamic ensembles. These comprehensive diagrams cover an extensive region of the phase spaces for both systems, offering insights into their phase behaviours. By analyzing SCFT solutions, we explore the correlation between system parameters, the distribution of blend components, and the properties of self-assembled spherical domains. Our findings qualitatively align with available experimental results on both polymeric blends and surfactant systems, enhancing

our understanding of the stabilization mechanisms of the FK phases in diverse soft matter systems involving amphiphilic molecules and selective solvents.

Theory of Complex Spherical Packing Phases in Diblock Copolymer/Homopolymer Blends

Jiayu Xie and An-Chang Shi*

Cite This: *Macromolecules* 2023, 56, 10296–10312

Read Online

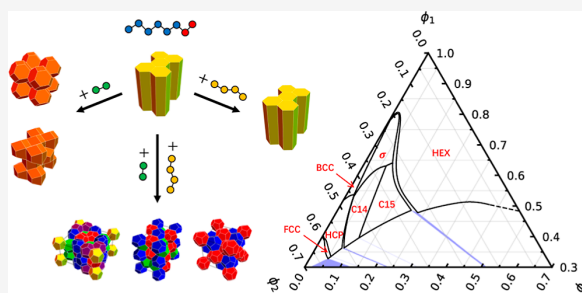
ACCESS |

Metrics & More

Article Recommendations

Supporting Information

ABSTRACT: The formation of complex spherical packing phases in binary and ternary diblock copolymer/homopolymer blends is studied using self-consistent field theory (SCFT). The polymeric blends are composed of A-sphere-forming AB diblock copolymers mixed with B-selective (C) homopolymers and A-selective (D) homopolymers, resembling surfactant/water and surfactant/water/oil systems. It is observed that the addition of C homopolymers stabilizes the Frank–Kasper (FK) σ and A15 phases, and further addition of D homopolymers enables the appearance of the Laves C14 and C15 phases. Compared with neat AB diblock copolymers, the FK σ phase is predicted to become an equilibrium phase in the AB/C blends at lower conformational asymmetry. In the AB/C/D blends, the C and D homopolymers are localized in the B-rich matrix and A-rich cores, respectively, synergistically stabilizing the complex spherical packing phases. The theoretically predicted phase behaviors of the AB/C and AB/C/D blends are consistent with experiments on polymeric blends and surfactant systems. These results provide insights into the emergence of complex spherical packings in soft matter systems composed of amphiphiles and selective additives.



INTRODUCTION

The packing problem is encountered ubiquitously in nature.¹ One well-known example is the search of the densest packing of identical hard spheres, which is solved in three-dimensions by packing the spheres on the face-centered cubic (fcc) or hexagonal close-packed (hcp) lattices.² In contrast to the packing of hard spheres, the packing problem in many soft condensed matter systems is much more complicated because the spherical domains are self-assembled from smaller molecules, allowing them to adjust their shapes and volumes. As a result, the equilibrium packing of these soft domains depends sensitively on the properties of the constituent molecules, and many different arrangements corresponding to various crystalline structures can emerge.

One ideal platform to study the packing of soft spheres is provided by block copolymers, which are macromolecules composed of more than one chemically distinct subchains or blocks covalently linked together.^{3,4} The simplest example of block copolymers is an AB diblock copolymer obtained by joining two homopolymers (A and B) through their ends. In AB diblock copolymer melts with shorter A blocks and longer B blocks, due to the chemical incompatibility between the A and B monomers, the copolymer chains could aggregate to form spherical domains consisting of A cores and B coronas, which in turn could pack into different crystalline structures with long-range order.^{3,5} It has been well established that the equilibrium spherical packing phases for the neat conformationally symmetric AB diblock copolymer melts are the body-

centered cubic (bcc) and hcp spheres, commonly referred to as the classical spherical phases.^{6,7}

Given the richness of crystalline structures, a natural question arises: can complex spherical packing phases or nonclassical spherical phases emerge from the self-assembly of block copolymers? An early instance of a nonclassical spherical phase in block copolymers is the self-assembly of a Frank–Kasper (FK) A15 phase from miktoarm AB_n block copolymers, which was predicted theoretically by Grason et al.^{8–10} and observed experimentally by Cho et al.¹¹ A significant breakthrough in the search of nonclassical spherical phases in block copolymers was the discovery of a FK σ phase in linear polyisoprene-*block*-polylactide diblock copolymer melts by Lee et al.¹² Since then, a large number of experimental and theoretical studies on the emergence and stability of complex spherical packing phases self-assembled from block copolymers have been carried out.^{7,13,14} Besides their appearance in neat block copolymer melts, these complex spherical phases, including two other FK phases, namely, the Laves C14 and C15 phases, have been found to be stable in binary AB diblock

Received: September 26, 2023

Revised: November 23, 2023

Accepted: November 27, 2023

Published: December 12, 2023



copolymer/A homopolymer (A_1B_1/A_2) blends^{15–18} and binary blends of AB diblock copolymers with different block compositions and/or degrees of polymerization (A_1B_1/A_2B_2).^{19–23} The discovery of these complex morphologies has greatly enriched the array of possible spherical packing phases accessible in polymeric systems containing block copolymers.¹⁴

Since the discovery of the FK phases in AB diblock copolymer systems, substantial efforts have been made to understand their formation mechanisms. There are two key features that distinguish the FK phases from the classical spherical phases, *i.e.* bcc, fcc, and hcp. The first feature is that the Wigner–Seitz cells (WSCs) of the FK phases are on average more rounder (having higher sphericity) than those of the classical spherical phases.¹³ In neat AB diblock copolymer melts, the stabilization of the FK phases is enabled by increasing the conformational asymmetry of the diblocks, quantified by the parameter ϵ that is defined by the ratio between the Kuhn lengths of the two blocks, $\epsilon = b_A/b_B$. Having $b_A > b_B$ leads to larger spherical domains, which in turn induces more pronounced polyhedral imprinting on the A–B interface toward the shape of their corresponding WSCs. Therefore, in comparison to the classical spherical phases, the FK phases with more spherical WSCs have less enthalpic penalty from warping the interface, making them more thermodynamically favored when ϵ is increased. This mechanism has been analyzed quantitatively by Grason *et al.* using the diblock foam model based on the strong-stretching theory (SST) and the WSC geometry of various spherical packing phases.²⁴

The second feature of the FK phases is the existence of several nonequivalent spherical domains enclosed by distinct WSCs with different sizes and shapes, in contrast to the classical spherical phases with only one type of spherical domain. This feature makes polymeric blends an ideal platform to stabilize the FK phases because the local segregation of the various components provides an effective mechanism to form domains with different sizes and shapes. The simplest recipe to formulate binary blends that stabilize the FK phases is to mix A homopolymers into A-sphere-forming AB diblock copolymers. Both theory^{16,17} and experiments^{15,18} have shown that the FK σ , C14, and C15 phases can be stabilized in the binary A_1B_1/A_2 diblock copolymer/homopolymer blends. Unlike the formation of the FK phases in neat AB diblock copolymers, which requires conformational asymmetry of the diblock chains, the emergence of the FK phases in the A_1B_1/A_2 blends does not necessitate conformationally asymmetric AB diblock copolymers. Detailed self-consistent field theory (SCFT) studies have provided direct evidence of the nonuniform distribution of the A homopolymers across different types of spherical domains, which is responsible for the formation of domains with largely different volumes commensurate with the size difference in the FK WSCs. These theoretical and experimental results have led to a good understanding of the emergence of the FK packings in the binary A_1B_1/A_2 blends.

For A-sphere-forming diblock copolymers, opposite to the effect of adding A homopolymers, the addition of B homopolymers swells the B matrix.^{25,26} In an experimental study of A_1B_1/B_2 blends composed of poly(ϵ -caprolactone)-*block*-polybutadiene (PCL-*b*-PB) diblock copolymers and polybutadiene (PB) homopolymers by Takagi and Yamamoto, a phase transition sequence of HEX \rightarrow σ \rightarrow bcc was detected as the homopolymer concentration increased.²⁷ A sensitive dependence of the presence and location of the σ phase

window on the molecular weight of the homopolymers was also observed. In a more recent experimental study of A_1B_1/B_2 mixtures composed of cylinder-forming poly(ethylene oxide)-*block*-poly(1,2-butadiene) (PEO-*b*-PB) diblock copolymers blended with either PB homopolymers or dodecylbenzene nonpolar foreign solvents, Chen *et al.* reported the discovery of the FK σ phase with a very low conformational asymmetry ($\epsilon \approx 1.2$) of the diblocks.²⁸ Moreover, the Laves C15 phase with a gigantic unit cell was discovered in salt-doped $A_1B_1/A_2/B_2$ pseudoternary polymer blends, where the AB copolymers act as compatibilizers between the A and B homopolymers.²⁹ These experimental results indicate that the complex spherical packing phases self-assembled from block copolymers could become more favored with the addition of corona-selective homopolymers alone or core- and corona-selective homopolymers together. Interestingly, the emergence of the FK phases, including the σ , A15, C14, and C15, has also been reported in surfactant/water and surfactant/water/oil systems exhibiting lyotropic liquid crystal (LLC) phases.^{30–33} The surfactant/water and surfactant/water/oil systems bear a strong similarity to the A_1B_1/B_2 and $A_1B_1/B_2/A_2$ polymeric blends, respectively, suggesting that they may share similar mechanisms in stabilizing these intriguing packing phases.

To our knowledge, the phase behaviors of the A_1B_1/B_2 and $A_1B_1/B_2/A_2$ blends involving complex spherical packing phases have not yet been systematically explored. In this work, we fill this gap by conducting a systematic study of the phase behaviors of these two blending systems using SCFT, aiming at a better understanding of the mechanisms governing the stability of the FK phases. We consider two generic model systems, that is, binary AB/C blends and ternary AB/C/D blends. In our model, all polymer chains are modeled as freely joined chains (FJCs). Compared to the commonly used continuous Gaussian chain (GC), the FJC is more suitable for modeling low-molecular-weight polymers and may even be a reasonable model for surfactant molecules.³⁴ The C and D homopolymers are B-selective and A-selective, respectively, by using appropriate Flory–Huggins χ parameters, that is, $\chi_{BC} < 0$ and $\chi_{AD} < 0$. These choices also make the two polymeric blends resemble surfactant/water and surfactant/water/oil systems. We explore a large region in the phase space of the systems of interest, and the phase behaviors are illustrated through a set of phase diagrams. The effects of various system parameters are demonstrated by comparing the phase diagrams with different parameters. A detailed analysis is also conducted to reveal the formation mechanisms of the complex spherical packing phases in the two systems. The theoretical results of the current work can be used to rationalize the available experimental observations from polymeric and surfactant systems, thus providing insights into the emergence of complex spherical packings in a broad range of systems consisting of amphiphilic molecules and selective additives.^{35–38}

■ THEORETICAL MODEL

In the following, we first introduce the theoretical model of the binary AB/C blends and then extend it to the ternary AB/C/D blends. For the binary AB/C blends, we consider n_1 AB diblock copolymers and n_2 C homopolymers, both modeled as FJCs, in a volume V . Each AB diblock copolymer is composed of N_A A and N_B B segments, resulting in a chain with $N = N_A + N_B$ segments connected by $N - 1$ bonds. To facilitate the development of the theory, we define a reference chain length N_0 and also define $\gamma_1 = \gamma_{AB} = N/N_0$. By choosing $N_0 = N$, we

have $\gamma_1 = 1$. For each diblock chain, the block composition, or volume fraction of the A block is $f_A = N_A/N = f$ and that of the B block is $f_B = N_B/N = 1 - f$. Each C homopolymer has N_C C segments and we define $\gamma_2 = \gamma_C = N_C/N$. For simplicity, we assume a uniform segment density ρ_0 so that $\rho_0 V = n_1 N + n_2 \gamma_C N$ according to the incompressibility condition. The average concentrations of the AB diblock copolymers (ϕ_1) and C homopolymers (ϕ_2) are given by

$$\phi_1 = \frac{n_1 N}{\rho_0 V}, \quad \phi_2 = 1 - \phi_1 = \frac{n_2 \gamma_C N}{\rho_0 V} \quad (1)$$

The bonded potential energy between two adjacent segments on a polymer chain is expressed as

$$b_\alpha(R_i) = -k_B T \ln \delta(R_i - b_\alpha) \quad (2)$$

where b_α represents the Kuhn length of the α segments. Equation 2 implies that the adjacent segments are connected by a bond with a fixed length and there is no angular dependence between adjacent bonds. The total nonbonded potential energy of the system is

$$U = k_B T \rho_0 \sum_{\alpha \neq \beta} \chi_{\alpha\beta} \int u(|\mathbf{r} - \mathbf{r}'|) \hat{\phi}_\alpha(\mathbf{r}) \hat{\phi}_\beta(\mathbf{r}') d\mathbf{r} d\mathbf{r}' \quad (3)$$

where $\chi_{\alpha\beta}$ is the Flory–Huggins parameter between the α and β segments, $\hat{\phi}_\alpha(\mathbf{r})$ is the microscopic density operator of the α segments, and $u(|\mathbf{r} - \mathbf{r}'|)$ is the interaction potential accounting for the finite-range interactions between chemically distinct segments. For the nonbonded interaction potential, we choose a Gaussian form

$$u(R) = \left(\frac{3}{2\pi r_0^2} \right)^{3/2} \exp\left(-\frac{3R^2}{2r_0^2} \right) \quad (4)$$

$$u(k) = \exp\left(-\frac{k^2 r_0^2}{6} \right) \quad (5)$$

which is normalized over the real space, that is, $\int u(R) d\mathbf{R} = 1$.

To consider the two-phase coexistence region, it is convenient to formulate the theory in the grand canonical ensemble in which the thermodynamic control parameters are the chemical potentials of the AB diblock copolymers, μ_1 , and the C homopolymers, μ_2 . The mean-field grand potential density is written as^{39,40}

$$\begin{aligned} \frac{N\Phi}{\rho_0 V k_B T} = & - \sum_{\kappa} e^{\mu_{\kappa}/k_B T} Q_{\kappa} - \frac{1}{V} \\ & \int d\mathbf{r} \left[\sum_{\alpha} N \omega_{\alpha}(\mathbf{r}) \phi_{\alpha}(\mathbf{r}) - \sum_{\alpha \neq \beta} \chi_{\alpha\beta} N \int u(|\mathbf{r} - \mathbf{r}'|) \right. \\ & \left. \phi_{\alpha}(\mathbf{r}) \phi_{\beta}(\mathbf{r}') d\mathbf{r}' + \eta(\mathbf{r}) \left(1 - \sum_{\alpha} \phi_{\alpha}(\mathbf{r}) \right) \right] \quad (6) \end{aligned}$$

where $\kappa (=1$ for AB diblock copolymers or 2 for C homopolymers) is used to label different types of polymer chains and α and β (=A, B, or C) are used to label different types of segments. $\phi_{\alpha}(\mathbf{r})$ is the ensemble average of $\hat{\phi}_{\alpha}(\mathbf{r})$ and $\omega_{\alpha}(\mathbf{r})$ is the conjugate field of $\phi_{\alpha}(\mathbf{r})$. $\eta(\mathbf{r})$ is the Lagrange multiplier that enforces the incompressibility condition. Minimizing the grand potential leads to a set of SCFT equations

$$\begin{cases} N \omega_{\alpha}(\mathbf{r}) = \sum_{\beta (\neq \alpha)} \chi_{\alpha\beta} N \int u(R) \phi_{\beta}(\mathbf{r} - \mathbf{R}) d\mathbf{R} + \eta(\mathbf{r}) \\ \phi_A(\mathbf{r}) = \frac{e^{\omega_A(\mathbf{r})}}{N} \sum_{i=1}^{N_A} q_1(i, \mathbf{r}) q_1^{\dagger}(i, \mathbf{r}) \\ \phi_B(\mathbf{r}) = \frac{e^{\omega_B(\mathbf{r})}}{N} \sum_{i=N_A+1}^{N_B} q_1(i, \mathbf{r}) q_1^{\dagger}(i, \mathbf{r}) \\ \phi_C(\mathbf{r}) = e^{\mu/k_B T} \frac{e^{\omega_C(\mathbf{r})}}{N} \sum_{i=1}^{N_C} q_2(i, \mathbf{r}) q_2(N_C - i + 1, \mathbf{r}) \\ \sum_{\alpha} \phi_{\alpha}(\mathbf{r}) = 1 \end{cases} \quad (7)$$

where $\mathbf{R} = \mathbf{r} - \mathbf{r}'$ and $R = |\mathbf{R}|$. Without loss of generality, in eq 7, we have set the chemical potential μ_1 for the diblock copolymers to 0 by using the incompressibility condition so the subscript of μ_2 has been dropped for brevity. Once eq 7 is solved, the average concentrations for different components can be calculated by

$$\phi_1 = Q_1, \quad \phi_2 = 1 - \phi_1 \quad (8)$$

The forward propagators $q(i, \mathbf{r})$'s in eq 7 are calculated via the iterative relation

$$q_{\kappa}(i+1, \mathbf{r}_{i+1}) = e^{-\omega_{\kappa}(\mathbf{r}_{i+1})} \int d\mathbf{r}_i g_{\alpha}(\mathbf{r}_{i+1} - \mathbf{r}_i) q_{\kappa}(i, \mathbf{r}_i) \quad (9)$$

where $g_{\alpha}(\mathbf{r}_{i+1} - \mathbf{r}_i)$ is the bond transition probability of the form $g_{\alpha}(\mathbf{R}_i) = \delta(|\mathbf{R}_i| - b_{\alpha})/4\pi b_{\alpha}^2$ with $\mathbf{R}_i = \mathbf{r}_{i+1} - \mathbf{r}_i$. The initial condition of the iteration is $q_{\kappa}(1, \mathbf{r}) = \exp[-\omega_{\alpha}(\mathbf{r})]$. The computation of the backward propagators is performed similarly, with the iterations running in the opposite direction. The single-chain partition function Q_{κ} is computed by

$$Q_{\kappa} = \frac{1}{V} \int d\mathbf{r}_{N_{\kappa}} q_{\kappa}(N_{\kappa}, \mathbf{r}_{N_{\kappa}}) \quad (10)$$

Another useful thermodynamic ensemble is the canonical ensemble, with the concentrations of different components being the control parameters. The Helmholtz free energy density is given by

$$\begin{aligned} \frac{NF}{\rho_0 V k_B T} = & - \sum_{\kappa} \frac{\phi_{\kappa}}{\gamma_{\kappa}} \ln \frac{Q_{\kappa}}{\phi_{\kappa}} - \frac{1}{V} \\ & \int d\mathbf{r} \left[\sum_{\alpha} N \omega_{\alpha}(\mathbf{r}) \phi_{\alpha}(\mathbf{r}) - \sum_{\alpha \neq \beta} \chi_{\alpha\beta} N \int u(|\mathbf{r} - \mathbf{r}'|) \right. \\ & \left. \phi_{\alpha}(\mathbf{r}) \phi_{\beta}(\mathbf{r}') d\mathbf{r}' + \eta(\mathbf{r}) \left(1 - \sum_{\alpha} \phi_{\alpha}(\mathbf{r}) \right) \right] \quad (11) \end{aligned}$$

Minimizing eq 11 results in a similar set of SCFT equations as eq 7 with some modifications for the equations calculating the different ϕ 's

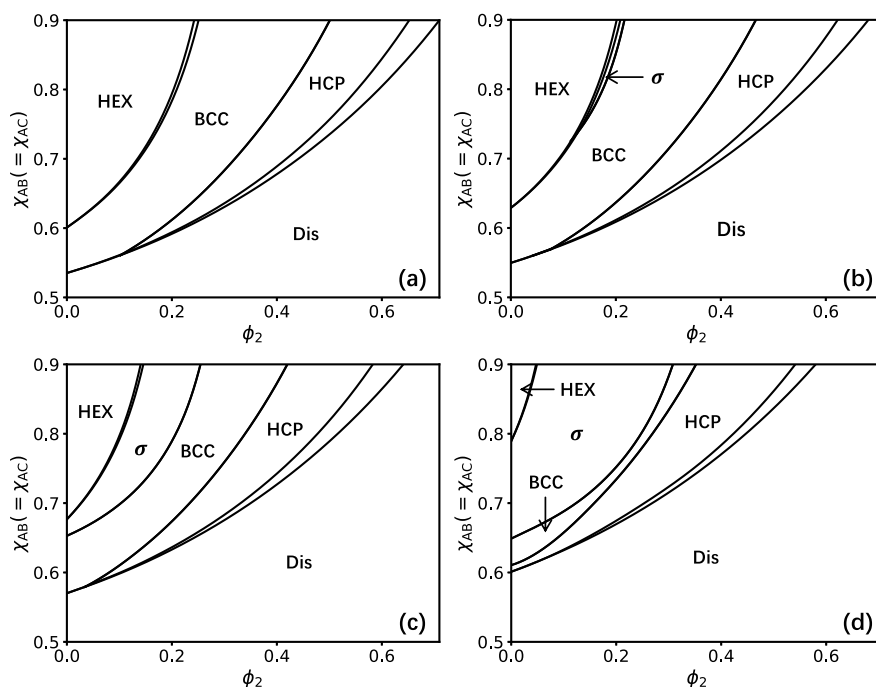


Figure 1. Phase diagrams in the $\phi_2 - \chi_{AB(= \chi_{AC})}$ plane with $\epsilon =$ (a) 1.0, (b) 1.1, (c) 1.25, and (d) 1.5 for the AB/C binary blends, where $N_A = 10$ ($f_A = 0.25$) and $N_C = 5$ are kept fixed. Unlabeled regions are the two-phase coexistence regions between two adjacent single phases.

$$\begin{cases} \phi_A(\mathbf{r}) = \phi_1 \frac{e^{\omega_A(\mathbf{r})}}{Q_1 N} \sum_{i=1}^{N_A} q_1(i, \mathbf{r}) q_1^\dagger(i, \mathbf{r}) \\ \phi_B(\mathbf{r}) = \phi_1 \frac{e^{\omega_B(\mathbf{r})}}{Q_1 N} \sum_{i=N_A+1}^{N_B} q_1(i, \mathbf{r}) q_1^\dagger(i, \mathbf{r}) \\ \phi_C(\mathbf{r}) = \frac{\phi_2}{\gamma_2} \frac{e^{\omega_C(\mathbf{r})}}{Q_2 N} \sum_{i=1}^{N_C} q_2(i, \mathbf{r}) q_2(N_C - i + 1, \mathbf{r}) \end{cases} \quad (12)$$

For the ternary AB/C/D blends, D homopolymers are also added to the system. Each D homopolymer contains N_D D segments and, similarly, we define $\gamma_3 = \gamma_D = N_D/N$. In the grand canonical ensemble, the thermodynamic control parameters for the ternary AB/C/D blends are the chemical potentials of the three components. Using the incompressibility condition, we can set μ_1 for the AB copolymers to 0 and we are left with two independent μ 's, that is, μ for the C homopolymers and μ' for the D homopolymers. The grand potential density takes the same form as eq 6, but with κ running through all three components, and α and β also running through D. Accordingly, the SCFT equations are the same as eq 7 with α (or β) = D also considered and one additional equation to calculate $\phi_D(\mathbf{r})$

$$\phi_D(\mathbf{r}) = e^{\mu'/k_B T} \frac{e^{\omega_D(\mathbf{r})}}{N} \sum_{i=1}^{N_D} q_3(i, \mathbf{r}) q_3(N_D - i + 1, \mathbf{r}) \quad (13)$$

Similarly, the average concentrations for the various components are readily computed by

$$\phi_1 = Q_1, \quad \phi_2 = \gamma_C e^{\mu/k_B T} Q_2, \quad \phi_3 = 1 - \phi_1 - \phi_2 \quad (14)$$

For the ternary blends, it is useful to introduce a semigrand canonical ensemble, where the thermodynamic control parameters are the chemical potentials of the AB copolymers (μ_1) and C homopolymers (μ_2) and the average concentration of D homopolymers (ϕ_3). The semigrand potential density is written as

$$\begin{aligned} \frac{N\Phi_{SG}}{\rho_0 V k_B T} = & - \sum_{\kappa \neq 3} e^{\mu_\kappa/k_B T} Q_\kappa - \frac{\phi_3 \ln Q_3}{\gamma_D \phi_3} - \frac{1}{V} \\ & \int d\mathbf{r} \left[\sum_\alpha N \omega_\alpha(\mathbf{r}) \phi_\alpha(\mathbf{r}) - \sum_{\alpha \neq \beta} \chi_{\alpha\beta} N \right. \\ & \left. \int u(|\mathbf{r} - \mathbf{r}'|) \phi_\alpha(\mathbf{r}) \phi_\beta(\mathbf{r}') d\mathbf{r}' + \eta(\mathbf{r}) (1 - \sum_\alpha \phi_\alpha(\mathbf{r})) \right] \end{aligned} \quad (15)$$

Similarly, μ_1 is set to 0, after which the remaining independent control parameters are μ for the C homopolymers and ϕ_3 for the D homopolymers. The corresponding SCFT equations are the same as those of the grand canonical ensemble, except the equation calculating $\phi_D(\mathbf{r})$ is replaced by

$$\phi_D(\mathbf{r}) = \frac{\phi_3}{\gamma_D} \frac{e^{\omega_D(\mathbf{r})}}{Q_3 N} \sum_{i=1}^{N_D} q_3(i, \mathbf{r}) q_3(N_D - i + 1, \mathbf{r}) \quad (16)$$

The average concentrations for the AB copolymers and C homopolymers are given by

$$\phi_1 = Q_1, \quad \phi_2 = 1 - \phi_1 - \phi_3 \quad (17)$$

For the ternary system, the propagators and single-chain partition functions are computed in the same manner as those for the binary system.

For both the AB/C and AB/C/D blends, we simultaneously solve the SCFT equations and optimize the unit cell

dimensions by implementing the pseudospectral method and variable-cell Anderson mixing for the FJCs.^{17,41} The phase diagrams are constructed by comparing the grand potential densities of different candidate phases. The phase boundaries are determined by identifying the intersections of the grand potential densities of adjacent phases. The candidate phases considered in the current study include the hexagonal close-packed cylinders (HEX), bcc, fcc, hcp, and disordered (Dis) phases, as well as the FK σ , A15, C14, C15, and Z phases. The schematics of these candidate phases, along with the numbers of grid points used to discretize their unit cells, are given in Table S1 of the Supporting Information. During our calculation, we found that in the AB/C blends, the grand potential density of the fcc phase is close to but always greater than that of the hcp phase, except in the close vicinity of the ODT, where they are nearly degenerate and become indistinguishable within the numerical accuracy of our calculation. Although a similar behavior is observed for the AB/C/D blends, the hcp to fcc transition, if it exists, remains identifiable near the ODT within the same numerical accuracy. For this reason, possible small stability windows of the fcc phase near the ODT are included in the AB/C/D blends but omitted in the AB/C blends. Additionally, we note that in some cases, particularly when either N_C or N_D is large, the SCFT equations become challenging to converge in regions very close to the ODT. When this occurred, we generated data points as close to the ODT as possible and used extrapolation to estimate the phase boundaries.

The parameter space of both systems considered in this study is dauntingly large, especially for the AB/C/D ternary mixtures. To focus on the phase space of interest, we fixed some of the parameters throughout the current study. Here, we introduce our choices of the system parameters that are applicable for both systems, and the specification for each system will be discussed in the following sections. For both the AB/C and AB/C/D mixtures, the number of segments N for the AB copolymers is kept at 40. In general, the conformational asymmetry of a molecule is defined as $\epsilon = \sqrt{(\rho_A b_A^2)/(\rho_B b_B^2)}$.^{42–44} Because of the assumption that $\rho_A = \rho_B = \rho_0$, we simply have $\epsilon = b_A/b_B$. When considering conformationally asymmetric AB copolymers, we set $b_A = 1$ and $b_\alpha = b_A$ for $\alpha = C$ and D , and the ϵ is tuned by adjusting b_B , unless stated otherwise. The range of the interactions is fixed to $\sqrt{3}b_A$. Furthermore, the Kuhn length of the bond at the AB junction connecting the A and B blocks is set to always be equal to b_A .

Compared to the standard GC,⁶ our choices of the FJC model and a relatively small N make the model more suitable for polymer chains with low-molecular weight. For the same reason, our model may also provide insights into the phase behaviors of surfactant systems involving these complex packings.

RESULTS AND DISCUSSION

Binary AB/C Blends. In this section, we provide a systematic examination of the phase behavior of the AB/C blends. We set $\chi_{AB} = \chi_{AC} > 0$ and fix $\chi_{BC} = -0.1$ throughout this section, unless otherwise specified. The phase diagrams depicting the phase behavior of the system will be presented in the 2-dimensional $\phi_2 - \chi_{AB}$ plane. Previous theoretical and experimental studies have demonstrated that conformational asymmetry between the A and B blocks plays a key role in the formation of complex spherical packing phases in AB diblock

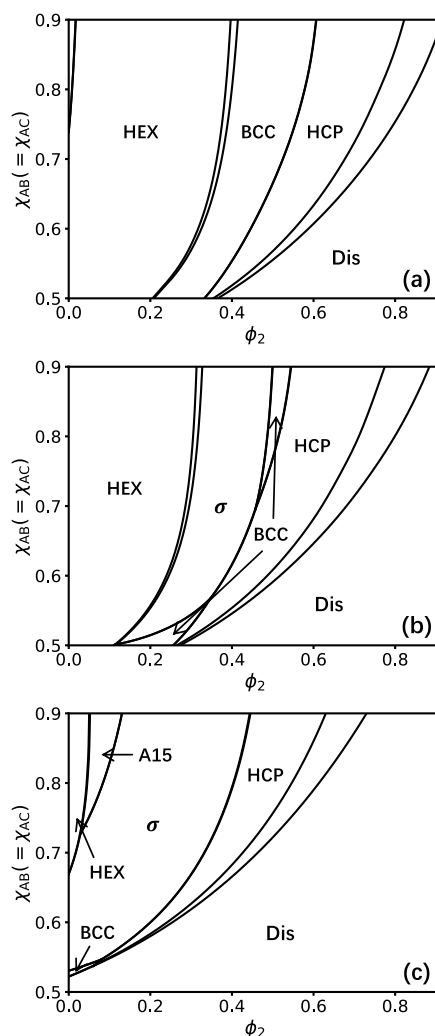


Figure 2. Phase diagrams in the $\phi_2 - \chi_{AB}(=\chi_{AC})$ plane with $\epsilon =$ (a) 1.0, (b) 1.25, and (c) 3.0, where $N_A = 13$ ($f_A = 0.325$) and $N_C = 5$ are kept fixed. Unlabeled regions are the two-phase coexistence regions between two adjacent single phases.

copolymer melts.^{45–47} SCFT calculations based on the GC model suggested that the critical value of ϵ for the stabilization of the FK σ phase is $\epsilon \sim 1.5$.⁴⁵ Further increasing ϵ to $\epsilon > 2.1$ could open up a stability window for the FK A15 phase at $\chi N \approx 40$.⁴⁷ Based on these previous results, the ϵ is expected to play a similar role in the AB/C blends in stabilizing the FK phases. To quantitatively examine the effect of ϵ on the equilibrium spherical packing phases in the presence of B-selective C homopolymers, we construct two sets of phase diagrams with different f and ϵ . The first set (Figure 1) includes 4 phase diagrams with fixed $N_A = 10$ ($f = 0.25$), $N_C = 5$, and varying ϵ from 1.0 to 1.5, while the second set (Figure 2) includes 3 phase diagrams with fixed $N_A = 13$ ($f = 0.325$), $N_C = 5$, and varying ϵ from 1.0 to 3.0.

Several common features emerge from the phase diagrams shown in Figures 1 and 2. Most notably, the system is driven from cylindrical to spherical phases by increasing the concentration of the C homopolymers (ϕ_2). Taking all the observed ordered phases into account, the progression of the

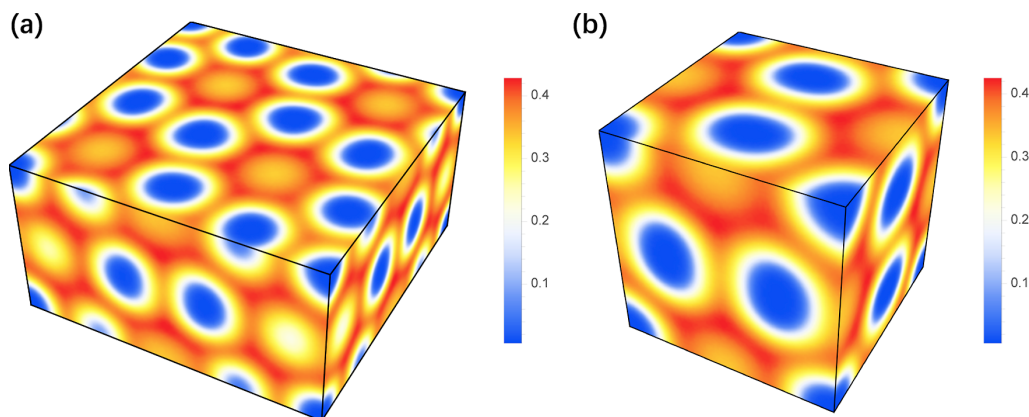


Figure 3. Density profiles of the C homopolymers for the FK (a) σ and (b) A15 phases taken from the SCFT solutions at the point $\{\phi_2, \chi_{AB}(=\chi_{AC})\}=\{0.3, 0.9\}$ on the phase diagram in Figure 1c.

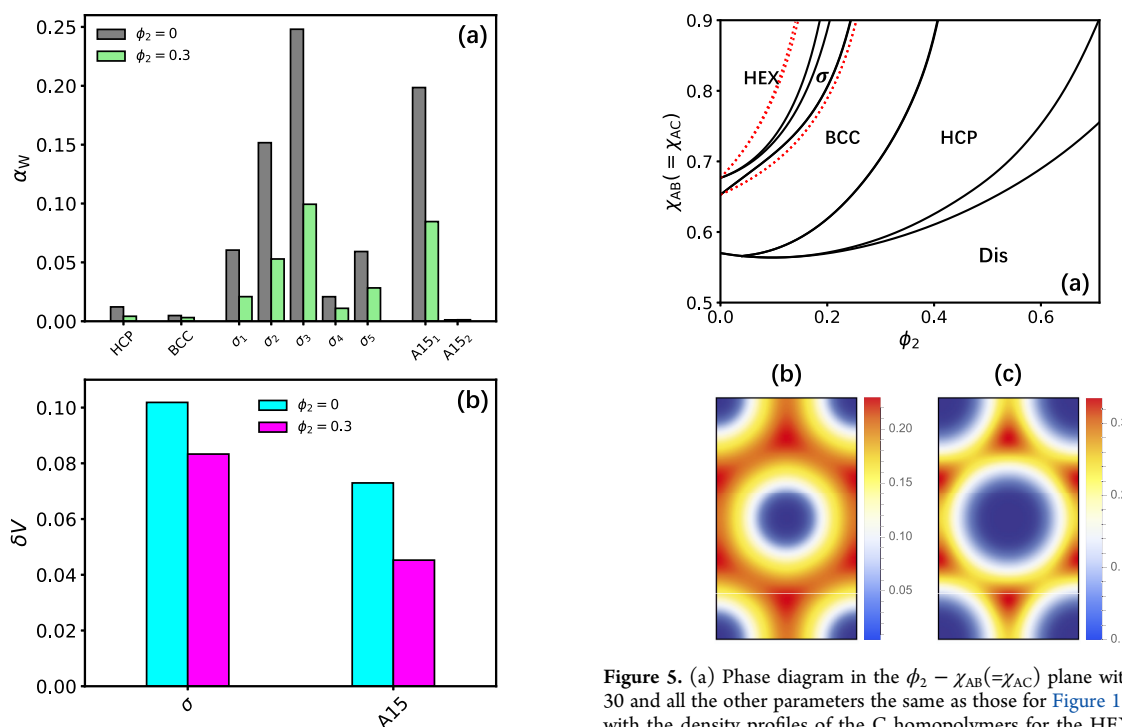


Figure 4. (a) Imprinting parameter α_w for all nonequivalent domains of the hcp, bcc, FK σ , and A15 phases and (b) the relative standard deviation of domain volumes of the FK σ and A15 phases. The density profiles used to generate the data are taken from the SCFT solutions with $N_A = 10$ ($f_A = 0.25$), $N_C = 5$, $\epsilon = 1.25$, $\chi_{AB} = \chi_{AC} = 0.9$, and two different values of ϕ_2 . Numbering of distinct types of domains/WSCs of the FK phases is shown in Figure S1. Bars for A15₂ in (a) are nearly invisible on the scale of the graph.

equilibrium morphology with increasing ϕ_2 is $\text{HEX} \rightarrow \text{A15} \rightarrow \sigma \rightarrow \text{bcc} \rightarrow \text{hcp}$. This generic phase transition sequence has been partially predicted by previous theoretical studies^{25,26} and observed in recent experiments on both diblock copolymer/homopolymer blends^{27,28} and surfactant solutions.^{30,32} It is noted that the progression of the equilibrium phase as the homopolymer concentration is increased in the AB/C blends (Figures 1 and 2) is identical to that observed for the AB

Figure 5. (a) Phase diagram in the $\phi_2 - \chi_{AB}(=\chi_{AC})$ plane with $N_C = 30$ and all the other parameters the same as those for Figure 1c, along with the density profiles of the C homopolymers for the HEX phase taken from the SCFT solutions at the point $\{\phi_2, \chi_{AB}(=\chi_{AC})\}=\{0.15, 0.9\}$ in (b) Figure 1c and (c) Figure 5a, respectively. Unlabeled regions in (a) are the two-phase coexistence regions between two adjacent single phases. To have a clear comparison, the HEX- σ and σ -bcc boundaries in Figure 1c are also plotted as red dotted lines in (a).

diblock copolymer melts as increasing the majority-block volume fraction.⁴⁵ An intuitively appealing explanation for this observation is given by an argument based on the overall volume fractions of the minority and majority blocks, that is, the addition of B-selective C homopolymers effectively increases the volume fraction of the majority B blocks in the system. However, the detailed phase behavior of the binary blends goes beyond this simple volume-fraction argument and exhibits a more intricate dependence on the specific distribution of the homopolymers, which will be elaborated later.

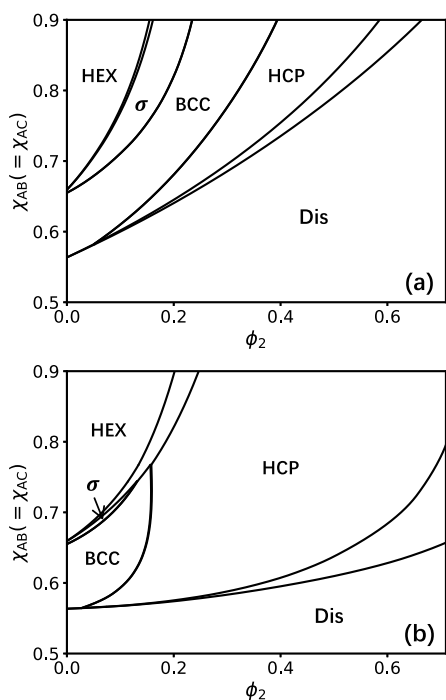


Figure 6. Phase diagrams in the $\phi_2 - \chi_{AB}(=\chi_{AC})$ plane with all parameters the same as those used for (a) Figure 1c and (b) Figure 5a, except that $\chi_{BC} = 0$, $b_B = b_C$, and $\epsilon = b_A/b_B = b_A/b_C = 1.2$ are used instead. These choices of parameters reduce the system to A_1B_1/B_2 blends. Unlabeled regions are the two-phase coexistence regions between two adjacent single phases.

The effect of the conformational asymmetry of the diblocks is revealed by comparing the phase diagrams with different values of ϵ . In Figures 1a and 2a, in which $\epsilon = 1$, none of the complex spherical phases is present. As ϵ is increased, a stability window of the FK σ phase appears between the HEX and bcc phases. Moreover, the A15 phase becomes stable between the HEX and σ when $\epsilon = 3.0$ in the case where $N_A = 13$ ($f_A = 0.325$), as could be seen in Figure 2c. These observations suggest that, similar to the neat AB diblock copolymers, the stabilization of the FK phases in the binary AB/C mixtures also requires some degrees of conformational asymmetry for the AB diblock copolymers. However, it is observed that adding C homopolymers generally increases the range of χ over which the FK phases are stable. Additionally, in Figures 1b and 2b,c, the FK σ or A15 phase is not an equilibrium morphology within the entire range of χ in the limit of the neat diblock copolymers corresponding to $\phi_2 = 0$, but they are stabilized by adding the C homopolymers. These observations provide clear evidence that the presence of C homopolymers promotes the stability of the FK phases.

Notably, the critical value of ϵ required to stabilize the FK phases is significantly lower in the AB/C blends compared with the neat AB diblock copolymers. In particular, a stability window of the FK σ phase, albeit narrow, is identified between those of the HEX and bcc phases in Figure 1b with $\epsilon = 1.1$. This prediction is in good agreement with the recent experiments of Chen et al., where the σ phase was observed in the PEO-*b*-PB diblock copolymers with $\epsilon \approx 1.2$ blended with PB-selective solvents.²⁸ It is worth noting that previous SCFT calculations based on the standard GC model predicted

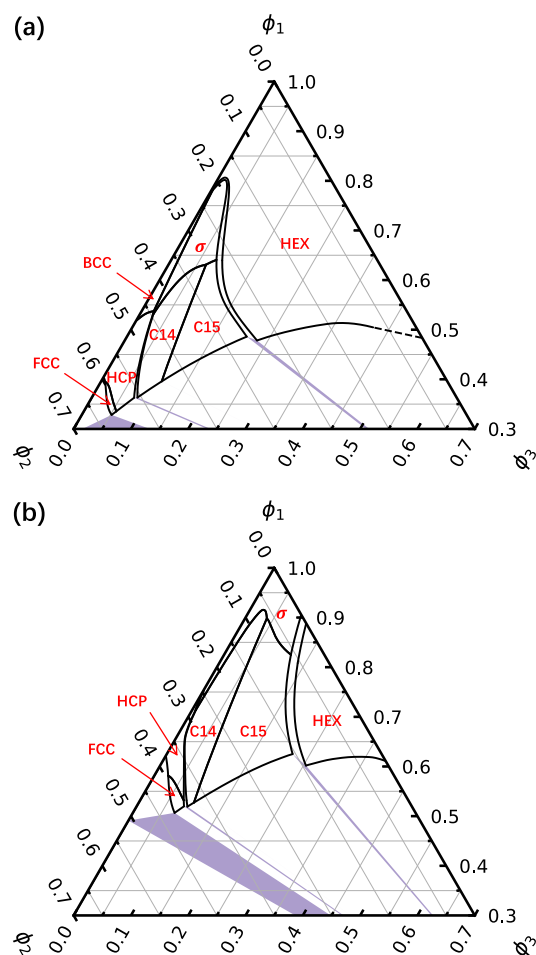


Figure 7. Ternary phase diagrams depicting the overall phase behavior of the AB/C/D blends with (a) $\epsilon = 1$ and (b) $\epsilon = 2$, where $\chi = 0.8$ and $\{N_A (f_A), N_C, N_D\} = \{10 (0.25), 5, 20\}$. Unlabeled regions are two-phase (white) and three-phase (blue) coexistence regions between the adjacent single phases. Dashed line in (a) is obtained from extrapolation.

a threshold $\epsilon \sim 1.5$ to stabilize the FK σ phase in the neat AB diblock copolymer melts.⁴⁵ In contrast, Figure 1c shows that the σ phase already has a moderate stability window at $\phi_2 = 0$, corresponding to the neat diblocks with $\epsilon = 1.25$. This lower critical ϵ predicted by SCFT based on the freely jointed chain model implies that the stability of the σ phase could be enhanced in systems of low-molecular-weight copolymers. However, a detailed investigation of the difference between these two chain models in stabilizing the FK phases is beyond the scope of the current work, and we will leave this topic for a future study.

While a simple volume-fraction argument could be used to rationalize the generic phase progression when ϕ_2 is increased, it is not sufficient to explain the intricate phase behavior of the system. Most notably, the reason behind the enhanced stability of the FK phases in the presence of the C homopolymers remains unclear. More detailed understanding of the effects of the C homopolymers in the binary AB/C blends is offered by the homopolymer distribution in the microdomains formed by

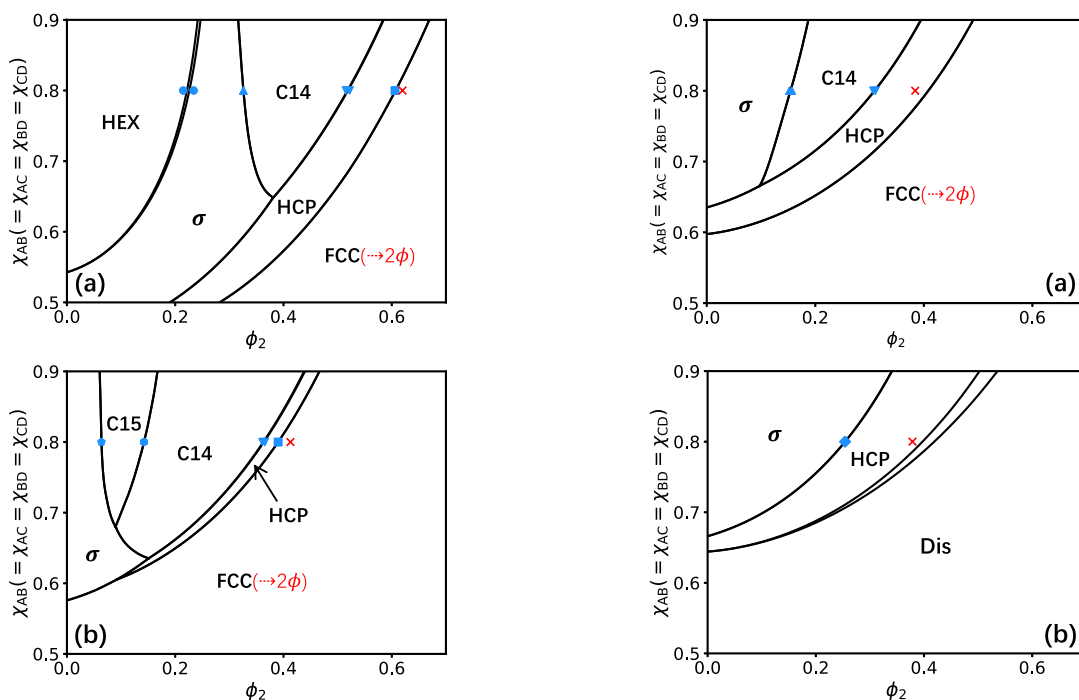


Figure 8. Phase diagrams in the $\phi_2 - \chi_{AB}(=\chi_{AC} = \chi_{BD} = \chi_{CD})$ plane with $\phi_3 = 0.05$, $N_C = 5$, $N_D = 20$, and $\epsilon =$ (a) 1.0 and (b) 2.0, respectively. Unlabeled regions are the two-phase coexistence regions between two adjacent single phases. The phase boundary between the fcc and order-disorder coexistence regions, fcc- 2ϕ , is not determined and this fact is noted by the red “($\rightarrow 2\phi$)”, following the “fcc” label. The markers are the phase boundaries encountered by traversing the paths with constant ϕ_3 in Figure 7, with a blue circle, upward triangle, downward triangle, square, pentagon, hexagon, and red cross denoting the HEX- σ , σ -C14, C14-hcp, hcp-fcc, σ -C15, C15-C14, and fcc-Dis boundaries, respectively. Many of the coexistence regions between the two adjacent phases are too narrow to be visible.

Figure 9. Phase diagrams in the $\phi_2 - \chi_{AB}(=\chi_{AC} = \chi_{BD} = \chi_{CD})$ plane with the same parameters as those used in Figure 8b except $\phi_3 =$ (a) 0.01 and (b) 0.001, respectively. Unlabeled regions are the two-phase coexistence regions between two adjacent single phases. The phase boundary between the fcc and order-disorder coexistence regions, fcc- 2ϕ , is not determined and this fact is noted by the red “($\rightarrow 2\phi$)”, following the “fcc” label. The markers are the phase boundaries encountered by traversing the paths with constant ϕ_3 in Figure 7, with the blue upward triangle, downward triangle, diamond, and red cross denoting the σ -C14, C14-hcp, σ -hcp, and hcp-Dis boundaries, respectively. Many of the coexistence regions between two adjacent phases are too narrow to be visible.

the copolymers. As an example of the homopolymer distribution, the density profiles of the homopolymers for the FK σ and A15 phases obtained from SCFT at the point $\{\phi_2, \chi_{AB}(=\chi_{AC})\} = \{0.3, 0.9\}$ on the phase diagram in Figure 1c are displayed in Figure 3a,b, respectively. The plots clearly show that the homopolymer densities exhibit strong spatial nonuniformity. Specifically, more concentrated homopolymers ($\phi_C(\mathbf{r}) \sim 0.4$) are found in the interstitial voids corresponding to the vertices and edges of the WSCs, enclosing the AB soft domains. As moving toward the center of the A domains, the homopolymer concentration gradually decreases. At the domain cores, there are almost no homopolymers ($\phi_C(\mathbf{r}) \ll 0.1$).

The nonuniform distribution of the C homopolymers shown in Figure 3 is driven enthalpically to minimize the unfavorable contacts between the A and C monomers. In addition, for all of the nonlamellar morphologies, the localization of the homopolymers at the interstitial voids releases the packing frustration.²⁶ For single-component systems such as AB diblock copolymer melts, the packing frustration originates from the conflict between the tendency for the soft domains to maintain their native shape and the need for the copolymer chains to fill the space without voids.⁵ This frustration could be

alleviated by the addition of the C homopolymers, which act as space fillers to fill the gaps that would otherwise be occupied by the diblock copolymers through excessive stretching. Furthermore, for the FK phases, the nonequivalent soft domains tend to have different sizes to accommodate the different geometric surroundings reflected by their corresponding WSCs. Thus, an additional source of packing frustration for the FK phases in single-component systems is the formation of domains with different volumes by aggregating copolymer chains with a uniform degree of polymerization, which inevitably results in unevenly stretched chains. In contrast, the binary AB/C blends could naturally overcome this type of packing frustration with the extra degree of freedom to partition the homopolymers into distinct WSCs differentially, which could explain the enhanced stability of the FK phases. Despite the high concentration at the interstitial regions, the homopolymers also penetrate into the coronas of the domains, driven by a gain in translational entropy, which increases the AB interfacial curvature accounting for the cylinders \rightarrow spheres transition observed in all phase diagrams in Figures 1 and 2.

It is worth emphasizing the differences between the stabilization mechanisms by adding core-selective and corona-selective homopolymers to the sphere-forming diblock copolymers. Previous studies demonstrated that adding core-

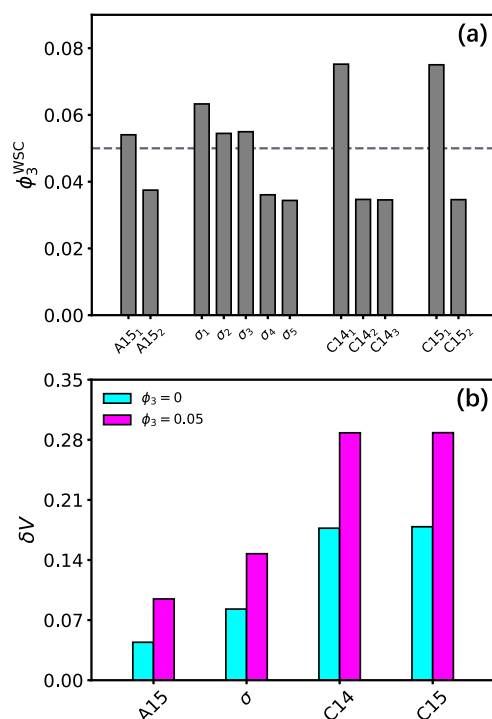


Figure 10. (a) Average concentrations of the D homopolymers within different FK WSCs, ϕ_3^{WSC} , at $\phi_3 = 0.05$. (b) Relative standard deviations of domain volumes, δV , at $\phi_3 = 0$ and 0.05 , evaluated for the four FK phases. Other parameters are $\epsilon = 2$, $\chi = 0.9$, $\phi_2 = 0.3$, and $\{N_A (f_A), N_C, N_D\} = \{10 (0.25), 5, 20\}$. Dashed line in (a) marks the unit-cell-averaged ϕ_3 . Numbering of distinct types of domains/WSCs of the FK phases is shown in Figure S1.

selective homopolymers into the AB diblocks stabilizes the FK phases by forming highly swollen domains.^{15–18} These swollen domains are more severely distorted toward the polyhedral shape of their WSCs, making the FK phases with higher average WSC sphericity more enthalpically favored than the bcc and hcp phases due to the lower AB interfacial energy. On the other hand, the nonuniform distribution of the core-selective homopolymers across distinct domains enlarges their size difference and, in turn, decreases the interfacial energy between the homopolymers and the corona blocks, which is responsible for the formation of the Laves phases.¹⁷ However, the mechanisms of stabilizing the FK phases by adding corona-selective components into the AB diblocks have opposite effects on the shapes and size dispersity of the soft domains. To quantitatively illustrate the effect of adding B-selective C homopolymers on the domain shapes and size difference, we evaluate the polyhedral warping parameter α_w for different domains and the relative standard deviation δV of the domain volumes. The polyhedral warping parameter is defined as²⁴

$$\alpha_w = \frac{1 - IQ^{-1/3}}{1 - IQ_{poly}^{-1/3}} \quad (18)$$

where IQ and IQ_{poly} are the isoperimetric quotients, i.e., $36\pi V^2/A^3$, of a domain and a polyhedron, respectively. This parameter measures the degree of domain deformation toward the polyhedron. An undeformed perfect sphere and a completely deformed polyhedron have $\alpha_w = 0$ or 1 ,

respectively. The α 's computed for the nonequivalent domains of the hcp, bcc, σ , and A15 phases with the same values for all parameters but two different values of ϕ_2 , i.e., 0.0 and 0.3 , are shown in Figure 4a. The IQ_{poly} for each domain is evaluated by assuming the shape of the WSC enclosing that domain. The δV 's computed for the σ and A15 phases are shown in Figure 4b with the same set of parameters used in (a). For the bcc and hcp phases, $\delta V = 1$.

From Figure 4a, it is seen that α decreases for all the domains as ϕ_2 changes from 0 to 0.3 , except A15₂, which has vanishingly small α and thus is not visible at the scale of the graph in both cases. This indicates that the observed homopolymer localization (Figure 3) releases the packing frustration and sustains soft domains closer to their native shape, i.e., a perfect sphere. The decrease in α is especially pronounced for the FK domains that have a large deformation in the absence of homopolymers, i.e., σ_1 , σ_2 , σ_3 , σ_4 , and A15₁. As can be seen in Figure 4b, the addition of the C homopolymers also decreases the volume difference between domains of different types for both the σ and A15 phases, suggesting that the differential distribution of the homopolymers could mitigate the need to form different-sized domains in the FK lattices and thus reduce uneven chain stretching. The behaviors of domain shapes and volume difference due to adding corona-selective homopolymers, as shown in Figure 4, are opposite to those observed in the case of adding core-selective homopolymers, reflecting the differences between the mechanisms of stabilizing the FK phases in these two cases. Compared to swelling the core, releasing the packing frustration in the corona proves to be less effective in promoting the stability of the FK phases. Particularly, our results suggest that the requirement of the conformational asymmetry of the diblock chains to stabilize the σ phase is not completely lifted by adding the corona-selective homopolymers into the AB diblocks, and this blending scheme cannot stabilize the Laves C14 and C15 phases.

Another parameter that can greatly affect the phase behavior of the binary AB/C blends is the degree of polymerization of the homopolymers. Numerous studies have demonstrated that the spatial distribution of the homopolymers in diblock copolymer/homopolymer blends is largely influenced by the molecular weight of the homopolymers.^{15–18,48–52} Due to the greater gain in entropy, shorter homopolymers penetrate deep into the microdomains formed by the affinity block (wet-brush behavior) compared to the longer ones that tend to be more excluded from the microdomains (dry-brush behavior). To investigate the effect of N_C , a phase diagram with the same parameters as that in Figure 1c except a larger $N_C = 30$, along with two C-homopolymer density plots, is presented in Figure 5. Specifically, the C-homopolymer density plots in Figure 5b,c are taken from the SCFT solutions for the HEX phase at $\{\phi_2, \chi_{AB}(=\chi_{AC})\} = \{0.15, 0.9\}$ in Figures 1c and 5a, respectively. It can be observed that increasing N_C from 5 to 30 enhances the localization of the homopolymers into the interstitial voids, as indicated by the more condensed red region and higher maximum density in the color bar in Figure 5c compared to Figure 5b. The change in the homopolymer distribution induced by increasing N_C clearly shows a transition from the wet-brush to the dry-brush behaviors of the homopolymers. The more isolated homopolymers have a stronger effect in alleviating the packing frustration associated with the WSC nonsphericity and a weaker effect on the interfacial curvature. Consequently, we observe that the bcc phase has slightly

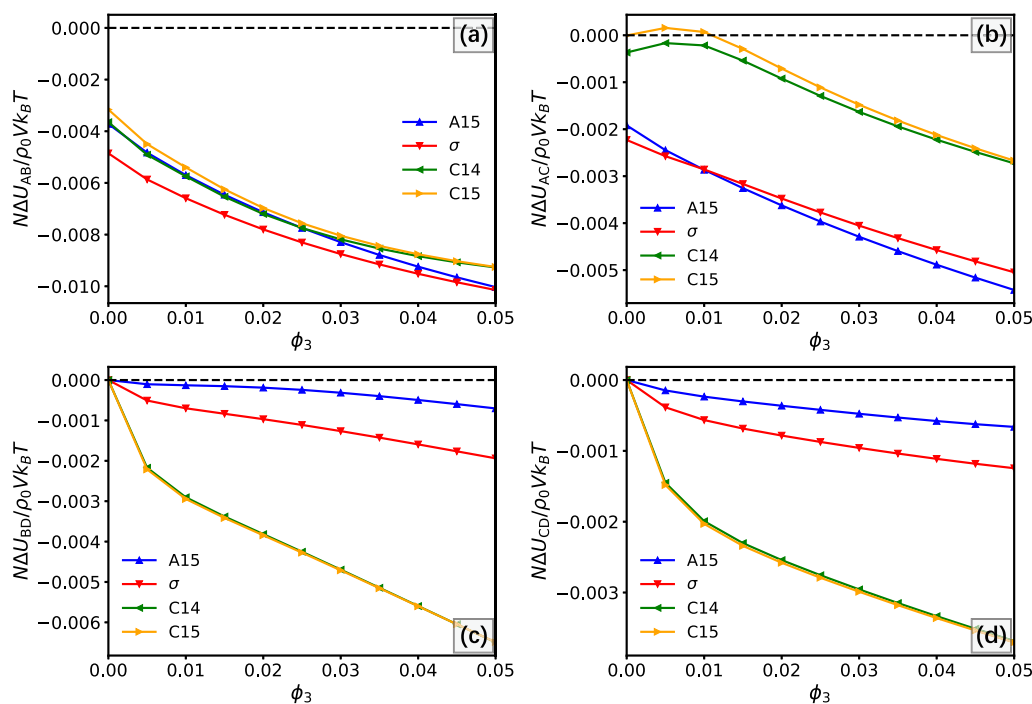


Figure 11. Four interfacial-energy contributions of the FK phases relative to those of the bcc phase, $N\Delta U_{\alpha\beta}/\rho_0 V k_B T$, where $\alpha\beta =$ (a) AB, (b) AC, (c) BD, and (d) CD, as a function of ϕ_3 . Other parameters are the same as those used in Figure 10.

increased stability against the σ phase and that the HEX phase is sustained to a larger ϕ_2 , together causing a shrinkage of the stability window of the σ phase. Besides, another obvious effect of increasing N_C is the increase of the hcp window and two-phase window between the copolymer-rich hcp phase and the homopolymer-rich disordered phase.²⁶

The destabilizing effect on the FK σ phase by increasing the homopolymer molecular weight was also observed experimentally in a study by Takagi and Yamamoto on the binary mixtures of polybutadiene-*block*-poly(ϵ -caprolactone) (PB-*b*-PCL) diblock copolymers and corona-selective PB homopolymers,²⁷ corresponding to a A_1B_1/B_2 system. They discovered that the σ phase is stable only when the chain length of the added B_2 homopolymer is smaller than the length of the corresponding block of the copolymer. When the molecular weight of the homopolymer is roughly 1.5 times that of the B_1 block, the σ phase is entirely absent. In our model, it is straightforward to reduce the AB/C to an A_1B_1/B_2 system by setting $\chi_{BC} = 0$ and $b_B = b_C$. For a detailed investigation of the effect of N_C in this case, we construct two phase diagrams with two different choices of N_C , i.e., 5 and 30, presented in Figure 6a,b, respectively. In Figure 6, all parameters are the same as those used in Figures 1c and 5a, except that $\chi_{BC} = 0$, $b_B = b_C$ and $\epsilon = b_A/b_B = b_A/b_C = 1.2$ are chosen. For convenience, we define the ratio $\alpha_R = N_C/N_B$. In Figure 6a where $\alpha_R = 0.167$, there is a sizable stable region of the σ phase that extends to higher χ . When α_R is increased to 1.0, the stable region of the HEX phase expands toward higher ϕ_2 , while that of the σ phase shrinks significantly and terminates at $\chi_{AB} = \chi_{AC} \sim 0.744$ and $\phi_2 \sim 0.131$, as shown in Figure 6b. In addition, the bcc stable region shrinks and terminates as well, with a terminating point close to that of the σ phase. Although the parameters used here do not exactly match the experimental samples by

Takagi et al.,²⁷ these theoretically predicted trends are in qualitative agreement with the experimental results. There are also some obvious discrepancies between the SCFT phase diagrams in Figure 6 and the experimental phase portraits. In particular, our SCFT results predict significantly enlarged regions for the hcp phase and macrophase separation upon increasing N_C , which were not observed in the experiment. We speculate that these regions near the ODT may have been missed in the experiment or largely affected by the fluctuation effect that is not captured by mean-field theory. It is worth noting that the diblock copolymers with $\epsilon = 1.2$ and the wet-brush homopolymers used in constructing the phase diagram in Figure 6a closely align with the experimental samples utilized by Chen et al.,²⁸ and the prediction from Figure 6a is in good qualitative agreement with their experimental results.

Ternary AB/C/D Blends. In this section, we turn our attention to the more complicated ternary blends consisting of AB diblock copolymers and two chemically distinct, C and D, homopolymer additives. The introduction of a third component dramatically increases the number of independent parameters in the model. To target the phase space of interest, where C and D homopolymers are B- and A-selective, respectively, we set $\chi_{AB} (= \chi_{AC} = \chi_{BD} = \chi_{CD}) = \chi > 0$ and $\chi_{BC} = \chi_{AD} = -0.3$. These choices of the interaction parameters make the ternary blends analogous to the $A_1B_1/B_2/A_2$ blends and surfactant/water/oil systems. The thermodynamics of the AB/C/D blends is described by the grand potential density (eq 6) in the grand canonical ensemble, which leads to ternary phase diagrams over the blend-composition (ϕ_1 - ϕ_2 - ϕ_3) triangle. Compared to the $\phi_2 - \chi_{\alpha\beta}$ phase diagrams (for example, Figure 1, etc.), each ternary phase diagram depicts the phase behavior only at a set of constant χ 's. To explore the χ dependence more conveniently, $\phi_2 - \chi_{\alpha\beta}$ phase diagrams can

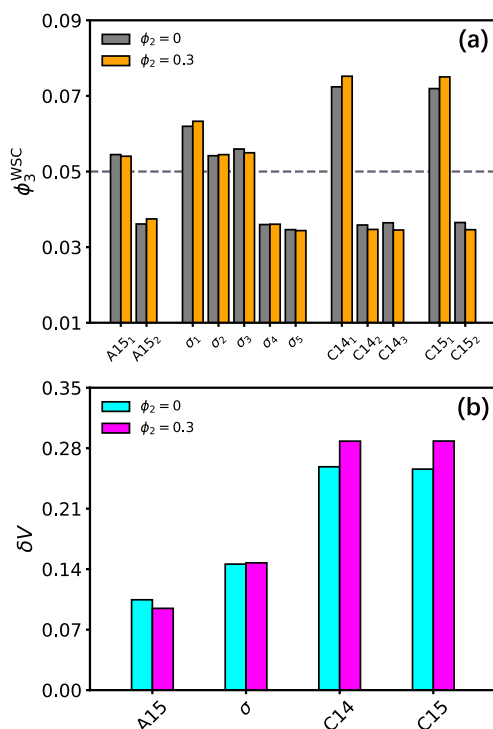


Figure 12. (a) Average concentrations of the D homopolymers within different FK WSCs, ϕ_3^{WSC} . (b) Relative standard deviations of domain volumes, δV . Both quantities are evaluated at $\phi_2 = 0$ and 0.3 for the four FK phases. Other parameters are $\epsilon = 2$, $\chi = 0.9$, $\phi_3 = 0.05$, and $\{N_A (f_A), N_C, N_D\} = \{10 (0.25), 5, 20\}$. Dashed line in (a) marks the unit-cell-averaged ϕ_3 . Numbering of distinct types of domains/WSCs of the FK phases is shown in Figure S1.

be constructed by working in the semigrand canonical ensemble, which amounts to considering systems with a constant concentration of the D homopolymers (ϕ_3). For ternary blends, macrophase separation could lead to three-phase coexistence regions in the phase space. Although those regions are not accessible in the semigrand canonical ensemble, they appear to be narrow when the two-phase coexistence regions are narrow. In what follows, we will first construct two ternary phase diagrams with $\epsilon = 1$ and 2, which provide a full picture of the phase behavior on the ϕ_1 - ϕ_2 - ϕ_3 triangle, and we will then use $\phi_2 - \chi_{\text{eff}}$ diagrams to investigate the effects of the other model parameters.

Previous studies on binary A_1B_2/A_2 blends demonstrated that the requirement of conformational asymmetry for diblock copolymers to stabilize the FK σ phase could be completely lifted by adding proper core-swelling homopolymers.^{16,17} In addition, stable Laves C14 and C15 phases could also form at higher homopolymer concentrations. For the current AB/C/D system, two ternary phase diagrams with $\epsilon = 1$ and 2 are presented in Figure 7a,b, respectively, with $\chi = 0.8$ and $\{N_A (f_A), N_C, N_D\} = \{10 (0.25), 5, 20\}$ held constant. In Figure 7a, the stable morphology at $\phi_2 = \phi_3 = 0$, corresponding to the neat diblocks, is HEX, which remains to be the only ordered phase on the entire right side of the triangle ($\phi_2 = 0$). This indicates that for the specific ternary blending system considered in Figure 7a, adding the core-swelling D homopolymers into the AB diblocks alone does not induce any of the complex spherical packing phases. On the left side of

the triangle ($\phi_3 = 0$), representing an AB/C blends without the D homopolymers, phase transitions from $\text{HEX} \rightarrow \text{bcc} \rightarrow \text{hcp}$ are observed, similar to those shown in Figure 1a. However, the simultaneous presence of the C and D homopolymers can stabilize the σ , C14, and C15 phases, resulting in large stability windows of these complex spherical packings in the left half of the phase diagram, as shown in Figure 7a. For example, the σ phase can be stabilized by adding a tiny amount of D homopolymers ($\phi_2 \gtrsim 0.001$) when there are about 22% C homopolymers in the system. When there are about 35% C homopolymers, increasing the concentration of D homopolymers induces the phase transitions from $\text{bcc} \rightarrow \sigma \rightarrow \text{C14} \rightarrow \text{C15}$. In the phase diagram with $\epsilon = 2$ shown in Figure 7b, the overall region of ordered morphologies is much smaller compared to Figure 7a, but the spherical region becomes dominant over that of the HEX. Due to the conformational asymmetry of the diblocks, the stable morphology at $\phi_2 = \phi_3 = 0$ becomes the σ phase. Adding either C or D homopolymers alone induces the transition from σ to hcp or HEX. The access of the two Laves phases requires adding the C and D homopolymers simultaneously, similar to the observation from Figure 7a. Both phase diagrams shown in Figure 7 demonstrate a synergistic effect of adding two selective homopolymers in promoting the complex FK packings, especially Laves C14 and C15, in the AB/C/D ternary blends.

Two $\phi_2 - \chi$ phase diagrams with $\epsilon = 1$ and 2 are constructed and shown in Figure 8, with $\phi_3 = 0.05$ and $\{N_A (f_A), N_C, N_D\} = \{10 (0.25), 5, 20\}$ held constant. A shrinkage of the overall ordered region and an enhancement in the dominance of the Laves phases as ϵ is increased are observed. In Figure 9, another two $\phi_2 - \chi$ phase diagrams with $\phi_3 = 0.01$ and 0.001 are presented, with $\epsilon = 2$ and all the other parameters the same as those used in Figure 8b. As ϕ_3 is decreased from 0.05 (Figure 8b) to 0.01 (Figure 9a), the C15 phase disappears. Further decreasing ϕ_3 to 0.001 (Figure 9b) destabilizes the C14 as well. These behaviors illustrated by Figures 8 and 9 are consistent with the observations from Figure 7. Additionally, both Figures 8 and 9 suggest that the stability windows for the Laves phases expand as χ becomes larger. Thus, the Laves region on the ϕ_1 - ϕ_2 - ϕ_3 triangle is expected to become more dominant with a larger χ . On the contrary, the Laves phases taper off and eventually disappear between the σ and hcp phases as decreasing χ . The synergistic effect between the two homopolymers in stabilizing the Laves phases is clearly revealed by comparing the different phase diagrams in Figures 8 and 9. It is seen that the Laves phases are stable only when both of the C and D homopolymers are added to the system. They are completely absent in the entire range of χ ($0 < \chi < 0.9$) when either $\phi_2 = 0$ or $\phi_3 = 0$.

To compare the phase boundaries determined from the grand canonical ensemble and semigrand canonical ensemble more quantitatively, we locate the phase boundaries encountered by traversing the corresponding paths with constant ϕ_3 in Figure 7 and reproduce them in Figures 8 and 9. The meaning of different markers is listed in the captions of the two figures. As can be seen from all the phase diagrams in Figures 8 and 9, for those areas with narrow phase-coexistence regions, the order-order phase boundaries determined by the two ensembles agree almost perfectly. One small difference is that the semigrand canonical ensemble tends to slightly underestimate the width of some of the coexistence regions, such as the $\text{HEX}-\sigma$ coexistence region in Figure 8a. However, in the area near the ODT, where large coexistence regions exist

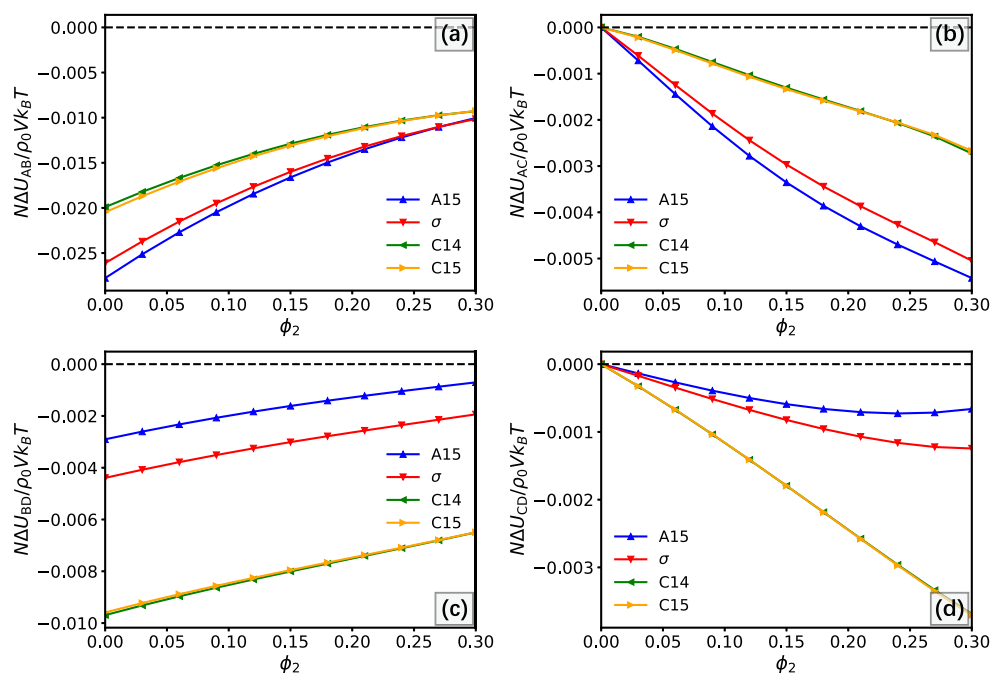


Figure 13. Four interfacial-energy contributions of the FK phases relative to those of the bcc phase, $N\Delta U_{\alpha\beta}/\rho_0 V k_B T$, where $\alpha\beta =$ (a) AB, (b) AC, (c) BD, and (d) CD, as a function of ϕ_2 . Other parameters are the same as those used in Figure 12.

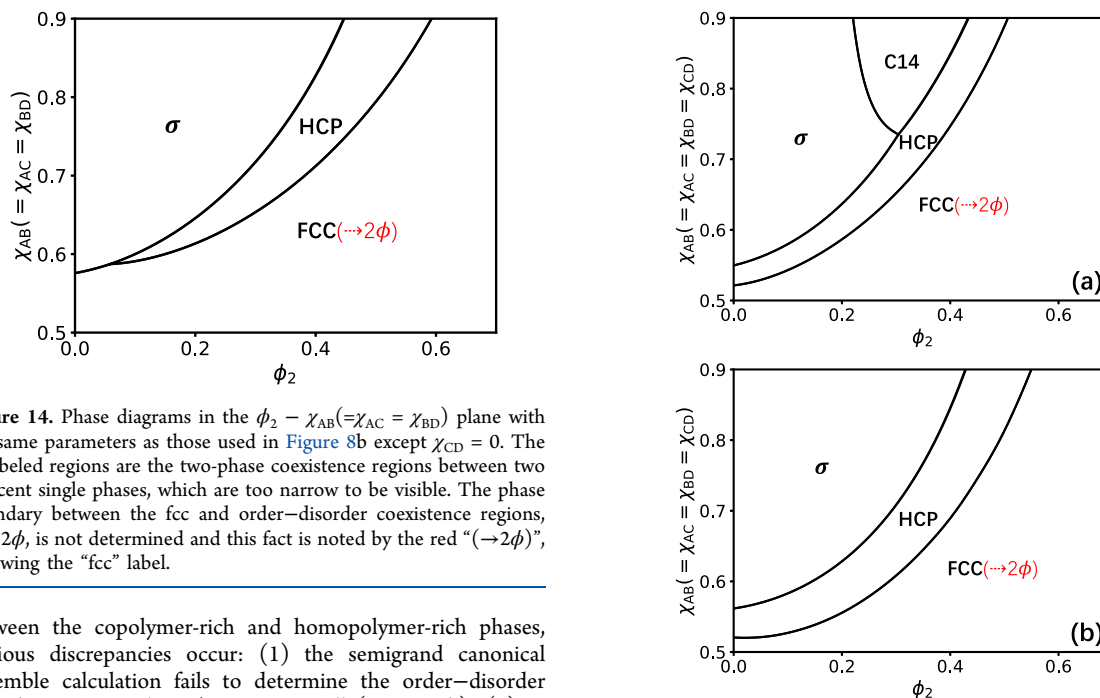


Figure 14. Phase diagrams in the $\phi_2 - \chi_{AB}(=\chi_{AC} = \chi_{BD})$ plane with the same parameters as those used in Figure 8b except $\chi_{CD} = 0$. The unlabeled regions are the two-phase coexistence regions between two adjacent single phases, which are too narrow to be visible. The phase boundary between the fcc and order-disorder coexistence regions, fcc- 2ϕ , is not determined and this fact is noted by the red “($\rightarrow 2\phi$)”, following the “fcc” label.

between the copolymer-rich and homopolymer-rich phases, obvious discrepancies occur: (1) the semigrand canonical ensemble calculation fails to determine the order-disorder boundary except when ϕ_3 is very small (Figure 9b); (2) in Figure 9b, even though the hcp-Dis boundary is identified in the semigrand canonical ensemble, the coexistence region is highly underestimated; and (3) in Figure 9a, a fcc phase is identified in the semigrand canonical ensemble, which is absent in the grand canonical ensemble with the same ϕ_3 . These discrepancies are due to the constraint $\phi_3 = \text{const.}$ imposed in the semigrand canonical ensemble, which is not strictly correct for accounting for phase coexistence. Nevertheless, these

Figure 15. Phase diagrams in the $\phi_2 - \chi_{AB}(=\chi_{AC} = \chi_{BD} = \chi_{CD})$ plane with the same parameters as those used in Figure 8b except $N_D =$ (a) 10 and (b) 6. The unlabeled regions are the two-phase coexistence regions between two adjacent single phases, which are too narrow to be visible. The phase boundary between the fcc and order-disorder coexistence regions, fcc- 2ϕ , is not determined and this fact is noted by the red “($\rightarrow 2\phi$)”, following the “fcc” label.

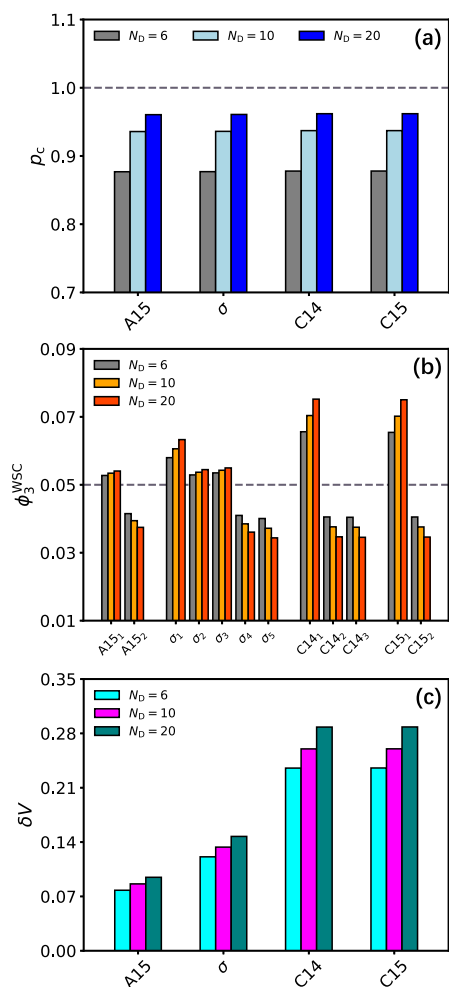


Figure 16. (a) Percentage contents of the D homopolymers within the A-rich domains, p_c . (b) Average concentrations of the D homopolymers within different FK WSCs, ϕ_3^{WSC} . (c) Relative standard deviations of domain volumes, δV . All quantities are evaluated at $N_D = 6, 10,$ and 20 for the four FK phases. Other parameters are $\epsilon = 2, \chi = 0.9, \phi_2 = 0.3, \phi_3 = 0.05,$ and $\{N_A (f_A), N_C, N_D\} = \{10 (0.25), 5, 20\}$. Dashed line in (a) marks 100% and the one in (b) marks the unit-cell-averaged ϕ_3 . Numbering of distinct types of domains/WSCs of the FK phases is shown in Figure S1.

discrepancies occur only when phase-coexistence regions become very large near the ODT and thus do not affect the regions consisting of the ordered phases, as focused by the current study.

The primary effect of the core-selective homopolymers is to act as space fillers and thus to swell the soft domains. The nonuniform partition of homopolymers into nonequivalent WSCs provides an effective mechanism to form domains with volumes conforming to those of the FK WSCs, which in turn optimizes the interfacial energy.¹⁷ For the AB/C/D ternary blends, the synergistic effect of the C and D homopolymers in strengthening the stability of the FK phases, particularly the Laves phases, observed in Figures 7–9, should be similarly attributed to optimized interfacial energies between chemically incompatible species. We will show that the formation of domains with large size dispersities helps to mitigate the

interfacial energies between all the repulsive pairs in the AB/C/D system. In Figure 10a, the average concentrations of the D homopolymers within different WSCs, ϕ_3^{WSC} , evaluated at $\epsilon = 2, \chi = 0.9, \phi_2 = 0.3, \phi_3 = 0.05,$ and $\{N_A (f_A), N_C, N_D\} = \{10 (0.25), 5, 20\}$ are shown. It is obvious that all four FK phases have a different ϕ_3^{WSC} in each nonequivalent WSC, and the deviation from the unit-cell-averaged value ϕ_3 (dashed line) for the two Laves phases is the largest. Figure 10b shows the relative standard deviations of the domain volumes, δV , evaluated at two different values for ϕ_3 , i.e., 0 and 0.05, for the various FK phases, with all the other parameters the same as those used in Figure 10a. The differential distribution of the core-selective D homopolymers is correlated with the increased size difference between these soft domains as ϕ_3 is increased, which is quantified by the increase in δV as ϕ_3 changes from 0 to 0.05, as seen in Figure 10b. These behaviors of ϕ_3^{WSC} and δV are similar to the A₁B₁/A₂ blends. More quantitatively, the different interfacial-energy contributions are measured by $N\Delta U_{\alpha\beta}/\rho_0 V k_B T$ ($\alpha\beta = AB, AC, BD,$ and CD). The four interfacial-energy contributions of the FK phases relative to those of their main competitor, i.e., the bcc phase, are plotted as a function of ϕ_3 in Figure 11. An overall drop is evidenced for all four contributions of the FK phases relative to those of the bcc phase upon increasing ϕ_3 . The drop in $N\Delta U_{BD}/\rho_0 V k_B T$ and $N\Delta U_{CD}/\rho_0 V k_B T$ is especially fast for the Laves phases compared to the σ and A15 phases, which are responsible for their stabilization over the σ phase in a large region in the phase diagrams with $\phi_2 > 0$ and $\phi_3 > 0$. These observations suggest that the FK phases have increasingly favorable interfacial energies between all the repulsive pairs in the ternary AB/C/D mixtures as the domain-size difference is enhanced by doping core-selective homopolymers in the presence of corona-selective homopolymers.

Another informative analysis to understand the synergistic effect between the two homopolymers is to investigate how increasing the concentration of the corona-selective homopolymers affects the existing core-selective homopolymers and its consequent impact on the various interfacial-energy contributions. For this purpose, Figure 12 shows the ϕ_3^{WSC} for different WSCs, along with the δV , at $\phi_2 = 0$ and 0.3 with $\epsilon = 2, \chi = 0.9, \phi_3 = 0.05,$ and $\{N_A (f_A), N_C, N_D\} = \{10 (0.25), 5, 20\}$, evaluated for the FK phases. As revealed by Figure 12a, increasing the concentration of the corona-selective component causes a slight redistribution of the core-selective component. Although the redistributions for all the FK phases are not significant, different behaviors are observed in these different packings. Specifically, the redistribution results in a clear growth in the interdomain deviation of the D homopolymer concentration for the Laves phases, that is, the ϕ_3^{WSC} of those domains with a value higher/lower than the unit-cell-averaged ϕ_3 (dashed line) is further increased/decreased with the addition of C homopolymers, which is not observed for the σ and A15 phases. The changes in concentration within the different σ WSCs do not show a clear trend. For example, σ_1 and σ_3 both have a higher-than-average ϕ_3^{WSC} value, but they change in opposite ways. For the A15 phase, the redistribution results in a drop in the deviation of ϕ_3^{WSC} , which is opposite of the observed trend for the Laves phases. These distinct behaviors in ϕ_3^{WSC} are correlated with the different trends in the change of δV , as shown in Figure 12b. It is seen that the δV has an obvious growth for the Laves phases, whereas the δV barely changes for the σ and slightly drops for the A15. The interfacial-energy analysis as a function

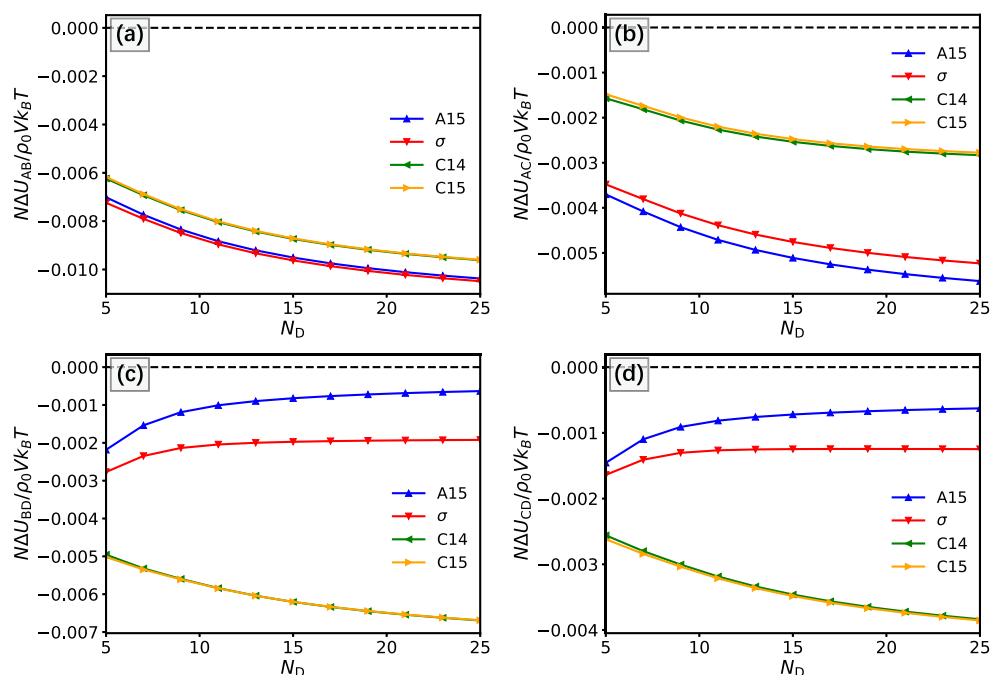


Figure 17. Four interfacial-energy contributions of the FK phases relative to those of the bcc phase, $N\Delta U_{\alpha\beta}/\rho_0 V k_B T$, where $\alpha\beta =$ (a) AB, (b) AC, (c) BD, and (d) CD, as a function of N_D . Other parameters are the same as those used in Figure 16.

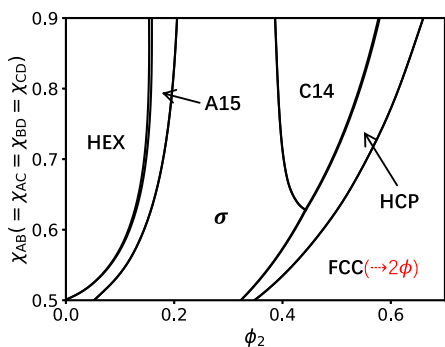


Figure 18. Phase diagram in the $\phi_2 - \chi_{AB}(=\chi_{AC} = \chi_{BD} = \chi_{CD})$ plane with the same parameters as those used in Figure 8b except $N_A = 13$ ($f = 0.325$). Unlabeled regions are the two-phase coexistence regions between two adjacent single phases. The phase boundary between the fcc and order-disorder coexistence regions, fcc- 2ϕ , is not determined and this fact is noted by the red “($\rightarrow 2\phi$)”, following the “fcc” label. Many of the coexistence regions between two adjacent phases are too narrow to be visible.

of ϕ_2 , provided in Figure 13 further reveals that the more dispersed domains make the Laves phases have more favorable CD interaction and less unfavorable AB interaction in comparison to the other two competing FK phases.

Both Figures 10 and 12 show that the Laves phases always greatly benefit from a more favorable CD interaction compared to the other competitive phases when increasing the concentration of either one of the C or D homopolymers at the presence of the other. This leads us to conclude that forming domains with very different sizes and packing into a Laves lattice provides an optimal way to compatibilize the immiscible C and D homopolymers, which explains the

synergistic effect of these two homopolymers in stabilizing the Laves phases. We believe that this mechanism is also the foundation of understanding the ubiquity of the Laves packings in a variety of soft matter systems composed of two incompatible species compatibilized by amphiphilic molecules.^{29,31,33,35–37} If the interaction between the C and D homopolymers is weakened, it is expected that the Laves phases would be less stable. To test this idea, a phase diagram with a fixed $\chi_{CD} = 0$ is constructed and shown in Figure 14, where all the other parameters are the same as those used for Figure 8b. Indeed, in contrast to Figure 8b, where a dominant Laves window exists between the σ and hcp phases, the Laves phases are completely absent in Figure 14, which confirms our speculation.

It has been established that the degree of polymerization of the core-swelling homopolymer plays an important role in determining the equilibrium morphology in AB/A-type blending systems.^{15–18,25,26,53} To illustrate the effects of N_D on the equilibrium spherical packing in the AB/C/D mixtures, Figure 15 shows two phase diagrams with $N_D = 10$ and 6, where the other parameters are the same as those for Figure 8b. Changes occur as N_D decreases from 20 (Figure 8b) to 10 (Figure 15a), including the overall shrinkage of the Laves region and the disappearance of the C15 phase. As N_D further drops to 6 (Figure 15b), the stability window of the C14 phase closes. As the D homopolymer behavior transitions from the dry-brush regime to the wet-brush regime by decreasing N_D , a weakened localization of the D homopolymers in the interior of the soft domains is expected. This is illustrated by Figure 16a, where the inner-domain percentage content p_c of the D homopolymers, defined as the fraction of the D homopolymers residing within the A-rich domains, is compared between cases with different N_D values for the four FK phases. The delocalization of the D homopolymers is reflected by the

decreased p_c when N_D becomes smaller. Furthermore, shorter homopolymers experience a more significant entropy loss when confined within domains with a substantial size difference compared to longer homopolymers. Therefore, the shorter D homopolymers are anticipated to distribute more evenly across the different WSCs, resulting in a smaller volume deviation for the FK phases. This is demonstrated by the changes in φ_3^{WSC} and δV , as shown in Figure 16b and c, respectively. Specifically, the φ_3^{WSC} 's for the various FK WSCs become closer to the unit-cell-averaged value and the δV 's for all FK phases decrease accordingly when lowering N_D . Consequently, the reduced difference in domain volumes diminishes the enthalpic favorability of the BD and CD contributions to the Laves packings, leading to the destabilization of both Laves phases. This is more directly demonstrated in Figure 17, where the relative interfacial-energy contributions are plotted as a function of N_D . In the Laves phases, the favorable BD and CD contributions gradually approach those of the other competitors as N_D decreases. Despite the presence of more repulsive pairs, whose interactions are all governed by the molecular weight of the core-selective homopolymers in the ternary AB/C/D blends, a similar dependence on the homopolymer molecular weight in phase behavior was also observed in the binary blends of miktoarm AB₄ copolymers and A homopolymers.⁵³

The equilibrium phase behavior of the AB/C/D system is also expected to be regulated by other factors, such as the block composition of the diblock copolymers. As an example, the phase diagram shown in Figure 18 depicts the phase behavior of the ternary blends, which have the same parameters as those used in Figure 8b except at a larger A-block composition $f = 0.325$. At this block composition of the diblock chains, the HEX phase with a lower interfacial curvature becomes more prominent, and an A15 stability window emerges between the HEX and σ . For neat AB diblock copolymer melts, a large diblock conformational asymmetry ($\epsilon \gtrsim 2.1$) is required to access the FK A15 phase at a comparable composition, i.e., $f \sim 0.3$.^{45,47} Although in the current ternary blends, this requirement may have been lowered due to the same argument applied to rationalize the emerging σ phase at low ϵ , the stabilization of the A15 phase in Figure 18 should still be largely attributed to the relatively large conformational asymmetry of the diblocks ($\epsilon = 2$). Moreover, the C15 phase becomes absent, leaving only the C14 phase between the σ and hcp. Notably, the phase transition sequence identified as increasing the concentration of the corona-selective homopolymers observed in the AB/C binary blends (Figure 2c), i.e., HEX \rightarrow A15 \rightarrow σ \rightarrow hcp, is preserved in the ternary AB/C/D blends, with the additional Laves window inserted at an intermediate ϕ_2 between the σ and hcp.

CONCLUSIONS

In summary, we have investigated the phase behavior of two polymeric blends containing AB diblock copolymers, i.e., the binary AB/C and ternary AB/C/D blends, by using the self-consistent field theory applied to the freely jointed chains. We have focused on the case where the diblock copolymers are sphere-forming and used the blends as a model system to obtain a better understanding of the ubiquitous emergence of the complex spherical packing phases in several analogous soft matter systems. For the AB/C binary blends, we predict a very low critical degree of conformational asymmetry with ($\epsilon \approx 1.1$) to stabilize the FK σ phase, which is consistent with recent

experimental observations. The occurrence of the FK σ phase at small ϵ is attributed to the aggregation of the corona-selective homopolymers at the interstitial voids, which releases the packing frustration induced by both the nonsphericity and nonuniformity of the polymeric domains. The extra degree of freedom offered by the homopolymer localization lowers the conformational-asymmetry requirement to access the FK packing in the binary blends. For the ternary AB/C/D blends, we observe that the simultaneous addition of the core- and corona-selective homopolymers greatly enhances the stability of the FK phases, particularly the Laves phases, suggesting a synergistic effect of the two incompatible homopolymers on the FK-packing formation. We further argued that the Laves packings offer the most effective arrangement to mitigate the interfacial-energy contributions from different repulsive block-pairs in the system owing to their largely different domain volumes enabled by the addition of the core-selective homopolymers. Especially, the Laves phases are greatly favored enthalpically due to a smaller CD interfacial-energy contribution. These observations offer a clear explanation for the observed synergistic effect and the wide stability windows of the Laves phases in the ϕ_1 - ϕ_2 - ϕ_3 triangular phase diagrams.

The two polymeric blends explored in this study have an enormously large phase space, especially the ternary AB/C/D blends, providing an illuminating model system to explore the emergence and stability of complex spherical packing phases. Although we have explored a large region in the phase space of the systems, further studies are required to have a more complete picture of the self-assembling behaviors outside the region covered by the current work. For example, the negative/positive interaction parameters $\chi_{\alpha\beta}$'s between different pairs of chemically distinct blocks were set to be equal, and this amounts to assuming that all the homopolymers are equally good or bad solvents. Relaxing this constraint to take into account the unequal miscibility will induce an asymmetry of the homopolymer-core and homopolymer-corona interactions and may, in turn, alter the equilibrium phase significantly. Another example is the recent experimental discovery of the C15 phase in a salt-doped pseudoternary polymeric system, where lamella-forming A₁B₁ diblock copolymers with symmetric block compositions were blended with A₂ and B₂ homopolymers both in the wet-brush regime.²⁹ Although there exist electrostatic interactions due to the addition of salt, the authors argued that electrostatic interactions are unlikely to be the source of the observed C15 packing. This suggests that the complex FK packings may also be accessed in salt-free A₁B₁/A₂/B₂ blends over an extended range of block compositions for the diblocks, provided that the homopolymer molecular weights and concentrations are carefully designed.

For systems in which ions and counterions play a significant role, such as surfactant solutions,^{30–33} a model incorporating electrostatic interactions is needed to provide a quantitative description of the phase behaviors.⁵⁴ Moreover, while the application of FJCs in the current work is suitable for modeling low-molecular-weight copolymers or even small amphiphilic molecules, the fluctuation effect is anticipated to have a greater impact on their phase behaviors, especially near the ODT. To accurately capture the phase behaviors near the ODT of these systems, a theoretical framework accounting for the fluctuation effect is required, such as field-theoretic simulation (FTS).^{55–57} Nevertheless, the mechanisms unraveled by the current work provide a solid foundation to explain the formation of these novel spherical packing phases not only

in neutral polymeric blends but also in systems involving electrostatic interactions and small amphiphilic molecules, thus shedding light on their emergence in a wide range of soft matter systems composed of amphiphiles and selective additives.

■ ASSOCIATED CONTENT

SI Supporting Information

The Supporting Information is available free of charge at <https://pubs.acs.org/doi/10.1021/acs.macromol.3c01973>.

Candidate phases and details of the four FK phases (PDF)

■ AUTHOR INFORMATION

Corresponding Author

An-Chang Shi – Department of Physics & Astronomy, McMaster University, Hamilton, Ontario L8S 4M1, Canada; orcid.org/0000-0003-1379-7162; Email: shi@mcmaster.ca

Author

Jiayu Xie – Department of Physics & Astronomy, McMaster University, Hamilton, Ontario L8S 4M1, Canada

Complete contact information is available at: <https://pubs.acs.org/doi/10.1021/acs.macromol.3c01973>

Notes

The authors declare no competing financial interest.

■ ACKNOWLEDGMENTS

This research is supported by the Natural Sciences and Engineering Research Council (NSERC) of Canada. The computation was made possible by the facilities of the Shared Hierarchical Academic Research Computing Network (SHARCNET).

■ REFERENCES

- Weaire, D.; Aste, T. *The Pursuit of Perfect Packing*; CRC Press, 2008.
- Hales, T. C. An overview of the Kepler conjecture. **1998**, arXiv Mathematics e-prints arXiv:math/9811071.
- Bates, F. S.; Fredrickson, G. H. Block copolymers—designer soft materials. *Phys. Today* **1999**, *52*, 32–38.
- Bates, C. M.; Bates, F. S. 50th Anniversary Perspective: Block Polymers—Pure Potential. *Macromolecules* **2017**, *50*, 3–22.
- Shi, A.-C. Frustration in block copolymer assemblies. *J. Phys.: Condens. Matter* **2021**, *33*, 253001.
- Matsen, M. W. The standard Gaussian model for block copolymer melts. *J. Phys.: Condens. Matter* **2002**, *14*, R21–R47.
- Li, W.; Duan, C.; Shi, A.-C. Nonclassical Spherical Packing Phases Self-Assembled from AB-Type Block Copolymers. *ACS Macro Lett.* **2017**, *6*, 1257–1262.
- Grason, G. M.; DiDonna, B.; Kamien, R. D. Geometric theory of diblock copolymer phases. *Phys. Rev. Lett.* **2003**, *91*, 058304.
- Grason, G. M.; Kamien, R. D. Interfaces in diblocks: A study of miktoarm star copolymers. *Macromolecules* **2004**, *37*, 7371–7380.
- Grason, G. M.; Kamien, R. D. Self-consistent field theory of multiply branched block copolymer melts. *Phys. Rev. E: Stat., Nonlinear, Soft Matter Phys.* **2005**, *71*, 051801.
- Cho, B.-K.; Jain, A.; Gruner, S. M.; Wiesner, U. Mesophase structure-mechanical and ionic transport correlations in extended amphiphilic dendrons. *Science* **2004**, *305*, 1598–1601.
- Lee, S.; Bluemle, M. J.; Bates, F. S. Discovery of a Frank-Kasper σ phase in sphere-forming block copolymer melts. *Science* **2010**, *330*, 349–353.
- Dorfman, K. D. Frank-Kasper Phases in Block Polymers. *Macromolecules* **2021**, *54*, 10251–10270.
- Xie, J.; Shi, A.-C. Phase Behavior of Binary Blends of Diblock Copolymers: Progress and Opportunities. *Langmuir* **2023**, *39*, 11491–11509.
- Mueller, A. J.; Lindsay, A. P.; Jayaraman, A.; Lodge, T. P.; Mahanthappa, M. K.; Bates, F. S. Emergence of a C15 Laves Phase in Diblock Polymer/Homopolymer Blends. *ACS Macro Lett.* **2020**, *9*, 576–582.
- Cheong, G. K.; Bates, F. S.; Dorfman, K. D. Symmetry breaking in particle-forming diblock polymer/homopolymer blends. *Proc. Natl. Acad. Sci. U.S.A.* **2020**, *117*, 16764–16769.
- Xie, J.; Shi, A.-C. Formation of complex spherical packing phases in diblock copolymer/homopolymer blends. *Giant* **2021**, *5*, 100043.
- Mueller, A. J.; Lindsay, A. P.; Jayaraman, A.; Weigand, S.; Lodge, T. P.; Mahanthappa, M. K.; Bates, F. S. Tuning Diblock Copolymer Particle Packing Symmetry with Variable Molecular Weight Core-Homopolymers. *Macromolecules* **2022**, *55*, 8332–8344.
- Liu, M.; Qiang, Y.; Li, W.; Qiu, F.; Shi, A.-C. Stabilizing the Frank-Kasper phases via binary blends of AB diblock copolymers. *ACS Macro Lett.* **2016**, *5*, 1167–1171.
- Kim, K.; Arora, A.; Lewis, R. M.; Liu, M.; Li, W.; Shi, A.-C.; Dorfman, K. D.; Bates, F. S. Origins of low-symmetry phases in asymmetric diblock copolymer melts. *Proc. Natl. Acad. Sci. U.S.A.* **2018**, *115*, 847–854.
- Lindsay, A. P.; Lewis, R. M.; Lee, B.; Peterson, A. J.; Lodge, T. P.; Bates, F. S. A15, σ , and a quasicrystal: Access to complex particle packings via bidisperse diblock copolymer blends. *ACS Macro Lett.* **2020**, *9*, 197–203.
- Lindsay, A. P.; Cheong, G. K.; Peterson, A. J.; Weigand, S.; Dorfman, K. D.; Lodge, T. P.; Bates, F. S. Complex Phase Behavior in Particle-Forming AB/AB' Diblock Copolymer Blends with Variable Core Block Lengths. *Macromolecules* **2021**, *54*, 7088–7101.
- Xie, J.; Li, Y.; Shi, A.-C. Binary blends of diblock copolymers: An efficient route to complex spherical packing phases. *Macromol. Theory Simul.* **2021**, *30*, 2100053.
- Reddy, A.; Buckley, M. B.; Arora, A.; Bates, F. S.; Dorfman, K. D.; Grason, G. M. Stable Frank-Kasper phases of self-assembled, soft matter spheres. *Proc. Natl. Acad. Sci. U.S.A.* **2018**, *115*, 10233–10238.
- Matsen, M. W. Stabilizing new morphologies by blending homopolymer with block copolymer. *Phys. Rev. Lett.* **1995**, *74*, 4225–4228.
- Matsen, M. W. Phase behavior of block copolymer/homopolymer blends. *Macromolecules* **1995**, *28*, 5765–5773.
- Takagi, H.; Yamamoto, K. Phase Boundary of Frank-Kasper σ Phase in Phase Diagrams of Binary Mixtures of Block Copolymers and Homopolymers. *Macromolecules* **2019**, *52*, 2007–2014.
- Chen, M.-Z.; Huang, Y.-T.; Chen, C.-Y.; Chen, H.-L. Accessing the Frank-Kasper σ Phase of Block Copolymer with Small Conformational Asymmetry via Selective Solvent Solubilization in the Micellar Corona. *Macromolecules* **2022**, *55*, 10812–10820.
- Xie, S.; Lindsay, A. P.; Bates, F. S.; Lodge, T. P. Formation of a C15 Laves phase with a giant unit cell in salt-doped A/B/AB ternary polymer blends. *ACS Nano* **2020**, *14*, 13754–13764.
- Kim, S. A.; Jeong, K.-J.; Yethiraj, A.; Mahanthappa, M. K. Low-symmetry sphere packings of simple surfactant micelles induced by ionic sphericity. *Proc. Natl. Acad. Sci. U.S.A.* **2017**, *114*, 4072–4077.
- Baez-Cotto, C. M.; Mahanthappa, M. K. Micellar mimicry of intermetallic C14 and C15 Laves phases by aqueous lyotropic self-assembly. *ACS Nano* **2018**, *12*, 3226–3234.
- Jayaraman, A.; Mahanthappa, M. K. Counterion-Dependent Access to Low-Symmetry Lyotropic Sphere Packings of Ionic Surfactant Micelles. *Langmuir* **2018**, *34*, 2290–2301.

- (33) Baez-Cotto, C. M.; Jackson, G. L.; Mahanthappa, M. K. Aqueous lyotropic mesophase behavior of gemini dicarboxylate surfactants swollen with n-decane. *Langmuir* **2020**, *36*, 2307–2321.
- (34) Matsen, M. Self-consistent field theory for melts of low-molecular-weight diblock copolymer. *Macromolecules* **2012**, *45*, 8502–8509.
- (35) Alexandridis, P.; Olsson, U.; Lindman, B. Structural polymorphism of amphiphilic copolymers: Six lyotropic liquid crystalline and two solution phases in a poly (oxybutylene)-b-poly (oxyethylene)- water- xylene system. *Langmuir* **1997**, *13*, 23–34.
- (36) Alexandridis, P.; Olsson, U.; Lindman, B. A record nine different phases (four cubic, two hexagonal, and one lamellar lyotropic liquid crystalline and two micellar solutions) in a ternary isothermal system of an amphiphilic block copolymer and selective solvents (water and oil). *Langmuir* **1998**, *14*, 2627–2638.
- (37) Uddin, M. H.; Rodríguez, C.; Watanabe, K.; López-Quintela, A.; Kato, T.; Furukawa, H.; Harashima, A.; Kunieda, H. Phase behavior and formation of reverse cubic phase based emulsion in water/poly (oxyethylene) poly (dimethylsiloxane) surfactants/silicone oil systems. *Langmuir* **2001**, *17*, 5169–5175.
- (38) Jayaraman, A.; Zhang, D. Y.; Dewing, B. L.; Mahanthappa, M. K. Path-dependent preparation of complex micelle packings of a hydrated diblock oligomer. *ACS Cent. Sci.* **2019**, *5*, 619–628.
- (39) Fredrickson, G.; et al. *The Equilibrium Theory of Inhomogeneous Polymers*; Oxford University Press on Demand, 2006.
- (40) Shi, A.-C. Self-consistent field theory of inhomogeneous polymeric systems. *Variational Methods in Molecular Modeling*; Springer, 2017; pp 155–180.
- (41) Thompson, R. B.; Rasmussen, K. O.; Lookman, T. Improved convergence in block copolymer self-consistent field theory by Anderson mixing. *J. Chem. Phys.* **2004**, *120*, 31–34.
- (42) Vavasour, J. D.; Whitmore, M. D. Self-consistent mean field theory of the microphases of diblock copolymers. *Macromolecules* **1992**, *25*, 5477–5486.
- (43) Vavasour, J.; Whitmore, M. Self-consistent field theory of block copolymers with conformational asymmetry. *Macromolecules* **1993**, *26*, 7070–7075.
- (44) Milner, S. T. Chain architecture and asymmetry in copolymer microphases. *Macromolecules* **1994**, *27*, 2333–2335.
- (45) Xie, N.; Li, W.; Qiu, F.; Shi, A.-C. σ phase formed in conformationally asymmetric AB-type block copolymers. *ACS Macro Lett.* **2014**, *3*, 906–910.
- (46) Schulze, M. W.; Lewis, R. M.; Lettow, J. H.; Hickey, R. J.; Gillard, T. M.; Hillmyer, M. A.; Bates, F. S. Conformational asymmetry and quasicrystal approximants in linear diblock copolymers. *Phys. Rev. Lett.* **2017**, *118*, 207801.
- (47) Bates, M. W.; Lequeieu, J.; Barbon, S. M.; Lewis, R. M.; Delaney, K. T.; Anastasaki, A.; Hawker, C. J.; Fredrickson, G. H.; Bates, C. M. Stability of the A15 phase in diblock copolymer melts. *Proc. Natl. Acad. Sci. U.S.A.* **2019**, *116*, 13194–13199.
- (48) Berney, C.; Cheng, P. L.; Cohen, R. Distribution of matrix homopolymer in block copolymers of spherical morphology. *Macromolecules* **1988**, *21*, 2235–2240.
- (49) Hashimoto, T.; Tanaka, H.; Hasegawa, H. Ordered structure in mixtures of a block copolymer and homopolymers. 2. Effects of molecular weights of homopolymers. *Macromolecules* **1990**, *23*, 4378–4386.
- (50) Tanaka, H.; Hasegawa, H.; Hashimoto, T. Ordered structure in mixtures of a block copolymer and homopolymers. 1. Solubilization of low molecular weight homopolymers. *Macromolecules* **1991**, *24*, 240–251.
- (51) Winey, K. I.; Thomas, E. L.; Fetters, L. J. Swelling of lamellar diblock copolymer by homopolymer: influences of homopolymer concentration and molecular weight. *Macromolecules* **1991**, *24*, 6182–6188.
- (52) Koizumi, S.; Hasegawa, H.; Hashimoto, T. Spatial distribution of homopolymers in block copolymer microdomains as observed by a combined SANS and SAXS method. *Macromolecules* **1994**, *27*, 7893–7906.
- (53) Zhao, M.; Li, W. Laves Phases Formed in the Binary Blend of AB4Miktoarm Star Copolymer and A-Homopolymer. *Macromolecules* **2019**, *52*, 1832–1842.
- (54) Shi, A.-C.; Noolandi, J. Theory of inhomogeneous weakly charged polyelectrolytes. *Macromolecular Theory And Simulations* **1999**, *8*, 214–229.
- (55) Düchs, D.; Ganesan, V.; Fredrickson, G. H.; Schmid, F. Fluctuation effects in ternary AB+ A+ B polymeric emulsions. *Macromolecules* **2003**, *36*, 9237–9248.
- (56) Delaney, K. T.; Fredrickson, G. H. Recent developments in fully fluctuating field-theoretic simulations of polymer melts and solutions. *J. Phys. Chem. B* **2016**, *120*, 7615–7634.
- (57) Spencer, R. K.; Matsen, M. W. Fluctuation effects in blends of A+ B homopolymers with AB diblock copolymer. *J. Chem. Phys.* **2018**, *148*, 204907.

NOTE ADDED AFTER ASAP PUBLICATION

This paper was published ASAP on December 12, 2023 with an incorrect link to the Supporting Information file. The corrected version was reposted on December 13, 2023.

Chapter 7

Stabilizing Binary Crystalline Phases in AB/CD Binary Diblock Copolymer Blends via Secondary Interactions

Publication: Xie, Jiayu, Chi To Lai, and An-Chang Shi. “Regulating the self-assembly of AB/CD diblock copolymer blends via secondary interactions.” *Journal of Polymer Science* (Published online: July 18, 2023).

Authors: **Jiayu Xie**, Chi To Lai, An-Chang Shi

Contribution: I am the first author of this paper. Chi To Lai and I developed the theoretical model and computational code together. We also collaborated on generating the data. I analyzed the data and drafted the initial manuscript. All authors collaborated on manuscript revisions, with guidance from Dr. Shi throughout the research.

Preface

In this chapter, we explore the possibility of stabilizing various binary spherical crystalline phases in binary AB/CD diblock copolymer blends with designed secondary interactions. The binary crystalline phases are composed of spheres, or “mesoatoms”, self-assembled from chemically distinct blocks, resembling the binary metallic alloys. The simplest block copolymer system that is capable of forming these structures is linear ABC triblock copolymers [130, 131]. However, the number of binary crystals that can be stabilized by this simple system is limited. One approach to expand the library of binary mesocrystals achievable through block-copolymer self-assembly is to use more complex multiblock copolymers with meticulously designed architectures. To this end, tetrablock and pentablock terpolymers were designed, which, as demonstrated by SCFT, successfully give rise to a diverse array of binary mesocrystals with various coordination numbers [46]. Moreover, the coordination number of the equilibrium crystal can be regulated by adjusting the relative compositions of the different matrix blocks of the terpolymer. Despite the promising opportunities presented by multiblock copolymers for producing desired binary crystals, the substantial synthesis effort required to construct a library of these polymers with precise block compositions poses a practical challenge.

Here, we adopt an alternative approach to attain binary mesocrystals — utilizing polymeric blends comprising architecturally simple components: AB and CD diblock copolymers. By employing SCFT, we demonstrate that this simple blending formulation, with properly designed segment-segment interactions, can stabilize binary crystals composed of A and C mesoatoms with varying A:C stoichiometries. Specifically, to promote the formation of binary crystals, a strong repulsion between A and C is required. However, such A-C repulsion will lead to macrophase separation of the system [76, 78]. To suppress the tendency of the blends to phase separate macroscopically, attractive interactions

need to be introduced between the B and D blocks. In experimental scenarios, the compatibilization of B and D blocks can be achieved by introducing secondary interactions, such as hydrogen bonding. The dependence of the equilibrium crystal on the different system parameters is illustrated by a set of phase diagrams. Furthermore, the chain packing within different binary crystalline phases is also analyzed, shedding light on the mechanism governing the selection of the equilibrium crystal in this system.

Regulating the self-assembly of AB/CD diblock copolymer blends via secondary interactions

Jiayu Xie | Chi To Lai | An-Chang Shi 

Department of Physics & Astronomy,
McMaster University, Hamilton,
Ontario, Canada

Correspondence

An-Chang Shi, Department of Physics &
Astronomy, McMaster University,
Hamilton, Ontario, Canada L8S 4M1.
Email: shi@physics.mcmaster.ca

Funding information

Natural Sciences and Engineering
Research Council of Canada; National
Science Foundation, Grant/Award
Number: PHY-1748958

Abstract

Designed multiblock copolymers with complex architectures offer unlimited opportunities to obtain novel nanostructured phases, however, their synthesis could be challenging and expensive. An alternative approach to access desired nanostructures is to use blends of block copolymers with simple chain architectures and designed block-block interactions. We use binary blends composed of AB and CD diblock copolymers as a model system to establish design principles of polymeric blends containing block copolymers. Specifically, we explore the phase behavior of AB/CD blends by using the polymeric self-consistent field theory to construct phase diagrams of the blends focusing on the sphere-forming regions in the phase space. We predict the formation of various spherical packing phases composed of either core-shell-structured spheres or binary spheres resembling metallic alloys. We demonstrate that the equilibrium morphology can be regulated by adjusting the blend composition and molecular parameters such as block fractions, conformational asymmetry, and segment-segment interactions. The strategy of using secondary interaction in polymeric blends to control the phase behavior explored in the current study can also be generalized to other soft matter systems.

KEYWORDS

block copolymer blends, Frank-Kasper phases, self-assembly of block copolymers, self-consistent field theory

1 | INTRODUCTION

Block copolymers are obtained when two or more chemically distinct blocks are tethered together via covalent bonds.¹ One of the unique features of block copolymers is that they possess opposing tendencies due to the block-block repulsion and chain connectivity; therefore, they are frustrated at the molecular level.² Block copolymers alleviate this frustration by microphase separation into polymeric domains, which in turn pack to form ordered

structures at 10–100 nanometer scale.^{3,4} The spontaneous emergence of long-range ordered structures in block copolymers not only leads to potential technological applications,^{5–9} but also offers an ideal platform to study the spontaneous emergence of structured matter.

A widely studied block copolymer is the AB diblock copolymer composed of two covalently bonded, A and B, subchains or blocks.^{3,4,10} Despite its simplicity, a rich array of ordered phases consisting of spheres, cylinders, bicontinuous networks and lamellae have been theoretically

This is an open access article under the terms of the [Creative Commons Attribution](#) License, which permits use, distribution and reproduction in any medium, provided the original work is properly cited.

© 2023 The Authors. *Journal of Polymer Science* published by Wiley Periodicals LLC.

predicted and experimentally observed in AB diblock copolymer melts. It is now well understood that the spontaneous formation of these intricate structures is due to a delicate competition between the interaction of incompatible blocks and the entropic chain stretching, or simply the frustration intrinsic to the system.² Extensive theoretical and experimental studies have established that the phase behavior of AB diblock copolymer melts is determined mainly by three parameters, namely the composition or volume fraction of the A block, f , the A/B interaction strength quantified by the product χN , where χ is the Flory-Huggins interaction parameter and N is the copolymer degree of polymerization, and the conformational asymmetry ϵ quantified by the ratio between the Kuhn lengths of the A and B blocks.^{11–13}

The number of accessible ordered phases in block copolymers could be drastically increased with increasing number of chemically distinct blocks and more complex chain architectures.^{1,14} A simple example is the introduction of a second A block to an AB diblock copolymer. As the tethering position of the additional A block changes from the AB junction point to the free end of the B block, the copolymer architecture transforms from miktoarm A_2B to linear ABA continuously, resulting in different phase behaviors as well as new ordered phases.¹⁵ Another example is replacing the added A block by a chemically distinct C block to form a linear ABC¹⁶ or a star ABC triblock copolymer,^{17,18} in which the number of accessible stable phases is further increased due to the more complex monomer-monomer interactions. From an application point of view, it is desirable to have the ability to inversely design macromolecules that are capable of self-assembling into certain target ordered structures. Driven by the demand of effective inverse molecular design, an active research direction is to understand the mechanisms and principles governing the self-assembly of block copolymers with different architectures via both theory^{12,19–24} and experiments.^{25–27}

Although multiblock copolymers with exotic molecular topologies offer great opportunities to enrich the phase behaviors of block copolymers, precise synthesis of copolymers with complicated architectures can be challenging and costly.^{1,14} One appealing alternative to fabricate and control novel polymeric structures is by using polymer blends. It has been shown that blending different types of block copolymers can stabilize new structures that are not equilibrium phases of the individual components. For instance, the binary A_1B_1/A_2B_2 diblock copolymer/homopolymer blends and A_1B_1/A_2B_2 diblock copolymer blends can stabilize various Frank-Kasper (FK) phases that are absent in the neat, conformationally symmetric, AB diblock copolymer melts.^{28–34} Extensive experimental and theoretical studies have revealed that the ability of polymeric blends to stabilize

these complex spherical phases could be attributed to the differential distribution of the second component.³⁵ Specifically, the added homopolymers could act as fillers swelling the spherical domains thus aiding the formation of large domains with different sizes, whereas the added copolymers could act as fillers and co-surfactants at the same time to regulate both the size of the spherical domains and the properties of the AB interface.³⁵

The complexity of polymeric blends containing block copolymers could be dramatically increased by introducing new chemically distinct components. For example, going from the binary A_1B_1/A_2B_2 blends to AB/B'C or AB/CD blends enlarges the phase space and thus alters the phase behaviors tremendously. Very recently, Dorfman and coworkers have reported theoretical studies on binary mixtures of AB/B'C diblock copolymers in search of a more robust platform to stabilize the Laves phases.^{36,37} By tailoring the molecular parameters to favor the formation of A and C spheres, or mesoatoms, with different volumes, interesting phase diagrams exhibiting an eutectic phase behavior resembling that of the binary metallic alloys were discovered, featuring the emergence of a Laves phase field. Moreover, an interesting observation by these authors was the decoupled control over the polyhedral imprinting of the A and C spherical domains by individually adjusting the conformational asymmetry of the AB and B'C copolymers.³⁷ However, one caveat of the binary AB/B'C blends is the dominance of macrophase separation due to the strong incompatibility between the AB and B'C diblocks. One possible approach to suppress macrophase separation is to introduce associations, or supramolecular interactions, between the different components.

On its own, the effects of supramolecular interactions such as hydrogen bonding on the phase behaviors of block copolymer blends have been an interesting research topic because it offers opportunities to access novel ordered structures.³⁸ In the case of a binary blend of AB/CD diblock copolymers with hydrogen bonding between B and D blocks, it has been observed experimentally that hierarchical structures could be formed.³⁹ Specifically, for symmetric AB and CD diblock copolymers, an hierarchical lamellar phase consisting of a mixed BD layer sandwiched by alternating phase-separated A/C layers was observed. If AB and CD are both asymmetric, the minority B and D blocks were observed to form mixed cylinders located at the interface of A and C lamellae. Moreover, the presence of hydrogen bonding between more than one pairs of blocks but with different strengths could result in competing associations, driving the system to form novel phases such as three-layered lamellae and core-shell cylinders.^{40–43} Recent theoretical studies using self-consistent field theory (SCFT)⁴⁴ and dissipative particle dynamics (DPD) simulations⁴⁵ also reported the formation of various complex structures in

supramolecular AB/CD blends. Furthermore, several novel structures including Archimedean and kaleidoscopic tilings were also experimentally observed in blends of block copolymers with more complicated architectures and selective interactions.^{46,47}

Previous theoretical and experimental studies have demonstrated that polymeric blends, especially those with secondary interactions such as hydrogen bonding, hold great promise to fabricate structures that are not available in the individual components. In this study, we aim to deepen our understanding of the self-assembling behaviors of polymeric blends involving secondary interactions by studying a simple model system composed of AB and CD diblock copolymers. By applying the polymeric self-consistent field theory (SCFT), we explore the phase behavior of sphere-forming AB/CD binary mixtures similar to the AB/B'C system studied by Dorfman and coworkers,^{36,37} with a focus on answering the following questions: (1) is it possible to suppress macrophase separation and consequently to enlarge the composition window over which the binary crystalline phases are stable by introducing attractive interaction between the B and D blocks; (2) what phases could be formed in this system in the presence of B–D association; and (3) how do the various system parameters alter the phase behavior of the system? Specifically, we construct phase diagrams in the $\phi_2 - \chi_{\alpha\beta}N$ planes, where ϕ_2 is the concentration of the CD diblock copolymers and $\chi_{\alpha\beta}N$ is the parameter quantifying the interaction between α - and β -type monomers with $\alpha(\neq\beta), \beta = A, B, C$ or D. In order to investigate the effects of different system parameters such as B–D association strength, block compositions and conformational asymmetry, a series of phase diagrams with different choices of parameters are constructed and compared. The dependence of the stability of different phases on the system parameters provides an effective route to manipulate the equilibrium morphology. An analysis of the structural properties is also conducted to elucidate mechanisms regulating the chain packing in various structures. The results from the current study provide valuable insights into the design principles for polymeric blends with appropriate secondary interactions to fabricate novel structures.

2 | THEORETICAL MODEL

We consider binary blends composed of AB and CD diblock copolymers in a volume V . Specifically, the model system contains n_1 chains of AB and n_2 chains of CD diblock copolymers described by the standard Gaussian chain model.¹⁰ Each AB and CD copolymer has the degree of polymerization of $N_1 = N_A + N_B$ and $N_2 = N_C + N_D$, respectively, where the alphabetical subscripts indicate

the monomer type. In our calculations, we choose N_1 as the reference N and define the ratio between the degrees of polymerization of the two copolymers as $\gamma = N_2/N_1$. The volume fractions of the A and B blocks in an AB copolymer are $f_A = N_A/N_1 = f_1$ and $f_B = N_B/N_1 = 1 - f_1$, respectively, and $f_C = N_C/N_2 = f_2$ and $f_D = N_D/N_2 = 1 - f_2$ are defined for the CD copolymer similarly. For simplicity, a uniform segment density ρ_0 is assumed and thus $\rho_0 V = n_1 N + n_2 \gamma N$ due to the incompressibility condition. The average concentrations of the AB and CD diblock copolymers are given by, $\phi_1 = \frac{n_1 N}{\rho_0 V}$ and $\phi_2 = 1 - \phi_1 = \frac{n_2 \gamma N}{\rho_0 V}$, respectively. The Kuhn length of the α segments is denoted by b_α ($\alpha = A, B, C$ or D).

For multi-component systems undergoing both microphase and macrophase separations, their phase behaviors can be accounted for most conveniently by using the grand canonical ensemble. The thermodynamic control parameters in the grand canonical ensemble are the chemical potentials, μ_1 and μ_2 , of the AB and CD diblock copolymers. Within the SCFT framework,^{48,49} the grand potential density of the system is given by,

$$\begin{aligned} -Q_1 - e^{\frac{\mu}{k_B T}} Q_2 - \frac{1}{V} \int d\vec{r} \left[\sum_\alpha \omega_\alpha(\vec{r}) \phi_\alpha(\vec{r}) \right. \\ \left. \frac{N\Phi}{\rho_0 V k_B T} = - \sum_{\alpha, \beta(\neq\alpha)} \chi_{\alpha\beta} N \phi_\alpha(\vec{r}) \phi_\beta(\vec{r}) \right. \\ \left. + \eta(\vec{r}) \left(1 - \sum_\alpha \phi_\alpha(\vec{r}) \right) \right], \end{aligned} \quad (1)$$

where μ_1 is set to 0 by using the incompressibility condition and thus the subscript of μ_2 is dropped for brevity. Upon minimizing the grand potential with respect to the density and conjugate fields, we obtain a set of SCFT equations,

$$\left\{ \begin{aligned} \omega_\alpha(\vec{r}) &= \sum_{\beta(\neq\alpha)} \chi_{\alpha\beta} N \phi_\beta(\vec{r}) + \eta(\vec{r}), \\ \phi_A(\vec{r}) &= \int_0^{f_1} ds q_1(s, \vec{r}) q_1^\dagger(s, \vec{r}), \\ \phi_B(\vec{r}) &= \int_{f_1}^1 ds q_1(s, \vec{r}) q_1^\dagger(s, \vec{r}), \\ \phi_C(\vec{r}) &= e^{\frac{\mu}{k_B T}} \int_0^{\gamma f_2} ds q_2(s, \vec{r}) q_2^\dagger(s, \vec{r}), \\ \phi_D(\vec{r}) &= e^{\frac{\mu}{k_B T}} \int_{\gamma f_2}^\gamma ds q_2(s, \vec{r}) q_2^\dagger(s, \vec{r}), \\ \sum_\alpha \phi_\alpha(\vec{r}) &= 1. \end{aligned} \right. \quad (2)$$

Here, the forward propagators $q(s, \vec{r})$ and backward propagators $q^\dagger(s, \vec{r})$ are obtained by solving the modified diffusion equations,

$$\begin{aligned} \frac{\partial}{\partial s} q_1(s, \vec{r}) &= b_1^2 \nabla^2 q_1(s, \vec{r}) - \omega_1(\vec{r}) q_1(s, \vec{r}), \\ -\frac{\partial}{\partial s} q_1^\dagger(s, \vec{r}) &= b_1^2 \nabla^2 q_1^\dagger(s, \vec{r}) - \omega_1(\vec{r}) q_1^\dagger(s, \vec{r}), \\ \frac{\partial}{\partial s} q_2(s, \vec{r}) &= b_2^2 \nabla^2 q_2(s, \vec{r}) - \omega_2(\vec{r}) q_2(s, \vec{r}), \\ -\frac{\partial}{\partial s} q_2^\dagger(s, \vec{r}) &= b_2^2 \nabla^2 q_2^\dagger(s, \vec{r}) - \omega_2(\vec{r}) q_2^\dagger(s, \vec{r}), \end{aligned} \quad (3)$$

where the reference N is set to 1 so $s \in [0, 1]$ for AB diblock copolymers and $s \in [0, \gamma]$ for CD diblock copolymers. The conjugate fields and Kuhn lengths are defined for the AB copolymers by $\omega_1(\vec{r}) = \omega_A(\vec{r})$, $b_1 = b_A$ when $s \in [0, f_1]$ and $\omega_1(\vec{r}) = \omega_B(\vec{r})$, $b_1 = b_B$ when $s \in [f_1, 1]$. Similarly, they are defined for the CD copolymers by $\omega_2(\vec{r}) = \omega_C(\vec{r})$, $b_2 = b_C$ when $s \in [0, \gamma f_2]$ and $\omega_2(\vec{r}) = \omega_D(\vec{r})$, $b_2 = b_D$ when $s \in [\gamma f_2, \gamma]$. The conformational asymmetry parameters depend on the Kuhn lengths via $\epsilon_1 = \sqrt{(\rho_A b_A^2)/(\rho_B b_B^2)} = b_A/b_B$ and $\epsilon_2 = b_C/b_D$ for the AB and CD copolymers, respectively. The initial conditions of the propagators are $q_1(0, \vec{r}) = q_2(0, \vec{r}) = q_1^\dagger(1, \vec{r}) = q_2^\dagger(\gamma, \vec{r}) = 1$. The average concentrations of the AB and CD diblock copolymers can be computed via,

$$\phi_1 = Q_1, \quad \phi_2 = 1 - \phi_1. \quad (4)$$

The single chain partition functions of AB and CD copolymers are given by,

$$Q_1 = \frac{1}{V} \int d\vec{r} q_1(1, \vec{r}), \quad (5)$$

$$Q_2 = \frac{1}{V} \int d\vec{r} q_2(\gamma, \vec{r}). \quad (6)$$

The SCFT equations (Equations 2) are solved numerically to obtain solutions corresponding to a set of candidate phases. A detailed description of the candidate phases included in this work is provided in the supplementary information (S1). The pseudo-spectral method^{50,51} is used to solve the modified diffusion equations (Equation 3). In addition, we apply variable-cell Anderson mixing method^{52,53} to simultaneously speed up the convergence of solutions to Equation 2 and to optimize the unit-cell

parameters. Finally, the phase diagram is constructed by comparing the grand potential densities of the candidate phases. Details about the phase diagram construction protocol used in the current study are also provided in the SI.

When the concentrations of different components need to be specified explicitly, it is more convenient to work in the canonical ensemble, where the thermodynamic control parameters are the concentration of the AB diblock copolymers, ϕ_1 , and the concentration of the CD diblock copolymers, ϕ_2 . The mean-field Helmholtz free energy density is given by,

$$\begin{aligned} \frac{NF}{\rho_0 V k_B T} &= -\phi_1 \ln \frac{Q_1}{\phi_1} - \frac{\phi_2}{\gamma} \ln \frac{Q_2}{\phi_2} - \frac{1}{V} \int d\vec{r} \left[\sum_\alpha \omega_\alpha(\vec{r}) \phi_\alpha(\vec{r}) \right. \\ &\quad \left. - \sum_{\alpha, \beta (\neq \alpha)} \chi_{\alpha\beta} N \phi_\alpha(\vec{r}) \phi_\beta(\vec{r}) \right. \\ &\quad \left. + \eta(\vec{r}) \left(1 - \sum_\alpha \phi_\alpha(\vec{r}) \right) \right]. \end{aligned} \quad (7)$$

A useful decomposition of the free energy given by Equation 7 is,

$$\frac{NF}{\rho_0 V k_B T} = \frac{N}{\rho_0 V k_B T} \left(\sum_{\alpha\beta} U_{\alpha\beta} - TS_1 - TS_2 \right), \quad (8)$$

where the different contributions are,

$$\begin{aligned} \frac{NU_{\alpha\beta}}{\rho_0 V k_B T} &= \frac{\chi_{\alpha\beta} N}{V} \int d\vec{r} \phi_\alpha(\vec{r}) \phi_\beta(\vec{r}), \\ -\frac{NTS_1}{\rho_0 V k_B T} &= -\phi_1 \ln \frac{Q_1}{\phi_1} - \frac{1}{V} \int d\vec{r} \sum_\alpha^{A,B} \omega_\alpha(\vec{r}) \phi_\alpha(\vec{r}), \\ -\frac{NTS_2}{\rho_0 V k_B T} &= -\frac{\phi_2}{\gamma} \ln \frac{Q_2}{\phi_2} - \frac{1}{V} \int d\vec{r} \sum_\alpha^{C,D} \omega_\alpha(\vec{r}) \phi_\alpha(\vec{r}). \end{aligned} \quad (9)$$

The term $U_{\alpha\beta}$ corresponds to the enthalpic contribution from the interactions between α - and β -type segments, while $-TS_1$ and $-TS_2$ are the entropic contributions from AB, and CD diblock copolymers, respectively. An analysis of Equations 9 could provide insights on the relative importance of the different contributions.

A general AB/CD binary blends contain 13 independent parameters, corresponding to an extremely large and complex phase space. Specifically, these are the six interaction parameters, that is, $\chi_{AC}N$, $\chi_{AB}N$, $\chi_{CD}N$, $\chi_{AD}N$, $\chi_{BC}N$ and $\chi_{BD}N$, the chain-length ratio γ , the volume

fractions of the A and C blocks of the respective diblock copolymers, f_1 and f_2 , the 4 Kuhn lengths for the different types of blocks, b_α with $\alpha=A, B, C$ or D (only 3 of them are independent by choosing one of them as the unit of length), and the concentration of the CD diblock copolymers ϕ_2 (or equivalently, ϕ_1 for the AB diblock copolymers). In what follows, we explore a much restricted phase space and construct phase diagrams on 2-dimensional planes with all the other parameters fixed at different values that are judiciously chosen to focus on the regions of interest. In addition, for the convenience of discussing conformational asymmetric copolymers, we assume $b_B = b_D$ and use the conformational asymmetry parameters $\epsilon_1 = b_A/b_B$ and $\epsilon_2 = b_C/b_D$ to re-parametrize b_A and b_C throughout the study.

3 | RESULTS AND DISCUSSION

3.1 | Regulating miscibility via B–D attraction

The self-assembling behaviors of the binary A_1B_1/A_2B_2 and AB/B'C diblock copolymer blends provide useful insights into the phase behavior of the AB/CD binary mixtures. Both theoretical^{28,29,54} and experimental^{30,31} studies have shown that several Frank–Kasper phases can be stabilized by mixing two AB diblock copolymers together with different block compositions and/or molecular weights. For the binary A_1B_1/A_2B_2 blends, mechanisms related to filler and co-surfactant behaviors due to intra- and inter-domain segregations have been revealed to act synergistically to modulate the sizes and shapes of the soft spherical domains or mesoatoms by forming core-shell structures, which is responsible for the stabilization of the FK phases. Unlike the A_1B_1/A_2B_2 blends, the AB/B'C blends with strong repulsive interactions between the A and C blocks are enthalpically driven to form separated A-rich and C-rich spheres and pack in ways that resemble metallic alloys.^{36,37} For these binary crystalline phases, the core-shell structures no longer exist and inter-domain segregation dominates. Due to the overall strong repulsion between AB and B'C diblocks, this system is prone to macrophase separation and single binary crystalline phases would only appear in a very narrow range over the blend composition.^{36,37}

In the current model system of binary AB/CD diblock copolymer blends, the A and C blocks are the minority blocks that form either mixed AC spherical domains (A + C) or separate A-rich and C-rich spherical domains (A/C). The interaction between the A and C blocks quantified by $\chi_{AC}N$ determines whether mixed (A + C) or separated (A/C) spherical domains are

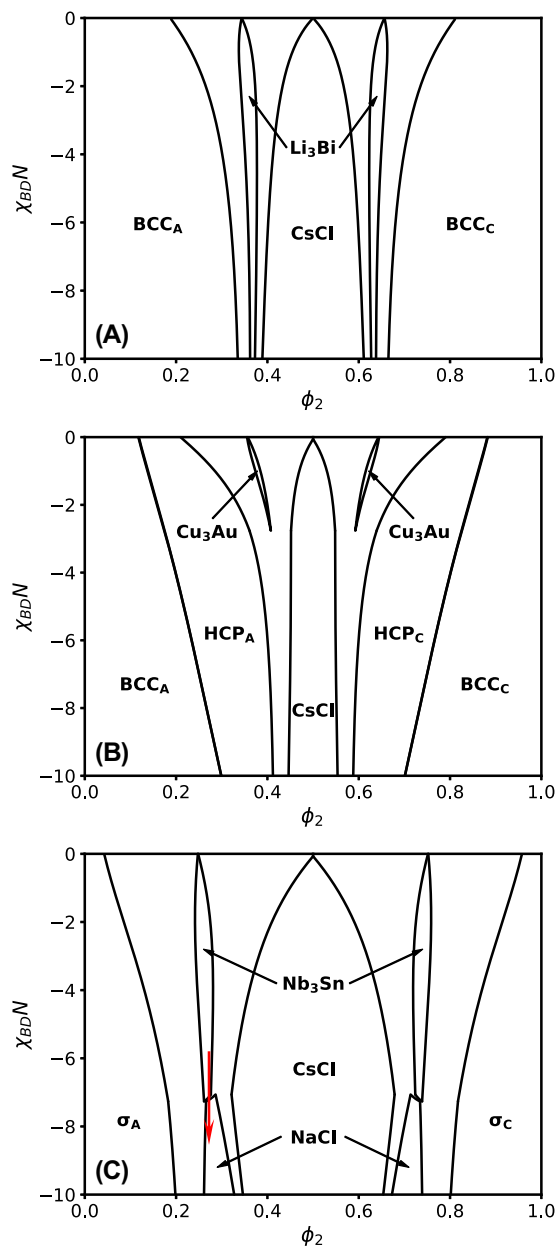


FIGURE 1 Phase diagrams in the $\phi_2 - \chi_{BD}N$ plane for (A) $f = 0.19$, $\epsilon = 1$, (B) $f = 0.19$, $\epsilon = 2$, (C) $f = 0.24$, $\epsilon = 2$, where $\chi_{AC}N$ and χN are fixed at 30 and γ is fixed at 1. Unlabeled regions are the two-phase coexistence regions between two neighboring single phases. The red arrow highlights order–order transition induced by increasing the strength of BD attraction. For phases with stoichiometry $\neq 1:1$, the ones on the left of the CsCl phase have more A spheres than those on the right and vice versa.

thermodynamically preferred. If A and C blocks are highly repulsive, i.e. with a large positive $\chi_{AC}N$, separated A and C spheres are preferred and thus binary crystalline phases could form. Moreover, to suppress macrophase

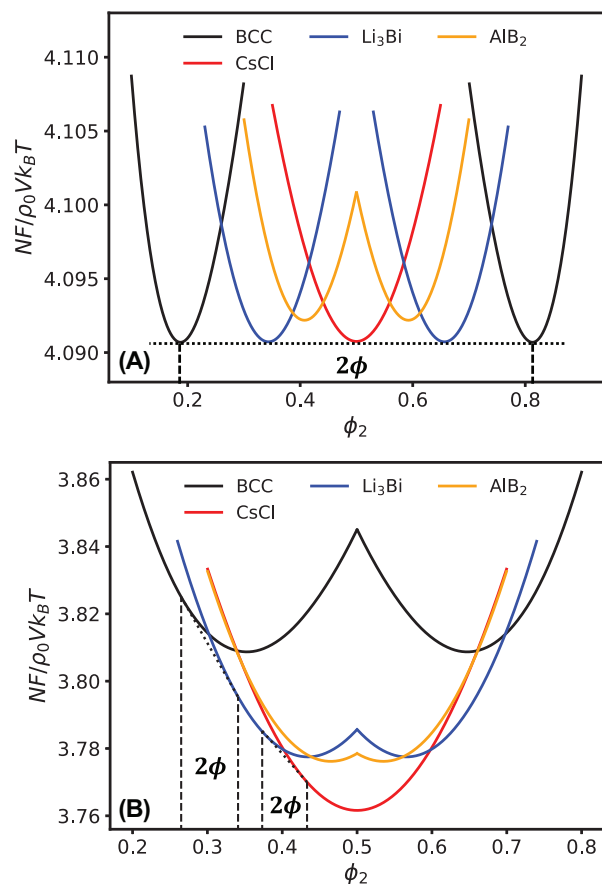


FIGURE 2 The free energy densities of several representative phases as a function of ϕ_2 along the phase path (A) $\chi_{BD}N = 0$ and (B) $\chi_{BD}N = -2$ in Figure 1A. The dotted lines are the double tangent of the free energies of two phases and the vertical dashed lines mark the boundaries of coexistence regions. Note that the difference between the minima of the black, blue and red curves in (A) is too small to be clearly visible at the scale of the plot.

separation and promote the formation of single ordered phases, attractive interactions are introduced between the majority B and D blocks by using a negative $\chi_{BD}N$.⁵⁵ It is expected that the simultaneous presence of a strong A–C repulsion and B–D attraction could result in larger regions of binary crystalline phases. To verify this idea, as well as to examine the effect of the strength of the attraction on the equilibrium morphology, we construct phase diagrams in the $\phi_2 - \chi_{BD}N$ plane. For simplicity, we set $\chi N = \chi_{AB}N = \chi_{CD}N = \chi_{AD}N = \chi_{BC}N$ and fix $\chi_{AC}N = 30$, $\gamma = 1$, $f_1 = f_2 = f$ and $\epsilon_1 = \epsilon_2 = \epsilon$. This choice of parameters leads to a symmetric system. The phase diagrams with different f and ϵ are given in Figure 1.

All phase diagrams shown in Figure 1 are presented for $\chi_{BD}N \leq 0$ and the strength of the attraction starts from zero and becomes greater as one moves downwards along

the y-axes (from $\chi_{BD}N = 0$ to -10). The horizontal lines at $\chi_{BD}N = 0$ correspond to the AB/B'C system and they exhibit very similar features. Specifically, as seen in Figure 1A, an A-rich spherical phase composed of A-core-C-shell spheres on a BCC lattice, denoted as the BCC_A phase, is stable at $\phi_2 \lesssim 0.2$. On the other side of the diagram in Figure 1A where $\phi_2 \gtrsim 0.8$, a BCC structure similar to the BCC_A but with A and C inverted (BCC_C) is stable. In the region where the concentrations of the AB and CD diblocks are more comparable, that is, $0.2 \lesssim \phi_2 \lesssim 0.8$, a large two-phase coexistence window between the AB-rich and CD-rich core-shell BCC phases is identified. In Figure 1B,C, similar behaviors where a wide two-phase region is sandwiched by two opposite core-shell HCP phases (Figure 1B) and σ phases (Figure 1C) are predicted for $\chi_{BD}N = 0$. In Figure 1B, transitions from the core-shell BCC to core-shell HCP phases are also identified prior to entering the two-phase region when moving from either side ($\phi_2 \sim 0$ or 1) to the middle ($\phi_2 \sim 0.5$) of the diagram. The free energy densities of several representative phases as a function of ϕ_2 along the phase path of $\chi_{BD}N = 0$ in Figure 1A are plotted in Figure 2A. It can be seen that the lowest free energy densities of different binary crystalline phases, except AlB_2 , are all nearly degenerate with the double tangent line between the BCC phases at low and high ϕ_2 . Nonetheless, the stability of the two-phase coexistence wins over those of the binary crystalline phases, giving rise to a dominant two-phase region. These behaviors for $\chi_{BD}N = 0$ are consistent with the results for the AB/B'C binary mixtures by Dorfman and coworkers.^{36,37}

Interesting behaviors are observed as $\chi_{BD}N$ becomes negative in all three phase diagrams shown in Figure 1. As the magnitude of the attractive $\chi_{BD}N$ is increased, the stable regions of the core-shell-structured phases expand towards the center. Several windows of binary crystals also open up in the central region of the phase diagrams. Consequently, the two-phase coexistence windows are suppressed. It is interesting to observe that at $\phi_2 \sim 0.5$, the CsCl is the stable morphology for all three phase diagrams whereas changing ϕ_2 away from 0.5 induces phase transitions to different binary crystalline phases as shown in Figure 1. Free energy plot similar to Figure 2A but along the phase path of $\chi_{BD}N = -2$ in Figure 1A is displayed in Figure 2B, showing clearly the effects induced by the attractive association between the B and D blocks. One obvious observation is that the free energy densities for all phases are lowered in Figure 2B compared to Figure 2A. We could also see that for different phases the free energy densities are lowered to different degrees by comparing their minimum values. Specifically, the benefit to the free energy by changing

$\chi_{BD}N$ from 0 to -2 increases from $BCC_A/BCC_C \rightarrow Li_3Bi \rightarrow AlB_2 \rightarrow CsCl$. In addition, the values of ϕ_2 at which the minima of the free energies of different phases occur shift toward 0.5. Most importantly, these changes of free energy result in the stabilization of two binary crystalline phases, that is, CsCl and Li_3Bi .

The various spherical packing phases can be categorized by the ratio between the numbers of the A and C spheres in a unit cell, that is, their stoichiometry. For the binary crystals considered in the current study, the included A/C sphere number ratios are 3:1(3A1C), 2:1(2A1C), 1:1(1A1C), 1:2(1A2C) and 1:3(1A3C). For convenience, we define the percentage of the C spheres $P_s^C = n_s^C / (n_s^A + n_s^C)$ for a spherical phase, where n_s^A and n_s^C denote the numbers of A and C spheres in its unit cell, respectively. For the A- and C-rich core-shell structures, P_s^C is taken to be 0 and 1, respectively. The existence of a minimum in the free energy of each phase indicates that there exists an optimal proportions of the AB and CD copolymers that is best compatible with the A to C spheres stoichiometry of the crystal structure with a given set of molecular parameters. In the left half of Figure 2A, the free energy densities of the BCC_A , Li_3Bi , AlB_2 and CsCl phases reach their minima roughly at $\phi_2 = 0.187, 0.344, 0.408$ and 0.5 , which have a positive correlation with their P_s^C , that is, 0.0, 0.25, 0.33 and 0.5, respectively. In Figure 2B, despite the overall shifts of the free energy minima towards $\phi_2 = 0.5$ for all the phases, the positive correlation is preserved. This correlation between the concentration of AB/CD copolymers and the stoichiometry of the different spherical phases could be used to control the relative stability of the phases with different P_s^C .

3.2 | Selecting crystals via block composition (f) and conformational asymmetry (ϵ)

The equilibrium morphology of the neat diblock copolymer melts and binary blends of diblock copolymers (A_1B_1/A_2B_2 and $AB/B'C$) is sensitive to the block composition f and conformational asymmetry ϵ .^{12,37,54} Particularly, recent studies on binary $AB/B'C$ blends^{36,37} explored the stability of the Laves binary crystals, or alloys, with different combinations of chain length asymmetry ($N_{B'C}/N_{AB}$) and conformational asymmetries (ϵ_{AB} and $\epsilon_{B'C}$). The stability of the Laves binary crystals was promoted by choosing the appropriate combinations of the above parameters such that the self-assembled domains have the volume asymmetry preferred by the Laves phases. Case et al. also demonstrated that individually increasing the conformational asymmetry of the

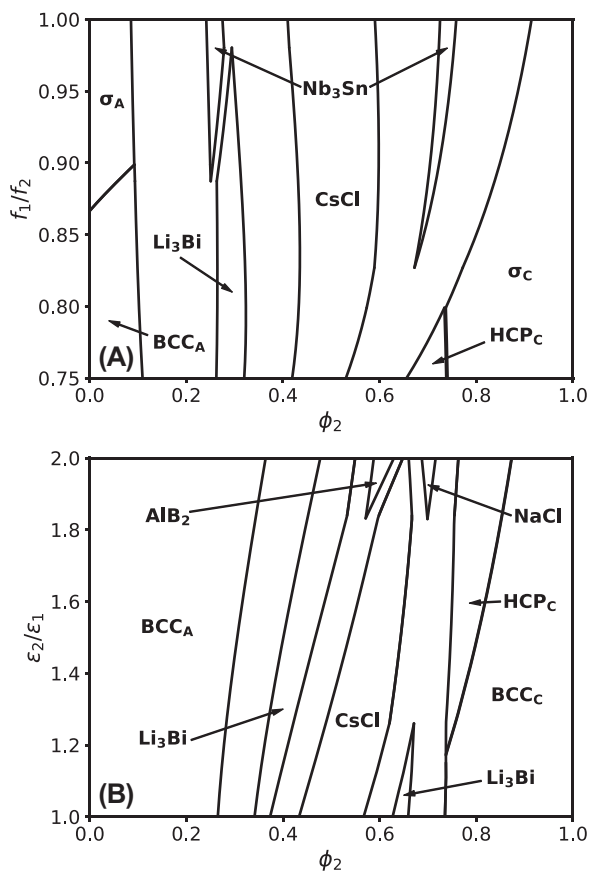


FIGURE 3 (A)Phase diagram in the $\phi_2 - f_1/f_2$ plane with $f_2 = 0.24$, $\epsilon_1 = \epsilon_2 = 2$ and (B) phase diagram in $\phi_2 - \epsilon_2/\epsilon_1$ plane with $\epsilon_1 = 1$, $f_1 = f_2 = 0.19$. $\chi_{AC}N$ and χN are fixed at 30, $\chi_{BD}N$ is fixed at -2 and γ is fixed at 1. Unlabeled regions are the two-phase coexistence regions between two neighboring single phases. For phases with stoichiometry $\neq 1:1$, the ones on the left of the CsCl phase have more A spheres than those on the right and vice versa.

copolymers forming the larger or smaller domains had a stabilizing or destabilizing effect on the Laves alloys, respectively, while increasing them simultaneously resulted in minimal effect because the opposite outcomes offset against each other. These effects due to changing the conformational asymmetries originate from the adjusted polyhedral imprinting and thus the interfacial energy of the spherical domains, which has been studied in details.^{56,57}

Different from the previous studies of the $AB/B'C$ blends,^{36,37} the chain-length ratio γ is kept at $\gamma = 1$ in the current study. We focus on examining the effects of f and ϵ on the equilibrium morphology in the presence of B–D attraction. Comparisons between different phase diagrams in Figure 1 highlight the effects of f and/or ϵ for the case of a symmetric system, i.e. $f_1 = f_2 = f$ and

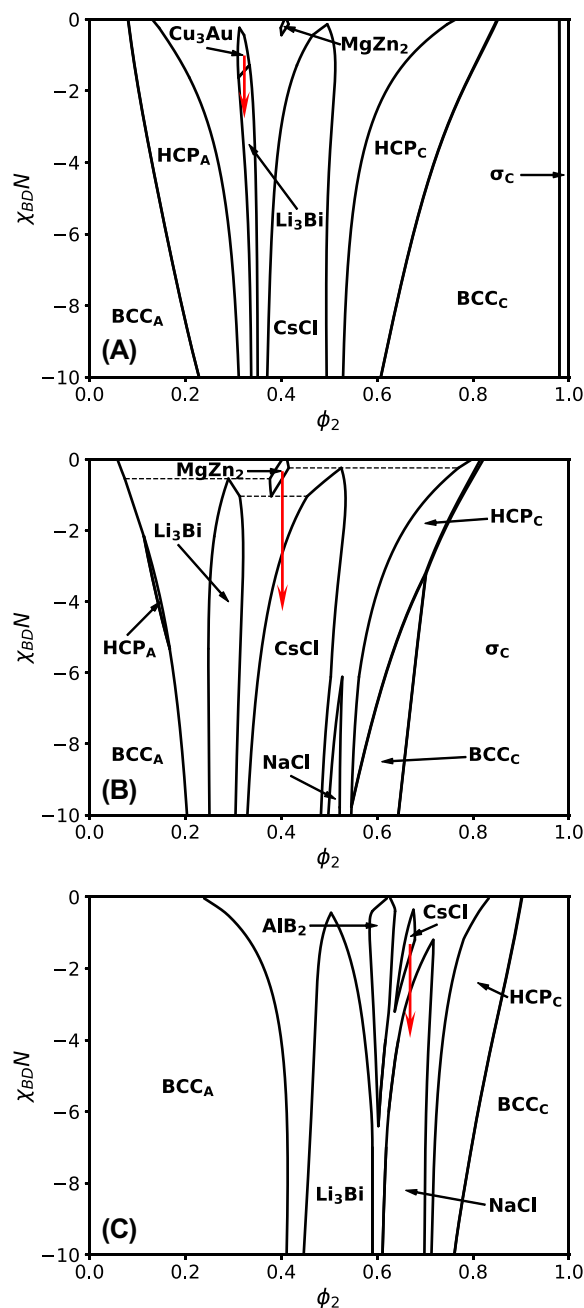


FIGURE 4 Phase diagrams in the $\phi_2 - \chi_{BD}N$ plane with (A) $\epsilon_1 = \epsilon_2 = 2, f_1 = 0.18, f_2 = 0.21$, (B) $\epsilon_1 = \epsilon_2 = 2, f_1 = 0.18, f_2 = 0.24$ and (C) $\epsilon_1 = 1, \epsilon_2 = 2, f_1 = f_2 = 0.19$. $\chi_{AC}N$ and χ_N are fixed at 30 and γ is fixed at 1. Unlabeled regions are the two-phase coexistence regions between two neighboring single phases. The red arrows highlight vertical transitions between binary crystalline phases. For phases with stoichiometry $\neq 1:1$, the ones on the left of the CsCl phase have more A spheres than those on the right and vice versa.

$\epsilon_1 = \epsilon_2 = \epsilon$. Interestingly, increasing ϵ from 1 (Figure 1A) to 2 (Figure 1B) with f fixed at 0.19 stabilizes phases with close-packing lattices instead of a BCC lattice. Specifically, the HCP_A/HCP_C phase emerges between the BCC_A/BCC_C and binary crystalline phases at the expense of the stability windows of the neighboring phases. Accordingly, the Li₃Bi with an underlying BCC lattice is replaced by the Cu₃Au phase which has the same stoichiometry but with a close-packed FCC lattice. Moreover, when f increases to 0.24 with $\epsilon = 2$, the stability windows of binary crystals expand at the expense of those of the core-shell phases and morphologies with complex FK lattices emerge. Notably, the equilibrium core-shell phases adopt a FK σ lattice and the Nb₃Sn with a FK A15 lattice stabilizes with the disappearance of the Cu₃Au. The preference of the FK lattices with sufficiently large ϵ and relatively large f is consistent with the phase behavior of the neat AB diblock copolymers.¹² In addition, when the B–D attraction is strong, the NaCl is stable over the Nb₃Sn. In all the phase diagrams shown in Figure 1, the CsCl crystal is always stable around $\phi_2 \sim 0.5$.

We now turn our attention to the asymmetric case with $f_1 \neq f_2$ and $\epsilon_1 \neq \epsilon_2$. To demonstrate the effects of f and ϵ asymmetries, phase diagrams in the $\phi_2 - f_1/f_2$ and $\phi_2 - \epsilon_2/\epsilon_1$ planes are constructed and shown in Figure 3. Specifically, the f_1/f_2 is varied by adjusting f_1 with fixed $f_2 = 0.24$ and the ϵ_1/ϵ_2 is varied by adjusting ϵ_2 with fixed $\epsilon_1 = 1$. Upon moving from symmetric to asymmetric f or ϵ , the phase diagram also becomes noticeably asymmetric with respect to ϕ_2 . In Figure 3A, as f_2 becomes larger than f_1 (C blocks become longer than A blocks), the 3A1C Nb₃Sn phase (left) undergoes a phase transition to the 3A1C Li₃Bi phase while the window of 1A3C Nb₃Sn (right) gradually narrows and eventually closes at $f_1/f_2 \sim 0.875$. The effect of asymmetric ϵ is different from that of f as shown in Figure 3B. With increasingly larger ϵ_2 than ϵ_1 (stiffer C blocks than A blocks), the window of the 3A1C Li₃Bi phase (left) grows wider while the window of the 1A3C Li₃Bi phase (right) shrinks and disappears at $\epsilon_2/\epsilon_1 \sim 1.25$. More intriguingly, the 2A1C AIB₂ phase and the NaCl phase emerge for extremely asymmetric ϵ , than is, $\epsilon_2/\epsilon_1 > 1.8$.

For the asymmetric case, phase diagrams in the $\phi_2 - \chi_{BD}N$ plane with specific combinations of asymmetric f or ϵ are displayed in Figure 4. In Figure 4A, with $\epsilon_1 = \epsilon_2 = 2$ and $f_1/f_2 = 0.18/0.21 \approx 0.857$, the 2A1C MgZn₂ binary crystal with a Laves C14 lattice is stable in a small window around $\phi_2 \sim 0.4$ and $\chi_{BD}N \gtrsim -0.5$ and its window expands in both the ϕ_2 and $\chi_{BD}N$ dimensions by enhancing the AB/CD compositional asymmetry (decreasing f_1/f_2 to $0.18/0.24 = 0.75$), as shown in

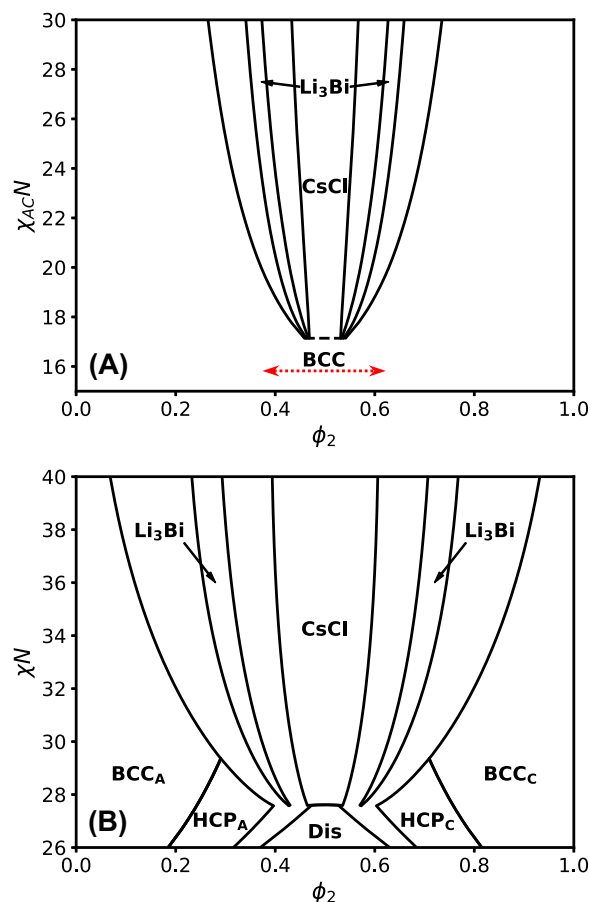


FIGURE 5 The phase diagram on the (A) $\phi_2 - \chi_{AC}N$ plane and (B) $\phi_2 - \chi N$ plane. For (A), χN is fixed at 30 and for (B), $\chi_{AC}N$ is fixed at 30. For the other parameters, $\chi_{BD}N = -2$, $\gamma = 1$, $f_1 = f_2 = 0.19$ and $\epsilon_1 = \epsilon_2 = 1$ are fixed in both cases. Unlabeled regions are the two-phase coexistence regions between two neighboring single phases. For phases with stoichiometry $\neq 1:1$, the ones on the left of the CsCl phase have more A spheres than those on the right and vice versa.

Figure 4B. This observation suggests that in the binary blends of conformationally asymmetric AB/CD (or AB/B'C) copolymers, unequal copolymer compositions could induce sufficient volume difference between different types of soft domains thus stabilizing the Laves alloys, which extends the results from previous studies.^{36,37} Interestingly, both of the MgZn_2 stability windows in Figure 4A,B disappear upon enhancing the B-D attraction. In Figure 4C with $f_1 = f_2 = 0.19$ and $\epsilon_2/\epsilon_1 = 2$, the 2A1C AlB_2 and NaCl crystals have sizeable stable regions, consistent with the prediction in Figure 3B. Note that neither AlB_2 nor MgZn_2 , composed of A and C spheres with distinct volumes, appear in the symmetric phase diagrams shown in Figure 1, indicating that the

compositional or conformational asymmetry between the AB and CD diblocks is critical to their formation in the AB/CD system. Furthermore, the 2A1C AlB_2 or MgZn_2 emerges instead of their 1A2C counterpart because having $f_1 < f_2$ with $\epsilon_2/\epsilon_1 = 2$ or $\epsilon_1 < \epsilon_2$ with $f_1 = f_2$ prefers the formation of larger CD-rich than AB-rich domains, which is in line with the WSC volume difference possessed by the 2A1C version of these two phases and opposes that of their 1A2C version (Table S1).

3.3 | Separated or mixed spheres: The effect of $\chi_{AC}N$ and χN

The repulsive interactions between different blocks play a critical role not only in the formation of A + C mixed spheres or A/C separated spheres, but also the ordering of the system. We examine the effects of the repulsive interactions by focusing on the $\chi_{AC}N$ and χN ($=\chi_{AB}N = \chi_{CD}N = \chi_{AD}N = \chi_{BC}N$) separately. To illustrate how the A-C repulsion influences the phase behavior, we first construct a phase diagram in the $\phi_2 - \chi_{AC}N$ plane with fixed $\chi N = 30$, $\chi_{BD}N = -2$, $\gamma = 1$, $f_1 = f_2 = 0.19$ and $\epsilon_1 = \epsilon_2 = 1$ (Figure 5A). The A-C repulsion is the key to determine the relative stability of the binary crystals and core-shell-structured phases. In Figure 5A, it could be observed that the stable binary crystalline phases are CsCl and Li_3Bi , which are sandwiched by a continuous region of the BCC phase. The binary crystalline regions are compressed by the widening BCC region as $\chi_{AC}N$ is decreased. The CsCl and Li_3Bi phases disappear at $\chi_{AC}N \sim 17.14$, which, marked by the black horizontal dashed line, is an approximate critical value to form binary crystalline structures with the current set of parameters. Clearly, a strong A-C repulsion is required to stabilize the binary crystalline phases. Note that the subscript of BCC has been dropped here since the BCC_A and BCC_C phases are essentially the same phase at low $\chi_{AC}N$. When moving along the red dotted double sided arrow in Figure 5A, no clear phase transition is identified. Instead, we observe that the core-shell spheres continuously evolve to spheres with uniformly mixed A and C blocks and then to the inverse core-shell spheres upon passing $\phi_2 = 0.5$.

To examine how the phase behavior depends on χN , the phase diagram on the $\phi_2 - \chi N$ plane with $\chi_{AC}N = 30$, $\chi_{BD}N = -2$, $\gamma = 1$, $f_1 = f_2 = 0.19$ and $\epsilon_1 = \epsilon_2 = 1$ is constructed (Figure 5B). Several ordered phases appear in Figure 5B, including the CsCl, Li_3Bi , HCP_A , HCP_C , BCC_A and BCC_C phases. With decreasing χN , the overall window of the core-shell-structured phases expands along the ϕ_2 dimension at the expense of the regions of the binary crystalline phases. The disordered (Dis) phase is

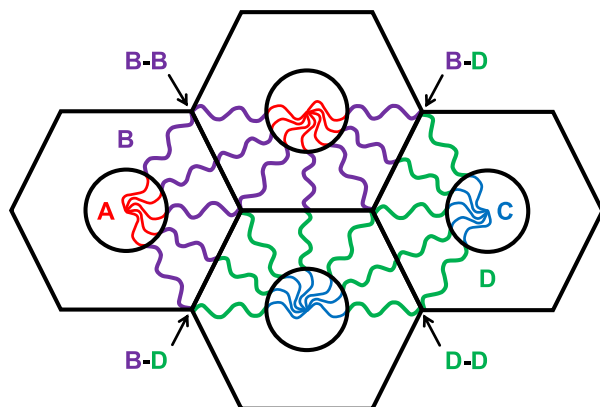


FIGURE 6 Illustration of the chain packing in binary crystalline phases. This example is in 2D where the A and C blocks form the core circles and the B and D blocks construct the coronas.

expected for pure AB or CD copolymers below $\chi N \sim 22$, which is where the order–disorder transition (ODT) takes place in the neat diblock copolymer melts with $f = 0.19$. In contrast, for the AB/CD binary blends, the disordered (Dis) phase occurs at $\chi N \sim 27.6$ in the vicinity of $\phi_2 = 0.5$, which is significantly higher than the value for the neat AB ($\phi_2 = 0$) or CD ($\phi_2 = 1$) diblocks. This resemblance to the eutectic phase behavior of binary alloys is similar to that of the AB/B'C binary mixtures reported by Dorfman and coworkers.^{36,37} However, a noticeably higher eutectic χN , or lower eutectic temperature, is predicted for the current AB/CD than for the previous AB/B'C mixtures. The occurrence of the Dis phase at a much higher χN here could be attributed to two factors: (1) in the current study $\chi_{AC}N = 30$ is used, which is lower than $\chi_{AC}N = 50$ used in the AB/B'C study, and (2) compared to the AB/B'C, a B–D attraction ($\chi_{BD}N = -2$) is introduced in the AB/CD mixtures. Both a lower $\chi_{AC}N$ and a negative $\chi_{BD}N$ favor a larger region of the Dis phase. These two factors could explain the observed occurrence of the Dis phase at a higher χN (a higher eutectic χN) in the AB/CD system studied here than in the AB/B'C system studied previously.

3.4 | Chain packing: Analysis and visualization of the density profiles

The distribution of different blocks of the AB and CD diblock copolymers offers insights into the mechanisms governing their phase behavior. A qualitative method to understand the packing of polymer chains is to assume that the soft domains, including both the spherical core and the polyhedral shell, formed by the diblock copolymers are approximately confined within their

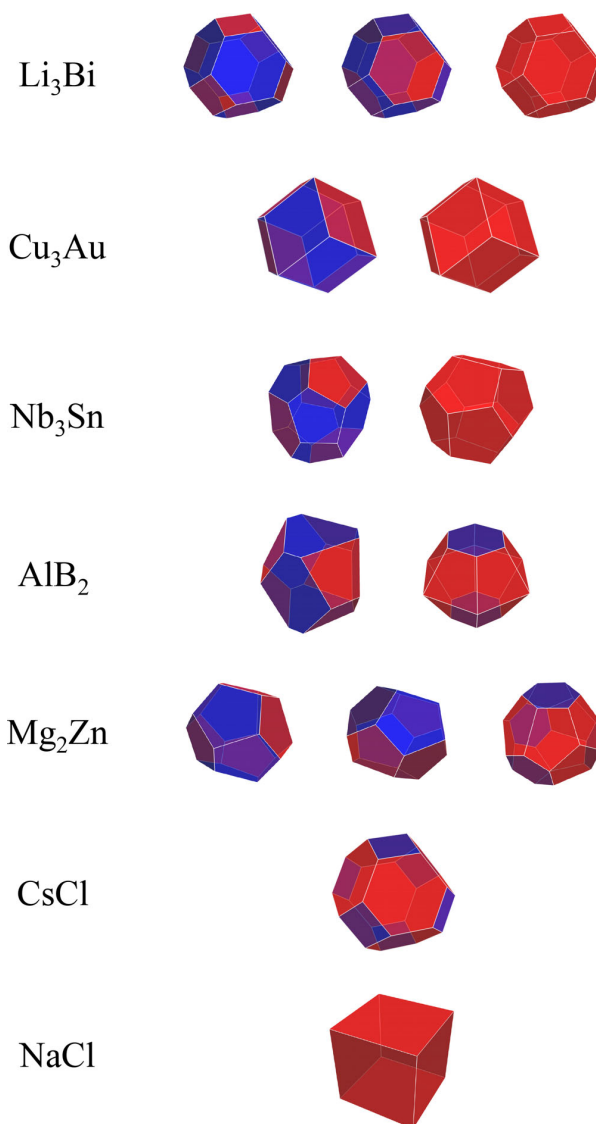


FIGURE 7 The WSCs of binary crystalline phases. The favorable and neutral faces are colored red and blue, respectively. More details of these WSCs are provided in Table S1 in the SI.

Wigner–Seitz cells (WSCs). For binary crystalline phases consisting of A and C spheres, the WSCs are composed of faces bisecting the lines connecting the centers of the A–A, A–C and C–C spheres. Under the assumption that each AB or CD domain is localized within its WSC, the B and D coronas contact roughly on the faces of the WSCs that bisect the lines connecting the A and C spheres (favorable faces). On the other hand, near the faces between A–A and C–C spheres (neutral faces), there are mostly only B–B and D–D contacts. A schematic illustrating the chain arrangement under this assumption is given in Figure 6. The distinct WSCs of all the relevant binary crystalline phases are also displayed in Figure 7,

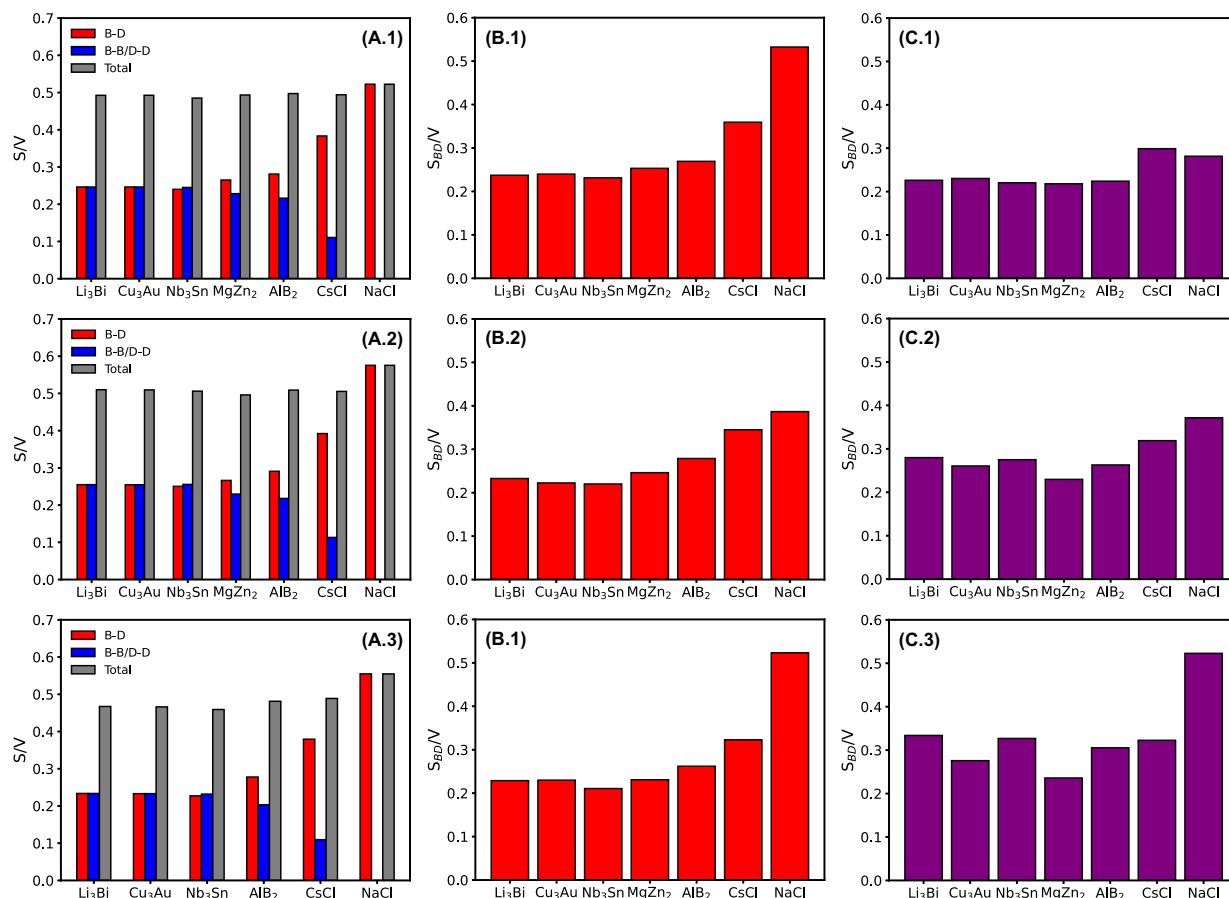


FIGURE 8 (A) The S/V of the favorable (B–D) and neutral (B–B/D–D) faces as well as of both faces (Total) of the WSCs of binary crystalline phases with three different sets of parameters: $\{f_1, f_2, \chi_{BD}N, \phi_2\} =$ (a.1) $\{0.19, 0.19, -1, 0.5\}$, (a.2) $\{0.18, 0.24, -5, 0.27\}$ and (a.3) $\{0.24, 0.24, -10, 0.29\}$. (B) The S/V of $\phi_B(\vec{r}) = \phi_D(\vec{r})$ isosurface (S_{BD}/V) of binary crystalline phases at their optimal ϕ_2 with $\{f_1, f_2\} =$ (b.1) $\{0.19, 0.19\}$, (b.2) $\{0.18, 0.24\}$ and (b.3) $\{0.24, 0.24\}$. (C) The S_{BD}/V for binary crystalline phases at $\phi_2 =$ (c.1) 0.36, (c.2) 0.44 and (c.3) 0.50 with $\{f_1, f_2\} = \{0.24, 0.24\}$. For all graphs, $\chi_{AC}N = \chi N = 30$, $\gamma = 1$ and $\epsilon_1 = \epsilon_2 = 2$ are kept fixed. In addition, $\chi_{BD}N = -2$ is used for (B) and (C). The data for the MgZn₂ phase is missing in (a.3) because it did not converge with that set of parameters.

where the favorable faces and neutral faces are colored red and blue, respectively. It is noted that B–D contacts do not occur on infinitely sharp interfaces because all the interfaces have a finite width. Nonetheless, the area of favorable faces per unit volume should still be a qualitative measure of the favorable B–D contacts for the various binary crystalline phases. In Figure 8A, we present the area per unit volume (S/V) of the favorable (B–D) and neutral faces (B–B/D–D), as well as the total of both faces (Total), of the WSCs of the relevant binary crystals for three different choices of the parameter set $\{f_1, f_2, \chi_{BD}N, \phi_2\}$ with fixed $\chi_{AC}N = 30$, $\gamma = 1$ and $\epsilon_1 = \epsilon_2 = 2$. These choices are made to compare the results from different combinations of f_1 , f_2 , $\chi_{BD}N$ and ϕ_2 . The favorable S/V is in an ascending order as the stoichiometry of the phase goes from 3:1 \rightarrow 2:1 \rightarrow 1:1 for all three sets of parameters, while the neutral S/V has

the opposite trend. Consequently, the total S/V is similar for all the phases. These trends are intuitive because the more comparable the numbers of A and C spheres are, the more neighboring A–C spheres (more B–D contacts) and less neighboring A–A and C–C spheres (less B–B and D–D contacts) there are. Moreover, the distributions of the three quantities across all the phases in all three graphs in Figure 8A are very similar, indicating that these observed trends are nearly independent of $\{f_1, f_2, \chi_{BD}N, \phi_2\}$.

A more accurate picture is that the soft domains are localized mostly within their WSCs only when the sizes of the domains are compatible with the corresponding WSCs. Intuitively, this compatibility is achieved at an optimal combination of the molecular parameters and ϕ_2 , which would be different for different phases. It is anticipated that when such compatibility between the properties of the polymer chains and the WSCs of

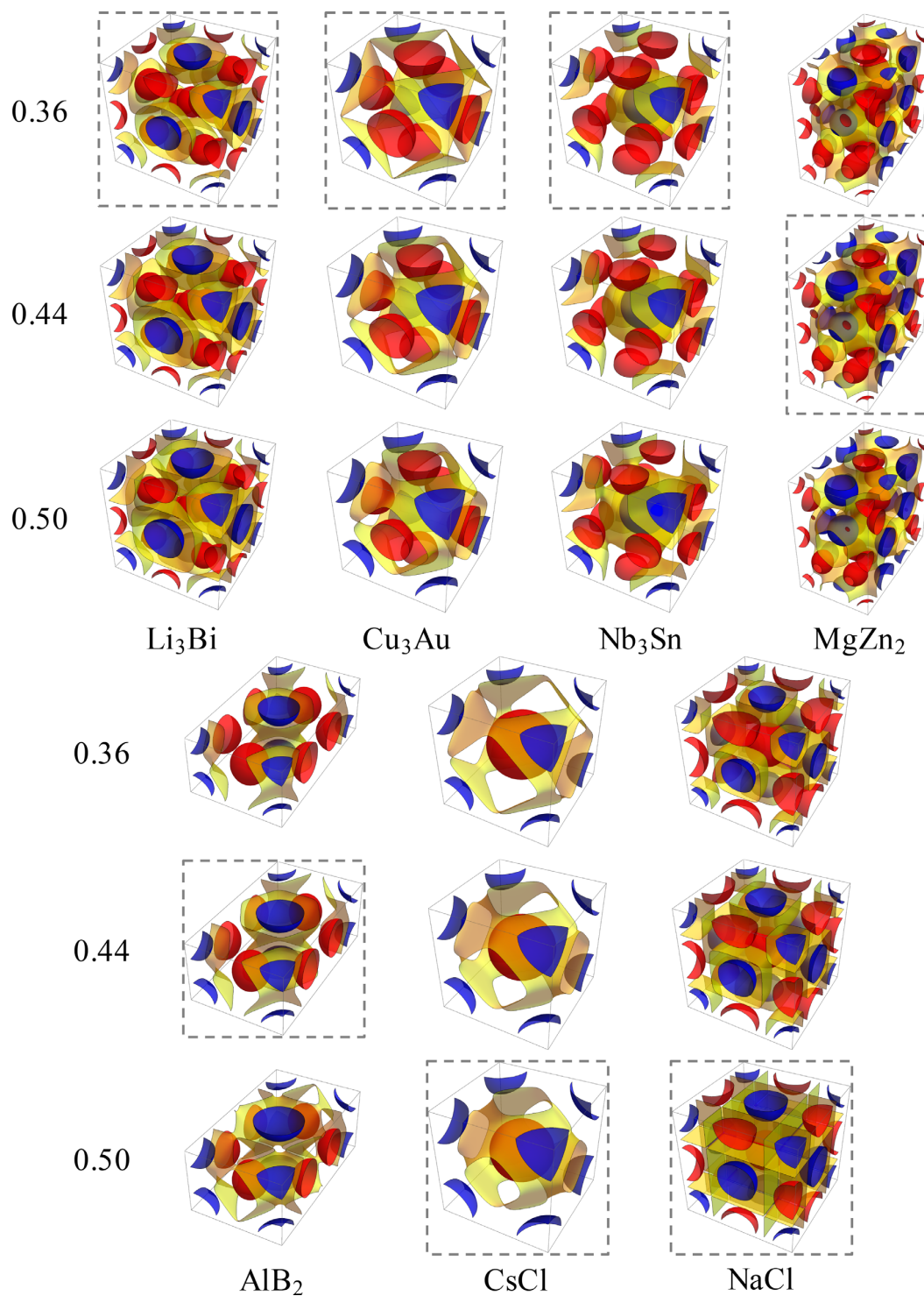


FIGURE 9 The isosurfaces of $\phi_A(\vec{r}) = 0.5$ (red), $\phi_C(\vec{r}) = 0.5$ (blue) and $\phi_B(\vec{r}) = \phi_D(\vec{r})$ (yellow) for the binary crystalline phases at $\phi_2 = 0.36, 0.44$ and 0.50 .

the self-assembled phase is satisfied, the copolymers would have an ideal chain packing and thus be less frustrated. For general alloy-forming binary AB/CD mixtures,

a rigorous optimization of all parameters simultaneously to find the solution that achieves the globally optimal chain packing of a particular phase is possible but would require

efficient optimization algorithms and a well-designed objective function.^{58,59} One simpler approach to determine a set of conditionally optimal, or nearly optimal parameters for a target phase is given by a two-step procedure: (1) start with a specific parameter set $p_m = \{f_1, f_2, b_B (= b_A/\epsilon_1), b_C, b_D (= b_C/\epsilon_2), N_1, N_2 (= \gamma N_1)\}$ (assuming that $b_A = 1$ is the unit of length) that is chosen to be compatible with the WSC properties of that phase, and (2) find the optimal ϕ_2 minimizing the free energy density (see, e.g., Figure 2). The resultant solution corresponds to the conditionally optimal chain packing for the target phase subject to p_m . Apparently, choosing p_m guided by the WSC properties is an approximation.

One approximate measure of the B–D interfacial area is given by the area of the $\phi_B(\vec{r}) = \phi_D(\vec{r})$ isosurface, which could be computed from the converged SCFT solution of a binary crystalline phase. The area per unit volume of the $\phi_B(\vec{r}) = \phi_D(\vec{r})$ isosurface, S_{BD}/V , is computed and shown in Figure 8B, for each binary crystalline phase at its optimal ϕ_2 with three sets of $\{f_1, f_2\}$, $\chi_{BD} = -2$ and all other parameters the same as those used for Figure 8A. We emphasize that these parameters are chosen for the purpose of illustrating the behavior under general conditions without targeting one particular phase, therefore, the p_m used here is not judiciously designed to favor the optimal packing of any morphology. Clearly, the distribution of S_{BD}/V across the 3A1C, 2A1C and 1A1C phases in all the three cases are quite consistent with the universal distribution of S/V computed for the favorable (B–D) faces of the WSCs (Figure 8A), indicating that the chain packing in various morphologies at their optimal ϕ_2 does roughly conform to the WSC construction (Figure 6). However, the optimal ϕ_2 for each phase is different. Thus, the distribution of S_{BD}/V across all phases evaluated at a fixed ϕ_2 is expected to deviate significantly from the ones in Figure 8A. Presented in Figure 8C are the results of S_{BD}/V for all the phases at $\phi_2 = 0.36, 0.44$ and 0.50 with $\{f_1, f_2\} = \{0.24, 0.24\}$ and all other parameters the same as those used in Figure 8B. These three values for ϕ_2 are chosen to be the average optimal values for 3A1C, 2A1C and 1A1C structures, respectively, determined by minimizing their free energy densities with respect to ϕ_2 . Indeed, the distribution of S_{BD}/V in Figure 6C evidently deviate from the distribution of S/V (B–D) in Figure 6A and that of S_{BD}/V evaluated at the optimal ϕ_2 of each phase in Figure 6B.

As a more direct visualization of chain packing, we plot the isosurfaces of $\phi_A(\vec{r}) = 0.5$ (red), $\phi_C(\vec{r}) = 0.5$ (blue) and $\phi_B(\vec{r}) = \phi_D(\vec{r})$ (yellow) for the binary crystalline morphologies in Figure 9 with the same

parameters as those used in Figure 8C. The $\phi_A(\vec{r}) = 0.5$ and $\phi_C(\vec{r}) = 0.5$ isosurfaces are reasonable representations of the cores of the A and C spheres. The $\phi_B(\vec{r}) = \phi_D(\vec{r})$ isosurfaces could be viewed as the surfaces separating the AB and CD copolymers. As expected, the yellow surfaces move towards the red A cores as the concentration of CD copolymers (ϕ_2) is increased. Because the three values for ϕ_2 approximately minimize the free energy density of 3A1C ($\phi_2 = 0.36$), 2A1C (0.44) and 1A1C (0.50) structures, the plots in the dashed gray boxes depict the chain packing closest to the ideal ones for these morphologies with the chosen molecular parameters. Indeed, the yellow isosurfaces in these plots also more closely match the favorable faces of the WSCs of the corresponding phases (Figure 7). Likewise, we anticipate that the actual chain packing and thus S_{BD}/V would also obviously deviate from the optimal ones predicted from the WSC construction for phases whose WSCs are highly incompatible with the choice of p_m .

The WSC construction can help us understand several aspects of the phase behavior examined in the previous sections. Notably, there are appreciable stability windows for the CsCl phase, whose WSCs have the same volume, in almost all phase diagrams (Figures 1, 3, 4 and 5). The ubiquity of the CsCl phase could be attributed to its larger S_{BD}/V compared to the other phases given by the WSC construction (Figure 8A), except the NaCl phase. Specifically, the higher the S_{BD}/V one phase has, the more enthalpic benefit is gained due to the B–D attraction. This explains why the stability windows of the 1:1-stoichiometric crystals generally widen the most rapidly when the B–D association becomes stronger (Figures 1 and 4A,B) and why the reduction in free energy from Figure 2A to Figure 2B for the 3:1-, 2:1- and 1:1-stoichiometric phases is in an ascending order. The NaCl has a higher S_{BD}/V than the CsCl, but its WSCs are much less spherical and thus have higher packing frustration.^{21,57,60} The NaCl phase could compete with the CsCl and become stable when the B–D attraction is sufficiently strong, as seen in Figures 1C, 3B, and 4B,C. Interestingly, the stability windows of NaCl usually occur at $\phi_2 \neq 0.5$ and/or asymmetric f or ϵ , indicating that the free energy of the NaCl is less affected by having asymmetric A and C soft domains than its competing crystalline phases.

The main reason why the AlB₂ crystal has less favorable free energy in Figure 2 and no phases with 1:2 stoichiometry are stable in the symmetric phase diagrams in Figure 1 is presumably because both of the 1:2-stoichiometric phases (AlB₂ and MgZn₂) have unequally sized WSCs (Table S1), which is less compatible with the

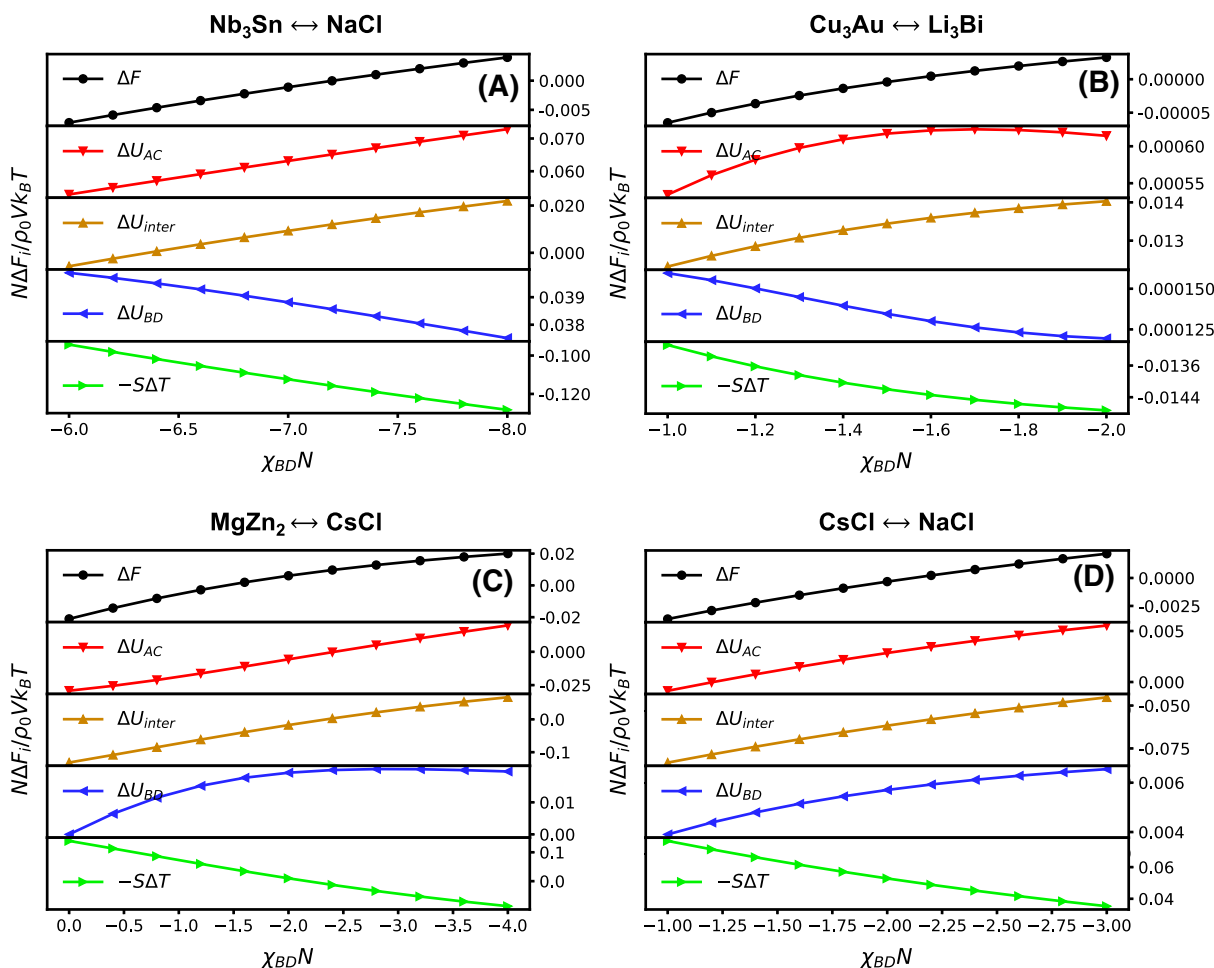


FIGURE 10 Plots of the difference of the total free energy along with that of the four contributions between the stable phase at the top and the one at the bottom for the highlighted transitions in (A) Figure 1C, (B) Figure 4A, (C) Figure 4B and (D) Figure 4C.

tendency for the symmetric AB and CD copolymers to form equally-sized soft domains. For the same reason, the AlB_2 and MgZn_2 phases become stable in the asymmetric phase diagrams in Figure 4. As the B–D attraction becomes stronger, both the AlB_2 and MgZn_2 windows close quickly between those of the 1:3- or 1:1-stoichiometric phases, which seems to be contradictory to the observation that they have overall intermediate S_{BD}/V according to the WSC construction (Figure 8A). One possibility is that the chosen molecular parameters are not fully compatible with their WSC volume asymmetries and thus the chain packing is still far away from being the global optimum even at ϕ_2 minimizing their free energies. This makes the WSC construction less accurate in depicting the chain packing for the AlB_2 and MgZn_2 with these choices of parameters. It would be interesting to see if these phases could stabilize in larger

regions with more carefully optimized molecular parameters, which we leave as a future study. Moreover, in Figure 3 with $\epsilon_1 = \epsilon_2 = 2$ a transition from the 3A1C Nb_3Sn to the 3A1C Li_3Bi is identified as decreasing f_1/f_2 (the AB diblocks becoming shorter than the CD diblocks). This could be explained by the fact that having shorter AB diblocks opposes the WSC volume asymmetry of the 3A1C Nb_3Sn phase, which has larger WSCs enclosing the A spheres than those enclosing the C spheres (Table S1), thus making the 3A1C Nb_3Sn more disfavored than the 3A1C Li_3Bi .

We would like to point out that, in contrast to the $\text{A}_1\text{B}_1/\text{A}_1\text{B}_2$ blends, the various factors contributing to the stability of different morphologies for the binary AB/CD blends are strongly entangled. One informative way to group the free energy in Equation 9 associated with different contributions is to divide the total free energy

density (Equation 7) into four parts: the interaction contribution between A and C spheres U_{AC} , the interfacial contribution $U_{inter} = U_{AB} + U_{CD} + U_{AD} + U_{CB}$, the attractive contribution U_{BD} and the entropic contribution $-TS = -T(S_1 + S_2)$, where the common factor $N/\rho_0 V k_B T$ appearing in all the terms has been omitted for simplicity. In Figures 1 and 4, several vertical paths of phase transitions are highlighted by red arrows. These transitions are all triggered by changing $\chi_{BD}N$. The difference of the total free energy along with that of the four contributions between the stable phases at the head and the tail of the arrows highlighting the four transitions in Figures 1 and 4 are shown in Figure 10. We can see that even though the phase transitions highlighted by the arrows are all induced by lowering $\chi_{BD}N$, the behaviors of the U_{BD} could be different. For Figure 10A,B, the trend of the U_{BD} contribution is even opposite to that of the total free energy. Therefore, the various energy contributions respond very differently to the change of one parameter and the stability of different morphologies is determined by the combined effect of all contributions.

4 | CONCLUSION

In summary, we have explored the phase behavior of binary blends of sphere-forming AB/CD diblock copolymers using polymeric self-consistent field theory. By constructing phase diagrams in different subspaces of the system, it is shown that phases composed of A + C mixed spheres or binary A/C separated spheres can form, and their stability depends sensitively on system parameters. Specifically, we have demonstrated that the formation of binary crystalline phases is promoted by having both large positive $\chi_{AC}N$ and negative $\chi_{BD}N$. The former drives the separation of the A and C blocks while the latter suppresses macrophase separation. We have also shown that phases with distinct stoichiometry are preferred at different blend compositions, which allows us to control the equilibrium morphology by adjusting the polymer concentration. Although only phases with 1:1 and 1:3 stoichiometry have been found stable for the systems with symmetric f and ϵ , it is possible for packing with 1:2 stoichiometry to appear in the asymmetric systems where $f_1 \neq f_2$ or $\epsilon_1 \neq \epsilon_2$. Moreover, the phase diagram of the AB/CD binary blends in the $\phi_2 - \chi N$ plane exhibits eutectic behavior similar to that observed for the AB/B'C blends.

By analyzing the density profiles of different morphologies, we have obtained valuable insights into the optimal chain packing, which is responsible for the selection of the stable binary crystalline phase. We have demonstrated that the WSC construction provides a useful estimate for the optimal chain packing. The favorable B–D

contacting area per unit volume (S_{BD}/V) obtained from the WSC construction yields a descending order when going from 1:1 \rightarrow 2:1 \rightarrow 3:1 stoichiometry. This distribution of S_{BD}/V across various binary crystalline phases is consistent with that computed from the $\phi_B(\vec{r}) = \phi_D(\vec{r})$ isosurfaces for these phases at their optimal ϕ_2 . The WSC construction can help to explain some of the observed phase behavior. Particularly, the abundance of the stable windows of the CsCl phase is largely due to both of the relatively less frustration possessed by its WSCs and the high S_{BD}/V . Moreover, enhanced stability has been evidenced for phases with WSC volume ratio more compatible with that of the soft domains formed by the AB and CD copolymers. We have also observed the disappearance of AlB₂ and MgZn₂ phases as the B–D attraction becomes stronger. An interesting future research direction is to explore the possibility of expanding the stable region of these phases with molecular parameters purposely designed to favor their formation. The parameter design could be carried out either by using information of their crystallographic characteristics or more rigorously by combining SCFT with advanced optimization algorithms such as the particle swarm optimization (PSO).^{58,59}

Compared to the theoretical studies of AB/B'C blends by Dorfman and coworkers,^{36,37} the current study explores the phase behavior of the more general AB/CD system with a focus on the formation of various binary crystalline phases enabled by the B–D attraction. It should be mentioned that the parameter space of the AB/CD system is extremely large. Although only a small fraction of the phase space is explored in the current study, the strategy of using secondary interactions such as hydrogen bonding to regulate the self-assembled structures is general. In the future, it would be interesting to study what morphologies are stable if the parent copolymers individually form cylinders, networks and lamellae, and how the non-spherical equilibrium structure is regulated by the various system parameters. Given the architectural simplicity of the diblock copolymers, it would be desirable to explore the phase behavior experimentally with precisely synthesized diblock copolymer pairs. In experiments, the attraction between two blocks could be realized via the association of different functional groups such as hydrogen bonding and electrostatic interaction,^{61–63} and the strength of the attractive interaction could be adjusted by, for example, the density of hydrogen bonding units⁶⁴ and the steric effects.^{65,66} The principles obtained from our theoretical study could be used to guide experiments and also serves as a starting point for future studies on the phase behaviors of polymeric blends with designed secondary interactions.

ACKNOWLEDGMENTS

This research was supported by the Natural Sciences and Engineering Research Council (NSERC) of Canada and was enabled in part by support provided by the facilities of SHARCNET (<https://www.sharcnet.ca>). This manuscript was completed while ACS is visiting the Kavli Institute for Theoretical Physics at UC Santa Barbara. This research was supported in part by the National Science Foundation under Grant No. PHY-1748958.

ORCID

An-Chang Shi  <https://orcid.org/0000-0003-1379-7162>

REFERENCES

- [1] C. M. Bates, F. S. Bates, *Macromolecules* **2017**, *50*(1), 3.
- [2] A.-C. Shi, *J. Phys.: Condens. Matter* **2021**, *33*(25), 253001.
- [3] I. W. Hamley, *The Physics of Block Copolymers*, Vol. 19, Oxford University Press, Oxford **1998**.
- [4] F. S. Bates, G. H. Fredrickson, *Phys. Today* **1999**, *52*(2), 32.
- [5] M. Park, C. Harrison, P. M. Chaikin, R. A. Register, D. H. Adamson, *Science* **1997**, *276*(5317), 1401.
- [6] W. A. Lopes, H. M. Jaeger, *Nature* **2001**, *414*(6865), 735.
- [7] C. M. Bates, M. J. Maher, D. W. Janes, C. J. Ellison, C. G. Willson, *Macromolecules* **2014**, *47*(1), 2.
- [8] G. Y. Kim, S. Kim, J. Choi, M. Kim, H. Lim, T. W. Nam, W. Choi, E. N. Cho, H. J. Han, C. H. Lee, et al., *Nano Lett.* **2019**, *19*(10), 6827.
- [9] R. Paxton Thedford, Y. Fei, W. R. T. Tait, K. Shastri, F. Monticone, U. Wiesner, *Adv. Mater.* **2023**, *35*(5), 2203908.
- [10] M. W. Matsen, *J. Phys.: Condens. Matter* **2001**, *14*(2), R21.
- [11] S. Lee, M. J. Bluemle, F. S. Bates, *Science* **2010**, *330*(6002), 349.
- [12] N. Xie, W. Li, F. Qiu, A.-C. Shi, *ACS Macro Lett.* **2014**, *3*(9), 906.
- [13] K. D. Dorfman, *Macromolecules* **2021**, *54*(22), 10251.
- [14] F. S. Bates, M. A. Hillmyer, T. P. Lodge, C. M. Bates, K. T. Delaney, G. H. Fredrickson, *Science* **2012**, *336*(6080), 20120306.
- [15] W. Jiang, Y. Qiang, W. Li, F. Qiu, A.-C. Shi, *Macromolecules* **2018**, *51*(4), 1529.
- [16] M. Liu, W. Li, F. Qiu, A.-C. Shi, *Macromolecules* **2012**, *45*(23), 9522.
- [17] G. Zhang, F. Qiu, H. Zhang, Y. Yang, A.-C. Shi, *Macromolecules* **2010**, *43*(6), 2981.
- [18] X. Weiquan, K. Jiang, P. Zhang, A.-C. Shi, *J. Phys. Chem. B* **2013**, *117*(17), 130417155037004.
- [19] Y. Qiang, W. Li, A.-C. Shi, *ACS Macro Lett.* **2020**, *9*(5), 668.
- [20] Q. Xie, Y. Qiang, W. Li, *ACS Macro Lett.* **2020**, *9*(2), 278.
- [21] Q. Xie, Y. Qiang, L. Chen, Y. Xia, W. Li, *ACS Macro Lett.* **2020**, *9*(7), 980.
- [22] Q. Xie, Y. Qiang, G. Zhang, W. Li, *Macromolecules* **2020**, *53*(17), 7380.
- [23] Q. Dong, W. Li, *Macromolecules* **2020**, *54*(1), 203.
- [24] C. Li, Q. Dong, W. Li, *Macromolecules* **2020**, *53*(24), 10907.
- [25] A. B. Chang, F. S. Bates, *ACS Nano* **2020**, *14*(9), 11463.
- [26] S. M. Barbon, J.-A. Song, D. Chen, C. Zhang, J. Lequieu, K. T. Delaney, A. Anastasaki, M. Rolland, G. H. Fredrickson, M. W. Bates, et al., *ACS Macro Lett.* **2020**, *9*(12), 1745.
- [27] M. W. Bates, S. M. Barbon, A. E. Levi, R. M. Lewis III, H. K. Beech, K. M. Vonk, C. Zhang, G. H. Fredrickson, C. J. Hawker, C. M. Bates, *ACS Macro Lett.* **2020**, *9*(3), 396.
- [28] M. Liu, Y. Qiang, W. Li, F. Qiu, A.-C. Shi, *ACS Macro Lett.* **2016**, *5*(10), 1167.
- [29] K. Kim, A. Arora, R. M. Lewis, M. Liu, W. Li, A.-C. Shi, K. D. Dorfman, F. S. Bates, *Proc. Natl. Acad. Sci.* **2018**, *115*(5), 847.
- [30] A. P. Lindsay, R. M. Lewis III, B. Lee, A. J. Peterson, T. P. Lodge, F. S. Bates, *ACS Macro Lett.* **2020**, *9*(2), 197.
- [31] A. P. Lindsay, G. K. Cheong, A. J. Peterson, S. Weigand, K. D. Dorfman, T. P. Lodge, F. S. Bates, *Macromolecules* **2021**, *54*(15), 7088.
- [32] A. J. Mueller, A. P. Lindsay, A. Jayaraman, T. P. Lodge, M. K. Mahanthappa, F. S. Bates, *ACS Macro Lett.* **2020**, *9*(4), 576.
- [33] G. K. Cheong, F. S. Bates, K. D. Dorfman, *Proc. Natl. Acad. Sci.* **2020**, *117*(29), 16764.
- [34] J. Xie, A.-C. Shi, *Giant* **2021**, *5*, 100043.
- [35] J. Xie, A. C. Shi, *Phase Behaviour of Binary Blends of Diblock Copolymers: Progresses and Opportunities*, Langmuir, **2023**.
- [36] B. R. Magruder, S. J. Park, R. P. Collanton, F. S. Bates, K. D. Dorfman, *Macromolecules* **2022**, *55*(7), 2991.
- [37] L. J. Case, F. S. Bates, K. D. Dorfman, *Soft Matter* **2023**, *19*(1), 90.
- [38] Y. Matsushita, A. Takano, M. Vayer, C. Sinturel, *Adv. Mater. Interfaces* **2020**, *7*(5), 1902007.
- [39] T. Asari, S. Matsuo, A. Takano, Y. Matsushita, *Macromolecules* **2005**, *38*(21), 8811.
- [40] W.-C. Chen, S.-W. Kuo, F.-C. Chang, *Polymer* **2010**, *51*(18), 4176.
- [41] T.-C. Tseng, S.-W. Kuo, *Macromolecules* **2018**, *51*(16), 6451.
- [42] T.-C. Tseng, S.-W. Kuo, *Molecules* **2018**, *23*(9), 2242.
- [43] C.-T. Tsou, S.-W. Kuo, *Macromolecules* **2019**, *52*(21), 8374.
- [44] X. Zhang, J. Lin, L. Wang, L. Zhang, J. Lin, L. Gao, *Polymer* **2015**, *78*, 69.
- [45] I. Ahmadian, A. J. Peters, *Soft Matter* **2020**, *16*(12), 3069.
- [46] T. Asari, S. Arai, A. Takano, Y. Matsushita, *Macromolecules* **2006**, *39*(6), 2232.
- [47] H. Miyase, Y. Asai, A. Takano, Y. Matsushita, *Macromolecules* **2017**, *50*(3), 979.
- [48] G. Fredrickson, *The Equilibrium Theory of Inhomogeneous Polymers*, 134, Clarendon Oxford University Press, Oxford **2006**.
- [49] A.-C. Shi, in *Variational Methods in Molecular Modeling* (Ed: W. Jianzhong), Springer, Singapore **2016**.
- [50] K. Ø. Rasmussen, G. Kalosakas, *J. Polym. Sci., Part B: Polym. Phys.* **2002**, *40*(16), 1777.
- [51] G. Tzeremes, K. Ø. Rasmussen, T. Lookman, A. Saxena, *Phys. Rev. E* **2002**, *65*(4), 41806.
- [52] R. B. Thompson, K. Ø. Rasmussen, T. Lookman, *J. Chem. Phys.* **2004**, *120*(1), 31.
- [53] A. Arora, D. C. Morse, F. S. Bates, K. D. Dorfman, *J. Chem. Phys.* **2017**, *146*(24), 244902.
- [54] J. Xie, Y. Li, A. C. Shi, *Macromol. Theory Simul.* **2021**, *30*(6), 2100053.
- [55] A. Dehghan, A.-C. Shi, *Macromolecules* **2013**, *46*(14), 5796.
- [56] S. Lee, C. Leighton, F. S. Bates, *Proc. Natl. Acad. Sci.* **2014**, *111*(50), 17723.

- [57] A. Reddy, M. B. Buckley, A. Arora, F. S. Bates, K. D. Dorfman, G. M. Grason, *Proc. Natl. Acad. Sci.* **2018**, *115*(41), 10233.
- [58] S. P. Paradiso, K. T. Delaney, G. H. Fredrickson, *ACS Macro Lett.* **2016**, *5*(8), 972.
- [59] M. R. Khadilkar, S. Paradiso, K. T. Delaney, G. H. Fredrickson, *Macromolecules* **2017**, *50*(17), 6702.
- [60] G. M. Grason, R. D. Kamien, *Macromolecules* **2004**, *37*(19), 7371.
- [61] C. B. Thompson, L. S. T. J. Korley, *ACS Macro Lett.* **2020**, *9*(9), 1198.
- [62] A. Harada, K. Kataoka, *Science* **1999**, *283*(5398), 65.
- [63] I. K. Voets, A. de Keizer, M. A. Cohen, J. J. Stuart, H. Schlaad, *Macromolecules* **2007**, *40*(6), 2158.
- [64] C. Tang, S.-m. Hur, B. C. Stahl, K. Sivanandan, M. Dimitriou, E. Pressly, G. H. Fredrickson, E. J. Kramer, C. J. Hawker, *Macromolecules* **2010**, *43*(6), 2880.
- [65] S.-C. Tsai, Y.-C. Lin, E.-L. Lin, Y.-W. Chiang, S.-W. Kuo, *Polym. Chem.* **2016**, *7*(13), 2395.
- [66] W. T. Du, T. L. Ma, S. W. Kuo, *Polymer* **2023**, *268*, 125694.

SUPPORTING INFORMATION

Additional supporting information can be found online in the Supporting Information section at the end of this article.

How to cite this article: J. Xie, C. T. Lai, A.-C. Shi, *J. Polym. Sci.* **2023**, *1*, <https://doi.org/10.1002/pol.20230306>

Chapter 8

Phase Behaviour of Triblock Copolymer and Homopolymer Blends: Effect of Copolymer Topology

Publication: Xie, Jiayu, and An-Chang Shi. “Phase Behaviour of Triblock Copolymer and Homopolymer Blends: Effect of Copolymer Topology.” *Physical Review Materials* (Accepted: December 18, 2023).

Authors: **Jiayu Xie**, An-Chang Shi

Contribution: As the first author, I developed the theoretical model and computational code, generated and analyzed the data, and drafted the initial manuscript. Dr. An-Chang Shi and I collaborated on the manuscript revisions, with Dr. Shi providing guidance throughout the research.

Preface

We have so far discussed the equilibrium phase behaviours of polymeric systems containing only homopolymers and/or diblock copolymers. For an AB diblock copolymer, the architectural simplicity leads to topological equivalency between the A and B blocks. In other words, the polymer chain remains invariant by interchanging the A and B blocks. However, for chains with more complex architectures, this equivalency may break down. One simple example is linear ABA and BAB triblock copolymers, formed by connecting two AB diblock chains through their B or A ends, respectively. The two homologous but topologically distinct triblock chains, i.e., ABA and BAB, exhibit slightly different equilibrium phase behaviours, reflected by the small asymmetry around the $f_A = 0.5$ axis in the $f_A - \chi N$ phase diagram of triblock copolymers [132, 133]. A natural question arises: How does the topological difference of the copolymers impact the equilibrium phase behaviour when they are blended with other polymers?

In this chapter, we address this question by examining a simple system composed of linear symmetric triblock copolymers and homopolymers. Using random-phase approximation and self-consistent field theory, we compare the phase behaviours of three homologous polymeric blends: AB/A, ABA/A, and BAB/A. We begin with the scenario where the copolymers form lamellae and investigate blend miscibility by comparing the spinodals and binodals of these systems. Next, we explore the case where the copolymers form spheres to understand how the topological differences influence the equilibrium spherical packing phase. Our results offer valuable insights into the topological effects in polymeric blends containing block copolymers with more complex architectures.

**Phase behavior of Triblock Copolymer and Homopolymer Blends:
Effect of Copolymer Topology**

Jiayu Xie^{1,*} and An-Chang Shi^{1,†}

¹*Department of Physics & Astronomy,
McMaster University, Hamilton, ON Canada L8S 4M1*

(Dated: December 31, 2023)

Abstract

Two distinct linear triblock copolymers with different block sequences, *i.e.* ABA or BAB, are obtained when two identical AB diblock copolymers are jointed at their B or A ends, respectively, resulting in three homologous, AB diblock, ABA and BAB triblock, copolymers with the same chemical composition but different topologies. We demonstrate that the topological effect on the phase behaviors of the copolymers is amplified when A homopolymers are added to the system. Specifically, the phase behaviors of binary blends composed of ABA or BAB linear triblock copolymers and A homopolymers are studied by using the random-phase approximation (RPA) and self-consistent field theory (SCFT). The RPA analysis predicts that the Lifshitz point for the ABA/A blends behaves like a “second-order transition” but that for the BAB/A blends behaves like a “first-order transition”. The Lifshitz point of the BAB/A mixtures is found to occur at a much lower homopolymer concentration than that of the ABA/A mixtures, indicating a poorer miscibility of the A homopolymers into the BAB than ABA triblocks, which is also confirmed by SCFT. For sphere-forming triblock copolymers mixed with homopolymers, the poorer miscibility and the more diffused distribution of the A homopolymers in the BAB/A blends result in a phase behavior drastically different from that of the ABA/A and AB/A blends. The ABA/A blends stabilize the Frank-Kasper (FK) phases similar to the AB/A blends, but the stability window of FK phases becomes negligibly small in the corresponding BAB/A blends. Our results demonstrate that the topological effect of block copolymers on the equilibrium phase behaviors can be more prominent in multi-component systems and thus more attention should be paid to copolymer topologies in the design of polymeric blends.

INTRODUCTION

Block copolymers composed of different blocks covalently bonded together are soft materials capable of self-assembling into ordered structures at the nanoscale [1, 2]. The spontaneous ordering of block copolymers originates from the frustration due to opposing tendencies: chemically distinct blocks tend to phase separate, whereas the covalent bonds hold them together [3]. The equilibrium structure of block copolymers depends on various fac-

* xiej33@mcmaster.ca

† shi@mcmaster.ca

tors such as the volume fractions of the different blocks, the copolymer architecture and temperature, *etc.* Such dependencies provide “knobs” by which the equilibrium morphology self-assembled from block copolymers can be regulated. Due to their rich phase behaviors, block copolymers not only hold promise in many applications such as lithography [4–7], photonics [8–10] and quantum materials [11, 12], but also serve as an ideal platform to study the spontaneous ordering of matter.

The simplest block copolymer system is AB diblock copolymer melts. Due to extensive theoretical and experimental studies [13–21], it has been well-established that the equilibrium phase behavior of neat AB diblock copolymers is controlled by three parameters: (1) the A (or B) block composition f_A (or f_B), (2) the interaction strength χN quantified by the product of the Flory-Huggins interaction parameter χ and degree of polymerization N , and (3) the conformational asymmetry parameter ϵ . Conformationally symmetric diblock copolymers ($\epsilon = 1$) exhibit a phase transition sequence from Dis \rightarrow HCP \rightarrow BCC \rightarrow HEX \rightarrow DG \rightarrow O⁷⁰ \rightarrow L as f_A changes from 0 to 0.5. Here Dis, HCP, BCC, HEX, DG, O⁷⁰ and L represent disordered phase, hexagonal close-packed spheres, body-centered cubic spheres, hexagonal close-packed cylinders, double-gyroid networks, *Fddd* networks, and lamellae [22]. For the case of $\epsilon = 1$, the $f - \chi N$ phase diagram is symmetric about $f = 0.5$, and further increasing f from 0.5 to 1 traverses the same morphologies but with A and B inverted and the order reversed. Another well-studied system is the symmetric linear AB-type triblock copolymers, which is obtained by joining two identical diblock chains through either their A ends or B ends. With the same overall block composition, there are two distinct architectures, *i.e.*, BAB and ABA, for an AB-type triblock copolymer. In contrast to the AB diblock copolymer melts, the $f - \chi N$ phase diagram for the linear symmetric AB-type triblock copolymer melts becomes slightly asymmetric about $f = 0.5$, due to the topological nonequivalency between the middle block and end blocks. However, the effect of this topological difference on the phase behavior is small and thus the phase diagram of the triblock copolymers remains largely analogous to that of the AB copolymers [22, 23].

One effective route to expand accessible morphologies self-assembled from block copolymers is by mixing different polymers (copolymer/copolymer or copolymer/homopolymer) together. Extensive experimental and theoretical studies have demonstrated that block copolymer blends can stabilize new morphologies that are not stable in the system composed of the individual parent species alone [24–38]. The greatest advantage of the blending strat-

egy for accessing new phases is that the architecture of each constituent polymeric species could remain simple, thus syntheses of complicated macromolecules could be avoided. The simplest polymeric blends that exhibit a rich phase behavior are binary AB diblock copolymer/A homopolymer blends. Depending on the block composition of the diblocks, the addition of appropriate homopolymers can stabilize a plethora of new morphologies including the Frank-Kasper (FK) σ , Laves C14 and C15, double diamond (DD) and plumber's nightmare (P) phases [14, 24, 26, 30, 31, 33, 39, 40].

Due to the incompatibility between the different components, an intrinsic feature of polymeric blends is their tendency to macrophase separate into two or more co-existing phases. Even for binary mixtures of two relatively simple polymeric components, the interplay between microphase and macrophase separations can lead to rather complex phase behaviors. For the simple binary AB/A blends, the addition of a small amount of homopolymers can induce order-order phase transitions, while the addition of excessive amount of homopolymers generally results in the coexistence between a copolymer-rich ordered/disordered phase and a homopolymer-rich disordered phase [13, 33]. One factor that strongly influences the solubility of the A homopolymers into the AB diblock copolymers as well as their spatial distribution is the ratio between the degrees of polymerization of the A homopolymer and the A block of the copolymer, *i.e.*, $\xi = N_{A,\text{homo}}/N_{A,\text{diblock}}$. For the case where $\xi \ll 1$ (wet-brush regime), the A homopolymers penetrate into the A micro-domains formed by the A blocks of the copolymers and the two components can remain miscible up to a high homopolymer concentration, while for the case where $\xi \geq 1$ (dry-brush regime), the opposite is true [30, 41–45]. Furthermore, the different behaviors of A homopolymers in the micro-domains formed by the diblocks result in different equilibrium morphologies. For example, adding homopolymers in the dry-brush regime into BCC-forming AB copolymers could stabilize the FK σ , C14 and C15 phases; however, these complex spherical phases are replaced by the HEX phase if the added homopolymers are in the wet-brush regime [30, 31, 33].

Because the phase diagram of the symmetric AB-type triblock copolymers is similar to the phase diagram of neat AB diblock copolymers, it is reasonable to expect that the new morphologies accessed by adding homopolymers into AB copolymers could also be accessed by blending homopolymers and triblock copolymers. A natural question is how the topological difference between the ABA and BAB architectures affects the equilibrium morphology when the A homopolymers are added. Theoretical and experimental studies of the AB-type

triblock copolymer/A homopolymer mixtures have been carried out. However, most of the existing studies focused on the effect of adding homopolymers on the bridging fraction and mechanical properties of the triblock copolymers, because of the commercial applications of triblock copolymers as thermoplastic elastomers [46, 47]. On the other hand, compared to the AB diblock copolymers, less efforts have been made to investigate the morphological phase behavior of their homologous triblock copolymers mixed with homopolymers [48–50], and, to our knowledge, none has examined the role played by the topology or sequence distribution of the triblocks. Therefore, the effect induced by the topological difference between the ABA and BAB triblock copolymers on the phase behavior of their mixtures with A homopolymers remains unexplored.

In this work, we examine the topological effect on the phase behavior of the binary blends composed of linear, ABA or BAB, symmetric triblock copolymers and A homopolymers. We employ the random-phase approximation (RPA) and the polymeric self-consistent field theory (SCFT), both applied to the freely-jointed chain (FJC) model, to study the microphase and macrophase separations of three homologous systems, *i.e.*, AB/A, ABA/A and BAB/A blends. To focus on the effect of the copolymer topology, we consider the case where the copolymers in these three systems have the same overall block fractions. In addition, the degree of polymerization of the two symmetric triblock chains are the same and both are twice of that of the AB diblock chain. We first focus on the case where the copolymers are lamella-forming and construct phase diagrams on the $\phi_2 - \chi_{AB}$ plane, where ϕ_2 is the homopolymer concentration, for the three systems to compare their phase behaviors. We then turn our attention to sphere-forming copolymers and examine the topological effect on the formation of the FK phases. In both cases, it is discovered that the AB/A and ABA/A blends have similar phase diagrams, whereas the BAB/A blends exhibit a drastically different phase behavior. Our results demonstrate that the topological effect in the neat AB-type triblock copolymers is amplified in their mixtures with A homopolymers and also provide insights into the topological effect in more complicated polymeric blends.

THEORETICAL FRAMEWORK

In this section, we present the theoretical framework used in the current study. We start with a description of the theoretical model based on the FJCs, followed by some details

of the RPA calculation for the study of the stability line of the homogeneous phase and the SCFT calculation for the study of the relative stability of different phases. We will compare the phase behaviors of the three homologous ABA/A, BAB/A and AB/A binary blends. Here the theoretical model is developed for the triblock copolymer/homopolymer blends. Similar theoretical formulation for the homologous AB/A blends can be found in our previous work [33].

Theoretical Model

We consider a binary blend composed of n_1 linear symmetric triblock copolymers and n_2 homopolymers in a volume V . Each triblock copolymer is composed of N_A A segments and N_B B segments, resulting in a chain with $N = N_A + N_B$ segments and $N - 1$ bonds. Two distinct topologies or sequences of the triblock copolymer are considered here, with the A or B blocks as the bridging block (BAB or ABA), respectively. The overall volume fractions of the A and B blocks for a copolymer are given by $f_A = f$ and $f_B = 1 - f$, respectively. Each homopolymer is composed of N_{Ah} A segments and the ratio between the number of A segments of an A homopolymer and that of a triblock copolymer is defined as $\gamma = N_{Ah}/N_A = N_{Ah}/fN$. We assume a uniform segment density ρ_0 so that $\rho_0 V = n_1 N + n_2 \gamma f N$ due to the incompressibility condition. The average concentrations of the triblock copolymers and the A homopolymers are given by,

$$\phi_1 = \frac{n_1 N}{\rho_0 V}, \quad \phi_2 = 1 - \phi_1 = \frac{n_2 \gamma f N}{\rho_0 V}.$$

The bonding potential between two adjacent segments in a polymer chain is given by,

$$v_\alpha(R_i) = -k_B T \ln \delta(R_i - b_\alpha), \quad (1)$$

where $R_i = |\mathbf{r}_{i+1} - \mathbf{r}_i|$ and b_α is the Kuhn length of the segments of type α with $\alpha=A$ or B. The non-bonded interaction energy U takes the form,

$$U = k_B T \rho_0 \chi_{AB} \int u(|\mathbf{r} - \mathbf{r}'|) \hat{\phi}_A(\mathbf{r}) \hat{\phi}_B(\mathbf{r}') d\mathbf{r} d\mathbf{r}', \quad (2)$$

where $\hat{\phi}_\alpha(\mathbf{r}) = (1/\rho_0) \sum_i \delta(\mathbf{r} - \mathbf{r}_{\alpha i})$ is the density operator of α segments, χ_{AB} is the Flory-Huggins parameter quantifying the incompatibility between A and B segments and $u(|\mathbf{r} - \mathbf{r}'|)$ describes the interaction potential as a function of inter-segment distance. The conformational asymmetry parameter can be defined as $\epsilon = b_A/b_B$.

Random-Phase Approximation (RPA)

In general, the Helmholtz free energy density functional of binary AB-type triblock copolymer/homopolymer blends can be written as an expansion with respect to small density fluctuations,

$$f = f^{(0)} + f^{(1)} + f^{(2)} + \dots \quad (3)$$

Of particular interest is the second order term,

$$\begin{aligned} f^{(2)} &= \sum_{\alpha,\beta} \int \frac{d\mathbf{k}}{(2\pi)^3} \Gamma_{\alpha\beta}(\mathbf{k}) \delta\phi_{\alpha}(\mathbf{k}) \delta\phi_{\beta}(-\mathbf{k}) \\ &= \sum_{\alpha,\beta} \int \frac{d\mathbf{k}}{(2\pi)^3} S_{\alpha\beta}^{-1}(\mathbf{k}) \delta\phi_{\alpha}(\mathbf{k}) \delta\phi_{\beta}(-\mathbf{k}), \end{aligned} \quad (4)$$

where $\Gamma_{\alpha\beta}(k)$'s are the second-order coefficients, $S_{\alpha\beta}(k)$'s are the Fourier-transformed density-density correlation functions and the subscript α or β labels the blocks made up of the α or β segments on different polymer chains. The RPA provides a systematic procedure to evaluate $S_{\alpha\beta}^{-1}(k)$'s, which can then be used to determine the stability line or spinodal of the system [51].

Following the formulation of Noolandi and coworkers [52, 53], the resultant $S_{\alpha\beta}^{-1}(\mathbf{k})$ computed by using RPA for binary AB-type copolymer/A homopolymer blends, denoted as $S_{\text{RPA}}^{-1}(\mathbf{k})$, is given by,

$$S_{\text{RPA}}^{-1} = -u\chi - \frac{(g_{AA} + 2g_{AB} + g_{BB})\phi_1 + \gamma g_{AhAh}\phi_2}{2N\phi_1[(g_{AB}^2 - g_{AA}g_{BB})\phi_1 - \gamma g_{AhAh}g_{BB}\phi_2]}, \quad (5)$$

where the quantities $g_{\alpha\beta}$'s are related to the correlation functions of the ideal, noninteracting polymer chains, which will be introduced shortly. For the homogeneous phase, $g_{\alpha\beta}$'s only depend on the magnitude of \mathbf{k} and this k dependence has been made implicit in Eq.5. The spinodal of the system is identified by the condition that the minimum of $S_{\text{RPA}}^{-1}(k)$ equals to zero. Denoting the k that minimizes $S_{\text{RPA}}^{-1}(k)$ as k^* , this condition also corresponds to the threshold beyond which the homogeneous phase becomes unstable against the fluctuation characterized by k^* .

The general expression of $g_{\alpha\beta}$ of a polymer chain is given by [51],

$$g_{\alpha\beta}(k) = \frac{1}{N_t^2} \sum_{i=1}^{N_t} \sum_{j=1}^{N_t} \Theta_i^{\alpha} \Theta_j^{\beta} P_{ij}, \quad (6)$$

where N_t is the total number of segments of the polymer chain and,

$$\Theta_i^\alpha = \begin{cases} 1, & \text{if the } i\text{th segment is of type } \alpha, \\ 0, & \text{otherwise.} \end{cases} \quad (7)$$

In Eq.6, the P_{ij} is the product of the k -space bond transition probabilities of all the segments that form the linear sub-chain bridging segments i and j . The current study focuses on the case where all segments have the same Kuhn lengths, *i.e.*, the bond transition probability $p(k)$ is the same across the whole chain, so we simply have $P_{ij} = p^{|i-j|}$. For a FJC, the real-space bond transition probability and its Fourier-transformed version are given by,

$$p(R) = \frac{1}{4\pi b^2} \delta(R - b), \quad (8)$$

$$p(k) = \frac{\sin(kb)}{kb}. \quad (9)$$

Using Eq.6, the $g_{\alpha\beta}$'s for polymers with different architectures can be computed. For the A homopolymer, we have,

$$g_{\text{AhAh}}(k) = \frac{2p(k) [p^{N_{\text{Ah}}}(k) - 1] - N_{\text{Ah}}p^2(k) + N_{\text{Ah}}}{N_{\text{Ah}}^2 [p(k) - 1]^2}. \quad (10)$$

For an AB diblock copolymer, using the same segmental-number notations (N , N_A and N_B) as the triblock for brevity, the g_{AA} and g_{BB} have the same form as Eq.10 but with ‘‘Ah’’ in the numerator replaced by ‘‘A’’ and ‘‘B’’, respectively, and the N_{Ah} in the denominator replaced by the total number of segment N . The inter-segment function g_{AB} is,

$$g_{\text{AB}}(k) = \frac{p(k) [p^{N_A}(k) - 1] [p^{N_B}(k) - 1]}{N^2 [p(k) - 1]^2}. \quad (11)$$

For the symmetric ABA triblock copolymer, the g_{BB} has the same form as that for the AB diblock, and the rest $g_{\alpha\beta}$'s are given by,

$$g_{\text{AA}}(k) = \frac{2p(k) \left[p^{\frac{N_A}{2}}(k) - 1 \right] \left[2 - p^{N_B}(k) + p^{\frac{N_A}{2} + N_B}(k) \right] - N_A p^2 + N_A}{N^2 [p(k) - 1]^2}, \quad (12)$$

$$g_{\text{AB}}(k) = \frac{2p(k) \left[p^{\frac{N_A}{2}}(k) - 1 \right] [p^{N_B}(k) - 1]}{N^2 [p(k) - 1]^2}. \quad (13)$$

Finally, for the symmetric BAB triblock copolymer, all the $g_{\alpha\beta}$'s have the same forms as those for the ABA triblock, but with the ‘‘A’’ and ‘‘B’’ swapped.

Self-Consistent Field Theory (SCFT)

The self-consistent field theory is used to determine the phase boundaries between different phases. For systems undergoing both microphase and macrophase separations, it is convenient to work in the grand canonical ensemble where the thermodynamic control parameters are the chemical potentials of the triblock copolymers, μ_1 , and the A homopolymers, μ_2 . Within the scope of mean-field theory, the grand potential density of the system is expressed as [54],

$$\begin{aligned} \frac{N\Phi}{\rho_0 V k_B T} = & -e^{\mu_1/k_B T} Q_1 - e^{\mu_2/k_B T} Q_2 - \frac{1}{V} \int d\mathbf{r} \left[N\omega_A(\mathbf{r})\phi_A(\mathbf{r}) + N\omega_B(\mathbf{r})\phi_B(\mathbf{r}) \right. \\ & \left. - \chi_{AB} N \int u(|\mathbf{r} - \mathbf{r}'|) \phi_A(\mathbf{r})\phi_B(\mathbf{r}') d\mathbf{r}' + \eta(\mathbf{r}) (1 - \phi_A(\mathbf{r}) - \phi_B(\mathbf{r})) \right], \end{aligned} \quad (14)$$

where Q_κ with $\kappa=1$ or 2 denotes the single-chain partition function of the triblock copolymer or the A homopolymer. $\phi_\alpha(\mathbf{r})$ represents the ensemble average of the density operator $\hat{\phi}_\alpha(\mathbf{r})$ and $\omega_\alpha(\mathbf{r})$ is the auxiliary field conjugate to $\phi_\alpha(\mathbf{r})$. $\eta(\mathbf{r})$ is the Lagrange multiplier enforcing the incompressibility condition. The total density profile of A segments in the system is given by,

$$\phi_A(\mathbf{r}) = \phi_{At}(\mathbf{r}) + \phi_{Ah}(\mathbf{r}),$$

where $\phi_{At}(\mathbf{r})$ and $\phi_{Ah}(\mathbf{r})$ are the density profiles of the A segments from the triblock copolymers and the A homopolymers, respectively.

Minimizing the grand potential density with respect to the densities and auxiliary fields yields the following set of self-consistent equations,

$$\left\{ \begin{aligned} N\omega_A(\mathbf{r}) &= \chi_{AB} N \int u(R)\phi_B(\mathbf{r} - \mathbf{R})d\mathbf{R} + \eta(\mathbf{r}), \\ N\omega_B(\mathbf{r}) &= \chi_{AB} N \int u(R)\phi_A(\mathbf{r} - \mathbf{R})d\mathbf{R} + \eta(\mathbf{r}), \\ \phi_A(\mathbf{r}) &= \frac{e^{\omega_A(\mathbf{r})}}{N} \sum_i^{N_A} q_1(i, \mathbf{r})q_1^\dagger(i, \mathbf{r}), \\ &+ e^{\mu/k_B T} \frac{e^{\omega_A(\mathbf{r})}}{N} \sum_{i=1}^{N_{Ah}} q_2(i, \mathbf{r})q_2^\dagger(i, \mathbf{r}), \\ \phi_B(\mathbf{r}) &= \frac{e^{\omega_B(\mathbf{r})}}{N} \sum_i^{N_B} q_1(i, \mathbf{r})q_1^\dagger(i, \mathbf{r}), \\ \phi_A(\mathbf{r}) + \phi_B(\mathbf{r}) &= 1, \end{aligned} \right. \quad (15)$$

where $\mathbf{R} = \mathbf{r} - \mathbf{r}'$ and $R = |\mathbf{R}|$. It is noted that the chemical potential μ_1 has been set to 0 by using the incompressibility condition so the subscript of μ_2 has been dropped for brevity. The concrete form for the summations over the segments of the triblock copolymer in Eqs. 15 depends on the architecture of the chain. Specifically, for ABA copolymer, we have,

$$\sum_i^{N_A} = \sum_{i=1}^{N_A/2} + \sum_{i=N_A/2+N_B+1}^{N_A+N_B},$$

$$\sum_i^{N_B} = \sum_{i=N_A/2+1}^{N_A/2+N_B},$$

and for BAB copolymer, we have,

$$\sum_i^{N_A} = \sum_{i=N_B/2+1}^{N_B/2+N_A},$$

$$\sum_i^{N_B} = \sum_{i=1}^{N_B/2} + \sum_{i=N_B/2+N_A+1}^{N_A+N_B}.$$

In Eqs.15, the forward propagator $q(i, \mathbf{r})$ is computed by iterating the equation,

$$q_\kappa(i+1, \mathbf{r}_{i+1}) = e^{-\omega_\alpha(\mathbf{r}_{i+1})} \int d\mathbf{r}_i p_\alpha(\mathbf{r}_{i+1} - \mathbf{r}_i) q_\kappa(i, \mathbf{r}_i), \quad (16)$$

with the initial condition $q_\kappa(1, \mathbf{r}) = \exp[-\omega_\alpha(\mathbf{r})]$, where $p_\alpha(\mathbf{r}_{i+1} - \mathbf{r}_i) (= p_\alpha(|\mathbf{r}_{i+1} - \mathbf{r}_i|) = p_\alpha(R))$ is the bond transition probability in Eq.8. The backward propagator is computed similarly by performing the iterations in the opposite direction along the chain. With the propagators, the single-chain partition function Q_κ is calculated via,

$$Q_\kappa = \frac{1}{V} \int d\mathbf{r} q_\kappa(N_\kappa, \mathbf{r}_{N_\kappa}), \quad (17)$$

and the average concentrations of the different species are calculated by, $\phi_1 = Q_1$ and $\phi_2 = 1 - \phi_1$.

The interaction potential is chosen to have a Gaussian form,

$$u(R) = \left(\frac{3}{2\pi r_0^2} \right)^{\frac{3}{2}} e^{-\frac{3R^2}{2r_0^2}}, \quad u(k) = e^{-\frac{k^2 r_0^2}{6}},$$

which is normalized in the real space, *i.e.*, $\int u(R) d\mathbf{R} = 1$. Throughout the current study, $r_0 = \sqrt{3}b_A$ is chosen and kept fixed.

The SCFT equations, *i.e.*, Eqs.15, are solved numerically by using the pseudo-spectral method combined with the variable-cell Anderson mixing for the FJCs. A detailed description of the numerical techniques can be found in our previous work[33]. For the construction of SCFT phase diagrams, various initial density fields corresponding to a set of candidate phases are used as inputs to Eqs.15, which are then numerically solved to obtain the converged grand potential densities for these phases. A list of schematics for all the ordered candidate phases considered in this work, along with the numbers of grid points used to discretize their unit cells in the SCFT calculations, is provided in Table S1 in the Supplemental Material. Phase transition boundaries are determined by comparing the converged grand potential densities. Different sets of candidate phases are used for different scenarios, which will be introduced later.

For the purpose of the current study, we restrict to the linear symmetric triblock copolymer with equal Kuhn lengths ($b_A = b_B$), *viz.* the triblock is also conformationally symmetric ($\epsilon = 1$). We also fix the total number of segments of the triblock chain to be 160. Under these restrictions, the free parameters of the binary AB-type triblock copolymer/A homopolymer mixtures include the A-block composition of the triblock (f), the triblock topology (ABA or BAB), the total numbers of segments of the homopolymer (N_{Ah}), the Flory-Huggins interaction parameter (χ_{AB}) and the homopolymer concentration (ϕ_2). Because the ABA and BAB triblocks considered here can be viewed as two identical diblocks covalently linked through their B and A ends, respectively, it is informative to also consider the homologous binary AB/A blends. To make direct comparison, all the parameters of the diblock/homopolymer blends are chosen to be the same as those of the triblock/homopolymer blends except that the diblock chain is obtained by cutting the triblock chain in half. Therefore, each AB diblock has 80 segments and the same f as the triblocks (and thus $N_{Ad} = N_A/2$). A convenient parameter to be defined is the segmental-number ratio ξ between the homopolymer and the A block of the AB diblock copolymer, *i.e.*, $\xi = N_{Ah}/N_{Ad}$. In the AB/A blends, the A homopolymers have the wet-brush behavior when $\xi \ll 1$ and the dry-brush behavior when $\xi \gtrsim 1$.

RESULTS AND DISCUSSION

We first consider the case with $f = 0.45$ ($N_A = 2N_{Ad} = 72$) so all the copolymers are lamella-forming. Fig.1 displays two phase diagrams in the $\phi_2 - \chi_{AB}$ plane for two values of ξ , *i.e.* $\xi = 0.5$ ($N_{Ah} = 18$) and $\xi = 1$ ($N_{Ah} = 36$), corresponding to the wet-brush and dry-brush regimes, respectively. Here the spinodal curve of a system signifies the point at which the homogeneous phase becomes unstable against fluctuations characterized by some wavevector k^* . For the binary mixtures considered in our study, the spinodals can be classified into two types denoted by the solid and dashed lines in Fig.1. The solid lines indicate the instability of the disordered phase against microphase separation, identified by that the $S_{RPA}^{-1}(k)$ first becomes negative at a non-zero k^* . In contrast, the dashed lines indicate the instability of the disordered phase against macrophase separation corresponding to $k^* = 0$. The point on the spinodal curve separating these two behaviors is the Lifshitz point, marked by a solid circle in the phase diagrams. Besides the spinodals, the phase boundaries between the L phase and the two-phase coexistence (2ϕ) region are also evaluated by SCFT and presented in Fig.1 as dash-dotted lines. We note that in constructing the diagrams in Fig.1, we only considered the L phase as the candidate ordered phase competing with the Dis phase for simplicity. Although other morphologies such as the network phases and HEX phase might be stable at large ϕ_2 , we expect their stability windows to be small with the chosen parameters and thus will not drastically, if at all, shift the boundaries between the overall ordered phases and their 2ϕ region with the homopolymer-rich disordered phase. In determining the L- 2ϕ boundaries in Fig.1, we found that for the ABA/A and AB/A blends, it becomes very hard to converge the L phase at the region very close to the boundaries especially at higher χ_{AB} . Whenever the L phase could not be converged beyond the L- 2ϕ boundaries, we performed SCFT calculation for the L phase as close to the boundaries as we could and then used extrapolation to find the location of the boundaries approximately. For the BAB/A phase, this issue does not exist and the L phase can converge easily within certain range beyond the L- 2ϕ boundaries.

A common feature of the spinodal curves in Fig.1 is that they are characterized by a non-zero k^* when ϕ_2 is small (solid lines) and as ϕ_2 is increased, k^* drops to zero at the Lifshitz point (solid circles), after which k^* stays at zero upon further increasing ϕ_2 (dashed lines). This reflects the fact that there is a threshold of the amount of homopolymers the micro-

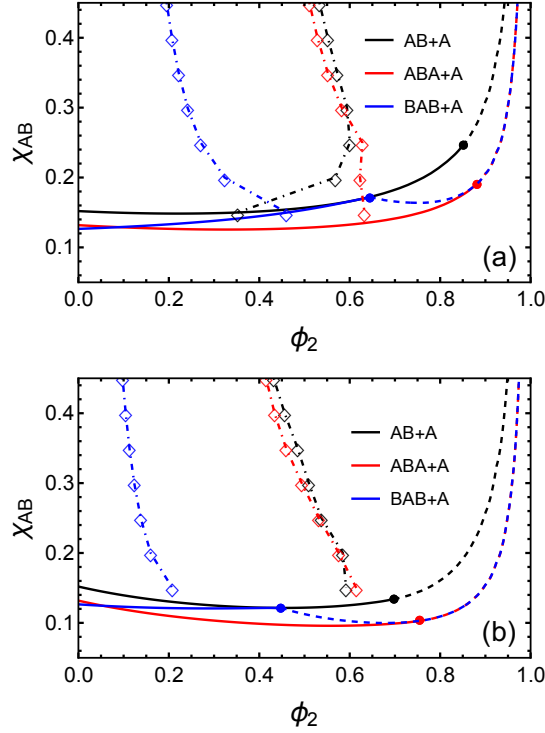


FIG. 1. The $\phi_2 - \chi_{AB}$ phase diagrams with (a) $\xi = 0.5$ ($N_{Ah} = 18$) and (b) $\xi = 1$ ($N_{Ah} = 36$), corresponding to the wet-brush and dry-brush regimes, respectively. The RPA-evaluated spinodal of each system is composed of a portion on the left characterized by a non-zero k^* (solid line) and a portion on the right characterized by a zero k^* (dashed line). The two portions are joined at the Lifshitz point (solid circle). The dash-dotted lines are the $L-2\phi$ boundaries evaluated by SCFT for different systems.

domains formed by the copolymers can accommodate, beyond which the two components tend to phase separate macroscopically. A comparison between the two diagrams shows clearly a shift of the Lifshitz point to smaller ϕ_2 for all blends in Fig.1(b) compared to Fig.1(a). This expanded instability of the disordered phase against macrophase separation is consistent with the enhanced tendency to macrophase separate in the AB/A system when the A homopolymers become longer, both observed experimentally [30, 42] and predicted theoretically [24, 33]. Moreover, a comparison between different systems in the same diagram reveals that the Lifshitz points for the AB/A and ABA/A blends occur at similar ϕ_2 's, which are noticeably higher than the ϕ_2 at which the Lifshitz point for the BAB/A blends occurs.

For instance, in Fig.1(a) corresponding to the wet-brush regime, the black and red circles are located at $\phi_2 \sim 0.86$ while the blue one is at $\phi_2 \sim 0.64$, which differ by $\Delta\phi_2 \sim 0.22$. In Fig.1(b), despite that all the Lifshitz points shift leftwards, the gap between their ϕ_2 's still exists and slightly enlarges, *i.e.*, $\Delta\phi_2 \gtrsim 0.25$. This indicates that the BAB/A blends have a stronger tendency to macrophase separate than the AB/A and ABA/A blends.

The SCFT-predicted L- 2ϕ boundaries for the three systems, denoted by the dash-dotted curves in Fig.1, behave consistently with their RPA-predicted spinodals and Lifshitz points. As ξ changes from 0.5 (Fig.1(a)) to 1 (Fig.1(b)), all the L- 2ϕ boundaries shift towards smaller ϕ_2 , clearly demonstrating a poorer miscibility of the copolymers and homopolymers. This behavior is consistent with the shift of the Lifshitz points. The diagrams also show that the L- 2ϕ boundaries for the AB/A and ABA/A blends locate very near to each other for most of the χ_{AB} range explored, except the region near $\chi_{AB} \sim 0.15$ in Fig.1(a), in which the L- 2ϕ boundary for the AB/A starts to shift to the left of that for the ABA/A. More notably, the L- 2ϕ boundary for the BAB/A blends appears at a significantly smaller ϕ_2 compared to those for the AB/A and ABA/A mixtures, regardless of ξ . This observation also coincides with the discovery that the homogeneous phase starts to become unstable against macrophase separation at a much lower ϕ_2 in the BAB/A blends compared to the other two systems. Combining the results from both the spinodals and L- 2ϕ boundaries, we conclude that for the binary AB/A blends linking the AB diblock chains through their B ends forming ABA triblocks roughly preserves the miscibility of the blends, whereas linking the diblocks through their A ends forming BAB triblocks drastically reduces the miscibility of the blends. Because the ABA and BAB triblocks have the same block composition and are both homologous to the AB diblock, the difference between their phase behaviors is entirely rooted in the topology or block sequence of the triblock copolymers.

An examination of the spinodal curves shown in Fig.1 reveals another interesting behavior due to the topology of the copolymers. As ϕ_2 is increased from 0, the spinodal curve of the BAB/A blends gradually approaches that of the AB/A blends. These two curves intersect at roughly the same location of the Lifshitz point of the BAB/A system. At its Lifshitz point, the BAB/A spinodal curve exhibits an abrupt change in its slope, and it gradually approaches and eventually overlaps with the ABA/A spinodal curve upon further increasing ϕ_2 . For a clearer view, two zoomed-in plots showing the vicinity of the BAB/A Lifshitz points (blue solid circles) in Fig.1(a) and (b) are provided in Fig.2(a) and (b), respectively.

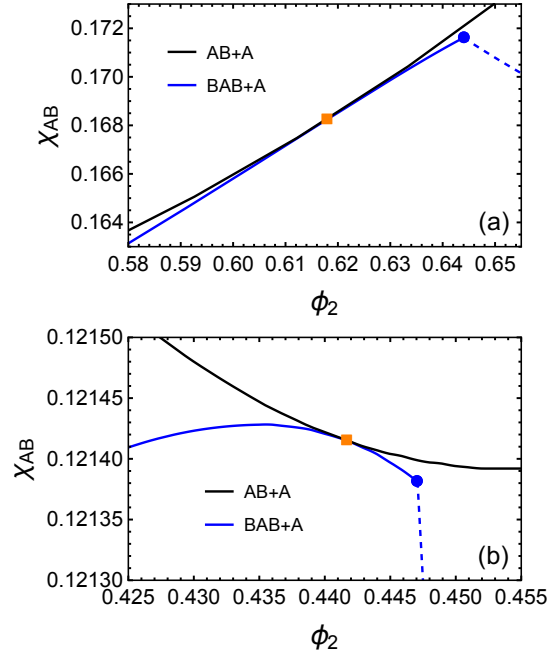


FIG. 2. The zoomed-in view of (a) Fig.1(a) and (b) Fig.1(b) in the vicinity of the Lifshitz point of the BAB/A system. The orange square in each diagram marks the estimated tangential point between the spinodals of the AB/A and BAB/A blends by interpolation.

Subject to numerical errors, our result suggests that the spinodals of the AB/A and BAB/A systems are tangential at their intersection, which is marked by a solid orange square in Fig.2. The BAB/A Lifshitz point occurs very close to and after the tangential point between the BAB/A and AB/A spinodals, as seen in both Fig.2(a) and (b).

In order to understand the discontinuous change in the slope of the BAB/A spinodal curve at the Lifshitz point, we take the $\xi = 1$ case as an example and plot k^* as a function of ϕ_2 for the ABA/A and BAB/A blends in Fig.3. It is very interesting that the behavior of k^* as a function of ϕ_2 is qualitatively different for the BAB/A and ABA/A blends. For the case of ABA/A blends (Fig.3(a)), the k^* reduces to zero continuously as ϕ_2 is increased. This resembles the behavior of the order parameter of a system undergoing a second-order phase transition if k^* is regarded as the order parameter and ϕ_2 as the temperature. On the other hand, for the case of BAB/A blends as shown in Fig.3(b), the k^* drops to zero discontinuously at the Lifshitz point, resembling a system undergoing a first-order phase transition. This difference stems from the behavior of the second-order

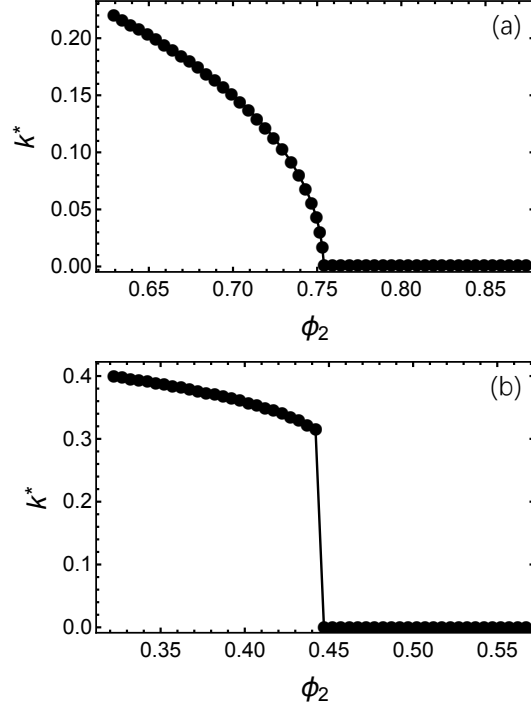


FIG. 3. Plots of k^* as a function of ϕ_2 for the (a) ABA/A and (b) BAB/A systems with $\xi = 1$ ($N_{\text{Ab}} = 36$). The Lifshitz point is defined as the position at which k^* turns from non-zero to zero. The behavior of k^* near the Lifshitz point of the AB/A blends has a similar feature to that of the ABA/A blends.

correlation function $S_{\text{RPA}}^{-1}(k)$ characterizing the fluctuations, which is shown in Fig.4 for several representative values of ϕ_2 along the spinodals of the ABA/A and BAB/A systems with $\xi = 1$. In Fig.4(a) for the ABA/A system, $S_{\text{RPA}}^{-1}(k)$ only exhibits one minimum, which approaches zero continuously as ϕ_2 is increased from 0.735 to 0.77. For the BAB/A system, $S_{\text{RPA}}^{-1}(k)$ exhibits one minimum when ϕ_2 is small, *e.g.*, $\phi_2=0.395$. However, a second local minimum, higher than the first one, appears at $k=0$ when ϕ_2 becomes larger, *e.g.*, $\phi_2=0.437$, as shown in Fig.4(b). Further increasing ϕ_2 makes the second minimum become equal to the first one, at which the Lifshitz point is identified. When ϕ_2 is increased further, the minimum at $k=0$ becomes the global minimum (*e.g.*, $\phi_2=0.452$ and 0.47) and the minimum at non-zero k eventually disappears (*e.g.*, $\phi_2=0.47$). The switch of the global minimum of $S_{\text{RPA}}^{-1}(k)$ from one to the other results in the sudden change in slope at the blue circles observed in Fig.1 and Fig.2. For the AB/A system, the Lifshitz point has the same second-

order transition feature as that of the ABA/A system. Therefore the spinodals of these two systems are smooth across the whole range of ϕ_2 .

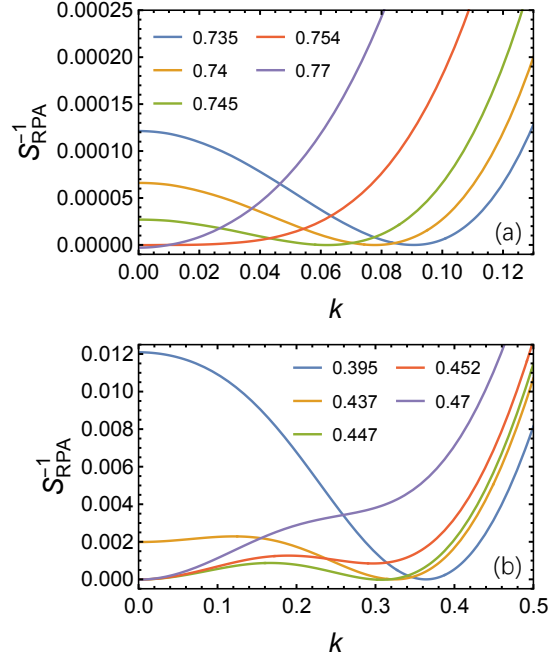


FIG. 4. Plots of $S_{\text{RPA}}^{-1}(k)$ at several representative values of ϕ_2 along the spinodals of the (a) ABA/A and (b) BAB/A systems with $\xi = 1$ ($N_{\text{Ah}} = 36$).

The different natures of the Lifshitz points indicate different topographical characteristics of the free energy landscapes of these blending systems, which, in turn, originate from the distinct chain topologies. In the case of the ABA/A and AB/A blends, the S_{RPA}^{-1} only has one minimum, that is, there is only one fluctuation mode leading the system from the homogeneous state to either microphase or macrophase separation. In contrast, for the BAB/A system, the mode driving the system to microphase separation coexists with the one driving it to macrophase separation within certain blend-composition range, *e.g.* from $\phi_2 = 0.437$ to 0.452 in Fig.4(b). When these two modes are comparable to each other, *i.e.* in the close vicinity of the Lifshitz point, the tendencies of the system to micro- and macrophase separate are in a close competition. In this regime, the BAB/A blends are expected to exhibit very interesting ordering dynamics, which would be of great interest for future research.

We now turn our attention to the case where the copolymers are sphere-forming by

choosing $f = 0.2$ ($N_A = 2N_{Ad} = 32$), and focus on the effect of triblock topology on the equilibrium ordered morphology in the triblock copolymer/homopolymer blends. Previous studies have revealed the capability of binary AB/A blends to stabilize the Frank-Kasper phases when the added homopolymers are in the dry-brush regime [30, 31, 33]. Because we are interested in the topological effect on the formation of the FK phases, we consider only the dry-brush case with $\xi = 1$ ($N_{Ah} = 16$). A preliminary examination of the phase behaviors of the three homologous systems, *i.e.*, the AB/A, ABA/A and BAB/A blends, is given by the spinodals obtained from the RPA (Fig.5). Despite the overall change of their shapes, the three spinodals preserve the features revealed in the lamella-forming case. In particular, the relative locations of the Lifshitz points suggest that the BAB/A would still have a much poorer miscibility than the AB/A and ABA/A mixtures.

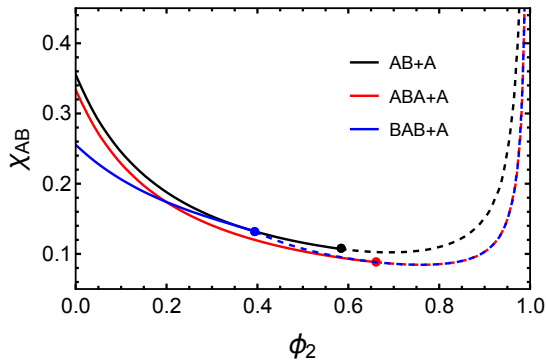


FIG. 5. Phase diagrams similar to those in Fig.1 but for the sphere-forming systems, *i.e.*, $f = 0.2$ ($N_A = 2N_{Ad} = 32$), where the homopolymers are in the dry-brush regime, *i.e.*, $\xi = 1$ ($N_{Ah} = 16$). Only the RPA-predicted spinodals are included here and more detailed phase diagrams predicted by SCFT are in Fig.6.

Fig.6 displays three detailed phase diagrams of the blends in the $\phi_2 - \chi_{AB}$ plane obtained by using SCFT. These phase diagrams are constructed by considering a number of candidate phases including the Dis, HCP, BCC and HEX as well as the FK σ and A15, and Laves C14 and C15 phases (Table S1). We note that the molecular parameters used in obtaining Fig.6(a) are the same as those used for Fig.3(a) in our previous paper [33]. The phase diagrams for the AB/A (Fig.6(a)) and ABA/A (Fig.6(b)) blends are remarkably similar. Despite a slight shift of the various phase boundaries towards lower χ_{AB} and a slight expansion of the ordered region towards higher ϕ_2 , the overall phase behavior is preserved when

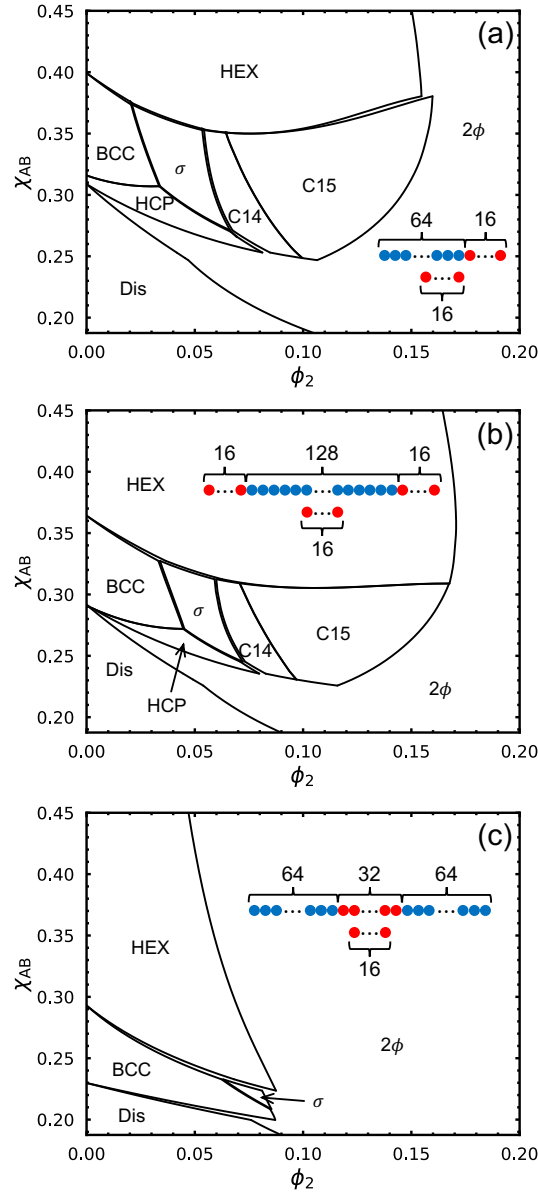


FIG. 6. Phase diagrams on the $\phi_2 - \chi_{AB}$ plane showing the SCFT-predicted phase boundaries for the sphere-forming (a) AB/A, (b) ABA/A and (c) BAB/A blends with the same parameters as those used for Fig.5. Schematics of the polymer chains that each system are composed of are also included in its phase diagram. In the schematics, the A and B segments are denoted by red and blue beads, respectively, and the number of beads of each block is also shown.

the AB diblock copolymers in the AB/A blends are transformed into the ABA triblocks by linking each pair of diblocks through their B ends. Particularly, the ABA/A blends preserve the ability to stabilize the FK σ , C14 and C15 phases and the stability windows of these complex phases appear in the same order as in the AB/A blends when the homopolymer concentration is increased.

In strong contrast, the BAB/A blends have a drastically different phase behavior compared to both the AB/A and ABA/A blends (Fig.6(c)). Specifically, adding A homopolymers into the BAB triblocks only induces a phase transition from the BCC to FK σ phase at $\chi_{AB} \approx 0.225$ and $\phi_2 \approx 0.07$. The stability window of the σ phase is very small, spanning a narrow range of $0.063 \lesssim \phi_2 \lesssim 0.085$ and $0.209 \lesssim \chi_{AB} \lesssim 0.233$. Furthermore, the HCP and Laves C14 and C15 phases are absent from the phase diagram. It is also observed that within the entire range of χ_{AB} covered in Fig.6(c), the ordered phase region only expands to $\phi_2 \approx 0.09$ upon the addition of the A homopolymers. Further increasing ϕ_2 induces macrophase separation. This more expanded 2ϕ region in the BAB/A compared to the other two systems is consistent with the RPA prediction (Fig.5). The depleted stability window of the FK phases, including the complete disappearance of the Laves C14 and C15 phases, is mainly due to the reduction of the single-phase region.

It is also observed from Fig.6(c) that the BCC- σ boundary shifts rightwards to higher ϕ_2 and the order-disorder coexistence region at $\phi_2 < 0.1$ diminishes compared to Fig.6(b). Similar tendencies have been observed when the homopolymer molecular weight in the binary AB/A blends is decreased, which makes the homopolymers less concentrated in the A-rich domains [33]. Thus, we suspect that the homopolymers should also have a more diffused distribution in the BAB/A than in the ABA/A blends. To verify this conjecture, we compare the homopolymer distribution at the same point, *i.e.*, $\phi_2 = 0.07$ and $\chi_{AB} = 0.297$, on the phase diagrams of these two systems, by plotting the $\phi_{Ah}(\mathbf{r})$'s of the ABA/A (light red) and BAB/A (light blue) systems on the xy plane passing through the center of one representative spherical domain of the BCC phase in Fig.7. Specifically, Fig.7(b) is a zoomed-in view of the region near to the domain center in Fig.7(a) and b_A is used as the unit of the x and y axes. It is seen that the $\phi_{Ah}(\mathbf{r})$ of the BAB/A blends is indeed lower than that of the ABA/A blends within a distance of more than $5b_A$ away from the domain center, confirming a more diffused distribution of the A homopolymers in the BAB/A blends. This observed broader homopolymer distribution in the BAB/A system has a different origin from that induced by

decreasing the molecular weight of the homopolymers, where the former should be related to the reduced configurational entropy of the A blocks of the triblock copolymers associated with the change of the molecular topology, while the latter is caused by the enhanced translational entropy of the homopolymers. The difference of these two mechanisms is also reflected by their different effects on the miscibility. Explicitly, decreasing N_{Ah} enhances the miscibility of the blends and thus expands the single-phase region towards higher ϕ_2 . On the contrary, the change of the triblock topology from ABA to BAB is observed to reduce the miscibility of the blends leading to a significantly smaller region of the single ordered phases.

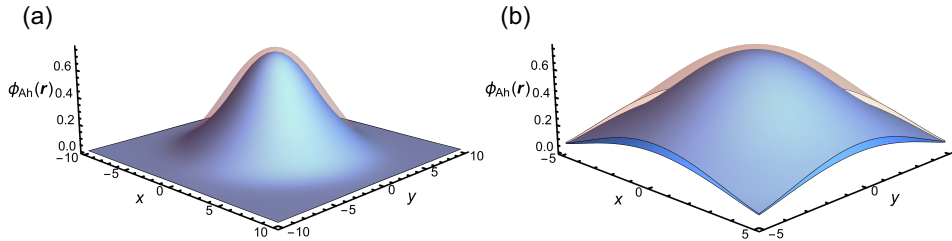


FIG. 7. Plots of the $\phi_{Ah}(\mathbf{r})$'s of the ABA/A (light red) and BAB/A (light blue) systems on the xy plane passing through the center of one representative spherical domain of the BCC phase. The density profiles are taken from the same point with $\phi_2 = 0.07$ and $\chi_{AB} = 0.297$ in Fig.6(b) for the ABA/A blends and in Fig.6(c) for the BAB/A blends. (b) is a zoomed-in view of the region near to the domain center in (a). In both (a) and (b), b_A is used as the unit of the x and y axes.

To provide a quantitative measure of the homopolymer distribution, we compute the average homopolymer concentrations within the nonequivalent A-rich domains (ϕ_2^D) of the C15 phase as a function of ϕ_2 along the path of $\chi_{AB} = 0.297$ and compare the results between the ABA/A and BAB/A systems in Fig.8. For each system, the curves in Fig.8 are evaluated before entering the 2ϕ region in the phase diagram. The FK phases are composed of more than one nonequivalent spherical domains with distinct sizes and shapes. Specifically, the C15 phase has two types of domains that differ significantly in volume. In Fig.8, the large and small domains of the C15 phase are labelled by 1 and 2, respectively. It is observed that for both the ABA/A and BAB/A blends, the larger domains always have a higher average homopolymer concentration than the smaller ones, which has been similarly observed in the AB/A blends. Moreover, for both the small and large domains, the average homopolymer

concentrations within the domains are constantly lower in the BAB/A than in the ABA/A system, which is consistent with the observation in Fig.7.

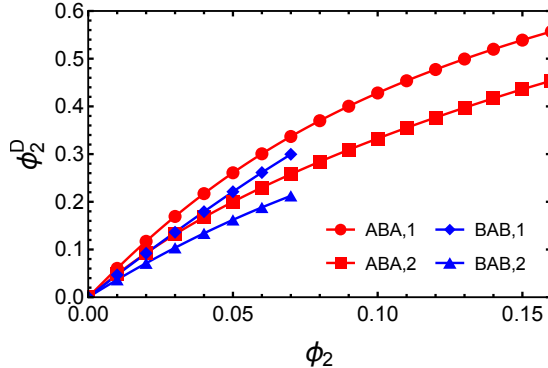


FIG. 8. The average concentrations of the homopolymers within the nonequivalent A-rich domains (ϕ_2^D) of the C15 phase as a function of ϕ_2 along the path of $\chi_{AB} = 0.297$. The curves for each system are evaluated before entering the 2ϕ region in the phase diagram. The large and small domains of the C15 phase are labelled by 1 and 2, respectively.

CONCLUSION

In summary, we have studied the topological, or block sequence, effect on the phase behavior of binary blends composed of linear symmetric ABA or BAB triblock copolymers and A homopolymers by using the random-phase approximation and self-consistent field theory applied to the freely-jointed chain model. Consistent phase behaviors have been obtained for lamella- and sphere-forming systems. For the case of lamella-forming systems, we examined the spinodals and L- 2ϕ boundaries of three polymeric mixtures, *i.e.*, AB/A, ABA/A and BAB/A, where the copolymers have the same block composition f . Our results indicate that the AB/A and ABA/A mixtures have similar miscibility and their Lifshitz points have a “second-order transition” feature; however, compared to the AB/A and ABA/A, the BAB/A mixtures have noticeably poorer miscibility and a Lifshitz point with a “first-order transition” feature. This feature results in a discontinuous change in the slope of the BAB/A spinodal at its Lifshitz point. For the case of sphere-forming copolymers, we demonstrated that the topological effect has a large influence on the equilibrium morphology of the system. Particularly, the transition of the BCC to FK phases can be induced by adding A

homopolymers into the ABA triblocks, which is similar to the phase behavior of the AB/A blends. In contrast, the FK phases are nearly absent in the BAB/A blends with the same block composition, which is due to a combined effect of the reduced miscibility and more diffused homopolymer distribution, both induced by the topological difference.

As demonstrated in previous SCFT studies [22, 23], the phase behaviors of the homologous ABA and BAB triblock copolymer melts are almost identical. The effect of triblock topology is reflected in small shifts of the phase boundaries, making the phase diagrams slightly asymmetric about $f = 0.5$. The results of the current study suggest that the topological effect of triblock copolymers on the equilibrium phase behavior can be greatly amplified in their mixtures with A homopolymers. We believe that such amplification mechanism is generic, which is also expected to be valid in other multicomponent systems containing copolymers with more complicated architectures. The discoveries in the current study provide a foundation for further research on the topological effect on the phase behaviors of more complex polymeric blends. Furthermore, recent advancements in polymer synthetic techniques have enabled copolymer samples with more precisely controlled block compositions and topologies [55–59]. The combination of theoretical and experimental studies will provide further understanding of the topological effect on the phase behaviors of polymeric blends containing block copolymers.

ACKNOWLEDGMENTS

This research was supported by the Natural Sciences and Engineering Research Council (NSERC) of Canada and was enabled in part by support provided by the facilities of SHARCNET (<https://www.sharcnet.ca>). ACS would like to thank the Isaac Newton Institute for Mathematical Sciences, Cambridge, and the Aberystwyth University for support and hospitality during the programme GeomPack: Geometry and packing in material structure and biology, where work on this paper was undertaken. This work was supported in part by EPSRC grant no EP/R014604/1.

-
- [1] Frank S Bates and Glenn H Fredrickson. Block copolymers—designer soft materials. *Physics today*, 52(2):32–38, 1999.

- [2] Yiyong Mai and Adi Eisenberg. Self-assembly of block copolymers. *Chemical Society Reviews*, 41(18):5969–5985, 2012.
- [3] An-Chang Shi. Frustration in block copolymer assemblies. *Journal of Physics: Condensed Matter*, 33(25):253001, 2021.
- [4] Joy Y Cheng, CA Ross, EL Thomas, Henry I Smith, and Gyula J Vancso. Fabrication of nanostructures with long-range order using block copolymer lithography. *Applied physics letters*, 81(19):3657–3659, 2002.
- [5] Chuanbing Tang, Erin M Lennon, Glenn H Fredrickson, Edward J Kramer, and Craig J Hawker. Evolution of block copolymer lithography to highly ordered square arrays. *Science*, 322(5900):429–432, 2008.
- [6] Julia D Cushen, Issei Otsuka, Christopher M Bates, Sami Halila, Sébastien Fort, Cyrille Rochas, Jeffrey A Easley, Erica L Rausch, Anthony Thio, Redouane Borsali, et al. Oligosaccharide/silicon-containing block copolymers with 5 nm features for lithographic applications. *ACS nano*, 6(4):3424–3433, 2012.
- [7] Christopher M Bates, Michael J Maher, Dustin W Janes, Christopher J Ellison, and C Grant Willson. Block copolymer lithography. *Macromolecules*, 47(1):2–12, 2014.
- [8] Augustine Urbas, Rachel Sharp, Yoel Fink, Edwin L Thomas, Maria Xenidou, and Lewis J Fetters. Tunable block copolymer/homopolymer photonic crystals. *Advanced Materials*, 12(11):812–814, 2000.
- [9] Andrew J Parnell, Andrew Pryke, Oleksandr O Mykhaylyk, Jonathan R Howse, Ali M Adawi, Nicholas J Terrill, and J Patrick A Fairclough. Continuously tuneable optical filters from self-assembled block copolymer blends. *Soft Matter*, 7(8):3721–3725, 2011.
- [10] Joshua Lequieu, Timothy Quah, Kris T Delaney, and Glenn H Fredrickson. Complete photonic band gaps with nonfrustrated abc bottlebrush block polymers. *ACS Macro Letters*, 9(7):1074–1080, 2020.
- [11] R Paxton Thedford, Fei Yu, William RT Tait, Kunal Shastri, Francesco Monticone, and Ulrich Wiesner. The promise of soft-matter-enabled quantum materials. *Advanced Materials*, 35(5):2203908, 2023.
- [12] Fei Yu and Ulrich Wiesner. The emerging field of block copolymer self-assembly-directed quantum materials. *Polymer*, 281:126063, 2023.
- [13] Mark W Matsen and Michael Schick. Stable and unstable phases of a diblock copolymer melt.

Physical Review Letters, 72(16):2660, 1994.

- [14] Mark W Matsen. Stabilizing new morphologies by blending homopolymer with block copolymer. *Physical review letters*, 74(21):4225, 1995.
- [15] Christopher A Tyler and David C Morse. Orthorhombic f d d d network in triblock and diblock copolymer melts. *Physical review letters*, 94(20):208302, 2005.
- [16] Mikihiro Takenaka, Tsutomu Wakada, Satoshi Akasaka, Shotaro Nishitsuji, Kenji Saijo, Hirofumi Shimizu, and Hirokazu Hasegawa. Orthorhombic fddd network in diblock copolymer melts. *arXiv preprint cond-mat/0605268*, 2006.
- [17] Sangwoo Lee, Michael J Bluemle, and Frank S Bates. Discovery of a frank-kasper σ phase in sphere-forming block copolymer melts. *Science*, 330(6002):349–353, 2010.
- [18] Nan Xie, Weihua Li, Feng Qiu, and An-Chang Shi. σ phase formed in conformationally asymmetric ab-type block copolymers. *Acs Macro Letters*, 3(9):906–910, 2014.
- [19] Sangwoo Lee, Chris Leighton, and Frank S Bates. Sphericity and symmetry breaking in the formation of frank–kasper phases from one component materials. *Proceedings of the National Academy of Sciences*, 111(50):17723–17731, 2014.
- [20] Morgan W Schulze, Ronald M Lewis III, James H Lettow, Robert J Hickey, Timothy M Gillard, Marc A Hillmyer, and Frank S Bates. Conformational asymmetry and quasicrystal approximants in linear diblock copolymers. *Physical review letters*, 118(20):207801, 2017.
- [21] Morgan W Bates, Joshua Lequieu, Stephanie M Barbon, Ronald M Lewis, Kris T Delaney, Athina Anastasaki, Craig J Hawker, Glenn H Fredrickson, and Christopher M Bates. Stability of the a15 phase in diblock copolymer melts. *Proceedings of the National Academy of Sciences*, 116(27):13194–13199, 2019.
- [22] Mark W Matsen. Effect of architecture on the phase behavior of ab-type block copolymer melts. *Macromolecules*, 45(4):2161–2165, 2012.
- [23] Mark W Matsen and RB Thompson. Equilibrium behavior of symmetric aba triblock copolymer melts. *The Journal of chemical physics*, 111(15):7139–7146, 1999.
- [24] Mark W Matsen. Phase behavior of block copolymer/homopolymer blends. *Macromolecules*, 28(17):5765–5773, 1995.
- [25] Daisuke Yamaguchi, Shuntaro Shiratake, and Takeji Hashimoto. Ordered structure in blends of block copolymers. 5. blends of lamella-forming block copolymers showing both microphase separation involving unique morphological transitions and macrophase separation. *Macro-*

- molecules*, 33(22):8258–8268, 2000.
- [26] Francisco J Martinez-Veracoechea and Fernando A Escobedo. The plumber’s nightmare phase in diblock copolymer/homopolymer blends. a self-consistent field theory study. *Macromolecules*, 42(22):9058–9062, 2009.
- [27] Zhiqiang Wu, Baohui Li, Qinghua Jin, Datong Ding, and An-Chang Shi. Phase behavior of binary blends of diblock copolymers. *The Journal of Physical Chemistry B*, 114(48):15789–15798, 2010.
- [28] Zhiqiang Wu, Baohui Li, Qinghua Jin, Datong Ding, and An-Chang Shi. Microphase and macrophase separations in binary blends of diblock copolymers. *Macromolecules*, 44(6):1680–1694, 2011.
- [29] Hideaki Takagi, Katsuhiko Yamamoto, and Shigeru Okamoto. Ordered-bicontinuous-double-diamond structure in block copolymer/homopolymer blends. *Europhysics Letters*, 110(4):48003, 2015.
- [30] Andreas J Mueller, Aaron P Lindsay, Ashish Jayaraman, Timothy P Lodge, Mahesh K Mahanthappa, and Frank S Bates. Emergence of a c15 laves phase in diblock polymer/homopolymer blends. *ACS Macro Letters*, 9(4):576–582, 2020.
- [31] Guo Kang Cheong, Frank S Bates, and Kevin D Dorfman. Symmetry breaking in particle-forming diblock polymer/homopolymer blends. *Proceedings of the National Academy of Sciences*, 117(29):16764–16769, 2020.
- [32] Aaron P Lindsay, Ronald M Lewis III, Bongjoon Lee, Austin J Peterson, Timothy P Lodge, and Frank S Bates. A15, σ , and a quasicrystal: Access to complex particle packings via bidisperse diblock copolymer blends. *ACS Macro Letters*, 9(2):197–203, 2020.
- [33] Jiayu Xie and An-Chang Shi. Formation of complex spherical packing phases in diblock copolymer/homopolymer blends. *Giant*, 5:100043, 2021.
- [34] Jiayu Xie, Yu Li, and An-Chang Shi. Binary blends of diblock copolymers: An efficient route to complex spherical packing phases. *Macromolecular Theory and Simulations*, 30(6):2100053, 2021.
- [35] Chi To Lai and An-Chang Shi. Binary blends of diblock copolymers: An effective route to novel bicontinuous phases. *Macromolecular Theory and Simulations*, 30(3):2100019, 2021.
- [36] Aaron P Lindsay, Guo Kang Cheong, Austin J Peterson, Steven Weigand, Kevin D Dorfman, Timothy P Lodge, and Frank S Bates. Complex phase behavior in particle-

- forming ab/ab diblock copolymer blends with variable core block lengths. *Macromolecules*, 54(15):7088–7101, 2021.
- [37] Jiayu Xie and An-Chang Shi. Phase behavior of binary blends of diblock copolymers: Progress and opportunities. *Langmuir*, 39(33):11491–11509, 2023.
- [38] Jiayu Xie and An-Chang Shi. Theory of complex spherical packing phases in diblock copolymer/homopolymer blends. *Macromolecules*, 56(24):10296–10312, 2023.
- [39] Francisco J Martinez-Veracoechea and Fernando A Escobedo. Bicontinuous phases in diblock copolymer/homopolymer blends: simulation and self-consistent field theory. *Macromolecules*, 42(5):1775–1784, 2009.
- [40] Hideaki Takagi and Katsuhiro Yamamoto. Effect of block copolymer composition and homopolymer molecular weight on ordered bicontinuous double-diamond structures in binary blends of polystyrene–polyisoprene block copolymer and polyisoprene homopolymer. *Macromolecules*, 54(11):5136–5143, 2021.
- [41] CV Berney, Pao Luo Cheng, and RE Cohen. Distribution of matrix homopolymer in block copolymers of spherical morphology. *Macromolecules*, 21(7):2235–2240, 1988.
- [42] Takeji Hashimoto, Hideaki Tanaka, and Hirokazu Hasegawa. Ordered structure in mixtures of a block copolymer and homopolymers. 2. effects of molecular weights of homopolymers. *Macromolecules*, 23(20):4378–4386, 1990.
- [43] Hideaki Tanaka, Hirokazu Hasegawa, and Takeji Hashimoto. Ordered structure in mixtures of a block copolymer and homopolymers. 1. solubilization of low molecular weight homopolymers. *Macromolecules*, 24(1):240–251, 1991.
- [44] Karen I Winey, Edwin L Thomas, and Lewis J Fetters. Swelling of lamellar diblock copolymer by homopolymer: influences of homopolymer concentration and molecular weight. *Macromolecules*, 24(23):6182–6188, 1991.
- [45] Satoshi Koizumi, Hirokazu Hasegawa, and Takeji Hashimoto. Spatial distribution of homopolymers in block copolymer microdomains as observed by a combined sans and saxs method. *Macromolecules*, 27(26):7893–7906, 1994.
- [46] Lisaleigh Kane, David A Norman, Scott A White, Mark W Matsen, Michael M Satkowski, Steven D Smith, and Richard J Spontak. Molecular, nanostructural and mechanical characteristics of lamellar triblock copolymer blends: effects of molecular weight and constraint. *Macromolecular rapid communications*, 22(5):281–296, 2001.

- [47] JP Baetzold, I Gancarz, X Quan, and JT Koberstein. Mechanical property modification and morphology of poly (styrene-*b*-hydrogenated butadiene-*b*-styrene)/poly (hydrogenated butadiene) blends. *Macromolecules*, 27(19):5329–5340, 1994.
- [48] X Quan, I Gancarz, JT Koberstein, and GD Wignall. Effect of homopolymer molecular weight on the morphology of block copolymer/homopolymer blends. *Macromolecules*, 20(6):1431–1434, 1987.
- [49] Suck-Hyun Lee, JT Koberstein, X Quan, I Gancarz, GD Wignall, and FC Wilson. Spatial distribution of a midblock-associating homopolymer blended into a triblock copolymer. *Macromolecules*, 27(12):3199–3206, 1994.
- [50] DA Norman, L Kane, SA White, SD Smith, and RJ Spontak. Triblock copolymer/homopolymer blends: conformational changes, microstructural transition and macrophase separation. *Journal of materials science letters*, 17(7):545–549, 1998.
- [51] Ludwik Leibler. Theory of microphase separation in block copolymers. *Macromolecules*, 13(6):1602–1617, 1980.
- [52] Kin Ming Hong and Jaan Noolandi. Theory of phase equilibria in systems containing block copolymers. *Macromolecules*, 16(7):1083–1093, 1983.
- [53] Mark Douglas Whitmore and Jaan Noolandi. Theory of phase equilibria in block copolymer-homopolymer blends. *Macromolecules*, 18(12):2486–2497, 1985.
- [54] Jiangzhong Wu, editor. *Variational Methods in Molecular Modeling*. Springer, Singapore, 2017.
- [55] Yanxiao Sun, Rui Tan, Zhuang Ma, Zhanhui Gan, Gang Li, Dongdong Zhou, Yu Shao, Wen-Bin Zhang, Rui Zhang, and Xue-Hui Dong. Discrete block copolymers with diverse architectures: resolving complex spherical phases with one monomer resolution. *ACS central science*, 6(8):1386–1393, 2020.
- [56] Suhua Duan, Xiaojie Yang, Ze Yang, Yuxin Liu, Qiunan Shi, Zhilin Yang, Haibing Wu, Yue Han, Yongquan Wang, Hang Shen, et al. A versatile synthetic platform for discrete oligo-and polyesters based on optimized protective groups via iterative exponential growth. *Macromolecules*, 54(23):10830–10837, 2021.
- [57] Dong Cai, Jinbin Li, Zhuang Ma, Zhanhui Gan, Yu Shao, Qian Xing, Rui Tan, and Xue-Hui Dong. Effect of molecular architecture and symmetry on self-assembly: A quantitative revisit using discrete aba triblock copolymers. *ACS Macro Letters*, 11(4):555–561, 2022.

- [58] Zhuang Ma, Rui Tan, Zhanhui Gan, Dongdong Zhou, Yida Yang, Wei Zhang, and Xue-Hui Dong. Modulation of the complex spherical packings through rationally doping a discrete homopolymer into a discrete block copolymer: a quantitative study. *Macromolecules*, 55(11):4331–4340, 2022.
- [59] Dongdong Zhou, Miao Xu, Zhuang Ma, Zhanhui Gan, Juncheng Zheng, Rui Tan, and Xue-Hui Dong. Discrete diblock copolymers with tailored conformational asymmetry: A precise model platform to explore complex spherical phases. *Macromolecules*, 55(16):7013–7022, 2022.

Chapter 9

Concluding Remarks and Future Outlook

In this thesis, we have conducted extensive studies on various polymeric blending systems using self-consistent field theory. Our focus has been on polymeric blends comprising simple components for two key reasons. Firstly, simple polymeric blends facilitate more comprehensive studies, allowing us to gain a deeper understanding of the fundamental mechanisms governing their phase behaviours. These mechanisms offer valuable insights into the phase behaviours of more complex polymeric blends and thus hold significant importance. Secondly, by maintaining simplicity in the architecture, we aim to explore the potential for using polymeric blends as a simpler yet effective alternative to architecturally complex block copolymers in the fabrication of desired novel structures.

In Chapter 3, we conducted a comprehensive review of progress made over the past three decades in the study of phase behaviours in binary diblock copolymer blends. Our primary focus was on binary A_1B_1/A_2B_2 blends, which consist of two diblock copolymers with varying degrees of polymerization and block compositions. Extensive studies have

revealed that the added A_2B_2 diblock copolymers serve either as fillers or cosurfactants, depending on their distribution within the polymeric domains formed by A_1B_1 diblock copolymers. The distribution of A_2B_2 diblocks is influenced by the A-block composition (f_{A2}), with symmetric diblocks primarily localizing at AB interfaces as cosurfactants, while asymmetric ones occupy central regions of A or B domains, thereby regulating the domain volume. These behaviours, further influenced by molecular weights, collectively mitigate packing frustrations and stabilize a variety of structures. These insights are applicable to more complex polymeric blends.

In chapters 4 and 5, we examined the phase behaviours of two simple polymeric blending systems: A_1B_1/A_2 and A_1B_1/A_2B_2 blends. Our primary focus was on the stability of the FK phases. In comparison to previous theoretical studies, our systematic investigation covered a significantly larger phase space for each system, leading to several new findings. For the A_1B_1/A_2 blends, $\phi_2 - \chi N$ phase diagrams are constructed with different combinations of $\{\epsilon, \alpha, f\}$. We confirmed that conformational asymmetry is not a necessary condition for the formation of complex spherical packing phases in this system, although a larger ϵ value can significantly expand the spherical phase region on the phase diagram. We also demonstrated that the observed $BCC \rightarrow \sigma \rightarrow C14 \rightarrow C15$ transition sequence with the addition of A homopolymers is strongly linked to the nonuniform distribution of A homopolymers among different A domains of the FK phases. Such distribution sustains domains with large size disparity reducing the AB interfacial area per unit volume of the FK phases, which serves as the main mechanism to stabilize these phases in the binary A_1B_1/A_2 mixture. In particular, the C14 and C15 phases are more stable than the σ phase at higher homopolymer concentration because of their favourable interaction energy between the A homopolymers and A blocks. We also illustrated the wet-brush behaviour of the homopolymers leading to a dramatically depleted FK stability

window on the phase diagram, which agrees well with the experiments. The consistent results between SCFT based on FJC and GC chains indicate that the formation of these complex packing is independent of the molecular details of the system.

For the A_1B_1/A_2B_2 blends, we parameterized the system with $\{f_1, f_2, \gamma\}$, offering a different perspective on phase behaviours compared to previous studies. We constructed $\phi_2 - \chi N$ phase diagrams using different combinations of $\{f_2, \gamma\}$ while keeping f_1 constant, covering a broad range of the phase space. Our analysis focused on the spatial distribution of various polymeric species, establishing correlations between structural formation and polymer segregation. We found that inter-domain segregation of different diblock copolymers results in varying domain volumes, while intra-domain segregation involves radial segregation of A blocks and lateral segregation of AB junctions, contributing to larger domain sizes and regulated domain shapes, respectively. These mechanisms synergistically open up a large stable region for the complex spherical packing phases on the phase diagrams. Furthermore, we discovered that the proper core-shell structure required to stabilize the FK phases could only form when the added A_2B_2 copolymer has a longer A block and an overall chain length larger than, or at least comparable to the host copolymer.

The A_1B_1/A_2B_2 blends represent a specific case of polydisperse diblock copolymers, known as bidisperse diblock copolymers. A natural extension of our study is to incorporate more diblock chains with varying molecular weights and block compositions. Polydisperse systems described by different molecular weight distributions have excessive degrees of freedom and are likely to further expand the stability window of complex spherical packings [134]. Even more excitingly, such systems potentially offer an effective platform for fabricating other novel structures, including the other Frank-Kasper phases that have not yet been discovered in block-copolymer self-assemblies [135].

In Chapter 6, we delved deeper into the study of two model systems: binary AB/C and ternary AB/C/D blends. In contrast to the A_1B_1/A_2 blends investigated in Chapter 4, the C homopolymers in the AB/C blends are matrix-selective. Our calculations revealed that the local segregation of C homopolymers promotes the stability of FK σ and A15 phases by mitigating the uneven chain stretching induced by packing frustration. Notably, we predict a very low critical conformational asymmetry ($\epsilon \approx 1.1$) required to stabilize the FK σ phase in binary blends comprising 40-segment diblock chains with $f_A = 0.25$ and 5-segment C homopolymers.

For AB/C/D blends, we observed a synergistic effect of the C and D homopolymers in stabilizing the FK packings, particularly the Laves packings. Our analysis suggests that the simultaneous presence of C and D homopolymers greatly promotes the stabilization of the FK σ , C14 and C15 phases due to their favourable interfacial energies between all repulsive pairs in the system. On the other hand, the addition of C homopolymers enhances the differential distribution of the existing D homopolymers across distinct domains, thereby increasing the domain-size dispersity of the Laves phases. This effect leads to a greater relative stability of the Laves packings primarily by strengthening their favourability in the CD interfacial energy over the other spherical packings. This indicates that the Laves packings offer an optimal way to compatibilize the immiscible C and D homopolymers. Our findings contribute to understanding the ubiquitous emergence of these novel spherical packing phases in a broad range of soft matter systems composed of amphiphiles and selective additives.

In Chapter 7, we explored the formation and stability of binary blends of sphere-forming AB/CD diblock copolymers. The promotion of binary crystalline phase formation was linked to large positive $\chi_{AC}N$ and negative $\chi_{BD}N$ values, driving A and C block separation while suppressing macrophase separation. Phases with distinct stoichiometries were

favoured at different blend compositions, enabling control over equilibrium morphology by adjusting polymer concentration. While only crystals with 1:1 and 1:3 stoichiometries were found stable in symmetric systems, asymmetric systems allowed for those with 1:2 stoichiometry. The $\phi_2 - \chi N$ phase diagrams exhibited eutectic behaviour similar to AB/B'C blends studies previously [76, 78]. Our density profile analysis illustrated that the optimal chain packing can be reasonably represented by the WSC construction, which sheds lights on the mechanisms governing the stable binary crystalline phase selection. The WSC construction of the chain packing explains the observed stability enhancement for phases whose WSC volume ratios are compatible with those of the A and C soft domains, and why the stability of the 1:1-stoichiometric crystals typically grows the fastest upon introducing the B-D association. The architectural simplicity of the AB/CD blends will potentially enable relevant experimental studies with precisely synthesized polymer samples.

The design space of the AB/CD blends is vast, holding great potential to stabilize a more diverse array of structures. One extension of our study would be to examine what morphologies are stable if the parent copolymers are cylinder-, network- or lamella-forming, and how the non-spherical equilibrium structure depends on the various system parameters. Another extension is to automate the AB and CD molecular design by employing advanced optimization algorithms such as the particle swarm optimization (PSO) [136, 137], which is expected to accelerate the molecular engineering towards desired structures.

Lastly, in Chapter 8, we explored the topological effect of linear symmetric triblock copolymers on their equilibrium phase behaviour when blended with homopolymers. To focus on the topological difference, we considered three homologous polymeric blends: AB/A, ABA/A, and BAB/A. Our results demonstrated that the AB/A and ABA/A

systems have very similar phase behaviours, while the BAB/A blends behave drastically differently. In both cases of lamella-forming and sphere-forming copolymers, the BAB/A blends exhibit significantly poorer miscibility than the AB/A and ABA/A blends. Moreover, different from the AB/A and ABA/A Lifshitz points behaving like a “second-order transition”, the BAB/A Lifshitz point possesses the feature of a “first-order transition”. Additionally, in the case of sphere-forming copolymers, the equilibrium morphology is largely influenced by the topological difference. Specifically, similar to the AB/A blends, the FK σ , C14, and C15 phases can also be stabilized in the ABA/A blends, but these phases are almost completely absent in the BAB/A blends.

Block copolymers with complex architectures have demonstrated capability to self-assemble into intricate structures [46, 49, 50, 47, 48, 51, 52]. As synthetic techniques progress, the incorporation of copolymers with complex architectures into polymeric blends may offer an even more robust route for fabricating designed nanostructures. The discoveries from the current simple blending system composed of triblock copolymers and homopolymers suggest that copolymer topology may exert more pronounced effects on phase behaviour when blended with other components. These results establish a foundation for future research on the role played by copolymer topology in polymeric blends containing block copolymers with more complex architectures.

Appendix A

Numerical Methods to Solve Modified Diffusion Equations

There are several numerical methods to solve the modified diffusion equations (Eqs. 2.25), with different advantages and drawbacks [115]. Broadly, these methods can be classified into three categories: real-space, spectral, and pseudo-spectral methods.

These three categories differ in the ways in which the spatial-coordinate dimensions are treated. Real-space methods [138], such as finite difference method, sample $q(s, \mathbf{r})$ at a set of discrete spatial points, and approximate ∇^2 by using different schemes in real space, such as centered space difference approximation. The advantages of real-space methods are that they do not require a pre-defined space group symmetry for the structure, and different boundary conditions can be readily implemented. A significant downside of the real-space method is that it requires a large number of spatial points to obtain an accurate solution, resulting in a high computational cost when dealing with high-dimensional problems.

Spectral methods, in contrast, handle the spatial dependence by expanding any spatial functions $f(\mathbf{r})$ into a complete set of basis functions. A common choice of basis functions is a series of plane waves [139]. In this case, a periodic function $f(\mathbf{r})$ can be expanded as:

$$f(\mathbf{r}) = \sum_j a_j \exp(i\mathbf{G}_j \cdot \mathbf{r}), \quad (\text{A.1})$$

where \mathbf{G}_j is a set of pre-selected reciprocal vectors satisfying the space-group symmetry of the target phase. One of the major advantages of spectral method is that it has spectral accuracy, and it is very computationally efficient when the target phase has a high symmetry because a relatively small number of plane waves are needed to obtain an accurate solution. However, for phases with a low symmetry, the computational cost is still high. Moreover, due to the pre-determined symmetry, the use of spectral method in exploring new morphologies is restricted.

Pseudo-spectral method solves the MDEs in both real and Fourier space [118]. Specifically, the following operator-splitting approximation is used:

$$\begin{aligned} q(s + \Delta s, \vec{r}) &= e^{(\nabla^2 - N\omega(\vec{r}))\Delta s} q(s, \vec{r}) \\ \longrightarrow q(s + \Delta s, \vec{r}) &= e^{-\frac{1}{2}N\omega\Delta s} e^{\nabla^2\Delta s} e^{-\frac{1}{2}N\omega\Delta s} q(s, \vec{r}) + o(\Delta s^3) \quad (\text{A.2}) \\ \longrightarrow q(s + \Delta s, \vec{r}) &\approx e^{-\frac{1}{2}N\omega\Delta s} e^{\nabla^2\Delta s} e^{-\frac{1}{2}N\omega\Delta s} q(s, \vec{r}) \end{aligned}$$

Because the operator ∇^2 in real space reduces to simple multiplication in Fourier space, we perform the calculation as follows:

$$q(s + \Delta s, \vec{r}) \approx e^{-\frac{1}{2}N\omega\Delta s} \text{FFT}^{-1} \left\{ e^{-k^2\Delta s} \text{FFT} \left[e^{-\frac{1}{2}N\omega\Delta s} q(s, \vec{r}) \right] \right\}, \quad (\text{A.3})$$

where “FFT” and “FFT⁻¹” represent forward and backward fast-Fourier transforms, respectively.

Due to the use of fast-Fourier transforms and its spectral accuracy, pseudo-spectral method generally has a higher computational efficiency than real-space methods. Furthermore, pseudo-spectral method has the ability to explore new morphologies, because the plane waves are based on a set of collocation points and no pre-defined symmetry is imposed. In this thesis, pseudo-spectral method is employed in all studies.

The accuracy of the solution also depends on the number of contour points used to discretize the variable s (N_s). In our calculation, we determine the proper N_s by ensuring that the computed phase boundaries do not have visible shifts upon further increasing N_s . The appropriate values of N_s vary between different systems. For instance, in the case of AB diblock copolymers, $N_s = 100$ would usually suffice when $\chi N \leq 40$.

Appendix B

Initial Ansatz for SCFT Calculation

In this appendix, we introduce the method employed to create an initial ansatz for each of the density fields used in the numerical SCFT calculation.

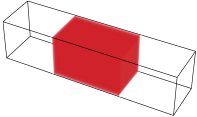
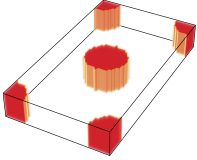
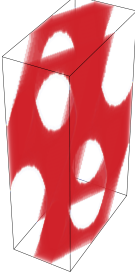
For the Dis phase, all density fields are initialized as constants, while ensuring that the total density adheres to the incompressibility constraint. In the case of spatially inhomogeneous (ordered) phases, we initialize ϕ_α by setting $\phi_\alpha = 1$ within the assumed α -rich domains and $\phi_\alpha = 0$ elsewhere. This initialization method is straightforward for the L phase and applicable to all the densities. For the other ordered phases, it is most convenient to first initialize the densities of monomers that comprise the core of the structure ($\phi_{\text{core}}(\mathbf{r})$) and then use the incompressibility condition to determine the initial densities for the monomers constituting the matrix ($\phi_{\text{matrix}}(\mathbf{r}) = 1 - \phi_{\text{core}}(\mathbf{r})$).

For phases consisting of discrete cylinders or spheres, cylindrical and spherical domains with appropriate radii are positioned to match the target crystalline structure. A method for determining reasonable values for the domain radii of a specific phase involves (1) assuming that all discrete domains have identical radii and (2) selecting a value for the radii such that the overall volume fraction of the minority blocks falls within the

appropriate range, e.g., from 0.2 to 0.3 for spherical morphologies. While convergence is generally not sensitive to the specific value chosen for the radii, it is important to ensure that discrete domains are not interconnected. For network phases, the networks are determined by using their level-set surfaces [140].

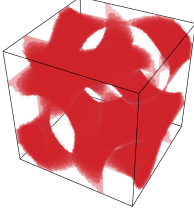
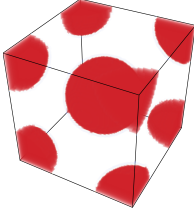
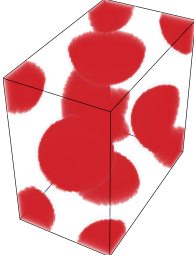
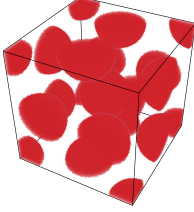
The following table shows the initial density profiles of the core-forming monomers for the classical morphologies in AB diblock copolymers and several Frank-Kasper phases. When applicable, the reduced coordinates of the centers of the discrete domains within the unit cell are also provided.

Table B.1 Initial density profiles of the core-forming monomers, and, when applicable, the reduced domain-center coordinates, for some typical ordered phases.

Phase Name	$\phi_{\text{core}}(\mathbf{r})$	Domain-Center Coordinates
L		$\{x\} = \{0.5\}$
HEX		$\{(x, y)\} = \{(0, 0), (1, 0), (0, 1), (1, 1), (0.5, 0.5)\}$
O70		/

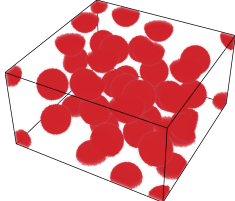
Continued on next page

Table B.1 – *Continued from previous page*

Phase Name	$\phi_{\text{core}}(\mathbf{r})$	Domain-Center Coordinates
DG		/
BCC		$\{(x, y, z)\} = \{(0, 0, 0), (1, 0, 0), (0, 1, 0), (0, 0, 1), (1, 1, 0), (1, 0, 1), (0, 1, 1), (1, 1, 1), (0.5, 0.5, 0.5)\}$
HCP		$\{(x, y, z)\} = \{(0.5, 0.1667, 0.5), (0.0, 0.6667, 0.5), (1, 0.6667, 0.5), (0, 0, 0), (1, 0, 1), (0, 1, 0), (0, 0, 1), (1, 1, 0), (1, 0, 0), (0, 1, 1), (1, 1, 1), (0.5, 0.5, 0), (0.5, 0.5, 1)\}$
A15		$\{(x, y, z)\} = \{(0, 0, 0), (1, 0, 0), (0, 1, 0), (0, 0, 1), (1, 1, 0), (1, 0, 1), (0, 1, 1), (1, 1, 1), (0.5, 0.5, 0.5), (0.75, 1, 0.5), (0.25, 1, 0.5), (0.5, 0.75, 0), (0.5, 0.25, 0), (1, 0.5, 0.25), (0, 0.5, 0.25), (1, 0.5, 0.75), (0, 0.5, 0.75), (0.5, 0.75, 1), (0.5, 0.25, 1), (0.75, 0, 0.5), (0.25, 0, 0.5)\}$

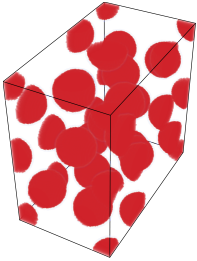
Continued on next page

Table B.1 – *Continued from previous page*

Phase Name	$\phi_{\text{core}}(\mathbf{r})$	Domain-Center Coordinates
σ		$\{(x, y, z)\} = \{(0, 0, 0), (1, 0, 1), (0, 1, 0), (0, 0, 1), (1, 1, 0), (1, 0, 0), (0, 1, 1), (1, 1, 1), (0.5, 0.5, 0.5), (0.0653, 0.7376, 0), (0.0653, 0.7376, 1), (0.2624, 0.9347, 0), (0.2624, 0.9347, 1), (0.5653, 0.7624, 0.5), (0.2376, 0.4347, 0.5), (0.7624, 0.5653, 0.5), (0.4347, 0.2376, 0.5), (0.7376, 0.0653, 0), (0.7376, 0.0653, 1), (0.9347, 0.2624, 0), (0.9347, 0.2624, 1), (0.3684, 0.9632, 0.5), (0.5368, 0.8684, 0), (0.5368, 0.8684, 1), (0.8684, 0.5368, 0), (0.9632, 0.3684, 0.5), (0.8684, 0.5368, 1), (0.0368, 0.6316, 0.5), (0.1316, 0.4632, 1), (0.1316, 0.4632, 0), (0.4632, 0.1316, 0), (0.6316, 0.0368, 0.5), (0.4632, 0.1316, 1), (0.3177, 0.6823, 0.7524), (0.3177, 0.6823, 0.2476), (0.8177, 0.8177, 0.2524), (0.8177, 0.8177, 0.7476), (0.6823, 0.3177, 0.7524), (0.6823, 0.3177, 0.2476), (0.1823, 0.1823, 0.7476), (0.1823, 0.1823, 0.2524), (0.1019, 0.8981, 0.5), (0.6019, 0.6019, 1), (0.6019, 0.6019, 0), (0.3981, 0.3981, 1), (0.3981, 0.3981, 0), (0.8981, 0.1019, 0.5)\}$

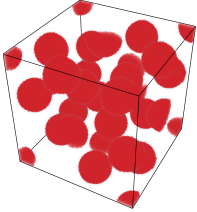
Continued on next page

Table B.1 – *Continued from previous page*

Phase Name	$\phi_{\text{core}}(\mathbf{r})$	Domain-Center Coordinates
C14		$\{(x, y, z)\} = \{(0, 0, 0), (0, 0, 1), (0, 1, 0), (0, 1, 1), (1, 1, 0), (1, 1, 1), (1, 0, 0), (1, 0, 1), (0.5, 0.5, 0.5), (0.5, 0.5, 0), (0.5, 0.5, 1), (1, 1, 0.5), (1, 0, 0.5), (0, 0, 0.5), (0, 1, 0.5), (0.74575, 0.91525, 0.75), (0.25425, 0.91525, 0.75), (1, 0.8305, 0.25), (0, 0.8305, 0.25), (0.5, 0.6695, 0.75), (0.75425, 0.58475, 0.25), (0.24575, 0.58475, 0.25), (0.75425, 0.41525, 0.75), (0.24575, 0.41525, 0.75), (0.5, 0.3305, 0.25), (1, 0.1695, 0.75), (0.74575, 0.08475, 0.25), (0.25425, 0.08475, 0.25), (0, 0.1695, 0.75), (0.5, 0.83334, 0.438), (0.5, 0.83334, 0.062), (1, 0.66666, 0.562), (1, 0.66666, 0.938), (0, 0.66666, 0.562), (0, 0.66666, 0.938), (1, 0.33334, 0.062), (1, 0.33334, 0.438), (0.5, 0.16666, 0.938), (0.5, 0.16666, 0.562), (0, 0.33334, 0.438), (0, 0.33334, 0.062)\}$

Continued on next page

Table B.1 – *Continued from previous page*

Phase Name	$\phi_{\text{core}}(\mathbf{r})$	Domain-Center Coordinates
C15		$\{(x, y, z)\} = \{(0.875, 0.375, 0.125), (0.875, 0.125, 0.375), (0.875, 0.875, 0.625), (0.875, 0.625, 0.875), (0.625, 0.875, 0.875), (0.625, 0.625, 0.625), (0.625, 0.375, 0.375), (0.625, 0.125, 0.125), (0.375, 0.875, 0.125), (0.375, 0.625, 0.375), (0.375, 0.375, 0.625), (0.375, 0.125, 0.875), (0.125, 0.375, 0.875), (0.125, 0.125, 0.625), (0.125, 0.875, 0.375), (0.125, 0.625, 0.125), (1, 0, 0), (1, 1, 0), (1, 0.5, 0.5), (1, 0, 1), (1, 1, 1), (0.75, 0.75, 0.25), (0.75, 0.25, 0.75), (0.5, 0.5, 0), (0.5, 0, 0.5), (0.5, 1, 0.5), (0.5, 0.5, 1), (0.25, 0.25, 0.25), (0.25, 0.75, 0.75), (0, 0, 0), (0, 1, 0), (0, 0.5, 0.5), (0, 0, 1), (0, 1, 1)\}$

References

- [1] George M Whitesides and Bartosz Grzybowski. Self-assembly at all scales. *Science*, 295(5564):2418–2421, 2002.
- [2] De-Liang Long, Eric Burkholder, and Leroy Cronin. Polyoxometalate clusters, nanostructures and materials: From self assembly to designer materials and devices. *Chemical Society Reviews*, 36(1):105–121, 2007.
- [3] Julia D Cushen, Issei Otsuka, Christopher M Bates, Sami Halila, Sébastien Fort, Cyrille Rochas, Jeffrey A Easley, Erica L Rausch, Anthony Thio, Redouane Borsali, et al. Oligosaccharide/silicon-containing block copolymers with 5 nm features for lithographic applications. *ACS nano*, 6(4):3424–3433, 2012.
- [4] Christopher M Bates, Michael J Maher, Dustin W Janes, Christopher J Ellison, and C Grant Willson. Block copolymer lithography. *Macromolecules*, 47(1):2–12, 2014.
- [5] William J Durand, Gregory Blachut, Michael J Maher, Stephen Sirard, Summer Tein, Matthew C Carlson, Yusuke Asano, Sunshine X Zhou, Austin P Lane, Christopher M Bates, et al. Design of high- χ block copolymers for lithography. *Journal of Polymer Science Part A: Polymer Chemistry*, 53(2):344–352, 2015.
- [6] Yoel Fink, Augustine M Urbas, Mounqi G Bawendi, John D Joannopoulos, and Edwin L Thomas. Block copolymers as photonic bandgap materials. *Journal of Lightwave Technology*, 17(11):1963–1969, 1999.
- [7] Augustine Urbas, Rachel Sharp, Yoel Fink, Edwin L Thomas, Maria Xenidou, and Lewis J Fetters. Tunable block copolymer/homopolymer photonic crystals. *Advanced Materials*, 12(11):812–814, 2000.
- [8] Andrew J Parnell, Andrew Pryke, Oleksandr O Mykhaylyk, Jonathan R Howse, Ali M Adawi, Nicholas J Terrill, and J Patrick A Fairclough. Continuously tuneable optical filters from self-assembled block copolymer blends. *Soft Matter*, 7(8):3721–3725, 2011.
- [9] Simeng Liu, Yi Yang, Lianbin Zhang, Jiangping Xu, and Jintao Zhu. Recent progress in responsive photonic crystals of block copolymers. *Journal of Materials Chemistry C*, 8(47):16633–16647, 2020.

- [10] Zhen Wang, Chun Lam Clement Chan, Tianheng H Zhao, Richard M Parker, and Silvia Vignolini. Recent advances in block copolymer self-assembly for the fabrication of photonic films and pigments. *Advanced Optical Materials*, 9(21):2100519, 2021.
- [11] Payam Zarrintaj, Joshua D Ramsey, Ali Samadi, Zhaleh Atoufi, Mohsen Khodadadi Yazdi, Mohammad Reza Ganjali, Leila Mohammadi Amirabad, Ehsan Zangene, Mehdi Farokhi, Krzysztof Formela, et al. Pluronic: A versatile tri-block copolymer for biomedical applications. *Acta biomaterialia*, 110:37–67, 2020.
- [12] Duy Toan Pham, Athittaya Chokamonsirikun, Vipasiri Phattaravorakarn, and Waree Tiyaboonchai. Polymeric micelles for pulmonary drug delivery: a comprehensive review. *Journal of Materials Science*, 56:2016–2036, 2021.
- [13] Maryam Radjabian and Volker Abetz. Advanced porous polymer membranes from self-assembling block copolymers. *Progress in Polymer Science*, 102:101219, 2020.
- [14] Luoxing Xiang, Qian Li, Chen Li, Qiqi Yang, Fugui Xu, and Yiyong Mai. Block copolymer self-assembly directed synthesis of porous materials with ordered bicontinuous structures and their potential applications. *Advanced Materials*, 35(5):2207684, 2023.
- [15] R Paxton Thedford, Fei Yu, William RT Tait, Kunal Shastri, Francesco Monticone, and Ulrich Wiesner. The promise of soft-matter-enabled quantum materials. *Advanced Materials*, 35(5):2203908, 2023.
- [16] Fei Yu and Ulrich Wiesner. The emerging field of block copolymer self-assembly-directed quantum materials. *Polymer*, page 126063, 2023.
- [17] Chen Yu and S Xiong. Directed self-assembly of block copolymers for sub-10 nm fabrication [j]. *International Journal of Extreme Manufacturing*, 2(03):129–162, 2020.
- [18] Richard AL Jones. *Soft condensed matter*, volume 6. Oxford University Press, 2002.
- [19] Michael Rubinstein, Ralph H Colby, et al. *Polymer physics*, volume 23. Oxford university press New York, 2003.
- [20] Mark W Matsen. The standard gaussian model for block copolymer melts. *Journal of Physics: Condensed Matter*, 14(2):R21, 2001.
- [21] Mark William Matsen. Fast and accurate scft calculations for periodic block-copolymer morphologies using the spectral method with anderson mixing. *The European Physical Journal E*, 30(4):361–369, 2009.
- [22] Ashish K Khandpur, Stephan Foerster, Frank S Bates, Ian W Hamley, Anthony J Ryan, Wim Bras, Kristoffer Almdal, and Kell Mortensen. Polyisoprene-polystyrene diblock copolymer phase diagram near the order-disorder transition. *Macromolecules*, 28(26):8796–8806, 1995.

- [23] Myung Im Kim, Tsutomu Wakada, Satoshi Akasaka, Shotaro Nishitsuji, Kenji Saijo, Hirokazu Hasegawa, Kazuki Ito, and Mikihiro Takenaka. Stability of the fddd phase in diblock copolymer melts. *Macromolecules*, 41(20):7667–7670, 2008.
- [24] An-Chang Shi. Frustration in block copolymer assemblies. *Journal of Physics: Condensed Matter*, 33(25):253001, 2021.
- [25] Frederick C Frank and John S Kasper. Complex alloy structures regarded as sphere packings. i. definitions and basic principles. *Acta Crystallographica*, 11(3):184–190, 1958.
- [26] Frederick C Frank and John S Kasper. Complex alloy structures regarded as sphere packings. ii. analysis and classification of representative structures. *Acta Crystallographica*, 12(7):483–499, 1959.
- [27] Sangwoo Lee, Michael J Bluemle, and Frank S Bates. Discovery of a frank-kasper σ phase in sphere-forming block copolymer melts. *Science*, 330(6002):349–353, 2010.
- [28] Nan Xie, Weihua Li, Feng Qiu, and An-Chang Shi. σ phase formed in conformationally asymmetric ab-type block copolymers. *Acs Macro Letters*, 3(9):906–910, 2014.
- [29] Sangwoo Lee, Timothy M Gillard, and Frank S Bates. Fluctuations, order, and disorder in short diblock copolymers. *AIChE Journal*, 59(9):3502–3513, 2013.
- [30] Sangwoo Lee, Chris Leighton, and Frank S Bates. Sphericity and symmetry breaking in the formation of frank-kasper phases from one component materials. *Proceedings of the National Academy of Sciences*, 111(50):17723–17731, 2014.
- [31] Morgan W Schulze, Ronald M Lewis III, James H Lettow, Robert J Hickey, Timothy M Gillard, Marc A Hillmyer, and Frank S Bates. Conformational asymmetry and quasicrystal approximants in linear diblock copolymers. *Physical review letters*, 118(20):207801, 2017.
- [32] Abhiram Reddy, Michael B Buckley, Akash Arora, Frank S Bates, Kevin D Dorfman, and Gregory M Grason. Stable frank-kasper phases of self-assembled, soft matter spheres. *Proceedings of the National Academy of Sciences*, 115(41):10233–10238, 2018.
- [33] Ronald M Lewis III, Akash Arora, Haley K Beech, Bongjoon Lee, Aaron P Lindsay, Timothy P Lodge, Kevin D Dorfman, and Frank S Bates. Role of chain length in the formation of frank-kasper phases in diblock copolymers. *Physical Review Letters*, 121(20):208002, 2018.
- [34] Morgan W Bates, Joshua Lequieu, Stephanie M Barbon, Ronald M Lewis III, Kris T Delaney, Athina Anastasaki, Craig J Hawker, Glenn H Fredrickson, and Christopher M Bates. Stability of the a15 phase in diblock copolymer melts. *Proceedings of the National Academy of Sciences*, 116(27):13194–13199, 2019.

- [35] Wei Zheng and Zhen-Gang Wang. Morphology of abc triblock copolymers. *Macromolecules*, 28(21):7215–7223, 1995.
- [36] Ping Tang, Feng Qiu, Hongdong Zhang, and Yuliang Yang. Morphology and phase diagram of complex block copolymers: Abc linear triblock copolymers. *Physical Review E*, 69(3):031803, 2004.
- [37] Christopher A Tyler, Jian Qin, Frank S Bates, and David C Morse. Scft study of nonfrustrated abc triblock copolymer melts. *Macromolecules*, 40(13):4654–4668, 2007.
- [38] Meijiao Liu, Weihua Li, Feng Qiu, and An-Chang Shi. Theoretical study of phase behavior of frustrated abc linear triblock copolymers. *Macromolecules*, 45(23):9522–9530, 2012.
- [39] Weihua Li, Feng Qiu, and An-Chang Shi. Emergence and stability of helical superstructures in abc triblock copolymers. *Macromolecules*, 45(1):503–509, 2012.
- [40] Ping Tang, Feng Qiu, Hongdong Zhang, and Yuliang Yang. Morphology and phase diagram of complex block copolymers: Abc star triblock copolymers. *The Journal of Physical Chemistry B*, 108(24):8434–8438, 2004.
- [41] Kenichi Hayashida, Atsushi Takano, Shigeo Arai, Yuya Shinohara, Yoshiyuki Amemiya, and Yushu Matsushita. Systematic transitions of tiling patterns formed by abc star-shaped terpolymers. *Macromolecules*, 39(26):9402–9408, 2006.
- [42] Kenichi Hayashida, Wataru Kawashima, Atsushi Takano, Yuya Shinohara, Yoshiyuki Amemiya, Yoshinobu Nozue, and Yushu Matsushita. Archimedean tiling patterns of abc star-shaped terpolymers studied by microbeam small-angle x-ray scattering. *Macromolecules*, 39(14):4869–4872, 2006.
- [43] Yushu Matsushita, Kenichi Hayashida, and Atsushi Takano. Jewelry box of morphologies with mesoscopic length scales—abc star-shaped terpolymers. *Macromolecular rapid communications*, 31(18):1579–1587, 2010.
- [44] Yushu Matsushita, Kenichi Hayashida, Tomonari Dotera, and Atsushi Takano. Kaleidoscopic morphologies from abc star-shaped terpolymers. *Journal of Physics: Condensed Matter*, 23(28):284111, 2011.
- [45] Weiquan Xu, Kai Jiang, Pingwen Zhang, and An-Chang Shi. A strategy to explore stable and metastable ordered phases of block copolymers. *The Journal of Physical Chemistry B*, 117(17):5296–5305, 2013.
- [46] Nan Xie, Meijiao Liu, Hanlin Deng, Weihua Li, Feng Qiu, and An-Chang Shi. Macromolecular metallurgy of binary mesocrystals via designed multiblock terpolymers. *Journal of the American Chemical Society*, 136(8):2974–2977, 2014.

- [47] Yicheng Qiang, Weihua Li, and An-Chang Shi. Stabilizing phases of block copolymers with gigantic spheres via designed chain architectures. *ACS Macro Letters*, 9(5):668–673, 2020.
- [48] Congcong Li, Qingshu Dong, and Weihua Li. Largely tunable asymmetry of phase diagrams of a (ab)_n miktoarm star copolymer. *Macromolecules*, 53(24):10907–10917, 2020.
- [49] Ya Gao, Hanlin Deng, Weihua Li, Feng Qiu, and An-Chang Shi. Formation of nonclassical ordered phases of a b-type multiarm block copolymers. *Physical Review Letters*, 116(6):068304, 2016.
- [50] Wenbo Jiang, Yicheng Qiang, Weihua Li, Feng Qiu, and An-Chang Shi. Effects of chain topology on the self-assembly of ab-type block copolymers. *Macromolecules*, 51(4):1529–1538, 2018.
- [51] Qiong Xie, Yicheng Qiang, and Weihua Li. Regulate the stability of gyroids of abc-type multiblock copolymers by controlling the packing frustration. *ACS Macro Letters*, 9(2):278–283, 2020.
- [52] Qiong Xie, Yicheng Qiang, Lei Chen, Yueming Xia, and Weihua Li. Synergistic effect of stretched bridging block and released packing frustration leads to exotic nanostructures. *ACS Macro Letters*, 9(7):980–984, 2020.
- [53] Frank S Bates, Marc A Hillmyer, Timothy P Lodge, Christopher M Bates, Kris T Delaney, and Glenn H Fredrickson. Multiblock polymers: Panacea or pandora’s box? *Science*, 336(6080):434–440, 2012.
- [54] Alexander D Vilesov, Georg Floudas, Tadeusz Pakula, Elena Yu Melenevskaya, Tatiana M Birshtein, and Yulia V Lyatskaya. Lamellar structure formation in the mixture of two cylinder-forming block copolymers. *Macromolecular Chemistry and Physics*, 195(7):2317–2326, 1994.
- [55] An-Chang Shi and Jaan Noolandi. Binary mixtures of diblock copolymers. phase diagrams with a new twist. *Macromolecules*, 28(9):3103–3109, 1995.
- [56] Mark W Matsen. Stabilizing new morphologies by blending homopolymer with block copolymer. *Physical review letters*, 74(21):4225, 1995.
- [57] Mark W Matsen. Phase behavior of block copolymer/homopolymer blends. *Macromolecules*, 28(17):5765–5773, 1995.
- [58] Mark W Matsen and Frank S Bates. One-component approximation for binary diblock copolymer blends. *Macromolecules*, 28(21):7298–7300, 1995.
- [59] Richard J Spontak, Jennifer C Fung, Michael B Braunfeld, John W Sedat, David A Agard, Lisaleigh Kane, Steven D Smith, Michael M Satkowski, Arman Ashraf, Damian A Hajduk, et al. Phase behavior of ordered diblock copolymer blends: effect of compositional heterogeneity. *Macromolecules*, 29(13):4494–4507, 1996.

- [60] Daisuke Yamaguchi, Shuntaro Shiratake, and Takeji Hashimoto. Ordered structure in blends of block copolymers. 5. blends of lamella-forming block copolymers showing both microphase separation involving unique morphological transitions and macrophase separation. *Macromolecules*, 33(22):8258–8268, 2000.
- [61] Takeshi Asari, Shigeo Arai, Atsushi Takano, and Yushu Matsushita. Archimedean tiling structures from aba/cd block copolymer blends having intermolecular association with hydrogen bonding. *Macromolecules*, 39(6):2232–2237, 2006.
- [62] Francisco J Martínez-Veracoechea and Fernando A Escobedo. Bicontinuous phases in diblock copolymer/homopolymer blends: simulation and self-consistent field theory. *Macromolecules*, 42(5):1775–1784, 2009.
- [63] Francisco J Martínez-Veracoechea and Fernando A Escobedo. The plumber’s nightmare phase in diblock copolymer/homopolymer blends. a self-consistent field theory study. *Macromolecules*, 42(22):9058–9062, 2009.
- [64] Zhiqiang Wu, Baohui Li, Qinghua Jin, Datong Ding, and An-Chang Shi. Phase behavior of binary blends of diblock copolymers. *The Journal of Physical Chemistry B*, 114(48):15789–15798, 2010.
- [65] Zhiqiang Wu, Baohui Li, Qinghua Jin, Datong Ding, and An-Chang Shi. Microphase and macrophase separations in binary blends of diblock copolymers. *Macromolecules*, 44(6):1680–1694, 2011.
- [66] Meijiao Liu, Yicheng Qiang, Weihua Li, Feng Qiu, and An-Chang Shi. Stabilizing the frank-kasper phases via binary blends of ab diblock copolymers. *ACS Macro Letters*, 5(10):1167–1171, 2016.
- [67] Haruko Miyase, Yusuke Asai, Atsushi Takano, and Yushu Matsushita. Kaleidoscopic tiling patterns with large unit cells from abc star-shaped terpolymer/diblock copolymer blends with hydrogen bonding interaction. *Macromolecules*, 50(3):979–986, 2017.
- [68] Tzu-Chun Tseng and Shiao-Wei Kuo. Hydrogen-bonding strength influences hierarchical self-assembled structures in unusual miscible/immiscible diblock copolymer blends. *Macromolecules*, 51(16):6451–6459, 2018.
- [69] Kyungtae Kim, Akash Arora, Ronald M Lewis III, Meijiao Liu, Weihua Li, An-Chang Shi, Kevin D Dorfman, and Frank S Bates. Origins of low-symmetry phases in asymmetric diblock copolymer melts. *Proceedings of the National Academy of Sciences*, 115(5):847–854, 2018.
- [70] Andreas J Mueller, Aaron P Lindsay, Ashish Jayaraman, Timothy P Lodge, Mahesh K Mahanthappa, and Frank S Bates. Emergence of a c15 laves phase in diblock polymer/homopolymer blends. *ACS Macro Letters*, 9(4):576–582, 2020.

- [71] Aaron P Lindsay, Ronald M Lewis III, Bongjoon Lee, Austin J Peterson, Timothy P Lodge, and Frank S Bates. A15, σ , and a quasicrystal: Access to complex particle packings via bidisperse diblock copolymer blends. *ACS Macro Letters*, 9(2):197–203, 2020.
- [72] Hideaki Takagi and Katsuhiko Yamamoto. Effect of block copolymer composition and homopolymer molecular weight on ordered bicontinuous double-diamond structures in binary blends of polystyrene–polyisoprene block copolymer and polyisoprene homopolymer. *Macromolecules*, 54(11):5136–5143, 2021.
- [73] Chi To Lai and An-Chang Shi. Binary blends of diblock copolymers: An effective route to novel bicontinuous phases. *Macromolecular Theory and Simulations*, 30(3):2100019, 2021.
- [74] Aaron P Lindsay, Guo Kang Cheong, Austin J Peterson, Steven Weigand, Kevin D Dorfman, Timothy P Lodge, and Frank S Bates. Complex phase behavior in particle-forming ab/abdiblock copolymer blends with variable core block lengths. *Macromolecules*, 54(15):7088–7101, 2021.
- [75] Qingyun Li, Dokyung Woo, Jin-Kon Kim, and Weihua Li. Truly “inverted” cylinders and spheres formed in the a (ab) $3/ac$ blends of b/c hydrogen bonding interactions. *Macromolecules*, 55(15):6525–6535, 2022.
- [76] Benjamin R Magruder, So Jung Park, Ryan P Collanton, Frank S Bates, and Kevin D Dorfman. Laves phase field in a diblock copolymer alloy. *Macromolecules*, 55(7):2991–2998, 2022.
- [77] Andreas J Mueller, Aaron P Lindsay, Ashish Jayaraman, Steven Weigand, Timothy P Lodge, Mahesh K Mahanthappa, and Frank S Bates. Tuning diblock copolymer particle packing symmetry with variable molecular weight core-homopolymers. *Macromolecules*, 55(18):8332–8344, 2022.
- [78] Logan J Case, Frank S Bates, and Kevin D Dorfman. Tuning conformational asymmetry in particle-forming diblock copolymer alloys. *Soft Matter*, 19(1):90–97, 2023.
- [79] Sukwon Kang, Jaeyong Lee, Hyeongkeon Yoon, Junho Jang, Eunyoung Kim, and Jin Kon Kim. Tetragonally packed inverted cylindrical microdomains from binary block copolymer blends with enhanced hydrogen bonding. *ACS Macro Letters*, 12:915–920, 2023.
- [80] Takeji Hashimoto, Komei Yamasaki, Satoshi Koizumi, and Hirokazu Hasegawa. Ordered structure in blends of block copolymers. 1. miscibility criterion for lamellar block copolymers. *Macromolecules*, 26(11):2895–2904, 1993.
- [81] Takeji Hashimoto, Satoshi Koizumi, and Hirokazu Hasegawa. Ordered structure in blends of block copolymers. 2. self-assembly for immiscible lamella-forming copolymers. *Macromolecules*, 27(6):1562–1570, 1994.

- [82] Satoshi Koizumi, Hirokazu Hasegawa, and Takeji Hashimoto. Ordered structure in blends of block copolymers. 3. self-assembly in blends of sphere-or cylinder-forming copolymers. *Macromolecules*, 27(15):4371–4381, 1994.
- [83] MW Matsen. Immiscibility of large and small symmetric diblock copolymers. *The Journal of chemical physics*, 103(8):3268–3271, 1995.
- [84] Hiroshi Morita, Toshihiro Kawakatsu, Masao Doi, Daisuke Yamaguchi, Mikihiro Takenaka, and Takeji Hashimoto. Competition between micro-and macrophase separations in a binary mixture of block copolymers. a dynamic density functional study. *Macromolecules*, 35(19):7473–7480, 2002.
- [85] CV Berney, Pao Luo Cheng, and RE Cohen. Distribution of matrix homopolymer in block copolymers of spherical morphology. *Macromolecules*, 21(7):2235–2240, 1988.
- [86] Takeji Hashimoto, Hideaki Tanaka, and Hirokazu Hasegawa. Ordered structure in mixtures of a block copolymer and homopolymers. 2. effects of molecular weights of homopolymers. *Macromolecules*, 23(20):4378–4386, 1990.
- [87] Hideaki Tanaka, Hirokazu Hasegawa, and Takeji Hashimoto. Ordered structure in mixtures of a block copolymer and homopolymers. 1. solubilization of low molecular weight homopolymers. *Macromolecules*, 24(1):240–251, 1991.
- [88] Karen I Winey, Edwin L Thomas, and Lewis J Fetters. Swelling of lamellar diblock copolymer by homopolymer: influences of homopolymer concentration and molecular weight. *Macromolecules*, 24(23):6182–6188, 1991.
- [89] Satoshi Koizumi, Hirokazu Hasegawa, and Takeji Hashimoto. Spatial distribution of homopolymers in block copolymer microdomains as observed by a combined sans and saxs method. *Macromolecules*, 27(26):7893–7906, 1994.
- [90] Guo Kang Cheong, Frank S Bates, and Kevin D Dorfman. Symmetry breaking in particle-forming diblock polymer/homopolymer blends. *Proceedings of the National Academy of Sciences*, 117(29):16764–16769, 2020.
- [91] Takeshi Asari, Shigeo Matsuo, Atsushi Takano, and Yushu Matsushita. Three-phase hierarchical structures from ab/cd diblock copolymer blends with complementary hydrogen bonding interaction. *Macromolecules*, 38(21):8811–8815, 2005.
- [92] Xu Zhang, Jingyuan Lin, Liquan Wang, Liangshun Zhang, Jiaping Lin, and Liang Gao. Supramolecular assembly of diblock copolymer blends with hydrogen-bonding interactions modeled by yukawa potentials. *Polymer*, 78:69–80, 2015.
- [93] Tzu-Chun Tseng and Shiao-Wei Kuo. Hierarchical self-assembled structures from diblock copolymer mixtures by competitive hydrogen bonding strength. *Molecules*, 23(9):2242, 2018.

- [94] Tzu-Chun Tseng and Shiao-Wei Kuo. Hydrogen bonding induces unusual self-assembled structures from mixtures of two miscible disordered diblock copolymers. *European Polymer Journal*, 116:361–369, 2019.
- [95] Cheng-Tai Tsou and Shiao-Wei Kuo. Competing hydrogen bonding interaction creates hierarchically ordered self-assembled structures of pmma-b-p4vp/pvph-b-ps mixtures. *Macromolecules*, 52(21):8374–8383, 2019.
- [96] An-Chang Shi, Jaan Noolandi, and Heinz Hoffmann. Diblock copolymer blends as mixtures of surfactants and cosurfactants. *Macromolecules*, 27(22):6661–6664, 1994.
- [97] An-Chang Shi and Jaan Noolandi. Effects of short diblocks at interfaces of strongly segregated long diblocks. *Macromolecules*, 27(11):2936–2944, 1994.
- [98] Eric K Lin, Alice P Gast, An-Chang Shi, Jaan Noolandi, and Steven D Smith. Effect of short diblock copolymers at internal interfaces of large diblock copolymer mesophases. *Macromolecules*, 29(18):5920–5925, 1996.
- [99] François Court and Takeji Hashimoto. Morphological studies of binary mixtures of block copolymers. 1. cosurfactant effects and composition dependence of morphology. *Macromolecules*, 34(8):2536–2545, 2001.
- [100] Takeji Hashimoto, Daisuke Yamaguchi, and François Court. Self-assembly in mixtures of block copolymers: “co-surfactant effects” on morphology control. In *Macromolecular Symposia*, volume 195, pages 191–200. Wiley Online Library, 2003.
- [101] François Court, Daisuke Yamaguchi, and Takeji Hashimoto. Morphological studies of binary mixtures of block copolymers: Temperature dependence of cosurfactant effects. *Macromolecules*, 39(7):2596–2605, 2006.
- [102] Feng Chen, Yoshiro Kondo, and Takeji Hashimoto. Control of nanostructure in mixtures of block copolymers: Curvature control via cosurfactant effects. *Macromolecules*, 40(10):3714–3723, 2007.
- [103] Iman Ahmadian and Andrew J Peters. Phase behavior of ab/cd diblock copolymer blends via coarse-grained simulation. *Soft Matter*, 16(12):3069–3081, 2020.
- [104] So Jung Park, Frank S Bates, and Kevin D Dorfman. Complex phase behavior in binary blends of ab diblock copolymer and abc triblock terpolymer. *Macromolecules*, 56(3):1278–1288, 2023.
- [105] Wangping He, Feng Wang, Yicheng Qiang, Yuchao Pan, Weihua Li, and Meijiao Liu. Asymmetric binary spherical phases self-assembled by mixing ab diblock/abc triblock copolymers. *Macromolecules*, 56(2):719–729, 2023.
- [106] Hideaki Takagi and Katsuhiko Yamamoto. Phase boundary of frank–kasper σ phase in phase diagrams of binary mixtures of block copolymers and homopolymers. *Macromolecules*, 52(5):2007–2014, 2019.

- [107] Meng-Zhe Chen, Yu-Ting Huang, Chun-Yu Chen, and Hsin-Lung Chen. Accessing the frank–kasper σ phase of block copolymer with small conformational asymmetry via selective solvent solubilization in the micellar corona. *Macromolecules*, 55(24):10812–10820, 2022.
- [108] Sung A Kim, Kyeong-Jun Jeong, Arun Yethiraj, and Mahesh K Mahanthappa. Low-symmetry sphere packings of simple surfactant micelles induced by ionic sphericity. *Proceedings of the National Academy of Sciences*, 114(16):4072–4077, 2017.
- [109] Carlos M Baez-Cotto and Mahesh K Mahanthappa. Micellar mimicry of intermetallic c14 and c15 laves phases by aqueous lyotropic self-assembly. *ACS nano*, 12(4):3226–3234, 2018.
- [110] Ashish Jayaraman and Mahesh K Mahanthappa. Counterion-dependent access to low-symmetry lyotropic sphere packings of ionic surfactant micelles. *Langmuir*, 34(6):2290–2301, 2018.
- [111] Carlos M Baez-Cotto, Grayson L Jackson, and Mahesh K Mahanthappa. Aqueous lyotropic mesophase behavior of gemini dicarboxylate surfactants swollen with n-decane. *Langmuir*, 36(9):2307–2321, 2020.
- [112] Shiao-Wei Kuo. Hydrogen-bonding in polymer blends. *Journal of Polymer Research*, 15:459–486, 2008.
- [113] Shiao-Wei Kuo and Cheng-Huo Hsu. Miscibility enhancement of supramolecular polymer blends through complementary multiple hydrogen bonding interactions. *Polymer international*, 59(7):998–1005, 2010.
- [114] Mark W Matsen. Self-consistent field theory and its applications. *Soft Matter*, 1, 2006.
- [115] Glenn Fredrickson. *The equilibrium theory of inhomogeneous polymers*. Number 134. Oxford University Press, 2006.
- [116] An-Chang Shi. Self-consistent field theory of inhomogeneous polymeric systems. *Variational Methods in Molecular Modeling*, pages 155–180, 2017.
- [117] Kim Ø Rasmussen and Georgios Kalosakas. Improved numerical algorithm for exploring block copolymer mesophases. *Journal of Polymer Science Part B: Polymer Physics*, 40(16):1777–1783, 2002.
- [118] G Tzeremes, Kim Ø Rasmussen, Turab Lookman, and Avadh Saxena. Efficient computation of the structural phase behavior of block copolymers. *Physical Review E*, 65(4):041806, 2002.
- [119] Christopher A Tyler and David C Morse. Stress in self-consistent-field theory. *Macromolecules*, 36(21):8184–8188, 2003.

- [120] Russell B Thompson, K O/ Rasmussen, and Turab Lookman. Improved convergence in block copolymer self-consistent field theory by anderson mixing. *The Journal of chemical physics*, 120(1):31–34, 2004.
- [121] Akash Arora, David C Morse, Frank S Bates, and Kevin D Dorfman. Accelerating self-consistent field theory of block polymers in a variable unit cell. *The Journal of chemical physics*, 146(24):244902, 2017.
- [122] Mark W Matsen. Self-consistent field theory for melts of low-molecular-weight diblock copolymer. *Macromolecules*, 45(20):8502–8509, 2012.
- [123] Pierre-Gilles De Gennes. *Scaling concepts in polymer physics*. Cornell university press, 1979.
- [124] Ludwik Leibler. Theory of microphase separation in block copolymers. *Macromolecules*, 13(6):1602–1617, 1980.
- [125] Kin Ming Hong and Jaan Noolandi. Theory of phase equilibria in systems containing block copolymers. *Macromolecules*, 16(7):1083–1093, 1983.
- [126] Mark Douglas Whitmore and Jaan Noolandi. Theory of phase equilibria in block copolymer-homopolymer blends. *Macromolecules*, 18(12):2486–2497, 1985.
- [127] Jin Kon Kim, Kohtaro Kimishima, and Takeji Hashimoto. Random-phase approximation calculation of the scattering function for multicomponent polymer systems. *Macromolecules*, 26(1):125–136, 1993.
- [128] Andreas Werner and Glenn H Fredrickson. Architectural effects on the stability limits of abc block copolymers. *Journal of Polymer Science Part B: Polymer Physics*, 35(5):849–864, 1997.
- [129] Shuyi Xie, Aaron P Lindsay, Frank S Bates, and Timothy P Lodge. Formation of a c15 laves phase with a giant unit cell in salt-doped a/b/ab ternary polymer blends. *ACS nano*, 14(10):13754–13764, 2020.
- [130] Mark W Matsen. Gyroid versus double-diamond in abc triblock copolymer melts. *The Journal of chemical physics*, 108(2):785–796, 1998.
- [131] Jian Qin, Frank S Bates, and David C Morse. Phase behavior of nonfrustrated abc triblock copolymers: weak and intermediate segregation. *Macromolecules*, 43(11):5128–5136, 2010.
- [132] Mark W Matsen and RB Thompson. Equilibrium behavior of symmetric aba triblock copolymer melts. *The Journal of chemical physics*, 111(15):7139–7146, 1999.
- [133] Mark W Matsen. Effect of architecture on the phase behavior of ab-type block copolymer melts. *Macromolecules*, 45(4):2161–2165, 2012.

- [134] Chi To Lai. *Theory of Disperse Diblock Copolymers*. PhD thesis, McMaster University, 2022.
- [135] Mathieu Dutour Sikirić, Olaf Delgado-Friedrichs, and Michel Deza. Space fullerenes: a computer search for new frank–kasper structures. *Acta Crystallographica Section A: Foundations of Crystallography*, 66(5):602–615, 2010.
- [136] Sean P Paradiso, Kris T Delaney, and Glenn H Fredrickson. Swarm intelligence platform for multiblock polymer inverse formulation design. *ACS Macro Letters*, 5(8):972–976, 2016.
- [137] Mihir R Khadilkar, Sean Paradiso, Kris T Delaney, and Glenn H Fredrickson. Inverse design of bulk morphologies in multiblock polymers using particle swarm optimization. *Macromolecules*, 50(17):6702–6709, 2017.
- [138] François Drolet and Glenn H Fredrickson. Combinatorial screening of complex block copolymer assembly with self-consistent field theory. *Physical Review Letters*, 83(21):4317, 1999.
- [139] Mark W Matsen and Michael Schick. Stable and unstable phases of a diblock copolymer melt. *Physical Review Letters*, 72(16):2660, 1994.
- [140] Meinhard Wohlgemuth, Nataliya Yufa, James Hoffman, and Edwin L Thomas. Triply periodic bicontinuous cubic microdomain morphologies by symmetries. *Macromolecules*, 34(17):6083–6089, 2001.